Michael Merten

Participation of Battery Storage Systems in the Automatic Frequency Restoration Reserve Market based on Machine Learning

Aachener Beiträge des ISEA Band 150

Participation of Battery Storage Systems in the Automatic Frequency Restoration Reserve Market based on Machine Learning

Von der Fakultät für Elektrotechnik und Informationstechnik
der Rheinisch-Westfälischen Technischen Hochschule Aachen
zur Erlangung des akademischen Grades eines Doktors der
Ingenieurwissenschaften genehmigte Dissertation

vorgelegt von

Michael Merten, M. Sc.
aus Linnich

Berichter:
Univ.-Prof. Dr. rer. nat. Dirk Uwe Sauer
Univ.-Prof. Dr.-Ing. habil. Christian Rehtanz

Tag der mündlichen Prüfung: 16. Juli 2020

AACHENER BEITRÄGE DES ISEA
Vol. 150

Editor:
Univ.-Prof. Dr. ir. h. c. Rik W. De Doncker
Director of the Institute for Power Electronics and Electrical Drives (ISEA)
RWTH Aachen University

ISSN 1437-675X

Institute for Power Electronics and Electrical Drives (ISEA), RWTH Aachen University
Jaegerstr. 17/19 • 52066 Aachen • Germany
Tel: +49 (0)241 80-96920
Fax: +49 (0)241 80-92203
post@isea.rwth-aachen.de

Michael Merten

Participation of Battery Storage Systems in the Automatic Frequency Restoration Reserve Market based on Machine Learning

Acknowledgements

This dissertation was written during my time as a research associate at the Institute of Power Electronics and Electrical Drives (ISEA) of the RWTH Aachen University. I would like to devote this section to thanking a few people who helped me during this time and contributed to the development of this dissertation. First, I would like to thank Univ.-Prof. Dr. rer. nat. Dirk Uwe Sauer, who gave me the opportunity to do my doctorate at his chair and who supported me in every possible way. I am particularly grateful for his support and encouragement to devote some of my time to develop a prototype for a business opportunity. His technical background and ability to interact with people were inspiring and showed me a new way of leadership. I would also like to thank Univ.-Prof. Dr.-Ing. habil. Christian Rehtanz for dedicating his time as secondary examiner. Further appreciation goes to all my colleagues at the institute for many technical discussions and the friendly social environment. I would like to pay a special attention to my longstanding office colleagues Tjark Thien, Hendrik Axelsen and Jeanette Münderlein who created a unique work environment. Special thanks also go to Kevin Jacqué and Christopher Olk for dedicating their time to the corrections of this work and for providing valuable feedback. I would also like to thank the secretary, the administration, the IT department, the mechanical workshop and the electrical workshop for their continuous support. For their support in my research, I would like to thank all students who worked for me during this time. Many thanks also go to my parents who made my studies possible, encouraged and supported me in the best possible manner. Finally, I would like to thank my girlfriend Laura, who endured me during the creation of this thesis, motivated and supported me all along.

Abstract

Automatic Frequency Restoration Reserve (aFRR) is one of three control reserve services in continental Europe to compensate imbalances in the electrical grid. Due to the transition towards a high degree of renewable sources, fewer conventional power plants will be available in the future to stabilize the electrical grid. However, new technologies are facing various entrance barriers because of the complex design of the aFRR market. This thesis provides a detailed aFRR market analysis and derives revenue potentials for different bidding strategies. By not relying on conventional power plants to stabilize the electrical grid, this work contributes in enabling a higher share of renewable sources.

To assist the creation of bidding strategies, a market prediction methodology is presented. For any potential bid, the acceptance probability in the next auction process is derived. Both statistical and machine learning based models are used for predicting key market quantities. An in-depth model comparison on numerous time series predictions reveals a usually better performance of statistical models. In only a few cases, the (recurrent) neural network models slightly outperform the statistical models. Exogenous data sources such as weather, electrical loads or market data did not significantly improve the prediction performance.

This work further developed an operating strategy for integrating Battery Energy Storage Systems (BESS) into existing virtual power plants (VPP) to jointly participate in the aFRR market. The operating strategy exploits the advantages of multiple technologies by selling a maximum of the generation capabilities on the market while the BESS instantly responds to aFRR requests and can recharge from the generation units. Based on an optimization process and the results from above mentioned predictions, a bidding strategy is presented that optimizes the bids to submit to the aFRR auction. An in-depth cost breakdown and battery-ageing model support the derivation of optimal bids and earning potentials. Special focus is on VPPs comprising only renewable sources and a BESS. With current costs of containerized BESS, an operation is not economically viable. Compared to the provision of Frequency Control Reserve (FCR), profits on the aFRR market were found to be lower. However, with a predicted cost breakdown for the year 2025, the pooled operation can generate profits and can contribute to grid stabilization in times of high levels of renewable sources.

Contents

1 Introduction

1.1 Motivation and Objective

To meet the climate objectives of the Paris Agreement, energy supply must shift away from conventional sources towards a high degree of renewable sources. As of December 2019, a total of 33 countries world-wide have declared to phase-out coal-fired generation [1]. Many countries, including Germany, are further phasing-out nuclear generation [2]. The transition process involves shutting down many conventional power plants.

In an electrical power system, a constant balance between production and consumption is required [3]. With fewer conventional power plants being active, services for stabilizing the electrical grid must increasingly be provided by other technical units. In continental Europe, various country-specific services are harmonized to benefit from a joint service procurement and a collaborative delivery. Of the three major control reserve services to stabilize the electrical grid, Frequency Control Reserve (FCR) has the shortest activation time and first responds to grid imbalances. Emerging technologies such as Battery Energy Storage Systems (BESS) already make up for a significant share of all FCR providers because the procurement process is easy and the business model is validated. However, this is different for subsequently activated control reserve services. In Germany, automatic Frequency Restoration Reserve (aFRR) and manual Frequency Restoration Reserve (mFRR) are dominated by a small number of providers with predominantly conventional generation [4]. Despite recent design changes, the aFRR and mFRR markets suffer from entrance barriers. Aside from technical requirements, the auction process is complex and revenue potentials are difficult to estimate.

This work aims at facilitating access to the aFRR market for technologies capable of storing electrical energy. A methodology for BESS participating in the aFRR market is presented and corresponding earning potentials are derived. Both the standalone operation of a BESS as well as the joint operation within a VPP comprising different types of generation facilities are considered. In joint operation, the properties of each technology are used to complement each other as effectively as possible. Special focus is on VPPs comprising only renewable sources and a BESS. By not relying on conventional power plants to stabilize the electrical grid, this work contributes in enabling an increasing share of renewable sources. Applying the proposed operating strategy allows a full utilization of renewable generation capabilities while stabilizing the electrical grid at the same time. These days, the aFRR market is undergoing frequent changes in the auction design and European-wide

collaboration. All simulations in this work are conducted on the conditions applying in Germany at the time between October 30th, 2018 and July 31st, 2019.

1.2 Structure

In chapter 2, various elements of the European/German electricity market are described. Of all three control reserve services, the aFRR market is analyzed at the highest degree of detail. The aFRR auction design is explained and game-theoretically regarded. An analysis of historical market data is conducted and revenues for different bidding behaviors are deduced. Since the operating methodology presented in this work trades on the day-ahead and intraday market, both markets are described as well.

The participation in the aFRR auction requires the submission of a bid comprising the offered capacity (MW), capacity price (€/MW) and energy price (€/MWh). Revenues strongly depend on the chosen bid components, other market participants and an unknown future request pattern. Chapter 3 proposes a methodology to predict key quantities of the aFRR market. The various predictions help estimating revenue potentials before submitting a bid and assist in deriving a bidding strategy. Multiple statistical and artificial intelligence based models are presented and compared with one another. Various data sources are made available for the learning process to increase the prediction accuracy. Based on the predictions, this work derives the acceptance probability associated with any choice of bid.

Chapter 4 presents an operating strategy that trades and dispatches the capabilities of a VPP with a connected BESS. At each point in time, energy is either traded on the various markets or used for recharging the BESS. Based on the results of the prediction methodology of the aFRR market, chapter 4 further presents a bidding strategy that derives the optimal bid for a VPP with a connected BESS. The optimal bid maximizes the expected earnings while considering costs for battery ageing as well as differential costs for the containerized BESS solution.

In the first section of chapter 5, results of the aFRR market prediction are presented. The performances of exponential smoothing models, seasonal autoregressive integrating moving average (SARIMA) models, neural network models and recurrent neural network models are compared with one another. According to the prediction methodology of chapter 3, three different aFRR market quantities are predicted: The marginal mixed price, the energy price and the deployment duration.

In the second section of chapter 5, the proposed bidding strategy is applied on different VPP configurations. Simulations are conducted for a BESS in standalone mode, in conjunction with a wind farm, in conjunction with a wind and PV farm and in conjunction with a wind farm, PV farm and thermal power plant. The economic viability is evaluated based on a BESS

cost breakdown of the year 2019 and a predicted cost breakdown for the year 2025. Earning potentials on the aFRR market are compared to earning potentials on the FCR market.

Chapter 6 summarizes the findings of this work.

2 Electricity Market Design

This chapter provides an overview of the European electricity market with a special focus on those market elements relevant for the presented prediction method (chapter 3) and bidding strategy (chapter 4). Multiple subsections of this chapter are based largely on a previous publication [5] of the author. In Europe, market liberalization was initiated by the European Commission in 1996 to unbundle the generation, transportation and sale of energy [6–8]. By this means, market monopolies are prevented in favor of creating a more efficient competitive market, which in particular allows participation of small, decentralized generation units. A further overall system cost reduction is targeted by uniting various national markets in order to increase the interexchange of energy and grid services. Both the Agency for the Cooperation of Energy Regulators (ACER) and the European Network of Transmission System Operators for Electricity (ENTSO-E) take a central role in creating Europe-wide common regulations. Extending the European cross-border electricity exchange allows the integration of large-scale renewable electricity generation. Several studies revealed that a larger market size reduce the generation and procurement costs of balancing power [9,10].

Since this thesis is closely coupled to a publicly funded large-scale stationary battery storage research facility located in Aachen, Germany, the German electricity market is considered in this work [11]. Figure 2-1 illustrates various methods of interacting with the electrical power system.

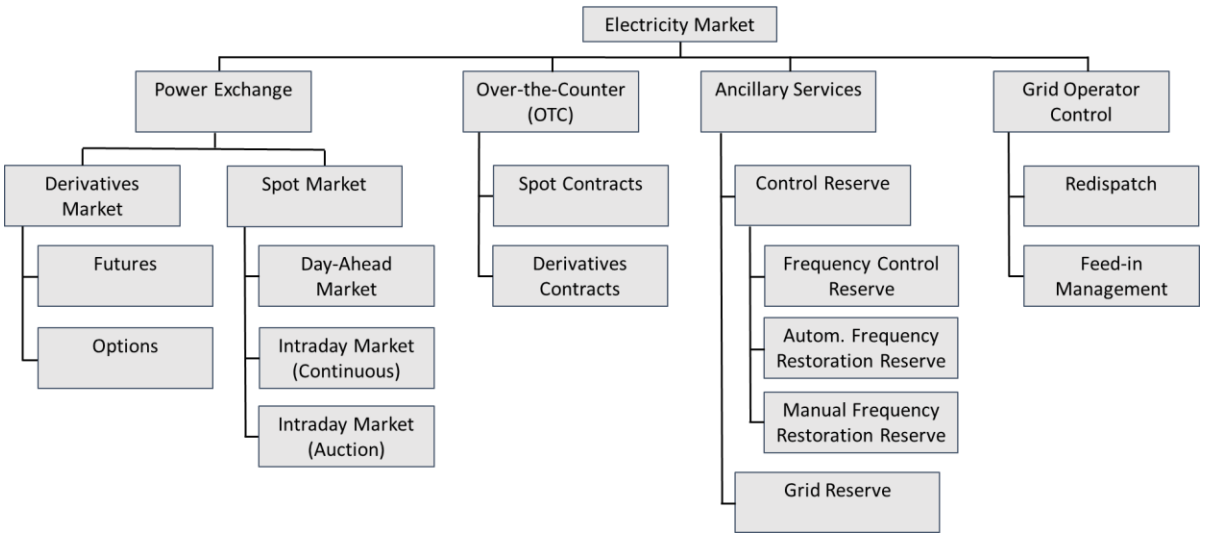

Figure 2-1: Electricity Market Design

Electrical energy can be traded at either the power exchange or over-the-counter (OTC), e.g. with bilateral contracts. The power exchange is divided into a facility for trading long-term

contracts and a facility for trading short-term contracts. Long-term contracts (weekly-, monthly-, quarterly- and yearly-basis) of up to 6 years in the future are traded on the derivatives market called European Energy Exchange (EEX) in Leipzig, Germany. Short-term contracts purchased for same-day or next-day delivery are traded at the European Power Exchange (EPEX) Spot located in Paris, France. Both the intraday and day-ahead short-term markets are explained in more detail in sections 2.2 and 2.3. For off-exchange trades (OTC), both long-term and short-term products exist and are commonly used.

In an electrical power system, generation and demand must be balanced at every time. To achieve balance, transmission system operators (TSOs) subdivide their responsibility into smaller balancing groups. Each balancing group is represented by a manager who ensures that the individual generation, consumption and traded energy within the corresponding zone are balanced. A balancing group is required to submit to the TSO a 15-minute resolution forecast of all activity for the next day. After the TSO has received all balancing group forecasts, a power-flow study is conducted to spot any grid bottlenecks. A grid bottleneck occurs if certain transmission line capabilities are too low to allow an energy flow as traded on the market. In this case, the power allocation must be changed by so-called “re-dispatch” measures. Generation units spatially in front of the bottleneck must be down-regulated to activate units behind the bottleneck. Down-regulated units are monetarily compensated.

TSOs counterbalance plant outages, load fluctuations and forecast errors by procuring control reserve, also referred to as balancing power. Control reserve compensates short term incidents and is indispensable for the stability of the power grid [12]. This topic is further explained in section 2.1. In addition to this market-oriented approach, the TSOs also maintain a so called “grid reserve” which mostly consists of power plants subject to decommissioning plans but classified as systemically relevant [13]. The power capabilities are reserved for scenarios with otherwise too little capacity to cover the demand. This might for example occur if market clearing on the wholesale market fails because the energy demand is higher than the energy supply. Both control reserve and grid reserve are referred to as ancillary services.

2.1 Control Reserve

Three different types of control reserve are procured by the TSOs, which technically differ in the maximum reaction time to the grid. Frequency Control Reserve (FCR) (section 2.1.1) must be fully activated within 30 s, automatic Frequency Response Reserve (aFRR) (section 2.1.2) within 5 min and manual Frequency Response Reserve (mFRR) (section 2.1.3) within 15 min after an imbalance causing event [14]. The minimum time that must be covered per incident also differs among the three control reserve types. Due to the diverse

specifications, not all generation unit types are equally capable of providing each control reserve service. Thermal power plants for instance often struggle with short activation times whereas long provision periods make stationary Battery Energy Storage Systems (BESS) uneconomic [15].

Figure 2-2 illustrates the activation procedure of FCR (also referred to as primary control reserve), aFRR (also referred to as secondary control reserve) and mFRR (also referred to as tertiary control reserve). The three control reserve types complement each other by being consecutively activated on the event of a grid balance disturbance. More information on each control reserve type is presented in the corresponding sections.

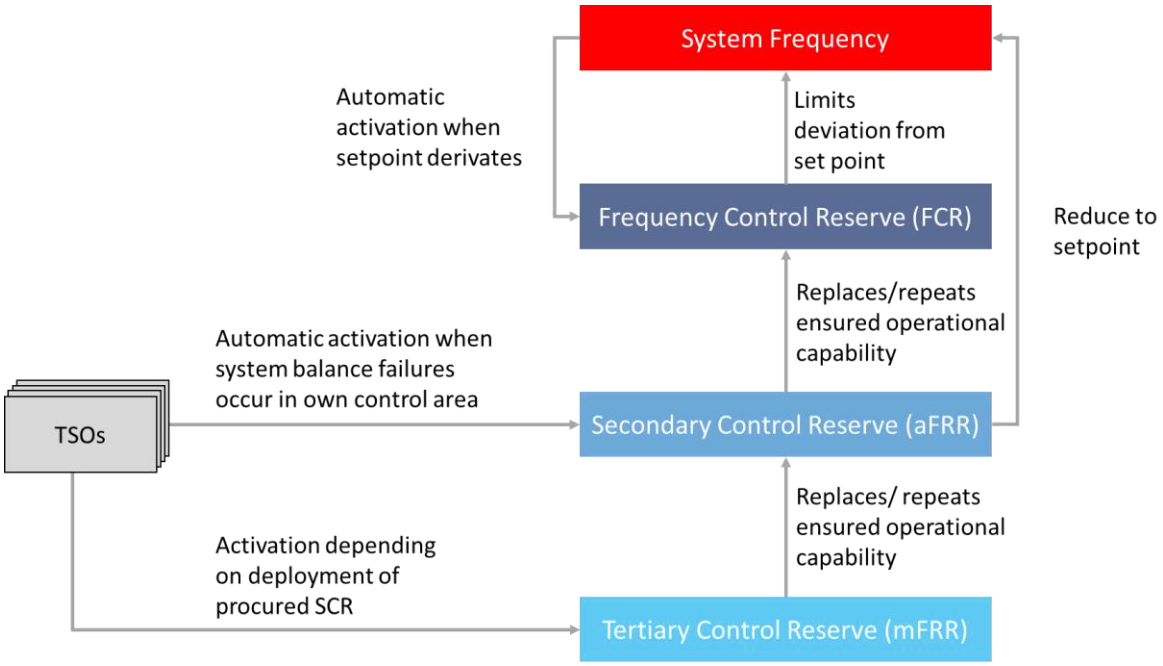

Figure 2-2: Activation of control reserve (based on [16])

The control reserve demand is procured in a multi-unit, open, discriminatory and transparent market auction to reach a cost optimal solution. Multi-unit auction refers to various independent auctions such as for the three different control reserve types and various time slots. Literature revealed that in “multi-unit auctions, the bidders' strategy spaces are substantially larger and more diverse than in single-unit auctions, and often a theoretic solution in form of a bidding equilibrium does not exist” [17].

Ambitions of the European Commission to merge the various control reserve markets within Europe shall reduce contrary power activation, increase flexibility, reduce CO_2 emissions, create a more competitive market and thus reduce the overall costs of electricity. Simulations verify the positive effects of a larger common control reserve market [18]. Multiple TSOs across Europe already collaborate on the provision of control reserve and jointly procure various products on a shared internet platform [14].

Before a unit can provide control reserve, numerous technical capabilities must be validated in a so-called prequalification process. Among others the prequalification process verifies whether the technical unit meets the requirement in terms of communication to the trading, IT security, energy availability (recharge strategy), power capabilities and service coverage by other units in case of a system failure (TransmissionCode 2007 [19]). The prequalification must be validated towards the spatially responsible TSO ("connecting TSO").

2.1.1 Frequency Control Reserve (FCR)

With the smallest activation time of all control reserve types, FCR first responds to grid imbalances. As opposed to the TSO activated aFRR and mFRR (see Figure 2-2), FCR providing units self-activate their service based on a measurement of the grid frequency. The TSOs define a set point frequency that serves as a reference for a balanced power flow in the grid. Grid frequencies above the set point indicate more generation than consumption whereas the opposite is true for frequencies below the set point. If the measured grid frequency deviates from the set point, FCR units feed-in or withdraw power proportionally to the frequency deviation. Figure 2-3 illustrates the grid interaction requirement (FCR power provision) with respect to the grid frequency and a set point of 50 Hz. A positive 100 % FCR provision (y-axis) refers to feeding-in with the capacity (MW) as assigned in the auction process (see below). At that point, the frequency is more or equal to 200 mHz below the set point. Symmetrically, frequencies above 200 mHz require the withdrawal with full assigned FCR power or a corresponding power set point reduction according to the schedule. For all frequencies within the ±200 mHz range, FCR power is activated linearly. FCR regulations allow a 20 % over-fulfillment of the power requirement derived from the measured frequency. Importantly, the additional power must be provided in the power direction

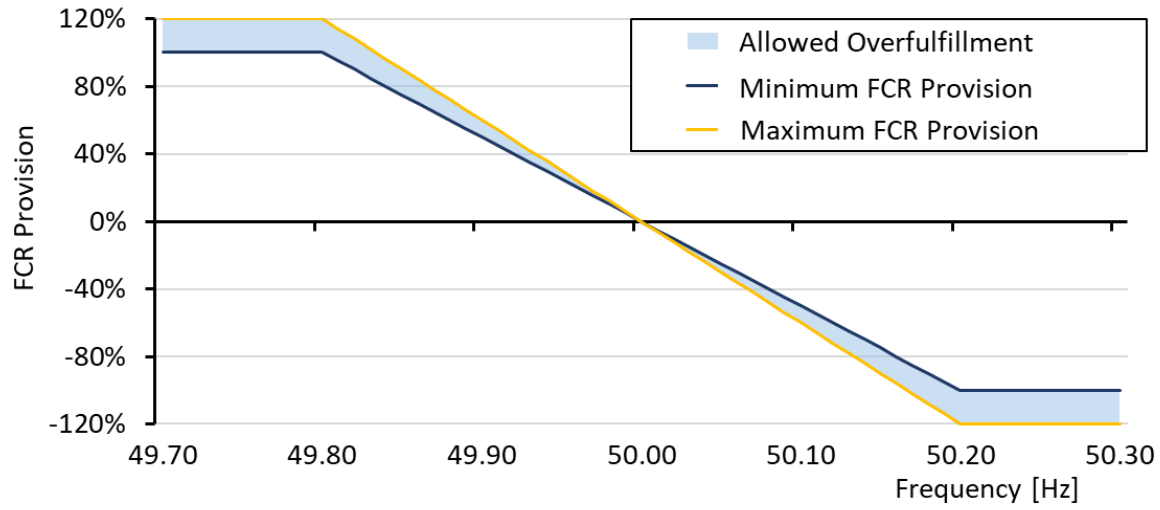

Figure 2-3: Frequency based activation of frequency control reserve (FCR)

counteracting the grid imbalances (feed-in for frequencies below the set point, withdrawal for frequencies above the set point). Within a so-called dead band of ±10 mHz around the set point, FCR provision is optional (given a high accuracy frequency measurement device).

A cooperation of multiple TSOs from the countries Austria, Belgium, France, Germany, Netherlands and Switzerland jointly conducts an auction process for delivering the total FCR demand across the spanned area. Since July 2019, the FCR demand has been procured in daily products with an auction closing of 2 days before delivery [20]. Starting from July 2020, the daily products have been replaced by six products per day (each with a duration of four hours) and an auction closing 1 day before delivery at 8 am. Bidders participating in the auction must be technically prequalified and submit their desired capacity (MW) in conjunction with an individual capacity price (€/MW). After auction closing, the TSOs sort all bids ascending by capacity price and accept the cheapest participants until the total FCR demand is met. Participants are paid a marginal price resulting from an allocation algorithm taking into account constraints such as import or export limitations.

2.1.2 Automatic Frequency Restoration Reserve (aFRR)

Automatic Frequency Restoration Reserve is the second-fastest frequency restoration measure aimed at timely replacing FCR. A prequalified technical unit must be able to produce a measurable power output after 30 s and deliver the full tendered power after 5 min. Each TSO operates its own load-frequency controller, which automatically distributes set point signals to connected technical units. The total aFRR demand (in MW) is calculated with probabilistic models and adjusted by the TSOs on a quarterly basis [14]. In the event of grid imbalances lasting longer than 15 min, aFRR is replaced by mFRR (section 2.1.3). The largest share of aFRR is provided by fast reacting power plants, such as combined cycle power plants, or by pumped hydroelectric energy storages (PHES). Virtual power plants comprising biogas systems or combined heat and power stations (CHPs) have recently gained momentum. BESS as standalone units are not well suited for aFRR due to the long minimum delivery duration of 4 hours and the associated high costs for battery capacity [15].

Among European countries, various country-specific market designs and procurement techniques are in place [21–23]. To reduce the aFRR provision costs of each TSO, an expansion of the grid control cooperation within Europe is being pursued. A larger control zone prevents counteracting control reserve activation by communicating imbalances between the load-frequency controllers of the TSOs. Control areas with insufficient power can cooperate with control areas with excess power to cancel out unnecessary aFRR activation. In 2011, the International Grid Control Cooperation (IGCC) was founded to exploit such benefits [22]. The efforts of the IGCC are divided into four modules. In the first module, counteracting aFRR activation is reduced by energy exchange between the control

areas. As of 2019, Austria, Belgium, Croatia, Czech Republic, Denmark, France, Germany, Netherlands, Slovenia and Switzerland cooperate on module one. Imbalance netting among the TSOs is only established if residual capacity is available on the transmission lines. Since no separate transmission capacity is reserved, the cooperation has no influence on the total procured aFRR demand. The module does not harmonize the markets but introduces a fair economic compensation for aFRR savings based on the individual costs. Modules two to four extend the cooperation among TSOs by introducing a common dimensioning, procurement and activation of aFRR. In case of transmission line bottlenecks, module 4 allows deviation from the merit order list of the auction. Since the beginning of 2019, a joint market up to module four exists for the four German TSOs (50Hertz, Amprion, TenneT and TransnetBW) and the Austrian TSO (APG). Cross-border capacities are determined in a weekly cost-benefit analysis and country-specific core shares are reserved [14]. Further steps towards an extended European cooperation are planned by the Platform for the International Coordination of Automated Frequency Restoration and Stable System Operation (PICASSO) [24].

2.1.2.1 Auction Design

The total aFRR demand is procured in a multi-unit, open, discriminatory, anonymous and transparent auction process. As opposed to FCR, a separate auction is held for the provision of positive and negative aFRR. Positive aFRR requests support the grid by supplying additional power. From left to right *Figure 2-4* summarizes the participation of market participants in the auction and operation process for one aFRR product type. The first step for each candidate is to acquire the prequalification of the connecting TSO (see section 2.1). Only prequalified units are allowed to participate in the auction process. Combined in a so-called bid tuple, each participant must submit the three quantities capacity (MW), capacity price (€/MW) and energy price (€/MWh). The capacity refers to the amount of power reserved for aFRR, the capacity price represents the monetary compensation the participant wishes to charge the system operator for holding the capacity available and the energy price describes the price the participant wishes to charge the TSOs for the delivery of actual energy. Each participant is allowed to submit multiple bid tuples for each aFRR product type. Energy prices can be positive and negative. With negative prices, the payment direction is reversed and market participants pay money to the TSOs. Negative energy prices are usually observed with negative aFRR products. A further discussion on negative aFRR prices is provided in section 2.1.2.3. After auction closing, all bids are collected by the TSOs and arranged ascendingly by capacity price (merit order). Starting from the lowest capacity price bid, consecutive bids are accepted until the total aFRR demand is met. The last accepted bid marks the marginal capacity price. If not all power of the last accepted bid is needed, a bid can also be accepted partially. Bids above the marginal capacity price are rejected. In the exceptional case of transmission line bottlenecks, a deviation from the merit order list is possible. All successful bidders are compensated for capacity reservation with

the capacity price as specified in the bid (pay-as-bid). To be considered, bids must be submitted until 8 am the day before delivery. Results are published 1 h after the submission deadline.

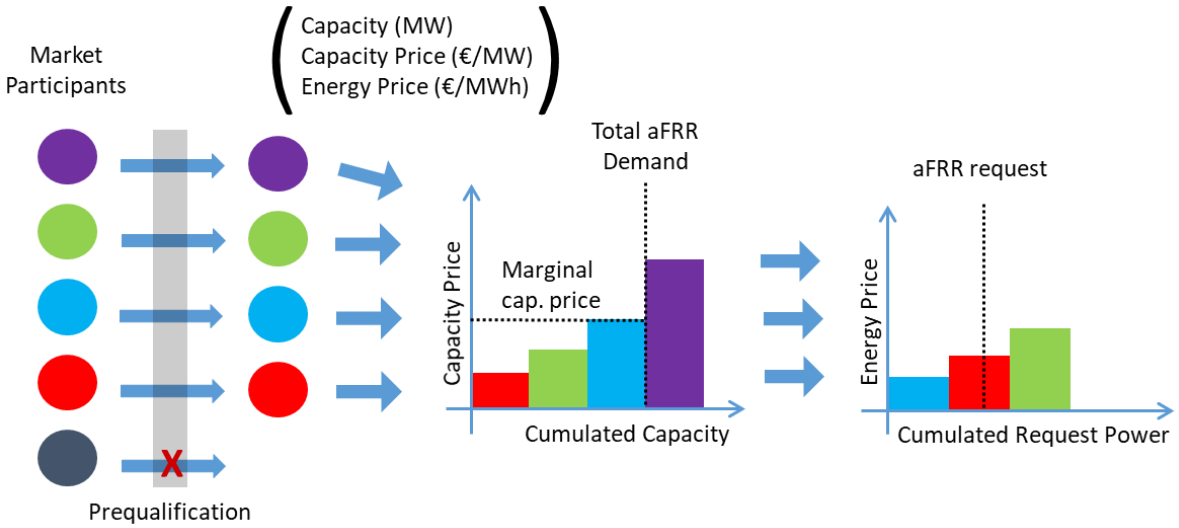

Figure 2-4: Working principle of the aFRR auction process (capacity price based)

Additional income can be generated if the reserved capacity is actually needed for stabilizing the grid. During the delivery period, all accepted bids are sorted in ascending order by energy price (merit-order). If grid imbalances require aFRR intervention, participants are activated starting with the one with the lowest energy bid until the power demand is met. The relative height of an energy bid determines the position in the merit-order list. Participants with low energy price bids are therefore activated more frequently than those with high energy prices.

Over the past years, the market and auction design has frequently changed. *Figure 2-5* illustrates a recent timeline of events for the Austrian/ German aFRR market. Before July 12th, 2018, aFRR was split into two time slices, one for all workdays between 8 am and 8 pm,

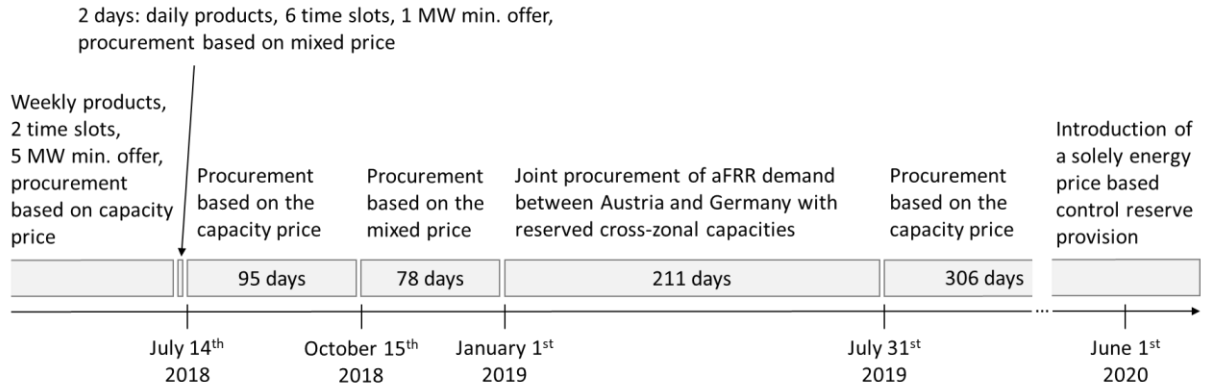

Figure 2-5: Changes in the aFRR market and auction design

the other one for all remaining periods. Only full delivery weeks were auctioned and the minimum capacity offer size was 5 MW. The demand of the four German TSOs was jointly procured. A revised market design was introduced on July 12th, 2018 to remove entry barriers for newly evolving market participants. Also literature revealed cost reductions for markets with smaller tender frequencies [25].

As illustrated in Figure 2-6, the new market design introduced separate daily auctions, 6 different time slices as well as both positive ("POS_xx_xx") and negative ("NEG_xx_xx") delivery directions. The minimum capacity size was reduced to 1 MW and the auction closing was moved closer to the day of delivery. Auctions are hold on a daily basis and bids can be submitted up until 9 am on the day before delivery [14].

12 am – 4 am	4 am – 8 am	8 am – 12 pm	12 pm – 4 pm	4 pm – 8 pm	8 pm – 12 am
POS_00_04	POS_04_08	POS_08_12	POS_12_16	POS_16_20	POS_20_24
NEG_00_04	NEG_04_08	NEG_08_12	NEG_12_16	NEG_16_20	NEG_20_24

Figure 2-6: Time slices in the new aFRR market design

Since the submitted energy price does not influence the awarding process, market participants can freely gamble with the energy price bid component. A disproportionately large energy price reduces the probability of being activated. Due to the rear position in the merit-order list, such a unit only responds to very rare grid emergency events. In the event of such a rare scenario, high profits are gained. For instance, on October 17th, 2017 mFRR energy was requested at a price of 77,777 €/MWh [26]. To prevent such gambling strategies from being successful, the new market rules introduced a mixed price auction scheme. As defined by equation (1), the mixed price for one product (B_{MP}) is based on the submitted capacity price (B_{C}), the submitted energy price (B_{E}) and a factor (a_M) published quarterly by the TSOs.

$$B_{\mathrm{MP}} = \frac{B_{\mathrm{C}}}{4h} + a_{\mathrm{M}} \cdot B_{\mathrm{E}} \tag{1}$$

The mixed price replaces the capacity price in the acceptance/ rejection process explained above. Since the mixed price is the sum of the capacity price in €/MW and the weighted energy price in €/MWh, no physical unit represents its meaning. For this reason, figures and references in this thesis that include the mixed price, do not come with a unit. With both the capacity and energy price component influencing the awarding of participants, the process is referred to as a scoring auction [27]. However, two days after coming into force, the Düsseldorf Higher Regional Court postponed the mixed-price based awarding until October 15th, 2018 to give market participants more time to adjust to the new procedure. After 289 days of a mixed price based procurement, the Düsseldorf Higher Regional Court

followed the outcome of a lawsuit and reactivated the capacity-based auction starting July 31st 2019. The mixed price procurement was considered an unfair market intervention and might be one reason for increased grid imbalances within that period [28]. Since the re-introduction of the capacity-based auction scheme, aggressive bidding behavior with energy prices in the order of 10,000 €/MWh was observed again. To promote sustainable competition and to prevent high energy prices from being requested, the German Federal Network Agency agreed on introducing a new market [29]. The new market shall be operated side-by-side to the existing control reserve markets. Solely based on energy price (€/MWh), prequalified technical units can then participate in the provision of grid stabilizing energy.

As mentioned in section 2.1.2, a joint procurement of aFRR has been carried out by Austria and Germany since the beginning of 2019. Due to reserved cross border capacities, a joint merit-order list awards participants irrespectively of their origin country.

The TSOs make various datasets available on the common platform regelleistung.net. The most relevant are the following [14]:

Anonymized successful bids: Includes the capacity, capacity price and energy price of each successful bid. Unsuccessful bids are not published.

Required balancing power: Every 3 months, the TSOs re-evaluate the amount of aFRR capacity required for grid operation. The demand (in MW) is publicly available before the auction starts.

Set point signal: With a 1 second resolution, the TSOs of Austria and Germany publish the set point signal of past aFRR activations.

2.1.2.2 Game-Theoretic Analysis

The daily aFRR demand is procured in separate auctions for the two power directions and the six 4 h time slices (Figure 2-6). Auctions are a subfield of game theory. Each of the 12 daily auctions share the following common properties, independent of whether a capacity- or mixed-price scoring scheme is applied:

Multi-unit

Multi-unit auctions refer to auctions in which a fixed number of identical units is traded. As for the aFRR auction, bidders compete for a predefined number of 1 MW (minimum block size) blocks corresponding to the predefined total capacity demand calculated by the TSOs. A bidder can specify a capacity price (€/MW) for an arbitrary number of 1 MW blocks (≤ prequalified capacity). It is also possible for a bidder to place multiple bids.

Pay-as-bid

If a bid is successful, both the capacity and energy price is paid as specified in the bid tuple. This is also referred to as a discriminatory price auction. In a future joint European aFRR market, the pricing rule might be switched to uniform pricing.

Partly homogeneous

The procured capacity pool is homogeneous since each capacity block is treated equally. As far as the energy price bid is concerned, the auction is not truly homogeneous since lower energy price bids result in more frequent calls.

Reversed

In a classical multi-unit forward auction, multiple units are simultaneously procured by the auctioneer. Each participant (bidder) of the auction can submit a different price for each unit. All bids are collected and the units are awarded to the highest submitted bids. In the aFRR auction design, multiple potential participants compete in selling their aFRR capacity until the predefined demand of the TSOs (auctioneer) is met. The payment direction is reversed and the auctioneer tries to reach minimum overall costs.

Sealed-Envelope

Up until auction closing, all bids submitted to the TSOs platform are kept secret. A participant has no insight in already submitted bids for the ongoing auction. Belayed strategy adaption of bidders is consequently not possible.

Anonymous

After auction closing, an anonymized list of successful bids is published. The list does not reveal the identity of the bidders and only contains the offered capacity, capacity price and energy price of each accepted bid. No information about rejected bids is given. However, the TSOs publish a list of prequalified suppliers of control reserve which limits the anonymity to a certain degree [4]. As of mid-2019, 37 potential suppliers are listed for aFRR. Based on the information provided, supplier identification or strategy deduction is hardly possible.

Repeated

A separate procurement process is conducted for each day of delivery. Apart from minor quarterly adaptions, the total procured aFRR demand per day and time slice is constant. In addition, the number of prequalified technical units is rather constant. An increase is only observed if multiple markets are joined or if new participants fulfil the prequalification requirements. However, due to the short lead times and the 4h-blocks, market participants

with a renewable generation portfolio can adapt their bids to predicted weather conditions. Still, a rather similar auction is repeated every day.

Efficiency

An electrical power system is considered efficient if an overall cost-minimal solution can be obtained. Hence, both the costs on the wholesale market and the costs arising from balancing power markets need to be minimized simultaneously [30]. Both markets interdepend on each other since a certain capacity of generation units can only be allocated to one market at a time. Only few literature covers the market interdependencies [23,31]. Ocker et al. [23] developed a game-theoretical market model for both the Austrian-German capacity-price auction and an auction based on a uniform pricing rule. Bayesian Nash equilibria were derived for the capacity (€/MW) and energy components (€/MWh) of the bids. All investigated market designs for both positive and negative aFRR were found to be theoretically efficient with competitive bids reflecting the particular technology of the generation unit.

Considering the pool of all units exchanging energy with the power grid, those units with the highest variable costs must be allocated for balancing power provision. Intuitively, the latter encourages units with low variable costs to continuously generate electrical energy for the wholesale market to keep the price for energy low. Conversely, units with high variable costs are only activated on rare grid supporting events. The allocation as just described is valid for both positive and negative aFRR whereas the activation of aFRR differs. Positive aFRR should be activated in the order of increasing variable costs for generation units or in the order of increasing opportunity costs for demand side management (reduction of consumption). This keeps the costs for additional energy demand (positive aFRR) low. Negative aFRR on the contrary should be activated first for units with high variable costs since reducing the power of those units has the highest cost saving potential.

The market equilibrium, as derived by the game theoretic model by Ocker et al. [23], is fundamentally different in the positive and negative aFRR auction. In the positive aFRR auction, both the capacity and energy price are greater than zero. Following the nomenclature of Müsgens et al. [30], an inframarginal (extramarginal) power plant is defined to have smaller (greater) variable costs than the timely corresponding price on the wholesale market (short-term or long-term contract). As indicated by equation (2), the lowest reasonable (economic) aFRR capacity price (€/MW) for an inframarginal power plant to offer (B_{Cmin}) depends on the lost profits of not trading power at an alternative market (B_{M}), the variable costs of the power plant (C_V) and the expected revenues based on the energy price B_{EE}.

$$B_{\mathrm{Cmin}} = B_{\mathrm{M}} + C_{\mathrm{V}} - B_{\mathrm{EE}} \quad (2)$$

If a power plant is extramarginal, due to its high variable costs it does not operate on the wholesale market and is presumably shut down. A capacity bid $\mathrm{B}_{\mathrm{Cmin}}$, as indicated by equation (3) must fully capture the variable costs C_{V}, include ramp-up costs C_{R} and compensate for usage costs C_{U} associated with running the plant at a minimal power to allow fast reaction times.

$$B_{\mathrm{Cmin}} = C_{\mathrm{V}} + C_{\mathrm{R}} + C_{\mathrm{U}} - B_{\mathrm{EE}} \quad (3)$$

The energy bid prices usually compensate at least for the variable costs C_{V}.

Market equilibrium for the negative market reveals according to game-theory a capacity price equal to zero and energy prices below zero [23]. Intuitively, zero capacity prices result from the fact that generation units do not need to withhold capacity for aFRR provision. Instead, variable costs can be prevented by ramping down the generation power traded on the wholesale market. Negative energy price bids (€/MWh) correspond to a reversed payment direction in which market participants pay for a power reduction. For generation units it is only reasonable to pay less for the power reduction than the variable costs. Offers above the variable costs (€/MWh) would result in a cost inefficient bidding strategy.

2.1.2.3 Price Settlement Analysis

Despite the existence of a theoretical aFRR market equilibrium (section 2.1.2.2), empirical analysis of past auction outcomes of the Austrian-German market reveal substantial deviations [17]. Prices in past auctions are on a higher level than the equilibrium suggests. Various research publications reveal that repeated auctions are susceptible to illegal price agreements among bidders [32–34]. The effect is called collusion and it is often observed in markets comprising a small number of dominant participants, as it is the case in the Austrian-German market.

For a limited time period, Heim et al. [35] were granted access to bidding data on the German market which also revealed the identity of auction participants. They found evidence for high prices due to “a reduction in supply of the most dominant supplier and the inter-action of the two most dominant suppliers’ bidding strategies afterwards”. Prices did not recover after the supply was back at its initial volume. Other research suggests that auction participants strongly adapt their bids according to previous auction results and by predicting the future marginal capacity price [30,36]. The latter conflicts with the theoretical market equilibrium in which participants place bids according to their true capacity costs.

Kraft et al. [12] analyzed bidding strategies on the German positive peak aFRR market in the period 2015 to 2017. Two dominant bidding strategies were observed. The first strategy

generates major revenues by energy provision and subordinates' revenues from capacity reservation. Conversely, the second strategy is based on capacity price revenues with only minor revenues from energy provision. At the end of the observation period, energy price bids increased whereas capacity price bids decreased. From a game-theoretic perspective, this is due to the repeated auction design and bidders having insight into previous outcomes. Across multiple auctions, bidders continuously reduce their capacity price bid to remain among those awarded for aFRR. Energy bids increase as bidders compensate for the losses on the capacity bid.

2.1.2.4 Historical Analysis

As for the market prediction (chapter 3) and the proposed bidding strategy (chapter 4), the outcomes of this thesis are derived from market data between October 20th, 2018 and June 6th, 2019. Within that period, auctions were awarded based on the mixed price. The following subsections analyze the market with respect to marginal mixed prices (subsection 2.1.2.4.1), energy prices (subsection 2.1.2.4.2), request durations (subsection 2.1.2.4.3) and revenue potentials based on the submitted energy bids (section 2.1.2.4.4).

2.1.2.4.1 Marginal Mixed Price

Of all mixed prices implicitly received from auction participants, the marginal mixed price denotes the highest awarded value. The bidder that submitted the marginal mixed price takes the last position in the merit order list and adds the last remaining capacity to the demand of the TSOs. Either the bidder's full capacity or a share of the capacity is awarded.

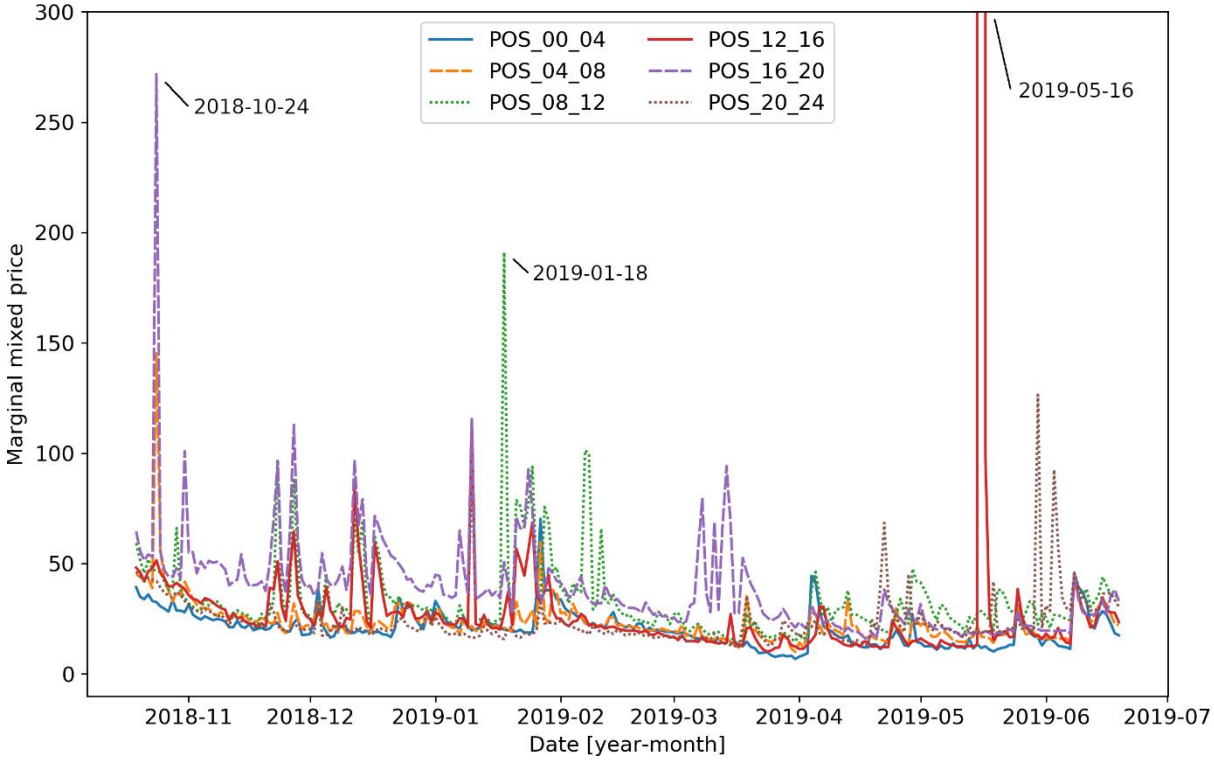

Figure 2-7: Marginal mixed prices for positive aFRR products

All bids above the marginal mixed price are rejected. Figure 2-7 illustrates a time series for each positive aFRR product type in the time period under consideration. Auctions for each product type were held daily. As supported by an STL (Seasonal and Trend decomposition using Loess) time series decomposition (see section 3.5), a minor downward trend can be observed across all product types. The downward trend is due to the mixed price scoring scheme being introduced five days before the start of the observation period. Market participants adjust their bids according to previous auction outcomes (collusive behavior) [23,35,36]. In addition, the price reduction might result from the market coupling of Germany and Austria at the start of 2019. Since then, a larger number of market participants compete for the procured capacity.

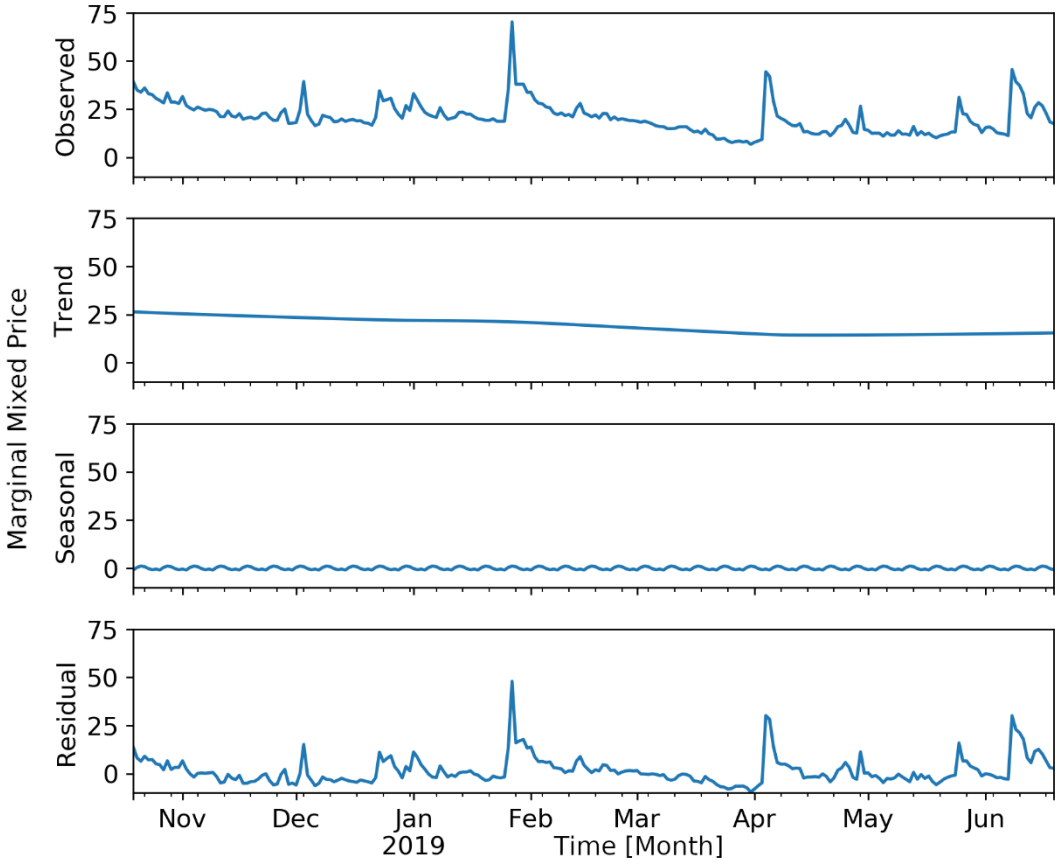

Figure 2-8: STL decomposition with a one-week seasonality of the POS_00_04 marginal mixed price series.

Multiple spikes are present in the various time series with magnitudes of around two to four times the prices of neighboring instances. Spikes of the various products often occur at the same day. The correlation is probably due to the same market participants bidding on multiple products with a similar bidding strategy. Any change of a participant acting on multiple time slices can then be observed on multiple products. Such a change might be associated to a change in the bidding strategy or a shortage of capacity (failure within a block of a power plant) which moves higher price participants down in the merit order list.

However, the simultaneous occurrence does not apply to all spikes and product types. The latter is an indication for a diverse market with bidders selectively participating in the various time slices and more reasonable price bids towards the end of the merit order list. As opposed to different time periods analyzed in [12,15], no obvious correlation to bank holidays or predominant vacation periods can be observed. In particular, during Christmas break many enterprises shut down their production causing the total power demand to go down. As a reaction, power plants with high variable costs also shut down and thus do not offer reserve capacity. Consequently, the reduced capacity at the grid has often resulted in high control reserve prices. On average, the POS_16_20 product reveals the highest marginal prices throughout the time under consideration.

As an example, Figure 2-8 illustrates the STL decomposition of the POS_00_04 marginal mixed price time series. A minor weekly-basis additive seasonal component is present but too small in magnitude to have any significant effect. After applying a first difference filter to the time series, the resulting time series can be considered stationary. The latter is justified by an ADF test on the differenced time-series. It reveals a statistic value of -11.13 that is smaller than the critical value of -2.87 at a 95 % confidence interval. Similar results are obtained when applying the STL decomposition on the other positive aFRR product types.

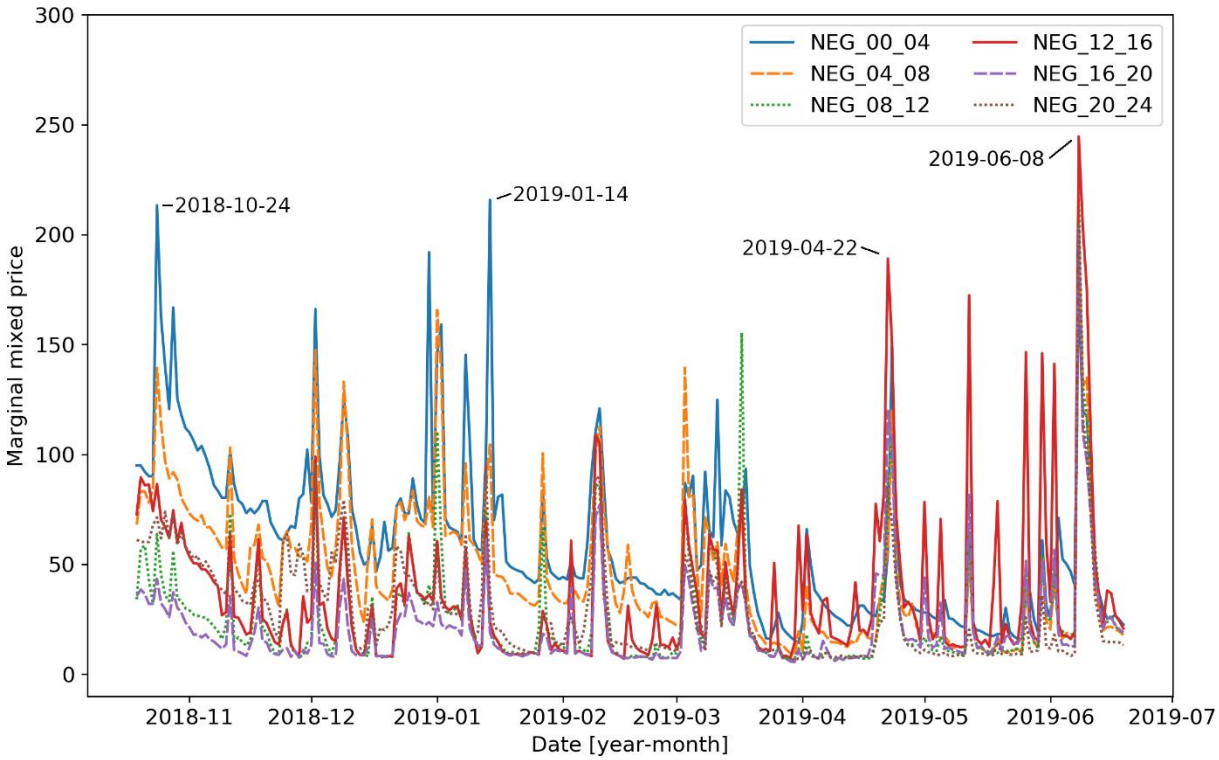

Figure 2-9: Marginal mixed prices for negative aFRR products

Figure 2-9 illustrates the marginal mixed prices for all negative aFRR product types. Compared to positive aFRR products, even more spikes are present. Individual spikes are

highly correlated with spikes of other aFRR products. As opposed to the game-theoretic findings of section 2.1.2.2, most capacity and energy bid prices are above zero (not visible in Figure 2-9). This is surprising since negative aFRR corresponds to a power reduction of generation units, which in turn corresponds to savings in variable costs. However, marginal mixed prices on average are on a higher level than corresponding positive aFRR products.

At the start of the observation period, marginal prices among the products differed substantially with the NEG_00_04 product yielding the highest prices. The start of the observation period is 5 days after the introduction of the mixed price auction scheme on October 15th, 2018. It appears, however, as though the market participants have tried different bidding strategies at the start of the new auction scheme. Towards the end of the observation period, marginal prices of the various product types continuously converge.

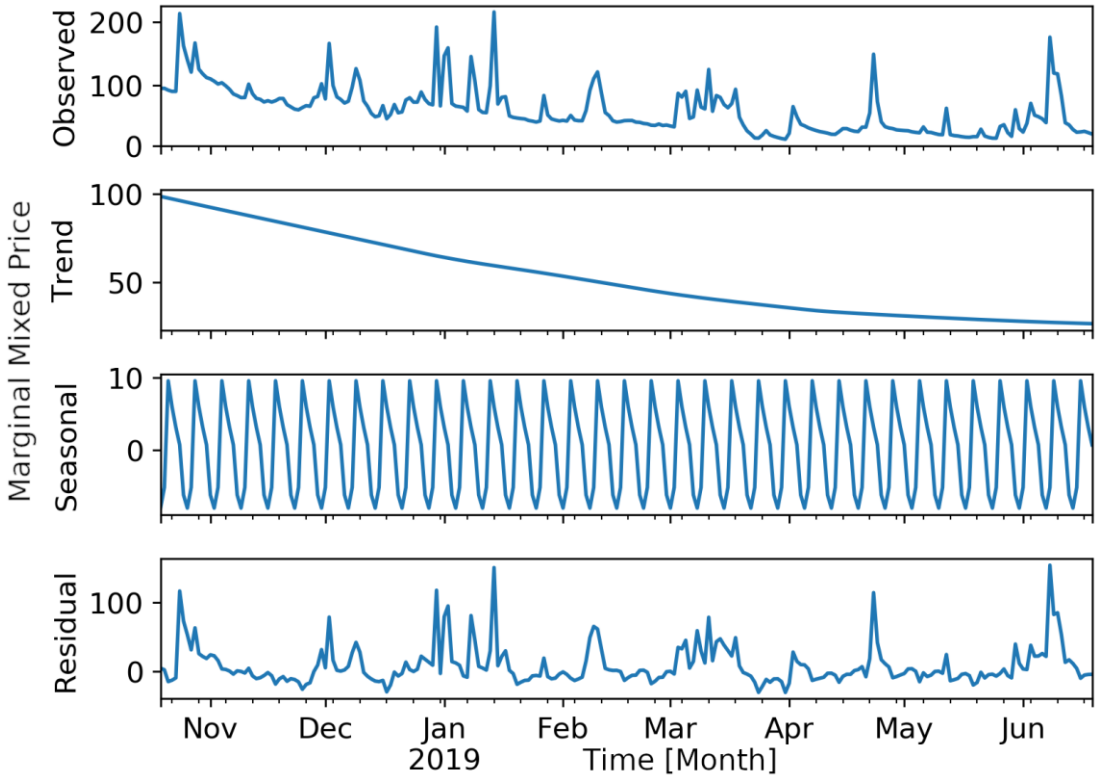

Figure 2-10: STL decomposition with a one-week seasonality of the marginal mixed price series (NEG_00_04)

Exemplary, Figure 2-10 illustrates the STL decomposition of the NEG_00_04 marginal mixed price time series. A clear, almost linear downward trend is apparent. Further, a minor additive seasonal component on a weekly basis is present in the series. A multiplicative seasonal component is not present. After applying a first difference filter to the time series, the resulting time series can be considered stationary. The ADF test on the differenced time-series reveals a statistic value of -11.11, which is smaller than the critical value at 5 % of

-2.87. This analysis was also conducted for all other negative product types, but due to a very similar outcome and for the sake of brevity is not further described.

2.1.2.4.2 Energy Prices

This subsection provides an overview of the energy prices submitted by the market participants. For each day and product type, all successful bid tuples are published by the TSOs. To illustrate the variance among the energy price bids, ten groups of equal capacity (section 3.2) are considered. The first group represents 10 % of the total capacity including those bids with lowest energy prices (merit order). Continuing in ascending order of the energy bids, the second group represents the 10 % to 20 % capacity range. For each group, the average energy price is calculated. Figure 2-11 illustrates the time series of the first (0 % - 10 %), 5th (50 % - 60 %) and last group (90 % - 100 %) of the NEG_00_04 product. The NEG_00_04 product type serves as an example.

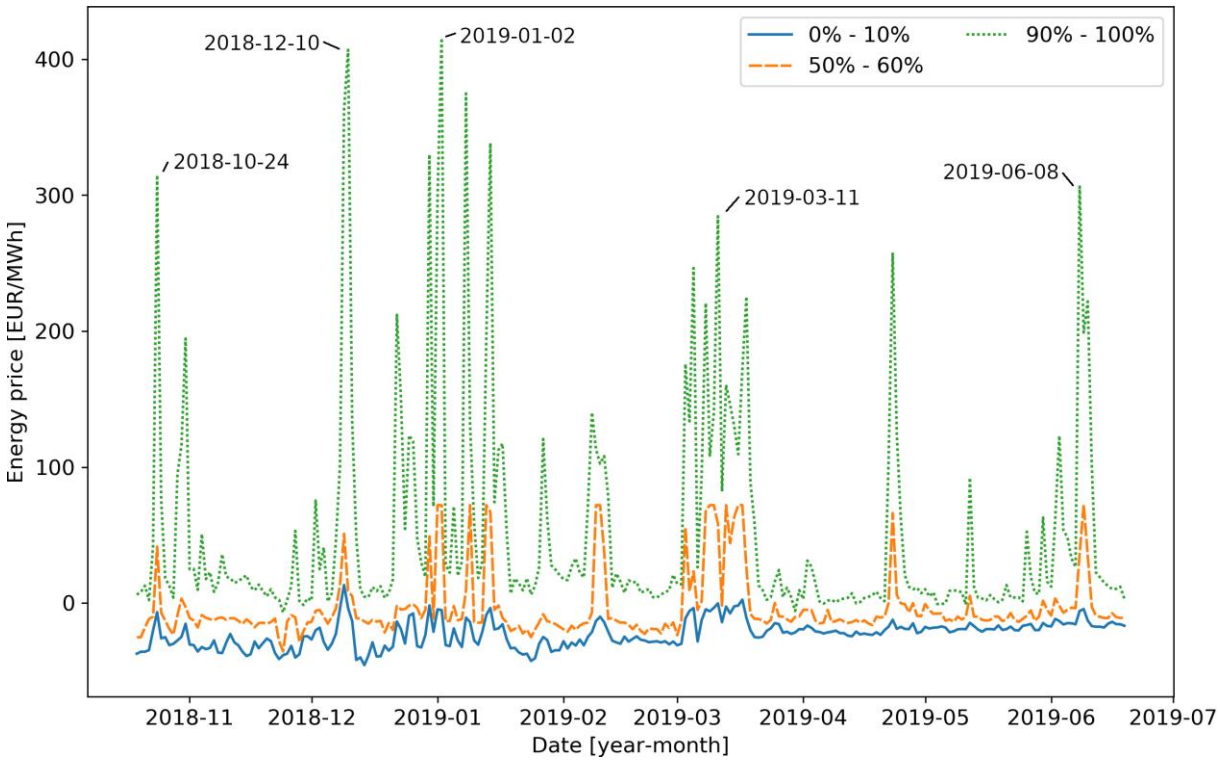

Figure 2-11: Energy price (€/MWh) time series for the NEG_00_04 product. Each graph represents a range within the sorted merit order list of all bids.

Energy prices in the first group are on average at around -20 €/MWh with fluctuations in the range ± 20 €/MWh. No clear trend is present and aside from two exceptions, the time series is negative. Because of rising energy prices within the merit order lists, subsequent groups are at higher price levels. The last group represents the highest energy price bids and is usually positively priced. Groups within higher ranges of the merit order list are subject to higher fluctuations. Peaks present in all groups increase in size the higher the group number is. For the last group peaks can reach magnitudes of 400 €/MWh whereas same day peaks in

the first group only reach 20€/MWh. High peaks in the last group are presumably rooted in bidding strategies aiming for low likelihood acceptance and low likelihood energy request. Because of the low awarding likelihood, high energy prices are claimed.

Likewise, Figure 2-12 illustrates the time series of the three groups for an exemplary positive aFRR product type (POS_08_12). As with the NEG_00_04 product, fluctuations are higher for groups towards the end of the merit order list. Prices are throughout positive since energy must be fed into the electrical grid. A downward trend can be observed in February 2019 with slowly recovering prices within the last few months.

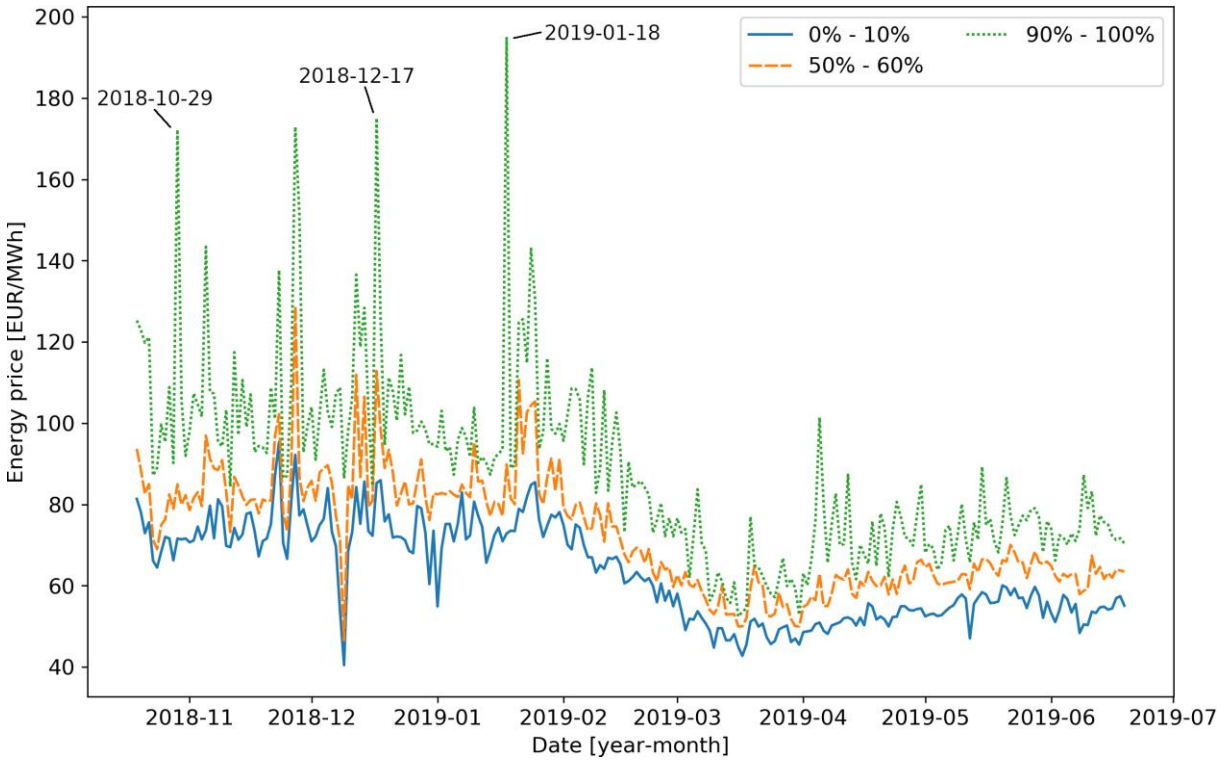

Figure 2-12: Energy price (€/MWh) time series for the POS_08_12 product. Each graph represents a range within the sorted merit order list of all bids.

2.1.2.4.3 Deployment Durations

This subsection provides an overview of the daily average deployment duration in the aFRR market. To what extend a participant is requested strongly depends on the submitted value of the energy bid. Since aFRR demands are covered according to the merit order list of all energy bids, bidders with low energy prices are requested more frequently than those with higher energy bids. The maximum possible deployment duration for an aFRR participant is 240 min, which corresponds to the duration of one aFRR product type. To show the bandwidth of deployment durations, the bids are placed into ten groups of equal capacity. As described in subsection 2.1.2.4.2, the first group covers the energetically cheapest 10% of all bids. Figure 2-13 illustrates the average deployment duration for three different groups within the NEG_00_04 product.

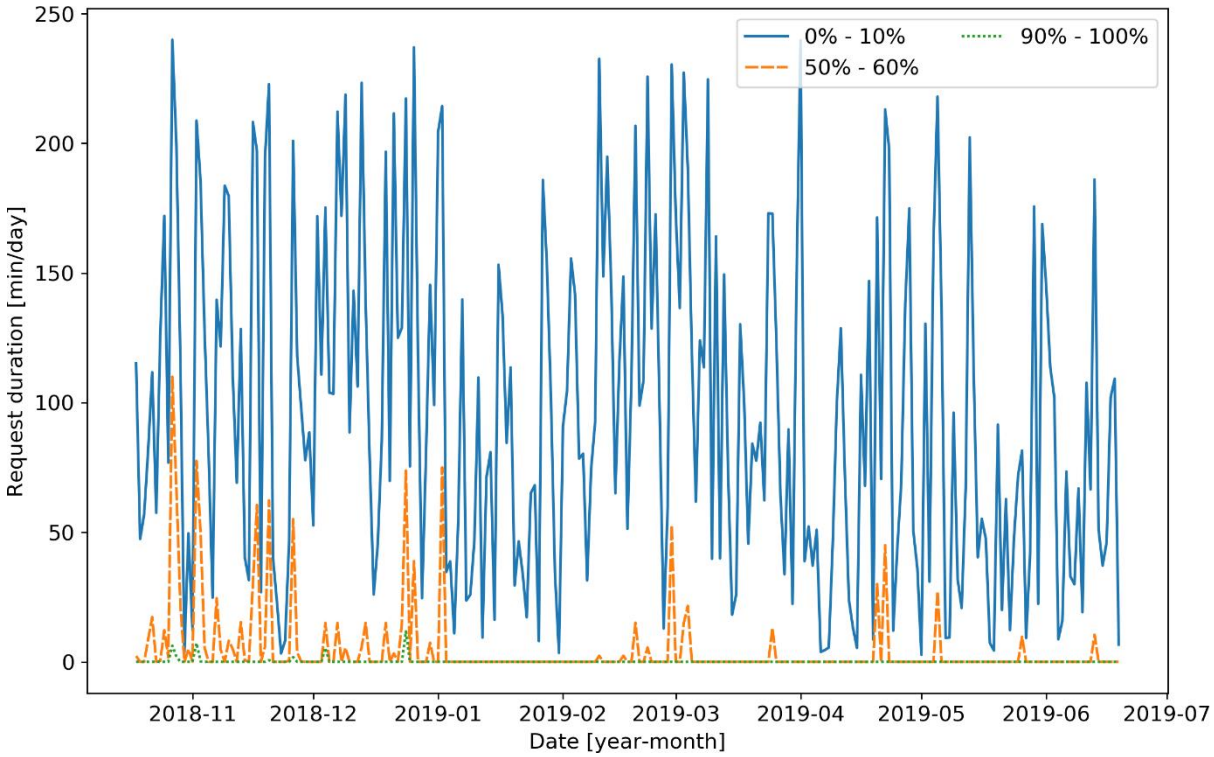

Figure 2-13: Time series of the daily request duration (in minutes per day) for the NEG_00_04 product. Each graph represents the average request duration for a range of bids within the merit order list.

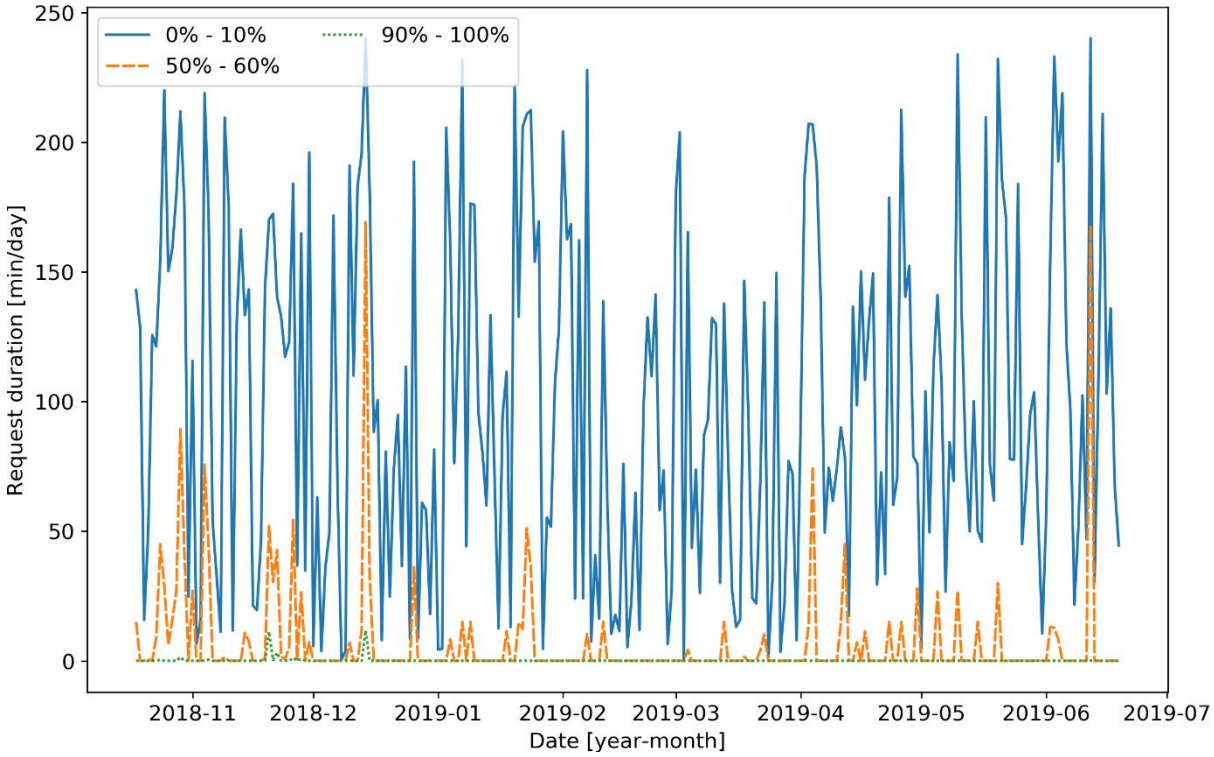

Figure 2-14: Deployment duration time series (in min) for the POS_08_12 product. Each graph represents the average request duration for a range of bids within the merit order list.

As expected, the first group has the highest average deployment duration. In some days, the maximum deployment duration is reached whereas in other days almost no power was requested. The time series significantly fluctuates and has no reoccurring patterns. In the 50 % - 60 % group, deployment durations are much smaller and no power is requested at all at many days. The last group covers the most expensive energy bids and in most days is not even requested once.

Figure 2-14 illustrates the three time series for the POS_08_12 product. In terms of average deployment duration and fluctuations, the time series are very similar to the negative product counterparts.

2.1.2.4.4 Revenue Potential

Depending on the energy price bid, this subsection presents an overview of historical revenues on the aFRR market. Table 2-1 summarizes the results for all positive aFRR product types. Each value represents the daily average over the considered time range between October 20th, 2018 and June 20th, 2019. All successful bids submitted for one product type and day are sorted in ascending order by energy price. Following the sorted list, the total capacity is divided into four blocks of equal size. The first block covers 25 % of the capacity corresponding to the lowest submitted energy prices. In the second block, all subsequent bids are placed until 50 % of the capacity is reached. This analysis only considers the revenues on the various aFRR markets but does not consider any marginal costs at the technical unit.

Across all product types, the highest revenues are yielded for energy price bids, which belong to the lowest 25 %. Due to the position in the merit order list, the corresponding deployment duration for aFRR requests is rather high. In four product types, the average energy provision per day is around 1 MWh. Revenues are generated from the quantity of energy rather than a high energy price. The capacity price contributes only little to the total revenue. In the subsequent capacity range (25 % - 50 %), only around a quarter of the energy is requested. Despite higher energy price bids, the total revenues are significantly lower than for the first capacity block. The average capacity prices are very similar in all product types and capacity ranges. No correlation with the submitted energy prices is present. Since almost no energy is requested for the latter two capacity ranges, the total revenues are dominated by the capacity price and in general are very low.

The results for all negative aFRR products are summarized in Table 2-2. Across all product types, the submitted energy prices are mostly negative and the capacity prices are low (~1 - 4 €/MW) but positive. Due to the negative energy prices, the total revenue is often negative as well, especially for the first 25 % of the capacity range. Market participants which submit negative energy bids benefit from energy supply at lower rates than on the intraday or day-ahead market. Thermal power plants for instance can offer energy prices below their

marginal costs to save on the consumption of fossil fuel. As with the positive aFRR product types, the average energy provision for the last two capacity ranges is very low. Consequently, the total average revenues are dominated by the capacity price. Per MW offered, the first range on average consumes around 1 MWh per day.

Table 2-1: Revenue potential on the positive aFRR market for various quartiles. Each value represents the daily average over the simulation period.

Product Type	Capacity Range	Minimum Energy Bid (€/MWh)	Maximum Energy Bid (€/MWh)	Average Energy Provision (MWh/MW)	Average Capacity Price (€/MW)	Total Average Revenue (€/MW)
POS_00_04	0% - 25%	51.80	63.61	0.682	1.56	41.98
	25% - 50%	63.61	67.39	0.115	1.49	8.82
	50% - 75%	67.39	71.00	0.013	1.55	2.40
	75% - 100%	71.00	98.35	0	1.19	1.19
POS_04_08	0% - 25%	54.49	66.14	0.997	1.98	64.13
	25% - 50%	66.14	69.96	0.268	1.87	20.04
	50% - 75%	69.96	73.31	0.054	2.02	5.84
	75% - 100%	73.31	103.49	0.005	1.53	1.88
POS_08_12	0% - 25%	56.58	67.98	1.136	2.90	78.13
	25% - 50%	67.98	71.73	0.359	2.67	28.76
	50% - 75%	71.73	75.33	0.09	2.80	9.90
	75% - 100%	75.33	127.76	0.016	2.27	3.60
POS_12_16	0% - 25%	55.34	66.15	1.034	2.18	69.74
	25% - 50%	66.15	69.88	0.283	1.76	22.22
	50% - 75%	69.88	73.19	0.047	1.79	5.56
	75% - 100%	73.19	513.79	0.007	3.08	3.77
POS_16_20	0% - 25%	57.07	68.60	1.173	3.93	78.20
	25% - 50%	68.60	73.35	0.364	3.64	28.45
	50% - 75%	73.35	78.39	0.074	3.68	9.04
	75% - 100%	78.39	144.34	0.007	3.04	3.59
POS_20_24	0% - 25%	55.31	65.70	0.845	1.94	52.77
	25% - 50%	65.70	69.15	0.209	1.78	14.89
	50% - 75%	69.15	72.69	0.04	1.89	4.42
	75% - 100%	72.69	103.33	0.004	1.51	1.79

Table 2-2: Revenue potential on the negative aFRR market for various quartiles. Each value represents the daily average over the simulation period.

Product Type	Capacity Range	Minimum Energy Bid (€/MWh)	Maximum Energy Bid (€/MWh)	Average Energy Provision (MWh/MW)	Average Capacity Price (€/MW)	Total Average Revenue (€/MW)
NEG_00_04	0% - 25%	-28.74	-14.39	0.985	3.86	-15.85
	25% - 50%	-14.39	-4.96	0.267	3.89	0.97
	50% - 75%	-4.96	4.09	0.07	4.38	4.19
	75% - 100%	4.09	125.26	0.011	2.95	3.13
NEG_04_08	0% - 25%	-29.39	-15.95	0.905	2.86	-15.70
	25% - 50%	-15.95	-7.33	0.273	3.02	0.38
	50% - 75%	-7.33	2.29	0.081	3.15	3.30
	75% - 100%	2.29	85.73	0.016	2.22	2.51
NEG_08_12	0% - 25%	-33.03	-20.60	0.921	1.87	-20.21
	25% - 50%	-20.60	-13.30	0.323	1.92	-2.52
	50% - 75%	-13.30	-2.31	0.086	1.95	1.84
	75% - 100%	-2.31	46.40	0.013	1.53	1.64
NEG_12_16	0% - 25%	-32.06	-18.77	0.899	2.41	-17.65
	25% - 50%	-18.77	-11.04	0.29	2.54	-0.42
	50% - 75%	-11.04	-0.98	0.081	2.66	2.89
	75% - 100%	-0.98	63.72	0.014	1.84	2.14
NEG_16_20	0% - 25%	-37.57	-21.23	0.81	1.79	-20.24
	25% - 50%	-21.23	-14.82	0.247	1.81	-3.17
	50% - 75%	-14.82	-4.32	0.073	1.69	0.96
	75% - 100%	-4.32	36.73	0.017	1.26	1.21
NEG_20_24	0% - 25%	-32.26	-19.68	1.046	1.77	-24.96
	25% - 50%	-19.68	-12.73	0.343	1.77	-4.51
	50% - 75%	-12.73	-3.91	0.104	1.80	0.63
	75% - 100%	-3.91	40.36	0.024	1.29	1.24

2.1.3 Manual Frequency Restoration Reserve (mFRR)

If power shortages or surpluses persist for more than 15 min, aFRR can be replaced by mFRR to make aFRR available again. Full power must be available 15 min after activation and the coverage period is 4 quarter-hours or up to several hours in case of several incidents [14]. As with aFRR, the total mFRR demand is adjusted quarterly by the TSOs and is currently (Q3 2019) 1,952 MW in the positive and 1,094 MW in the negative direction. Since 2012, the activation is based on a Merit-Order-List server operated by the TSOs (automatic activation). Due to the long reaction and provision times, mainly flexible gas-fired power plants or pumped storage power plants participate in the market. Virtual power plants which pool emergency power generators, combined heat and power (CHP) units, biogas plants and flexible electrical loads are recently emerging into the market [37].

As with aFRR, mFRR is procured daily with six different time slices and a distinction between positive and negative provision. Multiple changes in the auction design were done in parallel to the aFRR auction with the latest amendment dating back to July 12th, 2019. Each bid comprises the offered capacity (MW), a capacity price (€/MW) and an energy price (€/MWh). The scoring rule is based on the capacity price and energy is activated based on a merit-order list of the energy price bids. Both the capacity price is payed as bid for capacity reservation and the energy price is paid out for energy requests or feed-ins (discriminatory auction). Capacity and energy prices are subject to more severe market fluctuations than it is the case for aFRR. Overall, however, there has been a downward trend in average capacity prices over the past few years. One reason for this are the lower market entry barriers. With a reduced minimum lot size of 1 MW, more participants are entering the market. As a result, the costs of mFRR have fallen, effectively reducing the grid fees. Since mFRR, in chronological order, is the last control reserve type to react on grid imbalances, mFRR is called in a lower number of quarter-hours than aFRR.

2.2 Day-Ahead Market

Together with the two intraday markets, the day-ahead market belongs to the spot markets (Figure 2-1). Energy is traded either on the European Power Exchange (EPEX) in Paris or Over-The-Counter (OTC) in contracts negotiated off-exchange between suppliers and consumers [38]. At the power exchange, energy is traded for the following day in either one-hour slices or in standardized multi-hour products such as the base, peak or morning block. In the German market, participants must submit bids up until 12 noon the day before

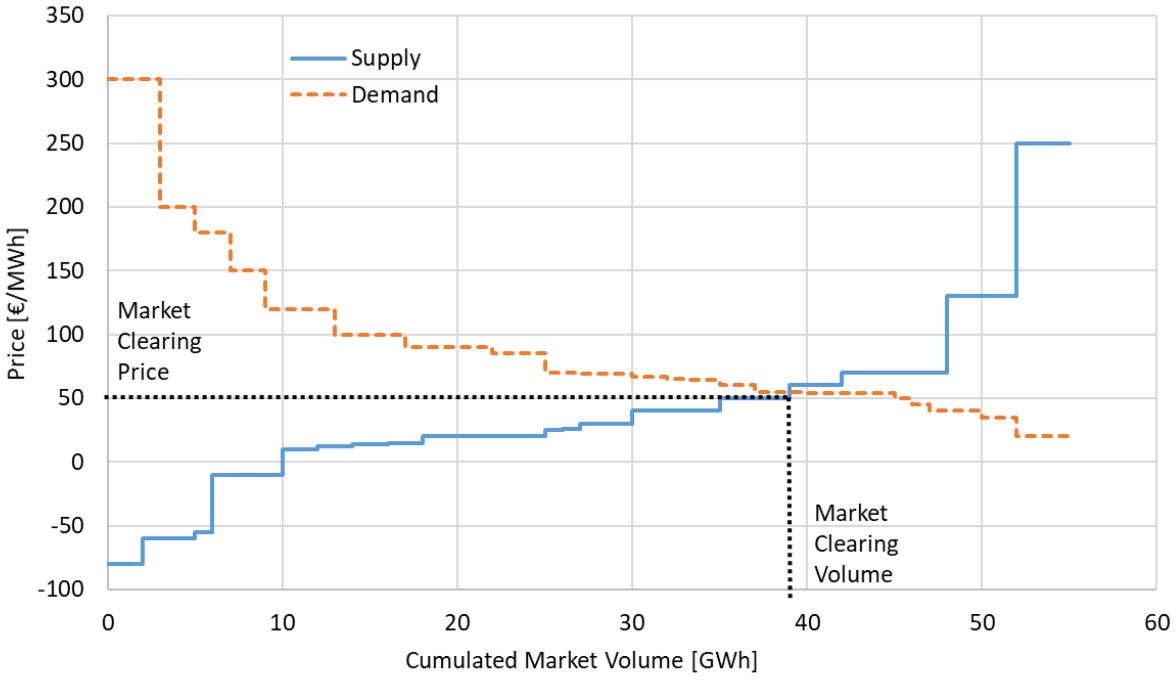

Figure 2-15: Demand curve, supply curve and market clearing price

delivery. Results are published 40 min after market closing to allow participation in the intraday trade, which opens at 3 pm the day before delivery. Trading is anonymous and takes place on all days, including bank holidays. The minimum quantity that can be traded is 0.1 MWh and prices are limited to a range between -500 €/MWh and 3,000 €/MWh [38]. For each hour traded, both electricity suppliers and consumers submit a bid comprising the desired quantity (MWh) and the corresponding energy price (€/MWh). After market closing, a supply curve for each hour is constructed by sorting all supply bids ascending by energy price and aggregating the corresponding offer (MWh). Similarly, a demand curve is constructed by sorting all demand bids descending by energy price and aggregating the corresponding offer (MWh). As illustrated by Figure 2-15, the intersection between the supply curve and the demand curve marks the so-called market clearing price (MCP) in this two-sided auction.

The MCP corresponds to the price of the last successful bid, which subsequently defines the price paid by all market participants for the respective product (uniform pricing). On the x-axis, the intersection marks the market clearing volume (MCV) which specifies the total quantity traded for the corresponding product. Energy prices (€/MWh) on the supply side can be negative if for instance the costs of ramping down a power plant exceed the losses from accepting negative prices or the production of renewable sources is unexpectedly high [12,39,40]. Even though a large European market is favored, cross-border capacities, as it is the case for Germany, often limit the exchange.

2.3 Intraday Market

Intraday trading takes place both on EPEX Spot in Paris and in OTC trading. With an auction based trading (section 2.3.1) and continuous trading (section 2.3.2), two different market designs are currently in place.

2.3.1 Auction

The auction based intraday market can be regarded as an extension to the day-ahead market and was introduced in December 2014 (in Germany). This daily auction allows the trading of electrical energy for every quarter of an hour of the following day. Subsequently to the day-ahead auction and before the beginning of continuous trading, all bids from the intraday auction are evaluated every day at 3 pm. The reason for the introduction of this additional quarter-hour trading is the increasing need to balance out the differences between the quarter-hourly and average hourly generation. With the additional auction, better planning and greater liquidity in the market were achieved. As with the day-ahead market, all bids for each block are aggregated to derive a unique MCP.

2.3.2 Continuous

While aforementioned auction-based markets rely on the principle of the MCP, the continuous intraday market uses a pay-as-bid method to determine the prices. Both, energy suppliers and potential buyers can place bids on the market. Each bid consists of the total energy to either offer (supplier) or request (buyer) and a corresponding price. If for instance a supplier offers energy on the market, a potential buyer must accept the price specified by the supplier or watch for a better offer. Consequently, there is no uniform price on the market, rather different prices for the same product occur depending on the time of trading.

Electricity is traded in both 15-minute and hourly blocks. Larger standardized block bids such as for base load or peak load are also possible. The lead times in intraday trading have been steadily reduced in recent years. A block can be traded up to 5 min before the start of delivery. This short-term trading primarily serves to keep the excess or shortage in balancing groups as small as possible to meet the previously issued forecasts. It allows counteracting unforeseen changes in electricity production or consumption prior to the use of control reserve. Intraday trading opens at 3 pm the day before delivery. As in day-ahead trading, the smallest tradable unit in intraday trading is 0.1 MWh. The possible price range for one MWh hour is -9,999 € to 9,999 €. All trades are handled anonymously. Electricity from conventional as well as from renewable energy sources is traded equally. The market was introduced in December 2011. Since then, the trade volume continuously increased and cross-border exchanges were enhanced [41].

3 Market Prediction for Automatic Frequency Restoration Reserve

This chapter is largely based on a previous publication of the author [5]. Revenues on the aFRR market depend on the total auctioned demand in the control zone, future SBP requests, the own bid tuple and the bid tuples submitted by competitors. The bid tuples of the competitors are unknown ahead of time because of the auction's sealed-envelope principle. Any future aFRR requests triggered by the TSOs are unknown as well and impossible to accurately predict with a high resolution. If latter were possible, the power could instead be traded on e.g. the Intra-Day market and there would be no need for balancing power.

This chapter presents an aFRR market prediction methodology to forecast key market quantities. A bidding strategy, which optimizes the bid tuple of a market participant, can build upon the predicted quantities. Section 3.1 reviews literature on related market predictions, section 3.2 to 3.5 describe the methodology and underlying input data used in this thesis. Section 3.6 estimates prediction intervals for the forecast quantity, section 3.7 derives the acceptance probability for any chosen bid tuple, section 3.8 to 3.12 explains how various prediction models are first trained and then evaluated. A detailed description of each prediction model is provided in section 3.13.

3.1 Literature Review

Literature on aFRR can be classified into the proposal of bidding strategies, market design analysis, market integration of renewables and market prediction techniques. This subsection focuses on the rare literature of market prediction techniques whereas the focus of subsection 4.1 is on bidding strategies and integration of renewables into the aFRR market.

Since the aFRR market design has changed in 2018, few literature was published on the new procurement process. For the old market design, Kraft et al. [12] examine the influence of exogenous factors on both the capacity and energy price structure. Exogenous quantities under investigation were the week ahead futures of the wholesale market, day-ahead spot prices and the forecast volatility of renewable energy sources. In a two-stage bivariate modelling process, the weighted average capacity and energy price is estimated. A bivariate multiple regression model is used in the first stage to quantify the influence of above-mentioned exogenous drivers. In the second stage, the influence of the lagged predictors are modelled in a multivariate vector autoregressive model. Applied to a two-year period,

both the volatility of wind and solar revealed a significant impact on the pricing whereas the day-ahead spot and week-ahead future market data did not.

Ocker et al. [17] analyze the German/Austrian aFRR old market design to derive bidding strategies of market participants. The focus is on thermal power plants for which a bidding strategy accordingly depends on the operation mode, capacity costs, calling costs and the empirical identification of acceptance and demand probability. It is assumed that previous auction results have a stronger influence on the individual bidding strategy than the actual power plant costs. The acceptance probability with respect to the capacity bid price is assumed to follow a linear function, which is obtained by analyzing historical bids. Since the marginal capacity price has a trend for the time range under consideration, the acceptance probability changes over time. Three different estimates of the linear acceptance probability function are proposed to compensate the trend. The demand probability as a function of the energy bid price is also modelled by a linear function taking into account the merit order position and prices of historical bids. Both approaches give a rough estimate of the corresponding probabilities by relying on averaging over historical data.

A fundamental market model for central Europe is introduced by Burgholzer [18] and computes the most economical dispatch of generation units such as thermal power plants, wind parks, PV (photovoltaic) parks, run-of-river plants and pumped hydro storages (PHS). The model implements balancing energy market mechanisms such as the procurement of balancing capacity and the activation of balancing energy due to control area imbalances [9]. Special focus is put on various market designs and the procurement of capacity. Other studies investigate the capabilities of aggregated volatile renewable sources to provide balancing power [21,42]. They aim at estimating a reliable day-ahead forecast for how much capacity can be offered on e.g. the aFRR market. Ma et al. [43] train two neural networks to forecast Locational Marginal Prices (LMP) before and after the day-ahead market for the PJM and New England market in the United States. Olsson et al. [44] model balancing market prices of the Scandinavian market by using combined SARIMA (section 3.13.3) and discrete Markov processes.

A somehow related research field to aFRR market prediction is electricity price forecasting (EPF). In most publications, the day-ahead electricity prices for liberalized markets around the world are predicted. Weron (2014) [45] published a thorough review of various approaches introduced in the last 15 years. A distinction of the forecast horizon is made between short-, medium- and long-term EPF. Short-term EPF generally refers to forecasts from a few minutes up to a few days, with one-step ahead forecast being the most common approach (also most interesting for this thesis). The vast majority of EPF papers evaluate the performance based on the mean absolute error (MAE), followed by the mean absolute percentage error (MAPE) and the root mean squared error (RMSE) (section 3.8). However,

most publications only calculate point forecasts but do not derive confidence intervals, prediction intervals or density forecasts (section 3.6). Only a few exceptions investigate prediction intervals or compare different approaches with one another [46–48]. Exogenous data sources are used in most approaches and almost always reveal a better performance than models only relying on autoregressive components of the time-series [45,49]. The following exogenous sources are considered to have a significant positive influence: Ambient weather conditions (temperature, wind speed, solar radiation and precipitation), system loads, fuel costs (oil, natural gas and to a minor extent coal), generation capabilities and scheduled maintenance of important power grid components [48]. For all sources, both historical data and predictions have been used to increase model performance. Aside from aforementioned quantitative sources, recent literature suggests the use of qualitative sources such as news feeds or social media posts (Twitter, Facebook) [50]. Techniques such as text mining and sentiment analysis can be used to feed information of these sources into a prediction model. Especially hybrid approaches use quantitative and qualitative sources have revealed a superior accuracy in various fields [51,52]. Due to the huge variety of prediction model types, Weron [45] introduced the following classification: Multi-agent models, fundamental methods, reduced-form models, statistical approaches and computational intelligence techniques. Statistical approaches predict the next observation by mathematically combining previous observations of the time series and exogenous sources. A huge variety of different statistical models such as regression, exponential smoothing or SARIMAX-GARCH models have achieved a high performance on EPF [53,54]. However, latter approaches often do not perform well if the time-series comprises spikes [55]. Multiple detection, filtering and spike modification methods have been proposed to solve this problem [48,56,57]. Computational intelligence techniques such as feed-forward neural networks, recurrent neural networks or support vector machines are well suited for handling complex and non-linear predictions with multiple exogenous features. However, the ability to adapt to non-linear and spiky time-series does not always guarantee a better performance than statistical models. For a more thorough overview of the various models used in literature, reference is made to [45].

3.2 Methodology

The following methodology refers to the market period between October 15th, 2018 and July 31st, 2019 in which the mixed price awarding scheme was present (see subsection 2.1.2.1). For the design of a bidding strategy, three different types of predictions are needed.

The first prediction quantity is the marginal mixed price as described in subsection 2.1.2.1. Of all submitted bids for one product, the marginal mixed price is the highest accepted mixed price. If the bidding strategy were to return a mixed price above the marginal mixed

price, the corresponding auction would be lost. All values below the marginal mixed price are accepted. This work implements several time series based prediction models (section 3.13) to obtain an estimate of the marginal mixed price. Since every prediction is accompanied by uncertainty, the predicted marginal mixed price or a smaller value does not guarantee acceptance within the auction. Section 3.6 derives intervals for the predicted value to quantify the statistical deviation from the true value. Based on the prediction intervals, section 3.7 derives the acceptance probability with respect to the mixed price.

If power is requested by the TSOs, starting from the cheapest energy price bid, bidders are called until the demand is met. The second prediction quantity is the energy price bid, which has a strong influence on the energy throughput and therefore the revenues. A low price energy bid corresponds to many requests and a high energetic throughput but relatively low revenue per MWh delivered. If a battery system is used for provision, a high energetic throughput causes increased cyclic aging and therefore deterioration costs. The opposite is true for high price energy bids. When the bidding strategy's optimizer selects an energy price from a range of possible values, the deterioration costs and revenues associated with each possible value must be considered. The latter requires an estimate of the provision duration, which is the third prediction value of this work.

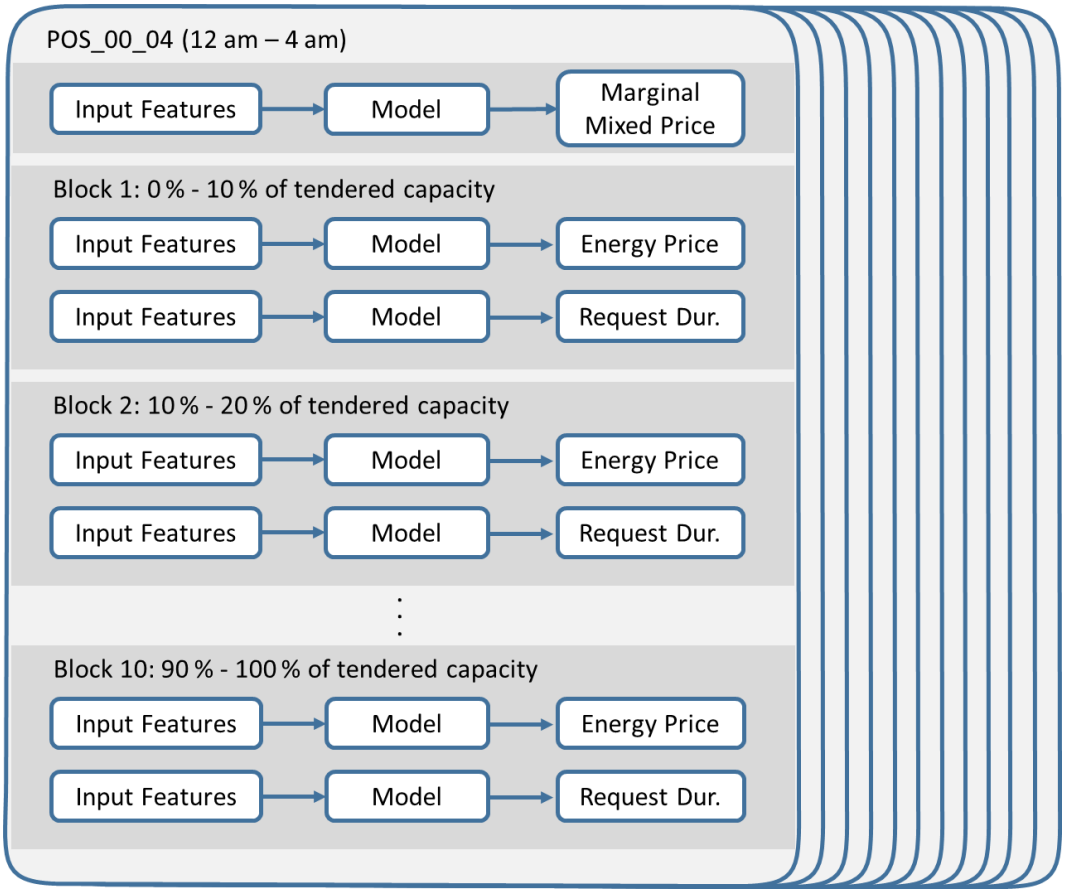

Figure 3-1: Prediction Methodology

The following sections describe the market prediction methodology for one aFRR product type and day. A graphical representation is depicted in Figure 3-1. The submission deadline for bids is at 10 am the day before delivery. Data available until this time is used for training time-series based models, which then make predictions for the day of delivery. The training data consists of an autoregressive component of the prediction quantity and multiple other data sources as described in section 3.3.

As illustrated in Figure 3-1, one model is trained for predicting the marginal mixed price, ten models are trained predicting the aFRR energy prices and ten models are trained for predicting the delivery durations. For both energy price and delivery duration prediction, all successful bids for a particular product type are sorted ascending by energy price. The total tendered aFRR capacity is then equally split into a predefined number of blocks. In this thesis, the total capacity is divided into ten blocks. Consequently, the first block covers all bids up until 10 % of the offered capacity; the second block covers all bids in the 10 % to 20 % range of all bids and so on. Starting from the cheapest energy bid, bids are put in into the first block until the 10 % block limit is reached. The following bids are put into the second block up until 20 % of capacity is reached. Since the tendered capacity is adapted over time, the absolute block size in MW is not constant in this approach. For each block, both the average energy price and delivery duration is calculated. Figure 3-2 illustrates the process. Bids overlapping the fixed block size are distributed proportionally to subsequent blocks.

Date	Product Type	Capacity Price (€/MW)	Energy Price (€/MWh) ↓	Offered Power (MW)
April 12th, 2019	POS_00_04	5.20	49.10	5
April 12th, 2019	POS_00_04	12.48	49.67	5
April 12th, 2019	POS_00_04	11.55	49.98	5
April 12th, 2019	POS_00_04	11.96	50.83	12
April 12th, 2019	POS_00_04	11.96	50.84	5
April 12th, 2019	POS_00_04	8.07	51.00	5
April 12th, 2019	POS_00_04	11.20	51.50	5
April 12th, 2019	POS_00_04	11.86	51.67	5
…	…	…	…	…
…	…	…	…	…
April 12th, 2019	POS_00_04	6.92	74.09	5
April 12th, 2019	POS_00_04	3.63	78.00	13

	Avg. Energy Price (€/MWh)	Avg. Delivery Duration (min)
Block 1 (0% – 10%)	49.90	172.4
Block 2 (10% – 20%)	50.98	130.6
…	…	…
Block 10 (90% – 100%)	76.44	0

Figure 3-2: Classification into blocks of equal capacity. The total procured capacity for this aFRR product type and date was 1,892 MW. Bids are sorted ascending by energy price.

This section justifies the chosen methodology against other approaches. Instead of distributing market participants into power blocks and then making a prediction for each power block, a multi-agent model could be deployed which derives each participant's

strategy based on historic data. The latter approach is not possible because auction results are published anonymously. A particular bidder cannot be identified across multiple auctions since no identification number is published. Bidders change their offered aFRR capacity as well as offered prices over time. Another approach could be to train a model for predicting the total delivery duration within one product as a function of the energy price and other features. That is a doable approach, which is accompanied by a few drawbacks. First, the delivery duration does not depend on the absolute value of the energy price but on the relative position of the energy price in the merit order list. The relative position is unknown before the auction ends since it depends on the closed-envelope bids of the competitors. A prediction for the delivery duration would therefore include the uncertainty of the position in the merit order list. Unlike this approach, the methodology presented above circumvents this problem since each capacity block represents a relative position in the merit order list. A second drawback of this approach is within the requirement of defining upper and lower boundaries for the delivery duration period. For very small energy prices, like 30€ below the true minimum, the model should not return unrealistically high delivery durations. This drawback is also circumvented by the methodology presented above.

3.3 Input Data and Feature Vectors

This section presents the data sources (predictors), which are available for training the various prediction models described in section 3.13. Table 3-1 states the type of time-series data with corresponding resolution and availability for the training process. As described in section 3.2, predictions are calculated one day before the actual day of delivery. The availability column states the data availability referred to the day of delivery/ prediction. For example, weather forecasts or German bank holiday data is available for the date of delivery, resulting in a Table 3-1 availability value of “D”. Stock exchange data or aFRR market data is only known and available up until one day before delivery (“D-1”). As for the aFRR energy prices and aFRR request set points, a separate series exists for each capacity block (see Figure 3-2). The weather data is obtained by averaging over data of 289 weather stations spread out all over Germany [58]. Since to the author’s knowledge no historic day-ahead forecasts are freely available, the actual measured values of the weather stations were used. This is justified by the fact that day-ahead weather forecasts have improved in recent years with accuracies in the range of 90-93 % [59,60]. All electrical data including the various load and generation time-series for Germany are based on freely available day-ahead predictions provided by ENTSO-E [61]. Gradients of the time series are derived to assist the learning process.

Feeding all data sources (also called features) to a model might negatively affect the model performance, since irrelevant or redundant data increases the model complexity, chances of

overfitting and training time. It is favorable to use only data sources that contribute information the prediction. Automatic feature selection techniques are widely discussed in literature [62]. A common approach is to statistically analyze each data source separately by e.g. a scatter plot or a correlation value. This approach is not applied in this thesis since latter approaches often only consider linear relationships and neglect interdependencies between data sources. Non-linear models such as neural networks are capable of e.g. treating a high PV-generation on a bank holiday differently than on a normal workday.

Table 3-1: Data Sources

Group	Data	Resolution	Availability	Feature Vector					Source
				1	2	3	4	5	
Market Data	aFRR Marginal Mixed Price	1 day	D-1	x	x	x	x	x	[14]
	aFRR Average Energy Price per Block	1 day	D-1	x	x	x	x	x	[14]
	aFRR Request Set Points per Block	1 sec	D-1	x	x	x	x	x	[14]
	aFRR Number of Bids	1 day	D-1	x		x	x	x	[14]
	aFRR Tendered Demand	1 day	D	x		x	x	x	[14]
Time Data	Calendar Year	1 year	D	x		x	x	x	
	Calendar Month	1 month	D	x		x	x	x	
	Calendar Day	1 day	D	x		x	x	x	
	Weekday	1 day	D	x		x	x	x	
	German Bank Holidays	1 day	D	x		x	x	x	[63]
Weather Forecast Data	Solar Irradiation	10 min	D	x			x		[64]
	Wind Speed	10 min	D	x			x		[58]
	Air Temperature	10 min	D	x			x		[65]
Stock Exchange Prices	EPEX Day-ahead Prices	1 hour	D-1	x			x		[38,61]
	DAX	1 day	D-1	x			x		[66]
	Oil Price	1 day	D-1	x			x		[67]
	Coal Price	1 day	D-1	x			x		[68]
	CO_2 Certificate Price	1 day	D-1	x			x		[69]
	Gas Price	1 day	D-1	x			x		[70]
Electrical Forecast Data	Load Profile Germany	15 min	D	x			x	x	[61]
	PV Gen. Germany	15 min	D	x			x	x	[61]
	Offshore Wind Gen. Germany	15 min	D	x			x	x	[61]
	Onshore Wind Gen. Germany	15 min	D	x			x	x	[61]
Derived Data	Gradients			x					

This thesis optimizes the use of features by regularization techniques as presented in section 3.13.4 and by evaluating models with five different feature vectors. Feature vector

one contains all data sources as listed in Table 3-1 and as such generates the highest number of parameters within models. In contrast, the second feature vector only contains the time series under consideration. The SARIMA model (section 3.13.3) and the exponential smoothing model (section 3.13.2) used in this work only make predictions based past observations of the time series (feature vector one). However, in the literature, statistical models, such as the SARIMAX model, exist which make use of additional data sources [71]. In this work, only the machine learning based models use additional data sources. Feature vector three contains aFRR market data and time data, feature vector four contains all data but derived gradients and feature vector five contains aFRR market data, time data and electrical forecast data.

3.4 Data Processing

To train prediction models, the input data listed in Table 3-1 must be transformed to a common temporal resolution. Since the resolution has an influence on the model accuracy, this work introduces the target resolution as a hyperparameter to the training process. In this context, hyperparameters are parameters specified before the learning (fitting) process of a model begins. Usually hyperparameters define the structure and data processing behavior of a model, such as the number of layers in a neural network. Depending on the source and target resolution, either downsampling (mean) or upsampling (forward fill) is applied.

Each product type in the aFRR market covers a 4 h period. Another hyperparameter to the model training is whether to extract the data for the full day or only data of the corresponding 4 h block.

Some machine learning models achieve higher accuracy if the input data has a consistent scale or distribution [72,73]. Two common methods are used in literature: Normalization describes the rescaling of input data to a range between 0 and 1 (min-max). Standardization involves rescaling the input data to a mean of zero and a standard deviation of 1 [73,74]. Both methods are evaluated in this work.

As suggested by literature, the input data is split into a training, validation and test set [75–77]. The training set is used for fitting the parameters (weights) of a specific model. Hyperparameter tuning and early stopping of the fitting process is done with the validation set [78]. The test set is set aside for an unbiased performance evaluation.

3.5 Time Series Analysis

Time series prediction is a big research area in which the one and best prediction approach for all problem types does not exist. Rather the performance of a prediction depends on the

model type, hyperparameters, predictors and the time series under consideration. This section analyses the inherent nature of the time-series to derive suggestions for model choice, hyperparameter selection and helpful data processing steps. Since analyzing all product types and prediction quantities as described in section 3.2 is beyond the scope of this section, the focus is on the univariate aFRR marginal mixed price time series for the 12 am to 4 am time slot (POS_00_04).

A common first step is to decompose the time series into a trend, seasonal and remainder component. Various different approaches have been analyzed in literature, including classical decomposition, X11 decomposition, SEATS (Seasonal Extraction in ARIMA Time Series) decomposition and STL (Seasonal And Trend Decomposition Using Loess) decomposition [79–81]. Compared to other approaches, STL decomposition has advantages in handling any type of seasonality, allowing the seasonal component to change over time, a smoothness parameter for the trend-cycle component and in the robustness against outliers [82]. On the downside, it only allows additive component decompositions. Figure 3-3 illustrates a line plot for the actual time-series at the top, followed by the components of the decomposition below.

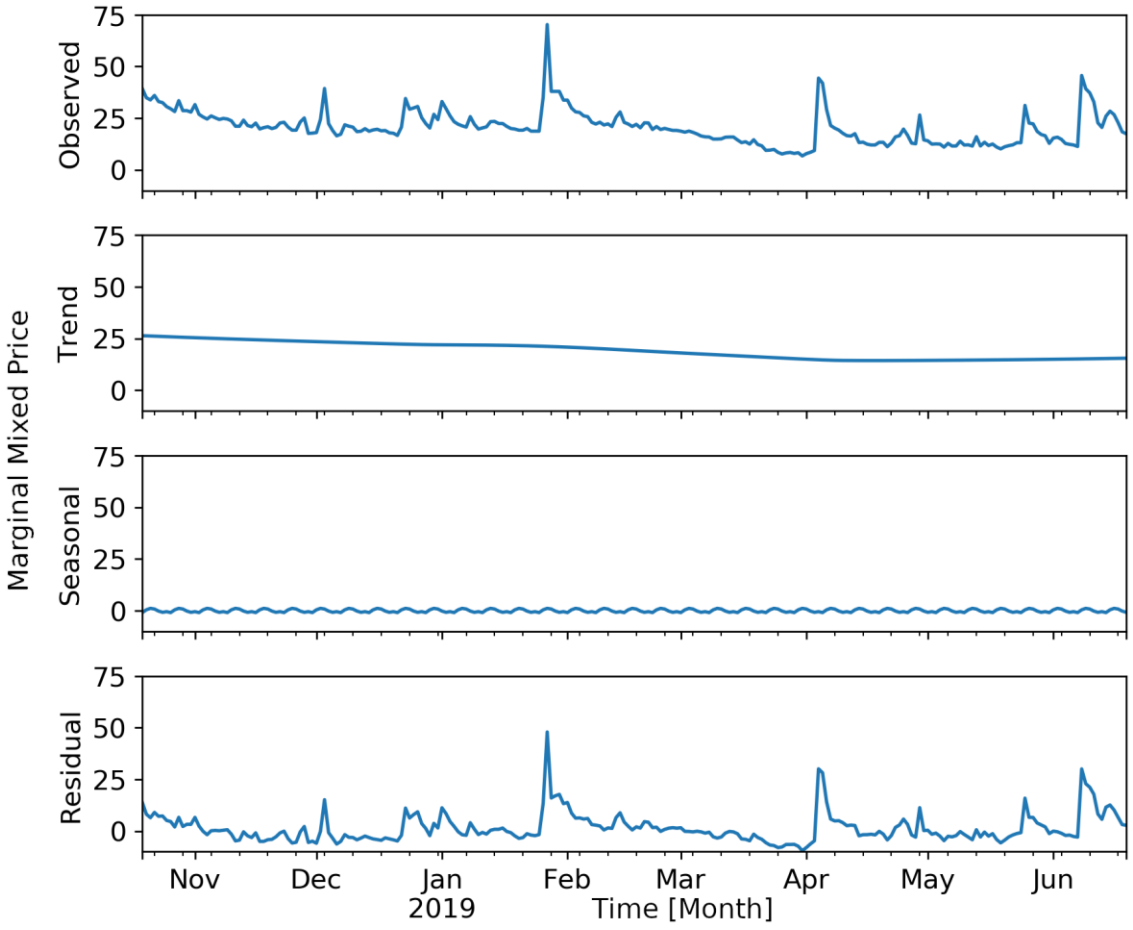

Figure 3-3: STL decomposition of the POS_00_04 marginal mixed price series

In the time range under consideration, a small trend towards lower marginal mixed prices is apparent. At the end of October 2018, the trend series starts at a value of around 25 and falls to a value of around 12 in start of May 2019. The downwards trend might be explained by the new auction design (introduction of mixed price tendering on October 15th, 2018) coming into force and the associated period to reach a market balance as participants are adjusting their bidding strategies.

Figure 3-3 also shows a seasonal component with a 7-day pattern. However, the very small variance of the seasonal component suggests that it is not relevant. This observation is in line with the autocorrelation (ACF) and partial autocorrelation (PACF) plot in *Figure 3-4*. The ACF plot shows the Pearson's correlation coefficient (y-axis) of the time series with the same time series lagged by k days (x-axis). The blue shaded (cone-like) area in the ACF plot represents 95 % confidence intervals, suggesting that spikes outside this area are significant (no white noise) with p-values less than 0.05 [83]. At the bottom of *Figure 3-4* is a PACF plot, that results from removing the effect of any correlations of shorter lags [84]. All spikes, except for the first lag spike in the PACF plot, are not significant (95 % confidence intervals). If seasonality is present in a time-series, a corresponding significant spike usually appears at the lag value of the periodicity.

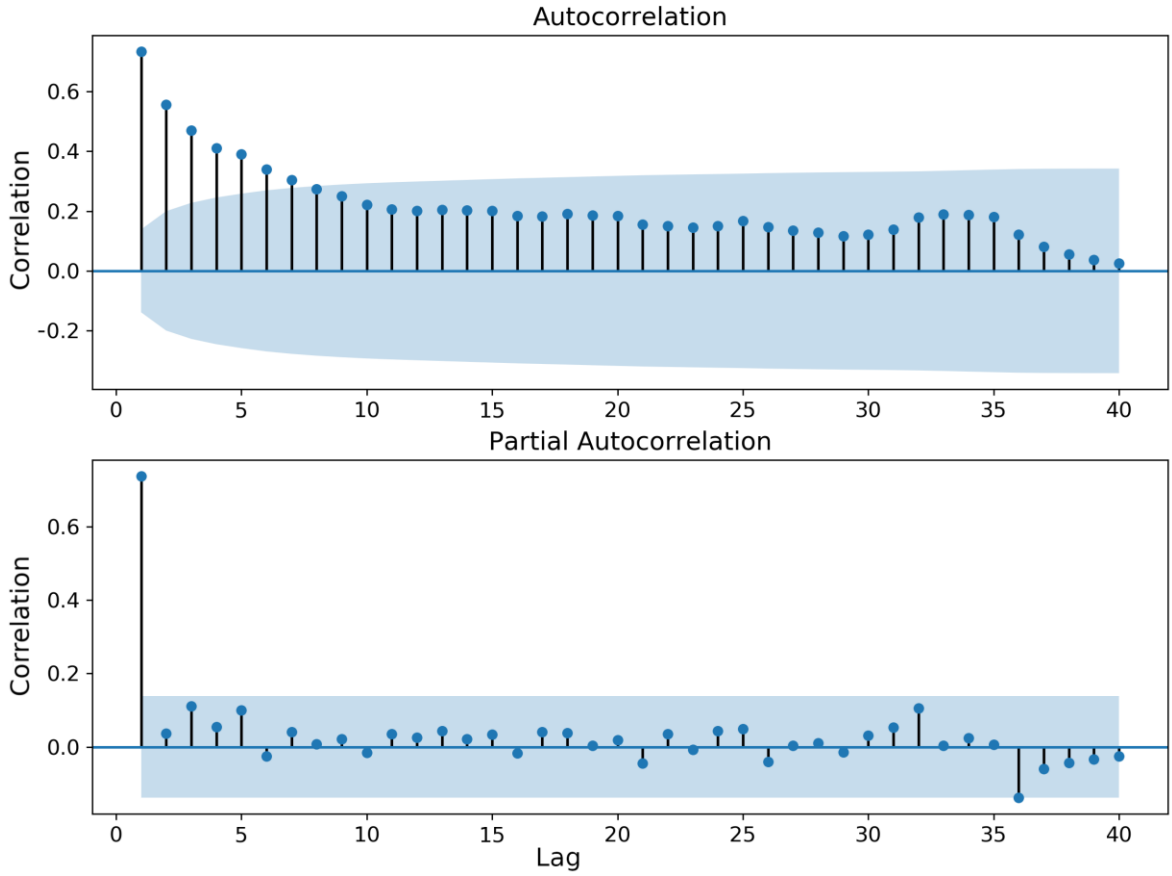

Figure 3-4: Top: Autocorrelation plot (POS_00_04 time series) with 40 days lag period. Bottom: Partial Autocorrelation plot with 40 days lag period.

A Gaussian-like distribution of the time series values can be seen in the histogram in Figure 3-5. The mean value is around 20 and some outliers are present towards larger values with the notable outlier of the 27th January 2018 with a value of 70.

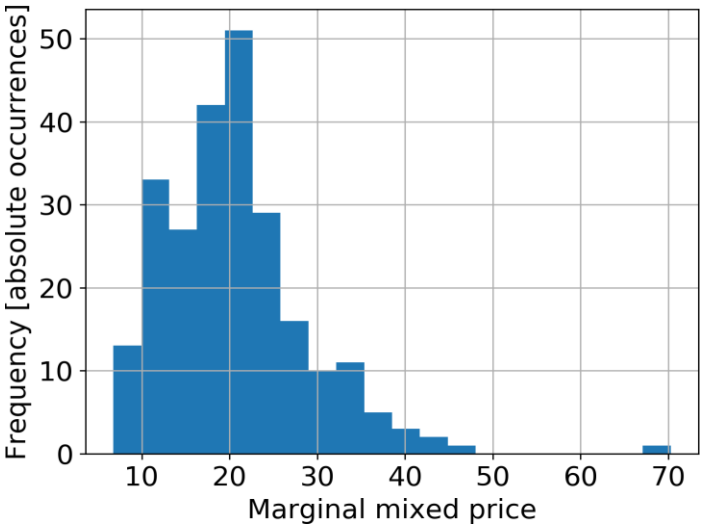

Figure 3-5: Histogram of the marginal mixed price (POS_00_04) time series

Many statistical prediction methods and available tools require the time series to be stationary. In a stationary time series the statistical properties such as mean, variance, autocorrelation, etc. are all constant over time [79]. A time series with a seasonality or trend component is not stationary, whereas a cyclic behavior by itself is stationary [79]. Since the time series under consideration has a trend, it is not stationary. Two common methodologies are used in literature to remove the trend component [83]. In the first approach, a usually low complexity model (linear or polynomial regression) is fitted to the trend component. The fitted model (function) is then subtracted from the time series (additive trend). In the second approach, the time series is detrended by applying a difference transformation. A linear trend can be removed by the first difference that subtracts the value of the series one-time lag before the current time period from the time series. If the series comprises a higher order trend, differencing must be applied multiple times. Figure 3-6 shows the first difference of the time series.

A time-series for which the variance is not constant over time is called heteroscedastic. To apply statistical models requiring stationarity (and therefore homoscedasticity) to such time-series, three common methods exist. First seasonal differencing could be applied if the time-series exhibits seasonality. Seasonal differencing subtracts the realization of the time series lagged by the periodicity from the current realization. The second method stabilizes the variance by applying power transformations to the time series such as the logarithm or Box-Cox transformations [85]. Thirdly, a method called Generalized Autoregressive Conditional Heteroscedasticity (GARCH) is used if the time series has a high volatility (time-

dependence) of variance [86]. GARCH models quantify the variance at a time step by using an autoregressive and a moving average component. Usually GARCH models are coupled with other statistical models such as the SARIMA models (section 3.13.3).

Figure 3-6: Differenced marginal mixed price (POS_00_04) time series

An objective way to determine if a time series is stationary is to use unit root tests, which are based on statistical hypothesis tests. Commonly used unit tests in literature are the augmented Dickey Fuller (ADF) and the Kwiatkowski–Phillips–Schmidt–Shin (KPSS) test [87,88]. Applying the ADF test on the differenced time-series reveals a statistic value of -10.08, which is smaller than the critical value at 5 % of -2.88. This suggests a rejection of the null hypothesis (nonstationarity) with a significance level of 5 % and a corresponding p-value of 1.19e-17. Since the stationarity test of the first difference was successful, no further stationarization transformations (as described above) are required.

3.6 Prediction Intervals

As described in section 3.2, one of the prediction quantities of interest is the marginal mixed price of a particular aFRR product type. Only if a bidder submits a bid lower than the actual marginal mixed price, participation in the product type is guaranteed. A time-series prediction model in its basis form only provides a point forecast for the day of interest. However, without quantifying the associated uncertainty, the point forecast is only of little value for a bidding strategy. A point forecast by itself does not state the range in which the real value is expected with a prescribed probability [89]. This section describes a methodology of how prediction intervals can be obtained. Wide prediction intervals are an

indication of presence of a high level of uncertainty in the underlying prediction model. Section 3.7 derives the acceptance probability for an aFRR product and day with respect to the mixed price value and the prediction interval.

By definition, an interval within which the true value is expected with a specified probability is called a prediction interval [79,89]. For example, if the forecast errors are normally distributed with a standard deviation of σ_{fe}, a prediction interval for a one-step ahead forecast is given by equation (4):

$$I_{\mathrm{P}} = \hat{\mathrm{y}}_{\mathrm{t+1}} \pm c \cdot \sigma_{\mathrm{fe}}, \tag{4}$$

where $\hat{\mathrm{y}}_{\mathrm{t+1}}$ represents the point forecast and c denotes the coverage probability (critical value from the Gaussian distribution). This thesis uses conventional 95 % prediction intervals with a corresponding $c = 1.96$ [90].

For prediction models without any estimated parameters, like the naïve model (subsection 3.13.1), the standard deviation of the forecast distribution σ_{fe} is identical to the standard deviation of the residuals σ_{re} [79]. This also applies to one-step forecasts of (S)ARIMA models (subsection 3.13.3) regardless of the parameters and orders [79]. More complex models involving multiple parameters to be estimated usually have a higher standard deviation of the forecast distribution than the residual standard deviation [91].

Prediction intervals quantify the uncertainty for a single specific point forecast. This sets them apart from confidence intervals which instead quantify the uncertainty in a population parameter such as a mean or standard deviation [92,93]. Confidence intervals are used to quantify the uncertainty of the estimated overall model performance. A mathematical description based on [93,94] is given as follows:

The time series under consideration consists of n data pairs $\{\overrightarrow{x_t}, y_t\}$, with y_t denoting the time series' actual values at step t and $\overrightarrow{x_t}$ denoting the input feature vector as described in section 3.3 including lagged values of y_t (auto regression). In this approach, target values y_t are assumed to be constructed by a target function $\mathrm{y}(\overrightarrow{x_t})$ given by equation (5):

$$y_t = \mathrm{y}(\overrightarrow{x_t}) = f(\overrightarrow{x_t}) + \xi(\overrightarrow{x_t}) \tag{5}$$

The target function $\mathrm{y}(\overrightarrow{x_t})$ is a theoretical construct that accurately maps a feature vector $\overrightarrow{x_t}$ to an observed value of the time series (y_t). In most cases, such as with the time series considered in this work, $\mathrm{y}(\overrightarrow{x_t})$ is unknown and cannot be mathematically derived. Nevertheless, it serves as a reference for prediction models. The target function consists of a deterministic component $f(\overrightarrow{x_t})$, denoted as the true regression function, and a (white) noise component $\xi(\overrightarrow{x_t})$ with zero mean.

The output of a trained prediction model, such as a neural network, is denoted by $g(\overrightarrow{x_t})$ and is referred to as hypothesis function. The hypothesis function is an estimate of $f(\overrightarrow{x_t})$. Confidence intervals, given by equation (6), quantify the model accuracy with respect to the true regression function:

$$I_{\mathrm{C}} = f(\overrightarrow{x_t}) - g(\overrightarrow{x_t}) \tag{6}$$

Prediction intervals on the other hand quantify the model accuracy with respect to the observed output. Prediction intervals are obtained by equation (7):

$$I_{\mathrm{P}} = \mathrm{y}(\overrightarrow{x_t}) - g(\overrightarrow{x_t}) = \left(f(\overrightarrow{x_t}) - g(\overrightarrow{x_t})\right) + \xi(\overrightarrow{x_t}) \tag{7}$$

Equation (7) shows that prediction intervals enclose the corresponding confidence intervals, thus are always wider [95].

Prediction intervals (one- and multi-step) can be mathematically derived for well-defined stochastic models such as the persistence models (subsection 3.13.1, [79]), exponential smoothing models (subsection 3.13.2, [96]) or (S)ARIMA models (subsection 3.13.3, [97,98]). Common model implementations such as in R [99,100] or Python (statsmodels library [101]) natively provide the calculation of prediction intervals.

In case of complex nonlinear models, such as artificial neural networks, it is a lot more challenging to create prediction intervals. In this case, the forecast errors are likely to be not normally distributed. Specialized techniques such as Bayesian [102,103], Delta [104,105], bootstrap [93,106–108] or mean-variance [109] estimation have been suggested in literature and applied in various fields [110,111]. The paper [112] evaluates the performance of aforementioned techniques with regard to the quality, repeatability, variability to uncertainty and computational effort within the scope of 12 real-world case studies. In conclusion, no technique outperforms the others in all regards.

This thesis uses the widely used and versatile bootstrap technique introduced by [106], since it can be used for all model types, calculation of confidence intervals, deriving prediction intervals and ensemble learning techniques [95,113–115]. The fundamental operating principle presented in the following is largely based on [93,94]. Originally, the bootstrap technique is applied to regression problems rather than to time series predictions. As opposed to regression problems, time series data additionally has interdependencies between consecutive data points. A data point depends on previous time series realizations. Almost all prediction model types make use of data points in the past to predict the future. The technique presented in the following allows usage of timely dependent data:

From the *n* input data pairs $\{\overrightarrow{x_t}, y_t\}$, the technique randomly samples *n* data pairs with replacement. This allows a given data pair to be included in the sample more than once. All pairs included in the sample make up the training set; all pairs left out make up the validation set. For large data sets n, the probability of an input pair becoming part of the validation set is $\left(1-\frac{1}{n}\right)^n \approx \frac{1}{e} \approx 0.37$ [93]. Even though it is not required to take a sample size *n* equal to the number of input data pairs, in machine learning applications, this is a very common approach [75]. After the creation of a random data set, the model under consideration, such as a neural network, is trained on the data set.

The process described above (random sampling and model training) is repeated n_{run}times with the same model (same hyperparameters). Considering all model realizations, a mean model estimate $\mathrm{m}(\overrightarrow{x_t})$ can be obtained from equation (8):

$$\mathrm{m}(\overrightarrow{x_t}) = \frac{1}{n_{run}} \cdot \sum_{k=1}^{n_{\mathrm{run}}} g_k(\overrightarrow{x_t}) \ , \tag{8}$$

where $g_k(\overrightarrow{x_t})$ describes the model output of the *k*-th model. Under the assumption that the ensemble of n_{run}networks provides an unbiased estimate of $f(\overrightarrow{x_t})$, the variance of $g_k(\overrightarrow{x_t})$ with respect to $f(\overrightarrow{x_t})$ is given by equation (9):

$$\sigma_c^2(\overrightarrow{x_t}) = \frac{1}{n_{\mathrm{run}} - 1} \cdot \sum_{k=1}^{n_{\mathrm{run}}} (g_k(\overrightarrow{x_t}) - \mathrm{m}(\overrightarrow{x_t}))^2 \tag{9}$$

The confidence interval, which quantifies how well the true regression function $f(\overrightarrow{x_t})$ can be approximated, is given by equation (10):

$$\mathrm{m}(\overrightarrow{x_t}) - c_c \cdot \ \sigma_c \ (\overrightarrow{x_t}) \leq f(\overrightarrow{x_t}) \leq \mathrm{m}(\overrightarrow{x_t}) + c_c \cdot \ \sigma_c \ (\overrightarrow{x_t}) \tag{10}$$

Where c_c denotes the critical value of the Student's t-distribution with a specified coverage probability (see above) and n_{run} degrees of freedom. The Student's t-distribution is a continuous probability distribution used when the population standard deviation is unknown and the sample size is small.

The next step is to derive prediction intervals that also account for the noise inherent to the real target values (equation (7)). If we assume the noise $\xi(\overrightarrow{x_t})$ to be approximately Gaussian, the variance σ_p^2 of the prediction with regard to the target values is given by equation (11):

$$\begin{aligned} \sigma_p^2(\overrightarrow{x_t}) &= var\big(\mathrm{y}(\overrightarrow{x_t}), \mathrm{m}(\overrightarrow{x_t})\big)^2 = var\big(f(\overrightarrow{x_t}), m(\overrightarrow{x_t})\big)^2 + var\big(\xi(\overrightarrow{x_t})\big)^2 \\ &= \sigma_c^2(\overrightarrow{x_t}) + \chi^2(\overrightarrow{x_t}) \end{aligned} \tag{11}$$

Where $\chi^2(\overrightarrow{x_t})$ denotes a model that must be fit to the remaining residuals $r^2(\overrightarrow{x_t})$ given by equation (12):

$$r^2(\overrightarrow{x_t}) = \max(\left(y_t - m_{\text{valid}}(\overrightarrow{x_t})\right)^2 - \sigma_c^2(\overrightarrow{x_t}), 0) \tag{12}$$

Equation (12) introduces $m_{\text{valid}}(\overrightarrow{x_t})$, which denotes a mean model estimate similar to $\text{m}(\overrightarrow{x_t})$ described by equation (8). The difference is that $m_{\text{valid}}(\overrightarrow{x_t})$ is only based on data pairs $\{\overrightarrow{x_t}, y_t\}$ that are part of the bootstrap validation set. As stated above, each data pair is part of the validation set in around 37 % of the n_{run} model evaluations. In comparison, $\text{m}(\overrightarrow{x_t})$ is based on data pairs used for model training, thus giving a biased view on the mean. Equation (3) states the definition for $m_{\text{valid}}(\overrightarrow{x_t})$, where $q_k(\overrightarrow{x_t}) = 1$ if $\overrightarrow{x_t}$ is in the validation set of model *k* and $q_k(\overrightarrow{x_t}) = 0$ otherwise.

$$m_{\text{valid}}(\overrightarrow{x_t}) = \left(\sum_{k=1}^{n_{\text{run}}} q_k(\overrightarrow{x_t}) \cdot g_k(\overrightarrow{x_t})\right) / \left(\sum_{k=1}^{n_{\text{run}}} q_k(\overrightarrow{x_t})\right) \tag{13}$$

As described above, each model realization g_k in the bootstrap process has a different and randomly selected validation set. The residual model $\chi^2(\overrightarrow{x_t})$ is trained only on validation set data of the n_{run} model evaluations, thus generating an almost unbiased estimate. This data selection method is beneficial because no extra test set must be set aside and the training data is not used, as this would underestimate the error.

A minus log-likelihood loss function for training the residual model is suggested by [93] and given by equation (14):

$$\text{L} = -\sum_{t=0}^{n-1} \log\left(\frac{1}{\sqrt{2\pi\chi^2(\overrightarrow{x_t})}} \cdot e^{\left(-\frac{r^2(\overrightarrow{x_t})}{2\chi^2(\overrightarrow{x_t})}\right)}\right) \tag{14}$$

After having determined $\chi^2(\overrightarrow{x_t})$, the prediction interval can be stated as follows (equation (15)):

$$\text{m}(\overrightarrow{x_t}) - c_p \cdot \sigma_p\ (\overrightarrow{x_t}) \leq f(\overrightarrow{x_t}) \leq \text{m}(\overrightarrow{x_t}) + c_p \cdot \sigma_p\ (\overrightarrow{x_t}) \tag{15}$$

As with the confidence interval, c_p denotes the critical value of the Student's t-distribution.

The number of bootstrap runs n_{run} influences both the computational complexity as well as the prediction interval accuracy. A simple test procedure is introduced in [116] that obtains n_{run} for a predefined significance level. Other literature suggests that the number of needed repetitions depends on the population parameter to be estimated, i.e. the number of bootstrap runs for estimating the variance is usually higher than for estimating the mean [117,118].

The bootstrap procedure as described in this section can be applied to obtain mean model point forecasts (equation (8)) and prediction intervals (equation (15)) for both one-step and multi-step forecasts. Since participation in the aFRR auction process only requires information for the next day, this thesis focuses on one-step forecasts. Multi-step forecasts were analyzed in literature and applied in various fields [119–121] including electricity price/ consumption forecasting [122,123].

3.7 Acceptance Probability

Following on the derivation of prediction intervals in section 3.6, this section derives the acceptance probability of a submitted bid tuple. Every participation of a prequalified unit in the aFRR auction process involves the use of a bidding strategy that is based on a programmatic approach, a judgmental technique or a combination thereof. Independent of the particular technique in use, the bidding strategy generates a bid tuple for each day and aFRR product type of interest. The bidding strategy's choice of capacity and energy price for a particular product type determines the mixed price on which the success in the auction depends upon. Qualitatively, a lower mixed price results in a higher auction acceptance (success) probability than a higher mixed price. Based on the point forecasts of the prediction models presented in section 3.13 and the bootstrap technique explained in section 3.6, this section quantitatively derives the acceptance probability for every possible choice of the mixed price. A bidding strategy can use this information to optimize the choice of capacity and energy prices.

Equation (8) states the mean point forecast $\mathrm{m}(\overrightarrow{x_t})$ of a series of n_{run} bootstrapped model evaluations. In the field of marginal mixed price predictions for the aFRR market, $\mathrm{m}(\overrightarrow{x_t})$ states the most likely occurring value. Equation (11) quantifies the variance $\sigma_p^2(\overrightarrow{x_t})$ of the forecast with regard to the unknown target value. The n_{run} bootstrapped model evaluations are assumed to follow a Student's t-distribution. For a sufficient number of model evaluations n_{run}, the Student's t-distribution closely approaches the normal distribution [124]. Since for this thesis, n_{run} >100, the true distribution function is approximated Gaussian. Figure 3-7 graphically illustrates the approximated Gaussian distribution function of the point forecasts.

If a bidding strategy were to choose $\mathrm{m}(\overrightarrow{x_t})$ as the mixed price, the acceptance probability would be 50%. Latter hypothesis is encouraged by $\mathrm{m}(\overrightarrow{x_t})$ being an estimate (without noise) of the true marginal mixed price and therefore if $\mathrm{m}(\overrightarrow{x_t})$ is slightly off towards lower values, the auction is won. Consequently, if $\mathrm{m}(\overrightarrow{x_t})$ slightly (e.g. infinitesimally) overestimates the true marginal mixed price, the auction is lost. The acceptance probability $\mathrm{P}(B_{\mathrm{MP}})$ of any possible choice of mixed price B_{MP} is given by the Q-function as stated in equation (16):

$$\mathrm{P}(B_{\mathrm{MP}}) = Q\left(\frac{B_{\mathrm{MP}} - \mathrm{m}(\overrightarrow{x_t})}{\sigma_p(\overrightarrow{x_t})}\right) \tag{16}$$

For an underlying Gaussian process, the Q-function states the probability of obtaining a value larger or equal to a random variable (e.g. B_{MP}) [125]. The Q-function is defined by equation (17) and can easily be obtained from the cumulative distribution function of the normal Gaussian distribution ($\mathrm{erf}(x)$).

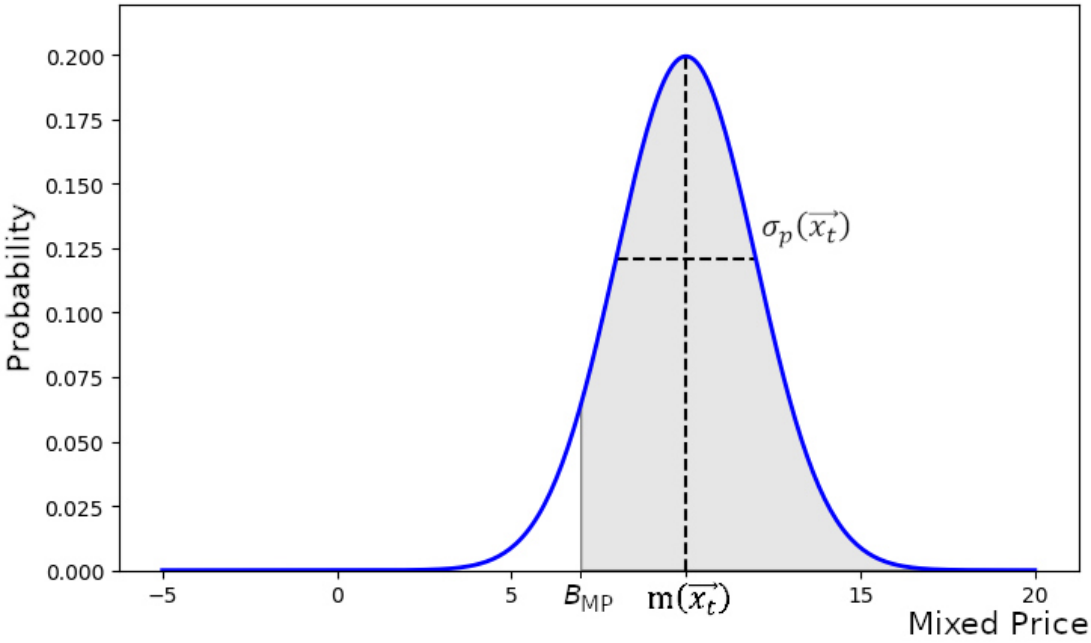

Figure 3-7: Exemplary probability density function for deriving the acceptance probability ($m(\overrightarrow{x_t}) = 10,\ \sigma_p^2(\overrightarrow{x_t}) = 2$)

$$\mathrm{Q(x)} = \frac{1}{\sqrt{2\pi}}\int_x^{\infty} e^{\left(-\frac{u^2}{2}\right)} du = 1 - \mathrm{erf}(x) \tag{17}$$

For a specific mixed price value B_{MP}, the shaded area in Figure 3-7 illustrates the corresponding acceptance probability $\mathrm{P}(B_{\mathrm{MP}})$ calculated by the Q-function.

3.8 Error Measures

The forecast error is defined as the difference between the true value of the time series and its prediction (equation (18)).

$$\mathrm{e_t} = y_t - \hat{y}_t \tag{18}$$

For each of the three data sets (training, validation, test), this thesis calculates the mean absolute error (MAE, equation (19)) and the root mean squared error (RMSE, equation (20)).

$$\mathrm{MAE} = \mathrm{mean}(|\mathrm{e_t}|) = \frac{1}{n} \cdot \sum_{t=1}^{n} |\mathrm{e_t}| \tag{19}$$

$$\mathrm{RMSE} = \sqrt{mean(e_t^2)} = \sqrt{\frac{1}{n} \cdot \sum_{t=1}^{n} e_t^2} \tag{20}$$

Both the MAE and the RMSE are the most widely used error measures in literature, even though there is no 'industry standard' [45]. Other error benchmarks such as percentage errors (e.g. mean absolute percentage error or symmetric mean absolute percentage error) or scaled error might be more suitable for a comparison between different datasets, but are accompanied by other drawbacks [79,126].

Rooted in stock market prediction, 'change direction' is another measure for performance evaluation. For each one-step ahead prediction $\hat{y}_{t+1}$, it is checked if the direction of change is predicted correctly. The quantity states the percentage of correctly predicted direction changes.

3.9 Model Performance Evaluation

This section presents how the performance of the used models (section 3.13) is evaluated and compared with one another. As described in section 3.4, the parameters of each model are fitted by using the training set data. Models with a large number of parameters such as neural networks (subsection 3.13.4) use an optional validation data set to early-stop the learning process to prevent overfitting. A test set, hold aside from any parameter learning or model selection task, is used to measure the performance on an unbiased (out-of-sample) scenario. Figure 3-8 schematizes the division into aforementioned data sets. In this thesis, the training set comprises 70 %, the validation set (if used) 15 % and the test set 15 % of the available data pairs $\{\overrightarrow{x_t}, y_t\}$. For models not prone to overfitting, the validation set data is used as additional training data.

Figure 3-8: Data separation of time-series

Each model used for prediction provides a set of hyperparameters that influences the performance on the data sets. If a model was evaluated on a range of various hyperparameters (section 3.10), the best model may only be selected based on the error measures of the training or validation set. Any peak on the test set would result in an overly optimistic estimate of the model skill [77,127].

3.10 Hyperparameter Optimization

As opposed to model parameters that are fitted during the training process of a model, hyperparameters are specified before the start of the training process. Hyperparameters define the structure of a model, such as the number of neurons per layer in a neural network. The field of hyperparameter optimization deals with obtaining a set of hyperparameters that yields the best model performance. Common to all techniques in literature is the first step, which for each hyperparameter defines the (numerical or textual) range under investigation. The upper and lower limit of a hyperparameter can be limited by model logic, e.g. the degree of differencing for a SARIMA model (subsection 3.13.3) must be a positive integer. Judgmental reasoning (or intuition) of where the best performance is expected is also often applied, e.g. the necessary degree of differencing for a SARIMA model is usually less or equal to two [128]. Equation (21) shows the objective function of hyperparameter optimization:

$$z^* = arg \min_{z \in Z} k(z), \tag{21}$$

where $k(z)$ denotes an objective function to minimize, Z represents all possible hyperparameter realizations, z is one realization of hyperparameters, and z^* is the realization of hyperparameters resulting in the lowest value of $k(z)$. This thesis uses an objective function $k(z)$ based on the model performance evaluation described in section 3.9 in combination with one of the error measures presented in section 3.8. More advanced model evaluation techniques, such as time series cross-validation (section 3.11) or the bootstrap procedure (section 3.6), are possible to use for $k(z)$ but require far more computational effort. In this thesis, the performance accuracy of the less advanced performance evaluation is considered sufficient to find a well performing set of hyperparameters.

Grid-Search is a hyperparameter optimization technique which trains a model on each possible parameter combination [129,130]. If the step size within the hyperparameter range is sufficiently small, the best solution is likely to be found. Since the computational expense grows exponentially with the number of hyperparameters, this thesis uses the Grid-Search approach only for models with a modest number of hyperparameters such as the SARIMA or Exponential Smoothing (subsection 3.13.2) models.

For complex models such as deep neural networks, the training and evaluation process is computationally expensive. This is particularly true for ensemble learning techniques, k-fold cross validation or if the bootstrap procedure (section 3.6) is applied (to obtain $k(z)$). With one set of hyperparameters, latter techniques involve multiple expensive training processes in order to obtain one error metric (section 3.8). Random search is another hyperparameter optimization technique, which evaluates a predefined number of randomly chosen evaluations $k(z)$ [131]. Grid-Search and random search do not exploit information from past evaluations, and as a result, often spend a significant amount of time evaluating less promising hyperparameters [132]. In favor of more efficient techniques, random search is not further considered in this thesis [133]. Hyperparameter optimization has been actively investigated in literature with common approaches using Bayesian optimization, genetic algorithms and various machine learning techniques including neural networks [132,134–136]. This thesis uses a Bayesian approach for tuning the hyperparameters of e.g. neural networks.

In contrast to Grid-search and random search, Bayesian hyperparameter optimization approaches use past evaluations to train a probabilistic model which maps hyperparameters to a probability of a score on the objective function $k(z)$ [137]. The probabilistic model is called a surrogate model of the objective function $k(z)$. Since the surrogate model's complexity is much lower than the complexity of evaluating $k(z)$, the surrogate model is used to find the next set of hyperparameters for evaluating $k(z)$. The optimization process can be described as follows:

1. Creation of a surrogate model for the objective function $k(z)$
2. From the surrogate model, the best performing hyperparameters are derived
3. Hyperparameters of step 2 are evaluated on the objective function $k(z)$
4. Update of the surrogate model with the result of step 3
5. Repetition of steps 2–4 until the specified number of iterations is reached

This methodology puts some computational effort into the selection of hyperparameters in order to save on the number of evaluations of the objective function. In each iteration, the surrogate model is updated to better estimate the true objective function. By using past evaluations, Bayesian methods usually require less evaluations of $k(z)$ to find high performance hyperparameters than e.g. the random search technique [138]. According to [139], Bayesian optimization methods can be differentiated at a high level by their surrogate models and the hyperparameter acquisition methodology. This thesis uses a Tree Parzen Estimators (TPE) surrogate model and "Expected Improvement" for hyperparameter selection, since promising results were achieved in literature [133,137].

3.11 Advanced Model Performance Evaluation

Section 3.9 introduced a model evaluation technique that withholds a section from the end of the time-series to obtain an estimate for the out-of-sample (test) error. Unfortunately, this technique is accompanied by drawbacks as explained in the following:

1. If the number of total data samples $\{\overrightarrow{x_t}, y_t\}$ is small, an allocation of training, validation and test set on a percentage basis might result in very few data samples for the test set. The performance estimate gets unreliable if too few data samples are used for calculation.

2. Since only one model is trained on the available data, there is no indication for whether the performance is consistent and reproducible. A different test set might produce results varying significantly from the test set under consideration. Using a different or a resampled training set could also result in a large variation.

For classification or regression problems, k-fold cross-validation is the most widely used technique in literature to cope with above drawbacks [95,140–142]. The technique divides the data into k sets of equal size. In multiple training processes, each of the k sets is once hold aside for evaluation whereas the remaining sets are used for training. A total of k model evaluations and metrics are generated. Training multiple models on different data sets enables quantifying the variation.

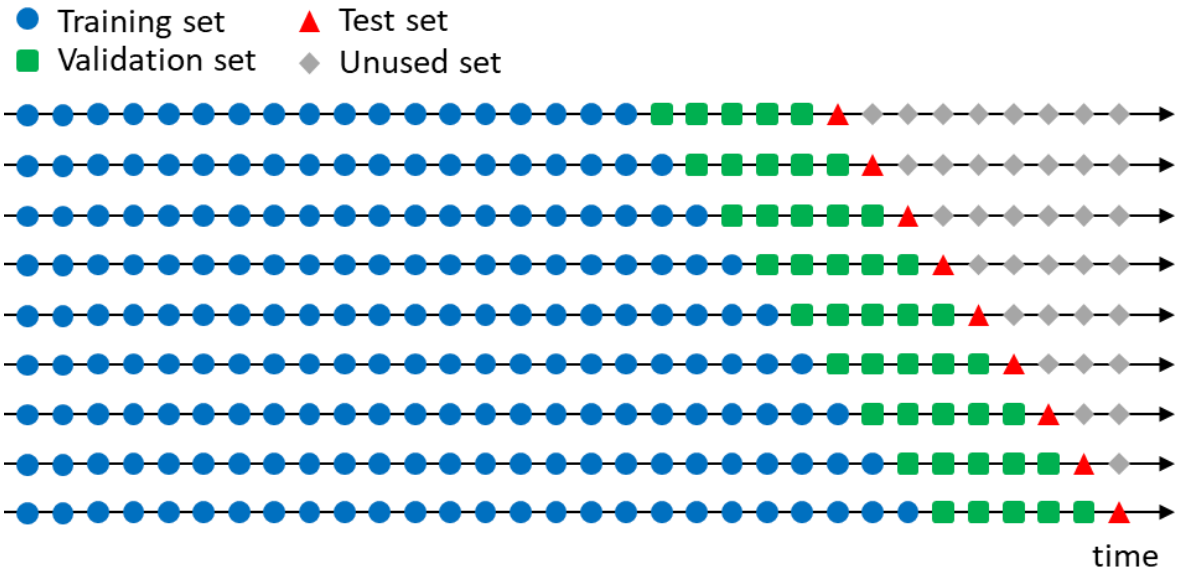

Figure 3-9: Time Series Cross-Validation

Unfortunately, k-fold cross-validation cannot easily be used for time-series predictions, since the samples temporally depend on each other [143]. A model trained on future samples can use this knowledge to better estimate the past. Training a model with future

samples therefore underestimates the error. Only with multiple restrictions, cross-validation can be applied to time-series predictions [144].

Cross-validation can however be adapted to be used for time-series prediction. In this procedure, the test set comprises one data sample and the corresponding training and validation set only comprise samples prior to the test set sample. The validation set has a fixed sample size and temporally follows the training set. Samples following the test sample (future values) are not used. A minimum training sample size must be defined for training the model. The first model is trained on the minimum training sample size and evaluated on the test sample. Each succeeding model uses one additional data sample and shifts all data sets one position forward in time. On each shift, the training set grows in size. The procedure is called walk forward validation and is illustrated in Figure 3-9. Each timeline (row) represents a separate model evaluation.

Models not requiring a validation step for early-stopping the learning process, use the validation set as additional training data. The procedure circumvents the two drawbacks stated at the beginning of the section by generating more evaluation samples on unseen data and by training a multitude of models. On the downside, the computational complexity is multiple times higher than the procedure explained in section 3.9. In comparison to the bootstrap approach, this procedure uses a variable training set size and resamples without replacement (each sample is only considered once).

3.12 Residual Analysis

As stated by equation (18), the residuals of a time series e_t are equal to the difference between the actual observation and the forecast value of a model at time t. Residuals can be used for analyzing how well a model represents the true underlying process of the input time series [79]. An adequate model for a particular time series exhibits the following properties:

1. Uncorrelated residuals
2. Zero mean residuals
3. Constant variance residuals
4. Normally distributed residuals

Exemplary, an ARIMA (10,0,0) model (subsection 3.13.3) was fit on the aFRR POS_00_04 time series. Figure 3-10 presents multiple plots, which guide through the residual analysis process. All plots are based on the standardized residual time series as defined by equation (22) and illustrated by the upper left plot in Figure 3-10:

$$e_{t\_std} = \frac{e_t}{\sqrt{var(e_t)}} \tag{22}$$

If the residuals are correlated, not all information is fully captured and the performance of the corresponding model can be improved. An ACF plot at the bottom right of Figure 3-10 shows the autocorrelation of the residuals r_k with multiple time lags k. In this particular example, the spikes indicate white noise since none is above the significance level illustrated

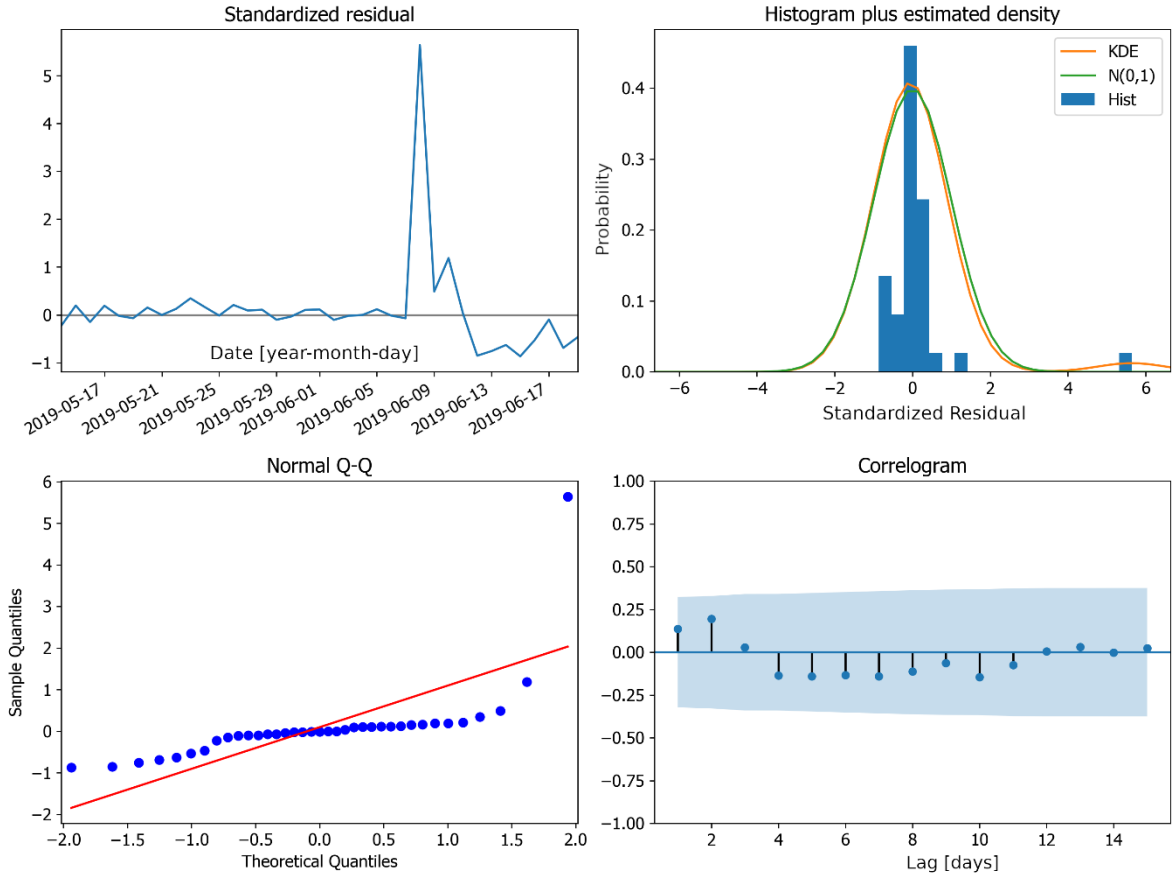

Figure 3-10: Residual plot. Upper left: standardized residual time series plot. Upper right: Histogram of standardized residuals, KDE distribution (orange) and standard normal distribution (green) for comparison. Bottom left: Q-Q-plot of standardized residuals and standard normal distribution. Bottom right: ACF plot of standardized residuals.

by the blue shaded area (section 3.5). If at least one of the r_k (autocorrelation for lag k) was above the significance level, a portmanteau test should be carried out to check if the residuals could still be white noise [79]. A portmanteau test checks whether a group of multiple r_k is significantly different from a white noise process. Latter group test is necessary since considering each r_k separately implicitly carries out multiple hypothesis tests, each one with a small probability of giving a false positive. For multiple such hypothesis tests, the probability of getting at least one false positive is high. A commonly

used portmanteau test for checking a group of r_k is the Ljung-Box test defined by equation (23) [145]:

$$\mathrm{Q} = \mathrm{n} \cdot (\mathrm{n}+1) \cdot \sum_{k=1}^{h} \frac{r_k^2}{n-k}, \tag{23}$$

where h denotes the maximum lag and n the sample size. Small values of Q indicate white noise.

Non-zero mean residuals indicate a model bias that can be resolved by adding a constant to the model. A model not fulfilling any of the first two properties can in general be improved. However, if both properties hold true, a model might still by improved [79].

It is beneficial for fitted models to have normally distributes residuals with constant variance. For example, prediction intervals statistically derived from the exponential smoothing (subsection 3.13.2) and SARIMA (subsection 3.13.3) models require the residuals to exhibit these properties. A model not fulfilling any of the last two properties might still perform well on predictions and cannot necessarily be improved. The histogram in the upper right corner of Figure 3-10 shows a discrete estimate of the probability density function (PDF) with a predefined bin size (blue bars). Two problems arise with histogram plots as firstly the PDF estimate is not smooth and secondly inaccuracies result from the fixed bin size [146]. The orange graph illustrates a continuous estimate of the PDF created by a kernel density estimation (KDE). In contrast to the histogram, KDE is a statistical and non-parametric methodology which centers a continuous kernel function at each data point [147,148]. All kernel functions are then superimposed to generate a continuous PDF based on a finite data sample, thus overcoming the drawbacks of a fixed bin size histogram. Equation (3) states the estimated density function $\mathrm{KDE_t}$ at time step t, with n denoting the total number of samples, K the kernel function, h the bandwidth of the kernel function and e_j the residual at time step j:

$$\mathrm{KDE_t} = \frac{1}{n} \cdot \sum_{j=0}^{n-1} K\left(\frac{e_t - e_j}{h}\right) \tag{24}$$

Various kernel functions $K(u)$ have been considered in literature. Gaussian kernels, as stated by equation (3), are most often used and applied in this thesis.

$$K(u) = \frac{1}{\sqrt{2\pi}} \cdot e^{-\frac{1}{2}u^2} \tag{25}$$

The shape of the estimated PDF depends on both the type of kernel function $K(u)$ and the bandwidth parameter h. A too small value of h results in an “undersmoothed“ PDF with

usually many spikes whereas a too large value of h results in an "oversmoothed" PDF obscuring the underlying structure. Automatic bandwidth selection methods for finding the optimal value of h have been developed and compared with one another in literature [149–153]. Plug-in selectors and cross validation selectors are usually considered to perform best over a wide range of data sets [154,155]. This thesis uses a cross validation approach based on maximum likelihood. Both the histogram and the KDE graphs can be compared to the standard normal distribution illustrated by the green graph.

Another approach for indicating the level of similarity between the residuals and a normal distribution is the quantile-quantile (Q-Q) plot depicted in the bottom left plot of Figure 3-10. A Q-Q plot compares two distributions by plotting the corresponding quantile values against each other [156]. This thesis computes a common statistical diagnostic plot that compares the distribution of the residuals to a standard normal distribution. The plot is created by first sorting the residuals in ascending order and then assigning a quantile to each residual. Each value of the standardized residual (y-axis) is then plotted against the corresponding quantile value of the standard normal distribution (x-axis). If the scatter plot closely follows the red diagonal line, the residual distribution can be considered normal. Latter does not apply to the exemplary residuals constituting Figure 3-10.

Prediction intervals statistically derived from SARIMA models are based on the assumption of uncorrelated and normally distributed residuals [79]. If the latter two properties are not present (as it is the case with above residuals), prediction intervals may be incorrect.

3.13 Prediction Models

Time-series prediction is a rather old research field in which multiple models have been developed, applied and statistically verified over time [157,158]. Up until now, no model or technique exists which outperforms all others at every discipline. It is necessary to apply multiple models on the time-series under consideration to find the best performing one. This section presents the various models, which are compared with one another.

Subsection 3.13.1 introduces the naïve persistence model that serves as an indication for whether a more complex model is worth considering. Exponential Smoothing, as presented in subsection 3.13.2, is a rather old prediction model which has motivated very successful forecasting methods [79]. One of the most popular and nowadays still frequently used stochastic time series models is the Seasonal Autoregressive Integrated Moving Average (SARIMA) model as described in subsection 3.13.3. With the cost-effective availability of computing resources, Neural Networks, as described in subsection 3.13.4, have recently received great attention [159]. A variant of neural networks, which is designed to better deal with sequentially dependent data, such as time series, is described in subsection 3.13.5 (Recurrent Neural Networks).

3.13.1 Persistence Model

For multiple different model types, this thesis quantitatively evaluates the performance of each model by applying the error measures presented in section 3.8 on the test set data. A low absolute error measure value is usually an indication for a well-performing model. A further method for classifying a model's performance is the comparison with a very simple model. The difference of the error measures between the simple model and the model under investigation quantifies the accuracy gain. In that sense, the simple model serves as benchmark [79] or persistence test. It reveals, if a complex and parameter-rich model justifies the additional effort and computational resources.

The persistence test applied in this thesis uses the naïve model, which is defined by equation (26):

$$\hat{y}_{t+1} = y_t \tag{26}$$

The observation of the previous time step y_t is used as the prediction for the next time step $\hat{y}_{t+1}$.

Other persistence models such as the seasonal naïve method, the average method or the drift method are sometimes used in literature but are not considered in this thesis [79].

3.13.2 Exponential Smoothing

Exponential smoothing is a time-series prediction model for which literature dates back to the 1950s at a time the model was extensively used in business and industry [157,160–162]. Simple exponential smoothing (SES) is the most basic model, suitable for time-series without a trend or seasonal component. Equation (27) describes the model:

$$\hat{y}_{t+1} = \alpha \cdot y_t + \alpha \cdot (1-\alpha) y_{t-1} + \alpha(1-\alpha)^2 y_{t-2} + \cdots \tag{27}$$

A prediction for the next time step $\hat{y}_{t+1}$ is additively generated from weighted past observations ($y_t, y_{t-1}, y_{t-2}, \cdots$), where the weights decrease exponentially depending on the parameter $\alpha \in (0, 1)$. The more recent the observation, the higher the associated weight [79].

Following the introduction of the SES model, the technique was step-wise extended to allow a trend coverage (additive [160] and multiplicative [163]), an associated trend "dampening" parameter [164], and a seasonal component (additive and multiplicative) [160,162]. A very common model with an additive trend and seasonal component for a one-step forecast is described as follows:

$$\hat{y}_{t+1} = l_t + b_t + s_{t+1-m} \tag{28}$$

$$\mathrm{l_t} = \alpha \cdot (y_t - s_{t-m}) + (1-\alpha) \cdot (l_{t-1} + b_{t-1}) \tag{29}$$

$$\mathrm{b_t} = \beta \cdot (\mathrm{l_t} - l_{t-1}) + (1-\beta) \cdot b_{t-1} \tag{30}$$

$$\mathrm{s_t} = \gamma(\mathrm{y_t} - l_{t-1} - b_{t-1}) + (1-\gamma) \cdot s_{t-m} \tag{31}$$

Equation (28) represents the overall forecast equation, equations (29) - (31) denote three smoothing components, one for the level $\mathrm{l_t}$, one for the trend $\mathrm{b_t}$ and one for the seasonality $\mathrm{s_t}$ [79]. Each of the three components has a corresponding smoothing parameter denoted α for $\mathrm{l_t}$, β for $\mathrm{b_t}$ and γ for $\mathrm{s_t}$. Depending on the sample rate, m denotes the frequency of the seasonality (e.g. $m = 12$ for a yearly seasonality and a monthly data resolution). The seasonal component $\mathrm{s_t}$ is a weighted average between the observation $(\mathrm{y_t} - l_{t-1} - b_{t-1})$ at time t and the same observation lagged by one season (m time steps). An estimated trend at time t is obtained by $\mathrm{l_t} - l_{t-1}$. Subtracting the estimated trend at time t from the previous estimate of the trend at $t-1$ results in the trend component $\mathrm{b_t}$. The level equation $\mathrm{l_t}$ is a weighted average between the seasonally adjusted observation $(y_t - s_{t-m})$ and the non-seasonal prediction $(l_{t-1} + b_{t-1})$.

Despite their age, Exponential smoothing models like the one described above are even today successfully employed in various fields [165–167] including electricity price/load forecasting [168–171]. One reason for the success in the past two decades is the introduction of statistical models which aside from point forecasts are also capable of generating prediction intervals [96,172,173].

3.13.3 Seasonal Autoregressive Integrating Moving Average

One of the most popular and widely used approaches for time series forecasting is the Autoregressive Integrated Moving Average (ARIMA) model [97,158]. The model is suitable for time series that are not necessarily stationary and where future values depend on both past observations and past forecast errors. If required, the model can be extended to deal with seasonal dependencies in the time series data (SARIMA). In comparison to exponential smoothing models (subsection 3.13.2), SARIMA models are based on autocorrelations properties of the time series, whereas exponential smoothing models are based on a description of the trend and seasonality in the data [79]. Either as a standalone model or in conjunction with other approaches, SARIMA models are used in various fields [174–176] including electricity price/load forecasting [123,177,178]. SARIMA models consist of various components, which are described in the following:

Autoregressive component

A purely autoregressive model computes the forecast as a linear combination of past observations of the time series [79]. Equation (32) states the definition of an autoregressive model of order p:

$$\hat{y}_{t+1} = c_a + \varphi_1 \cdot y_t + \varphi_2 \cdot y_{t-1} + \cdots + \varphi_p \cdot y_{t-p+1} \quad (32)$$

The predictors y_t are lagged values of the time series weighted by the parameters φ_i. Superimposed by noise, $\hat{y}_{t+1}$ is a one-step prediction of the true future value y_{t+1}. Autoregressive models are best applied on stationary data. The AR component of the SARIMA model is an autoregressive model of order p applied on the differenced time series.

Differencing

In statistics, differencing refers to a transformation applied to time series that is supposed to make it stationary. As described in section 3.5, the statistical properties of a stationary time series are independent of the time. Mathematically, differencing computes the difference between two consecutive time steps (equation (33)) of the series:

$$y'_t = y_t - y_{t-1} \quad (33)$$

To obtain a stationary time series, it may be necessary to difference the data multiple times. Since the SARIMA model requires stationary time series, it is necessary to carry out successive differencing until the requirement is met [179]. As a side effect, the higher the order of differencing, the more the prediction intervals increase in size [79]. The capital I in the SARIMA model stands for “integrated” because the original time series can be recovered by a repeated summation process.

Moving average component

A moving average (MA) model is a linear regression model which uses past forecast errors as predictors [79]. Forecast errors at time step t are denoted ε_t. Past forecast errors up until q time steps back (model order) are weighted with the parameters σ_i. Equation (34) formulates the model:

$$\hat{y}_{t+1} = c_m + \sigma_1 \cdot \varepsilon_t + \sigma_2 \cdot \varepsilon_{t-1} + \cdots + \sigma_q \cdot \varepsilon_{t-q+1} \quad (34)$$

Non-seasonal ARIMA model

Combining autoregression with differencing and a moving average model results in the non-seasonal ARIMA model. A model description is stated by equation (35):

$$\hat{y}'_{t+1} = c_n + \varphi_1 \cdot y'_t + \varphi_2 \cdot y'_{t-1} + \cdots + \varphi_p \cdot y'_{t-p+1} + \quad (35)$$

$$\sigma_1 \cdot \varepsilon_t + \sigma_2 \cdot \varepsilon_{t-1} + \cdots + \sigma_q \cdot \varepsilon_{t-q+1},$$

where $\hat{y}'_{t+1}$ denotes the one-step ahead prediction on the differenced time series. Depending on the time series, the differencing might have been applied multiple times (d=degree of differencing). The first predictors are similar to the autoregressive model with

order p. Latter predictors represent the moving average component of order q. A full model description is given by the notation ARIMA(p,d,q).

Seasonal ARIMA model

The ARIMA model can be extended with additional predictors to the regression to deal with seasonal time series. However, as with the non-seasonal case, the first step is to generate a stationary time-series. Depending on the time series, seasonal differencing must by applied:

$$y'_t = y_t - y_{t-m} \tag{36}$$

Equation (29) differences the observation at time step t and the corresponding observation at the previous season m time steps before. The seasonal component then adds predictors to the regression similar to those of the non-seasonal components but m time steps shifted backwards. A full model can then be denoted by SARIMA $(p,d,q)\ (P,D,Q)_m$, where the lower case letters denote specified non-seasonal hyperparameters and the upper case letter the seasonal counterparts [79].

Model selection

By visually analyzing the time series plot, it is not possible to derive the hyperparameter set which yields the best forecast performance. Figure 3-11 illustrates a common multi-step process for SARIMA order selection. At first, a Box-Cox transformation is applied if the variance of the time series is not constant over time [85]. Aforementioned hyperparameters can then be selected either automatically or manually.

Common automatic selection processes are either based on algorithms provided by the used library or by a grid-search approach. The programming language R for instance uses a variation of the Hyndman-Khandakar algorithm, which combines unit root tests, minimization of the AICc (see below) and maximum likelihood estimates (MLE) [180]. Since algorithmic approaches do not always find the best hyperparameter set and computational power has become cheap, the grid-search approach tries all possible parameter combinations within specified boundaries to find the best performing model.

Manual hyperparameter selection is carried out by first successively differencing the time series until a unit root test (see section 3.5) assures stationarity [87,88]. Appropriate orders of p, q, P and Q are then selected using autocorrelation (ACF) and partial autocorrelation (PACF) plots as illustrated in Figure 3-4.

Various candidate models are than compared with one another using Akaike information criterion for small sample sizes (AICc) [181]. AICc provides a mean for model selection as it quantifies how well a model fits the underlying time series while taking into account the

model complexity (number of parameters) [182]. Special care must be taken since AICc values of models with a different degree of differencing are not comparable [180].

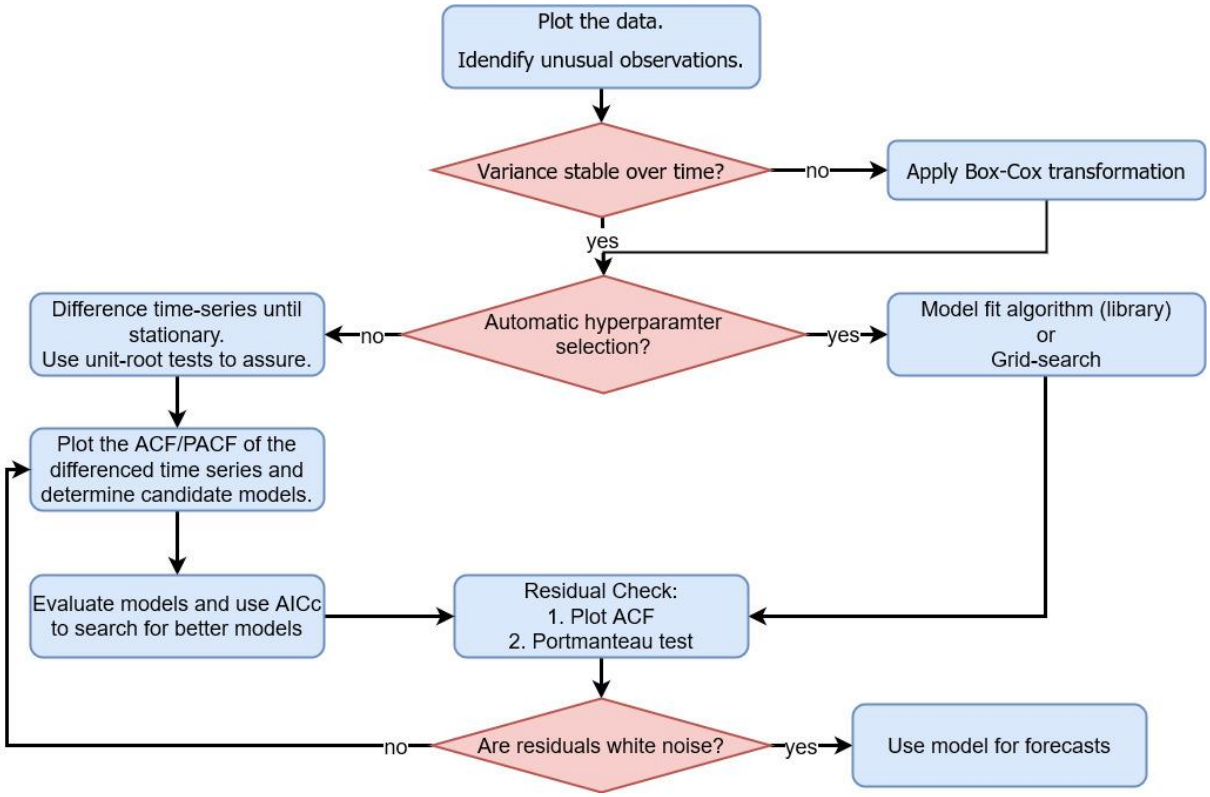

Figure 3-11: Hyperparameter selection process (Box and Jenkins approach) based on [79]

After the selection of a candidate model, the corresponding residuals must be checked for being uncorrelated, having zero mean, constant variance and follow a normal distribution. A more detailed residual check procedure including a Portmanteau test is described in section 3.12. If the residual conditions do not apply, different candidate models should be evaluated.

Prediction intervals

Common SARIMA model implementations provide a means to automatically calculate prediction intervals, without the necessity of applying complex procedures (e.g. bootstrap) as described in section 3.6. The calculations are usually based on the residual assumptions stated above [79]. If either of the assumptions is not fulfilled, the result will be incorrect.

Having obtained the standard deviation of the residuals σ_{re}, one-step ahead prediction intervals can be calculated with equation (4), substituting σ_{re} for σ_{fe}. Multi-step prediction intervals are mathematically complex to derive [97]. Common model implementations provide multi-step prediction intervals.

3.13.4 Neural Network

In recent years, neural networks (NN) have gained tremendous momentum in various fields including image-, speech, handwriting-recognition, sentiment analysis, dialog systems, autonomous driving and time series forecasting among many more [157,183,184]. The technology dates back to 1943, when neurophysiologists first discovered the potential of applying the biologically inspired concept of neural networks to electrical circuits [185]. A key finding from 1989 proclaimed the use of multilayer feedforward networks as "universal approximators" capable of implementing any function including XOR [186]. Though, it was not until around 20 years later that neural networks became successful in various fields. The recent success is due to the availability of huge computational power including GPU processing, availability of large training data sets, improved algorithms and new model structures [183]. In a review of 100 studies of various fields, Paliwal et al. [105] concluded that NN outperform traditional statistical techniques in the majority of cases. A number of papers have reported excellent performance on electricity price forecasting [45].

All forecasting techniques in the previous subsections only use the time series and lagged observations of it (autoregression) as input for the prediction. Neural networks allow the inclusion of additional information like weather data, holidays or stock exchange data as described in section 3.3. Due to their inherent structure, NN can perform well on non-linear and non-stationary time series [159].

As illustrated in Figure 3-12, a neural network consists of an input layer to which all data sources are fed, a predefined number of hidden layers, which is the root of all functional logic, and an output layer, which returns the model estimate.

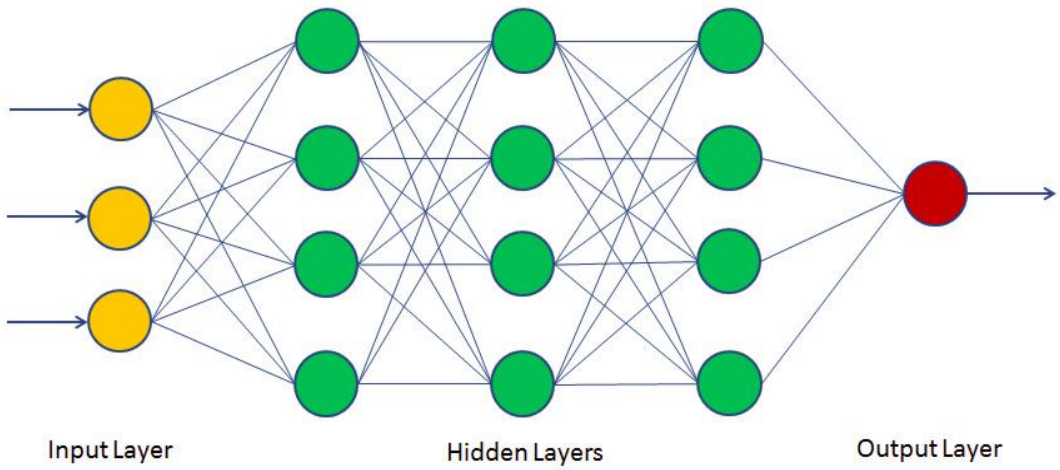

Figure 3-12: Neural network structure [187]

Each layer comprises a predefined number of neurons that are interconnected by trainable weights. In a multilayer feed-forward network, the output of a neuron is a function of the

weighted outputs of neurons from the previous layer. Equation (37) states an expression for the output value of neuron j of layer k:

$$o_{k,j} = \varphi\left(b_{k,j} + \sum_{i=1}^{n_{k-1}} o_{k-1,i} \cdot w_{k-1,i,j}\right), \tag{37}$$

Where φ is an activation function, $b_{k,j}$ is a bias for each neuron (not illustrated in Figure 3-12), $n_{k-1}$is the number of neurons in layer $k-1$, $o_{k-1,i}$ is the output of neuron i in layer $k-1$ and $w_{k-1,i,j}$ is the trainable weight between a neuron from the previous layer $(k-1)$ and the current neuron. If no hidden layers are used and the activation function φ is omitted, the model is equal to a simple regression model, also called single-layer perceptron [45].

As for neural network models, the selection of the number of hidden layers and neurons per layer is not straightforward and strongly depends on the complexity between input and output data [159,188]. Many literature concluded that a small number of hidden layers (≤ 2) is sufficient for a wide range of applications [189]. As for the number of neurons, multiple rule-of-thumb selection methods exist which can be used as a starting point. Underfitting occurs if too few neurons are available for covering the complexity of the data. Overfitting occurs if the neural network is fit too closely to the training data, which results in a large generalization error. This can be due to a too small training data set or due to too high model complexity (e.g. many neurons). In this thesis, hyperparameter optimization (section 3.10) is used to find a good compromise for above parameters.

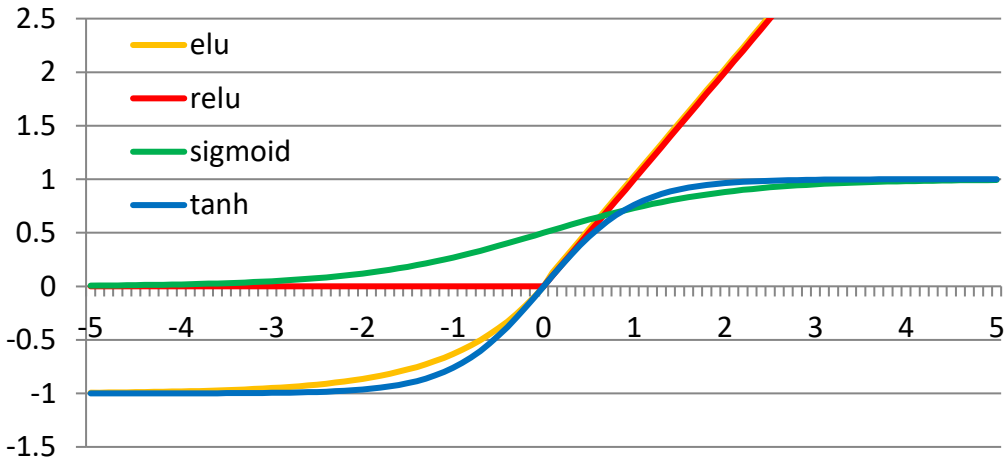

Figure 3-13: Activation functions

If a neural network is constructed without an activation function φ as stated by equation (37), the output results from multiple addition and multiplication operations and thus is not able to model non-linear behavior [183]. Using a non-linear activation function φ solves this

issue. A wide range of various activation functions (> 30) have been investigated in literature over time, each having advantages and drawbacks. Figure 3-13 illustrates a commonly used selection of activation functions.

Up until around 10 years ago the sigmoid (equation(38)) and tanh functions were the mostly used activation functions in neural networks [190]. Both functions however suffer from saturation as they asymptotically converge for small and large input values. During the learning process, errors are back propagated through the network and decrease with each additional layer. This is referred to as the vanishing gradient problem which is caused by saturation (gradients converge to zero) and prevents further model improvement [191]. Another drawback of both functions is the sensitivity to only a small input range around their mid-point. Since the tanh has a wider sensitivity range, the function has often achieved better predictive performance [190].

$$\varphi(x) = \frac{1}{1 + e^{-x}} \tag{38}$$

To overcome the vanishing gradient problem, the rectifier linear unit (ReLU) activation function as stated by equation (39) has been invented [191].

$$\varphi(x) = \max(0, x) \tag{39}$$

It's a piecewise linear function which only saturates towards negative values and requires low computational effort. Most current papers which achieve state-of-the-art performance make use of the ReLU function [190,192,193]. Nevertheless, ReLU has drawbacks in not being zero centered, not being differentiable at zero and vanishing gradients for negative input values (dying ReLU) [194]. Alternatives such as the exponential linear unit (ELU) or LeakyReLU have been suggested by literature to overcome some of the latter issues by introducing a non-zero slope for negative values [194].

After the specification of the model structure, which includes the choice of an activation function, the weights of the network must be initialized before starting the training process. Proper weight initialization prevents gradients from exploding and vanishing during the backpropagation training process. Weights should within certain boundaries be randomly initialized in order for the stochastic learning algorithm to properly work [195]. Various techniques presented in literature suggest that weight initialization has a tremendous effect on the overall performance of a model [190,196,197].

For sigmoid and tanh activation functions, Xavier initialization has become the de facto standard [198]. The technique aims at keeping the variance constant across multiple layers to prevent exploding or vanishing gradients. Weights are randomly sampled from a Gaussian distribution with zero mean and a variance according to equation (40).

$$var(w_{ij}) = \frac{2}{n_{in} + n_{out}}, \tag{40}$$

where $w_{ij}$is a weight in the network, $n_{in}$is the number of neurons in the previous layer and n_{out} is the number of neurons in the next layer. If ReLU or an adapted version is used as the activation function, a modified Xavier technique called “He initialization” is proposed by literature in order to prevent gradient issues [194].

Following the initialization process, the weights must be adapted to account for the pattern inherent in the training data [159]. The weights are stepwise updated by first forward propagating a predefined subset of the input data, usually referred to as the batch size, through the network. An error measure (loss function) such as the RMSE, as defined in section 3.8, is then obtained from the output of the network $\widehat{y_t}$ and the actual value of the time series y_t. The error is then back-propagated through the network in order to update the weights of each neuron according to the size and direction of the corresponding gradient. Repeating the procedure gradually fits the network to the training data.

Multiple different optimization algorithms have been suggested and evaluated in literature. Mini-batch stochastic gradient descent is the traditionally most used approach which only relies on the gradients and a predefined learning rate [199]. However, the associated constant learning rate often suffers from either slow convergence, oscillations or overshooting of the minimum. Stochastic gradient descent with momentum applies exponential smoothing to gradients of past evaluations to accelerate the learning process and to overcome the convergence and oscillation problems [200]. Today, latter approach often reveals the best performance [201]. Many more optimization techniques such as Adagrad, Adadelta, RMSprop, Adam, AdaMax were published to tackle various issues, improve performance or speed up the learning process [202,203]. Of latter approaches, Adam has attracted special attention specifically for training deep neural networks. According to [204], the approach “is computationally efficient, has little memory requirements, is invariant to diagonal rescaling of the gradients, and is well suited for problems that are large in terms of data and/or parameters”. The approach calculates adaptive learning rates for each individual weight and many papers have revealed superior performance. Though in some cases the algorithm does not properly converge and the performance turns out to be slightly worse than e.g. stochastic gradient descent (with momentum) [201,205,206]. This thesis uses the Adam optimizer.

Complex models, such as neural networks suffer from overfitting weights too closely to the training data set. In such cases, the noise of the training data is captured which results in a high performance on the training set accompanied by a low generalization performance on the validation and test set. Overfitting can be prevented by using less complex models (e.g. less neurons), applying less features (section 3.3), using a larger training data set, cross-

validation, ensemble learning and regularization techniques. In machine learning, regularization describes a multitude of techniques aiming at overfitting prevention. Lasso regression (L1) and ridge regression (L2) are two commonly used methods which discourage model complexity by penalizing weights in the loss function [140]. Both methods assume that smaller weights generate simpler models that are less prone to overfitting. As described by equation (41), Lasso Regression (Least Absolute Shrinkage and Selection Operator) updates the loss function of the optimizer by adding the sum of all weights (absolute value) to it:

$$\sum_{t=1}^{n}(y_t - \hat{y_t})^2 + l_1 \cdot \sum_{i,j}\left|w_{i,j}\right| \tag{41}$$

As for equation (41), a mean squared error function is assumed, where $(y_t - \hat{y_t})$ is the difference between the actual time series value and the prediction at time t, n is the sample size (batch size), l_1 is a hyperparameter affecting the influence of the regularization and latter sum adds up the absolute values of all weights $w_{i,j}$ in the network. Bias terms of the network are not considered. Lasso regression shrinks the weights of less important features to zero which corresponds to an algorithmic feature selection.

Ridge regression as described by equation (42) works very similar to lasso regression but adds the squared magnitude of all weights as penalty term to the loss function. The influence of ridge regression is determined by the hyperparameter l_2.

$$\sum_{t=1}^{n}(y_t - \hat{y_t})^2 + l_2 \cdot \sum_{i,j}\left(w_{i,j}\right)^2 \tag{42}$$

In this thesis, a combination of L1 and L2 regularization, called Elastic net regularization is used [207].

Another method of preventing overfitting is ensemble learning. Multiple models with different configurations are trained on the same data to generate a set of predictions. By combining (e.g. averaging) the set of predictions, a model can be obtained which has less variance and a better overall performance [192,208]. “The reason that model averaging works is that different models will usually not make all the same errors on the test set” [190]. Despite the advantages, ensemble learning is computationally expensive and more demanding in maintaining multiple models.

Dropout is a technique which simulates having multiple models with different configurations by randomly muting some neurons during the training process of a single model [209]. This way, a layer randomly behaves like a layer with a different number of neurons and connectivity to the previous layer. It is a computationally cheap method to reduce

overfitting and the generalization error. This thesis applies dropout to the hidden layers of the network and introduces the probability at which neurons are dropped out as another hyperparameter.

Another and probably the most effective overfitting prevention method used in this thesis is early-stopping. After each epoch (iteration) on the training set, the model is evaluated on the validation set. One epoch corresponds to one training cycle on the training set. The epoch is finished as soon as all training data was used one time. If for a predefined number of iterations the performance on the validation set is not increased, the learning process is stopped.

3.13.5 Recurrent Neural Network

Neural networks calculate predictions only based on the input features of the current time step. If no lagged observations are fed to the network as additional input variables, a neural network is incapable of using information from the past. Recurrent neural networks (RNNs) solve latter drawback by handling an internal state, also called memory, which allows information of previous time steps to persist. As opposed to the feed forward networks introduced in subsection 3.13.4, RNNs exhibit loops, which feed information backwards. To train RNNs similar to NNs, a gradient based technique called backpropagation through time (BPTT) was invented which unfolds RNNs a predefined number of time [210–212]. Figure 3-14 illustrates a three times unfolded network in which multiple copies of the same network pass their output to the successor.

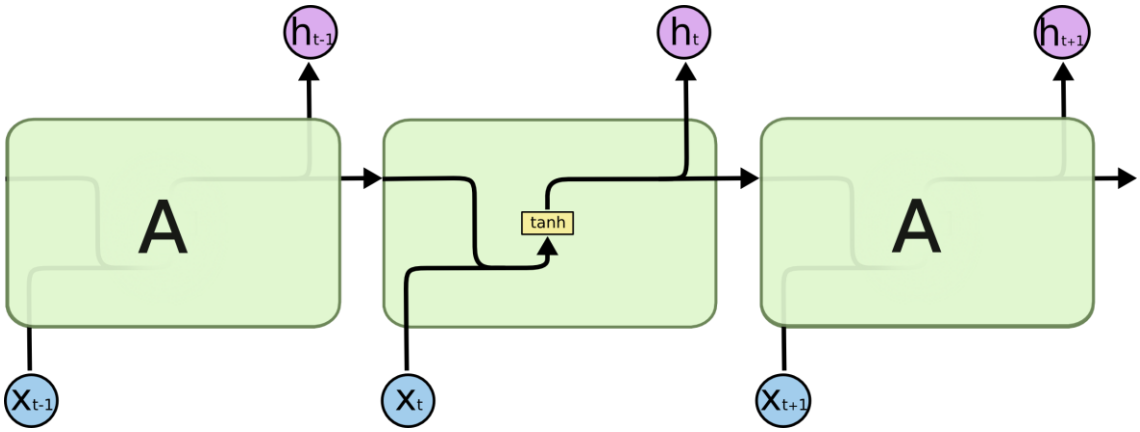

Figure 3-14: Unfolded Elman-type recurrent neural network [213]

Because RNNs are capable of handling long-term dependencies, they have in the last few years been successfully applied to a variety of problems including speech recognition and generation, handwriting recognition and generation, human language translations, text classifications, dialog systems, image captioning and time-series predictions [199]. In the field of electricity price forecasting, RNNs have outperformed many alternatives [214,215].

The most basic RNN types are the Jordan and Elman model, which differ primarily in that the Jordan model maintains the history of the output layer in memory whereas the Elman model (*Figure 3-14*) keeps the history of the hidden layer in memory. Both cell types have a simple structure, such as the single tanh layer as illustrated in Figure 3-14. Two problems arise with both models. First the BPTT unfolding propagates errors many times over a cell leading to vanishing or exploding gradients [216]. Second, it is very difficult to train the models to capture long-term dependencies because gradients decrease exponentially over time [45,217].

The most popular RNN type is long short-term memory (LSTM) network, which solves the long-term dependency problem. LSTM networks contain additional gate elements which are capable of selectively memorizing and forgetting parts of the sequence [218]. As illustrated in *Figure 3-15*, unfolded LSTM networks are also chained together for training but compared to the previous approaches have a more sophisticated cell structure. A cell consists of four interacting layers, each with corresponding trainable weights. Central to LSTMs is the cell state (horizontal line running through the top of *Figure 3-15*) which can be numerically adapted by the so called forget and input gate. An output gate decides how much information from the cell state is used to generate the output value.

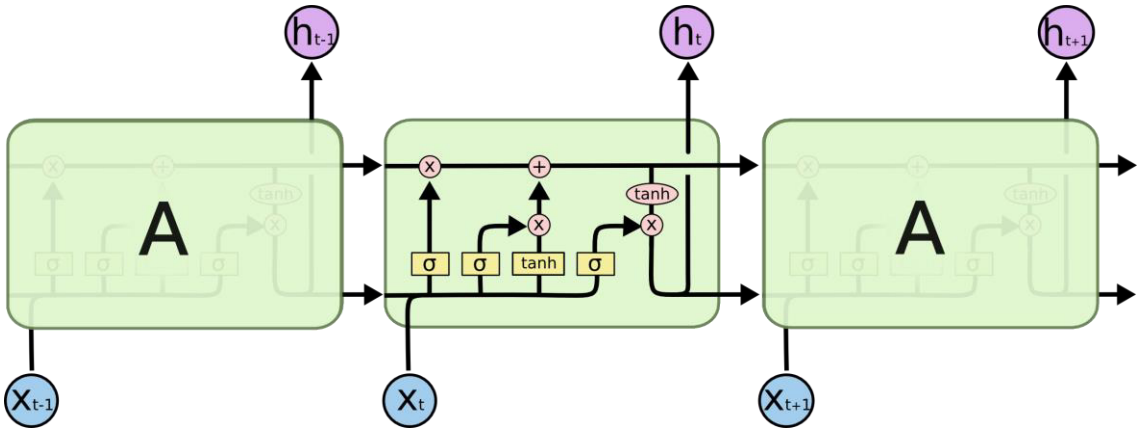

Figure 3-15: Unfolded long short term memory (LSTM) network [213]

LSTM networks have been applied with huge success to a large variety of problems [219]. A very common adaption on LSTM cells is the Gated Recurrent Unit (GRU) introduced by [220]. As opposes to LSTM cells, the forget and input gate are combined into one update gate. Also, among other minor changes, the cell state and hidden state are merged. Overall, the GRU model is less complex and therefore computationally favorable. Compared to LSTM, many papers found a similar performance [221]. This thesis evaluates Elman, LSTM and GRU type RNNs. In literature, RNN development has gained a lot attraction lately with many publications on various model types [222,223].

4 Bidding and Operating Strategy

This chapter is based largely on a previous publication of the author [224]. To participate on the automatic Frequency Restoration (aFRR) market, a system operator must both fulfil the technical requirements of the TSO as described in section 2.1 and submit a bid tuple (section 2.1.2.1). The bid tuple consists of a capacity price (€/MW), an energy price (€/MWh) and the offered capacity (MW) for each of the six time slots and both power delivery directions.

Revenues on the aFRR market strongly depend on the submitted bid tuple of an auction participant. This chapter presents a bidding strategy that maximizes the profit for a particular generation pool by deriving the optimal bid tuple. It relies on the day-ahead aFRR market prediction as described in chapter 3. Section 4.1 reviews literature on related bidding strategies, section 4.2 describes various pool configurations analyzed in this work, section 4.3 presents the underlying data sources of the simulation, section 4.4 describes the operation strategy of a pool, section 4.6 describes the battery model used for estimating aging effects, section 4.7 describes the optimization approach, section 4.8 presents the multi-agent framework used for market modelling and section 4.9 concludes with the profit evaluation procedure.

4.1 Literature Review

This section provides an overview of literature related to bidding strategies for the electricity market with a special focus on the aFRR market. Predominant foundations for building bidding strategies are based on either fundamental market simulations, multi-agent models or game-theoretic derivations.

Fundamental models assume an efficient market and complete information for all market participants. The system load is covered at minimal overall costs since the distribution of resources can be optimized [225]. However, under the assumption of complete information, strategic bidding or exploitation of market power cannot be investigated. For latter effects to be considered, a multi-agent or game-theoretic based simulation is more suitable.

A multi-agent based simulation of the German control reserve and day-ahead market was conducted in [226]. The aim of the research was to find bidding strategies that simulate the behavior of market participants in aforementioned markets as close to reality as possible. An analysis revealed that a bidding strategy is influenced by the auction design, price development expectations, the portfolio of the individual market participant and the repeated procurement process. In case of the day-ahead market, bidding strategies offering prices close to the marginal costs revealed the most realistic results. Offering at the marginal price increases the awarding probability of market participants and in most cases

contributes to covering fixed costs as well. The contribution to the fixed costs is due to a unit market price (market clearing price) on the day-ahead market, which is usually higher than the offered price (section 2.2). Strategic bidding plays a minor role. In the aFRR market, participants are payed-as-bid. Offers at marginal costs therefore do not cover fixed costs. The research revealed that strategic bidding strategies, which learn from previous auction outcomes, produce the most realistic results. Offered prices were above the marginal costs.

Another detailed multi-agent based model was presented by [227] and is able to simulate the day-ahead as well as the intraday market. Major agents in these markets are modelled individually. Aside from short-term simulations, the model also allows to derive investment decisions by analyzing multiple years [228].

To extend the country-specific balancing power markets to a European-wide solution, the auction design must be harmonized. Compared to the German/ Austrian market design, the European Commission aims at implementing two design modifications [229]. First, the pay-as-bid awarding scheme is to be replaced by uniform pricing and second an additional energy-price based market is planned. A game-theoretical model for both auction designs was implemented by [23]. Both market designs were found to theoretically provide efficient auction outcomes and competitive prices. However, imperfections were also revealed in historical market data. Empirical evidence was presented which suggests that market participants coordinate on non-competitive price levels (collusive bidding behavior) by taking into account previous auctions results [35,36]. The collusion and abuse of market power can in part be explained by only four market participants providing most of the aFRR capacity in Germany. Historical market data does therefore not match with game-theoretic predictions. Based on above findings, [17] proposes a bidding strategy which integrates the results of previous auctions to derive optimal capacity and energy price bids. A subjective acceptance probability and demand probability was derived from historic prices. It was found that the capacity and energy price depend on each other. Validating the bidding strategy on real market data revealed a high correlation to bidding strategies actually used in the market.

A two-player competitive market model was developed by [230]. The first player represents a single market participant whereas the second player represents the remaining market. The simulation environment implements a power market, ancillary services and corresponding auction processes. From a defined combination of bidding strategies, game theory techniques developed in this research can locate optimal Nash equilibrium solutions. In addition, the dominant bidding strategy, which maximizes the revenues for a single market participant, can be derived.

In [12], bidding strategies on the German aFRR market are derived by analyzing the historical capacity and energy prices. A two-stage bivariate modelling process is presented

which first analyses the influence of exogenous data sources to the aFRR prices. In the second stage, the influence of the lagged predictors is modelled in a multivariate vector autoregressive model. Based on the findings from the time series modelling, two dominant bidding strategies were derived and explained by game-theory.

To allow wind power farms to provide ancillary services to the grid, [231] implemented a probabilistic generation forecasts model. Based on the forecast, an offering strategy was developed which accounts for the market rules, operational capabilities of the turbines and the joint market participation. The research revealed that the provision of control reserve provision by wind farms is technically feasible but does not always generate more revenues. Related research estimates the amount of aFRR capacity which can reliably by provided by a renewable generation plant consisting of wind and photovoltaic [42,232]. Multiple strategies are derived which either optimize for maximizing revenues or for minimizing the risk of underfulfilment. The research used aFRR price forecasting techniques and is evaluated on real aFRR market data.

Only a few investigations are published which deal with BESS participating on the aFRR market. Lithium-ion and sodium Sulphur based grid-scale energy storages were analyzed in [233]. For the British market, an arbitrage algorithm was extended to also allow participation in control reserve services. Both a stand-alone operation as well as a joint operation with a wind farm was considered. Despite a tripling of profits, the high investment costs of BESS were found to prevent an economic viable operation. A revenue potential analysis of BESS offering congestion relief services and providing arbitrage trading was conducted by [234]. However, ancillary services were not considered. Various research suggests that BESS which provide aFRR in a standalone mode cannot be operated economically beneficial [15,235]. According to this research, the energetic capacity costs of BESS are too high for meeting the 4 h minimum operating criterion of aFRR.

No literature was found which provides an in-depth analysis of BESS participating on the aFRR market in conjunction with a VPP. This research is aimed at filling this gap.

4.2 Pool Configurations

The objective of the bidding strategy presented in this section is to evaluate the benefits of adding a BESS to an existing pool of various generation units. A pool is also referred to as a virtual power plant (VPP). By adding a BESS to an existing pool, generation capacity utilization shall be maximized while simultaneously proving aFRR services to the grid. This section describes multiple pool configuration scenarios, which differ in the types of generation facilities and corresponding nominal capacities. The particular pool configuration influences the generated revenues since it influences the total capacity which can be offered on the aFRR market (subsection 4.5.2). For all pool configurations considered in this

work, one dispatch and trading unit must be able to control all generation facilities and the BESS.

Various different generation type facilities and corresponding properties such as generation profile time series, marginal costs or idle capacities are included in the simulation framework designed for this work. Among the included facilities are various wind parks (onshore and offshore), solar parks, biomass generation, nuclear power plants, fossil gas power plants and lignite power plants. This work, however, does not use specific generation facilities at individual locations but instead uses scaled profiles of the overall generation in Germany. To obtain for example the wind onshore profile of 100 MW nominal capacity, the overall German wind onshore generation time series is scaled according to the overall installed nominal capacity. A few advantages arise from scaled generation profiles for this investigation. Outages of individual generation units due to failures or maintenance measures do not affect the results. In real life, dispatch and trading facilities, which operate multiple generation units and BESS, would compensate the lost capacity by ramping up other units. Therefore, a BESS providing aFRR could dynamically be pooled with other generation units. A scaled profile does better reflect that behavior. In addition, depending on the data source, individual generation profiles are often at a resolution of less than 15 min (e.g. 1 h resolution) which does not match the simulation time base. Furthermore, individual generation profiles are often not freely available which would make this work not reproducible.

Table 4-1 provides an overview of the considered pool configurations in this work. On purpose, the configurations do not reflect the generation units of any specific trading, administration and dispatch facility. Instead, the used configurations could be part of any utility-scale or municipal-scale trading facility portfolio.

Table 4-1: Generation Pools

Confi-guration	**BESS Power Capabilities P_{Nom} [MW]**	**BESS Energetic Capacity E_{Nom} [MWh]**	**Wind Onshore – Nominal Capacity [MW]**	**PV – Nominal Capacity [MW]**	**Lignite-Fired Power Plant – Nominal Capacity [MW]**
1	20	20	0	0	0
2	30	20	100	0	0
3	30	20	100	100	0
4	30	20	100	100	400

For this work a common, as of 2019 in Germany, stationary BESS size with 20 MWh storage capacity was assumed. In case the BESS is operated in standalone mode, 20 MW of inverter capacity is considered whereas in the pooled operation mode, 30 MW of inverter capacity is

considered. The difference in the energy to power ratio arises from the fact that in standalone mode a BESS must be capable of providing 4 h the full tendered aFRR power. In pooled operation, the BESS can recharge from other generation units during aFRR provision and therefore requires a lower energy to power ratio (see subsection 4.5.2).

Both the PV and onshore wind park have nominal capacities of 100 MW. The lignite power plant has a nominal capacity of 400 MW. Table 4-1 states four configurations in which the introduced BESS is operated in stand-alone mode, coupled with onshore wind, coupled with onshore wind and PV and coupled with onshore wind, PV and a lignite power plant.

4.3 Input Data

This section describes the various input data sources used for running the simulation described in this chapter. All aFRR market related data is published on a web-based platform operated by multiple European TSOs (regelleistung.net) [14]. The data is open-access and includes anonymized bids of all successful market participants, the aFRR request time series (1 sec and 15-min resolution) and the quarterly published mixed price factors (section 2.1.2.1). Since the operation strategy (section 4.4) trades on the day-ahead and intraday market, corresponding electricity prices are obtained from the European Network of Transmission System Operators for Electricity (ENTSO-E) and the European Power Exchange (EPEX) [38,61]. Wind onshore, PV and lignite-powered generation profiles of Germany (15-min resolution) are freely accessible on the ENTSO-E web platform [61].

4.4 System Cost Breakdown

To evaluate the economic performance of stationary BESS, a financial analysis is necessary. Detailed cost breakdowns are rare in this area because system integrators often keep information of individual components confidential. Prices strongly depend on the ordered quantities.

Table 4-2: Utility-scale cost parameters of BESS in the year 2019

Component	**Costs**
Battery system	189 €/kWh [236]
Bi-directional Inverter	70 €/kW [237]
BOS	81 €/kWh [237,238]
EPC	55 €/kWh [238]
Soft Costs	60 €/kWh [236,238]
Maintenance and Operation	1 % of hardware invest per year
Contingency	3 % of invest [236]

Parameters used in this work are largely based on an utility-scale BESS benchmark provided by the U.S. National Renewable Energy Laboratory [237], a BESS analysis conducted by McKinsey [238] and data derived from the stationary BESS located in Aachen, Germany [11].

Container based solutions are currently the most cost-effective approach in building BESS. As mentioned in section 4.2, this work focuses on a utility-scale 30 MW, 20 MWh lithium-ion based container system. Table 4-2 provides an overview of the components and corresponding costs of the BESS. The battery system includes all cells, modules, cell state monitoring devices, racks, DC circuit breaker, DC bus bar, DC connection point and the battery management system. The balance of system (BOS) encompasses the container, all mounting structures, cabling, transformers (e.g. to medium voltage), electrical components, documentation, installation works, fire suppression system, gas extinguishing system (if available) and the HVAC (heating, ventilation and air conditioning) system. Due to the increased availability of container-scale components, design advances and efficiency gains in manufacturing, BOS costs decreased by 78 % between 2012 and 2017 [238]. EPC (engineering, procurement and construction) reflects costs associated to project management, procurement, permissions, site preparation, construction and commissioning. Similar to BOS costs, EPC costs decreased by 75 % in aforementioned range [238]. This decline is attributable to increased standardization, enhanced design and installation techniques, increased competition and gained experience of the EPC companies. Soft costs include customer acquisition, land acquisition, permitting and interconnection among others. By standardized processes and an increase in experience, soft costs have decreased over the past years as well.

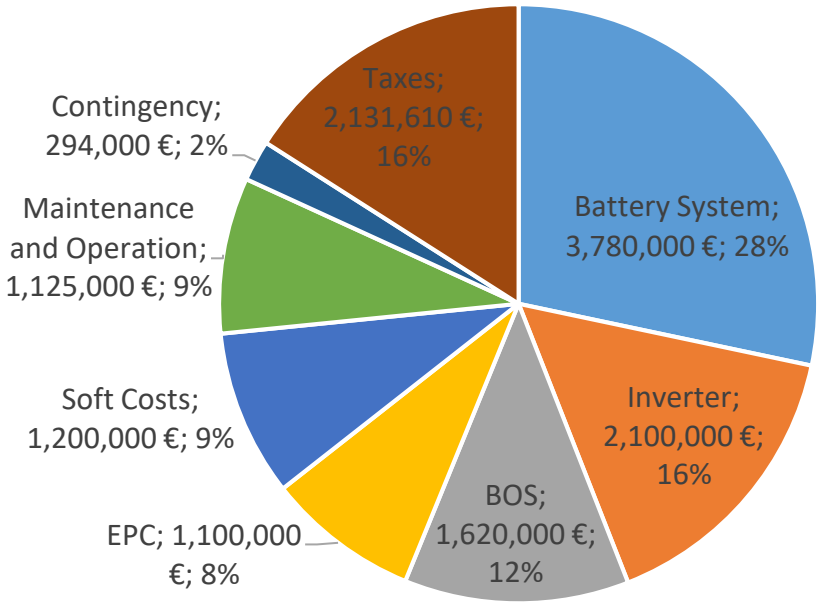

Figure 4-1: Cost Breakdown of a 30MW, 20MWh BESS

Based on the cost parameters provided by Table 4-2, Figure 4-1 illustrates a cost breakdown of the 30 MW/ 20 MWh BESS used in this work. At this scale, the total costs amount to 13,350,610 €. All battery system related costs contribute 28 % to the total costs. The second highest positions are taxes and inverter costs. Dividing the total costs by the energetic capacity reveals specific costs of 668 €/ kWh. If only the hardware costs (battery system, inverter, BOS) and taxes are considered, specific costs of 482 €/ kWh are obtained. Latter specific hardware costs correspond to the entries of a BESS database provided by [239]. The database offers free access to BESS data provided by various manufacturers and system integrators. Aside from technological information and multiple system size ranges, the database offers pricing information.

Aside from the battery system (section 4.6), all components are simulated with a lifetime of 15 years.

4.5 Operating Strategy

For a pool comprising different generation units and a BESS, the operating strategy handles the dispatch and trading of energy at each instance in time. Generation capabilities are either placed on the day-ahead or on intraday market. Other trading channels aside from aforementioned markets are possible but due to the complexity are not further considered in this work. Here, any unpredictable aFRR request is instantly provided by the BESS. By the use of a reserved power band, the generation units are capable of recharging the BESS after an aFRR request. The operating strategy assures that in each instance of time, the aFRR requirements of the TSOs are met and the energy trading generates maximum revenues. Subsection 4.5.1 investigates time parameters relevant for the operating strategy, subsection 4.5.2 derives the maximum possible aFRR capacity (MW) a pool can offer, subsection 4.5.3 describes the handling of time slices in which aFRR must be provided and subsection 4.5.4 describes the handling of time slices without aFRR obligation.

4.5.1 Continuous Intraday Market Rules

As described in subsection 2.3.2, the smallest time period to be traded on the continuous intraday market is a 15 min block (t_{Block}) and the minimum lead time of sale is 5 min (t_{Lead}). To give trading partners an opportunity to consider and buy a certain block, some arbitrary time > 0 must be taken into account (t_{Sale}). This work assumes a sale opportunity time of t_{Sale} = 30 mins. Figure 4-2 illustrates aforementioned time constants for an exemplary 15 min block (hatched area). The decision point marks the instance in time at which the sell decision for the hatched block must be made.

Aside from the intraday market prices, additional expenses apply when exchanging energy. These additional expenses are country-specific and consist of for example various taxes,

network charges, metering costs, concession fees, renewable energy surcharges and various apportionments. For each MWh of energy fed into the grid, the revenue is equal to the market price since the final consumer is charged for all additional expenses. If, however, energy is withdrawn from the electrical grid to e.g. charge the BESS, some specific expenses apply. For all calculations, this work uses the same fees that apply for the stationary M5BAT BESS located in Aachen. In total, 12.01 €/MWh are charged for each MWh obtained from the grid. This includes among others concession fees and multiple apportionments (power-heat coupling, §19 Strom-NEV [240], etc.).

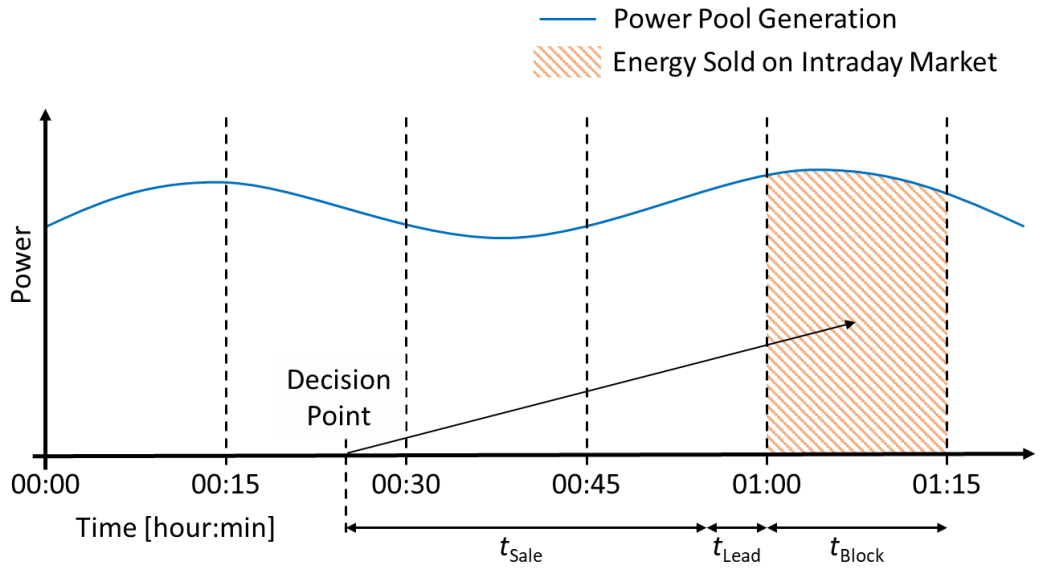

Figure 4-2: Time Constants of the Intraday Market

4.5.2 Determination of Maximum aFRR Capacity

As described in section 2.1.1, units prequalified for aFRR are required to deliver the accepted capacity (MW) up to 4 h. Based on discussions with grid operators, an aFRR prequalified VPP must not rely on intraday recharging during a 4 h aFRR provision period. It cannot be guaranteed that an energy seller is available which in consequence means that the VPP must be capable to fulfil the 4 h criterion without external market recharge. The maximum capacity a standalone BESS can offer on the aFRR market is therefore given by equation (43):

$$P_{\mathrm{aFRR\_Standalone}} = \min\left(P_{\mathrm{Nom}}, \frac{E_{\mathrm{Nom}}}{4\mathrm{h}}\right), \tag{43}$$

where P_{Nom}represents the maximum power capabilities and E_{Nom} represents the energetic capacity (in MWh) of the BESS.

If, however, the BESS is operated in conjunction with a generation pool as described in section 4.2, more capacity can be offered on the aFRR market. This work only considers

positive aFRR as this is generally more profitable and, if combined with other generators, can be realized without a derating of generators. Figure 4-3 illustrates how energy can be recharged from the pool while the BESS provides aFRR. The total pool generation power (P_{Pool}), as the sum of all units (e.g. PV + Wind + Thermal), is given by the continuous line. Some of the total pool generation power is traded on various channels, e.g. on the day-ahead market as indicated by the hatched blue area. Another share of the total pool generation power is reserved for recharging the BESS after an aFRR request. The reserved power is equal to the accepted aFRR capacity. If no aFRR energy is requested from the BESS, the reserve band can continuously be sold on the intraday market. The latter is indicated by the hatched red area. If, however, an aFRR request discharged the BESS, the reserve band can be used for recharging. Prediction uncertainties in the wind and PV generation are not particularly considered in this work. However, uncertainties could be compensated by the reserved power band or an extension of the reserved power band.

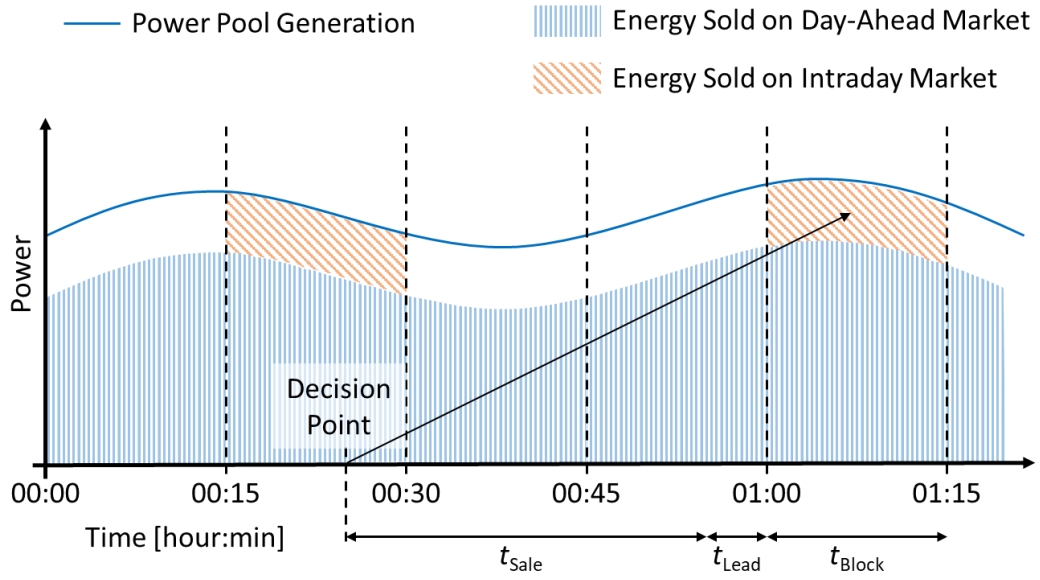

Figure 4-3: Recharge strategy for aFRR Provision

According to section 4.5.1, the decision to either sell or not sell a quarter-hour block on the intraday market must be made $t_{\text{Sale}} + t_{\text{Lead}}$ before the start of the block. If in the worst case scenario, a full and continuously lasting aFRR request is triggered right after the decision to sell a block, the BESS must at least be able to provide the delivery duration (t_{Delivery}) as indicated by equation (44):

$$t_{\text{Delivery}} = t_{\text{Sale}} + t_{\text{Lead}} + t_{\text{Block}} \tag{44}$$

If the pool continuously provides a reserve band over the aFRR product duration, the maximum possible aFRR capacity to offer ($P_{\text{aFRR\_Pool\_max}}$) is given by equation (45):

$$P_{\text{aFRR\_Pool\_max}} = \min\left(P_{\text{Nom}}, \frac{E_{\text{Nom}}}{t_{\text{Delivery}}}\right) \tag{45}$$

In case the generation profile of the pool does not continuously provide the possibility to recharge the BESS, the aFRR capacity to offer on the market is less then $P_{\text{aFRR\_Pool\_max}}$. Figure 4-4 illustrates a generation pool scenario for the POS_04_08 aFRR product type (4 am to 8 am). From the start of the product type at 4 am until 6:30 am, in this example, no pool generation power is available to support the BESS in case energy must be recharged due to an aFRR request.

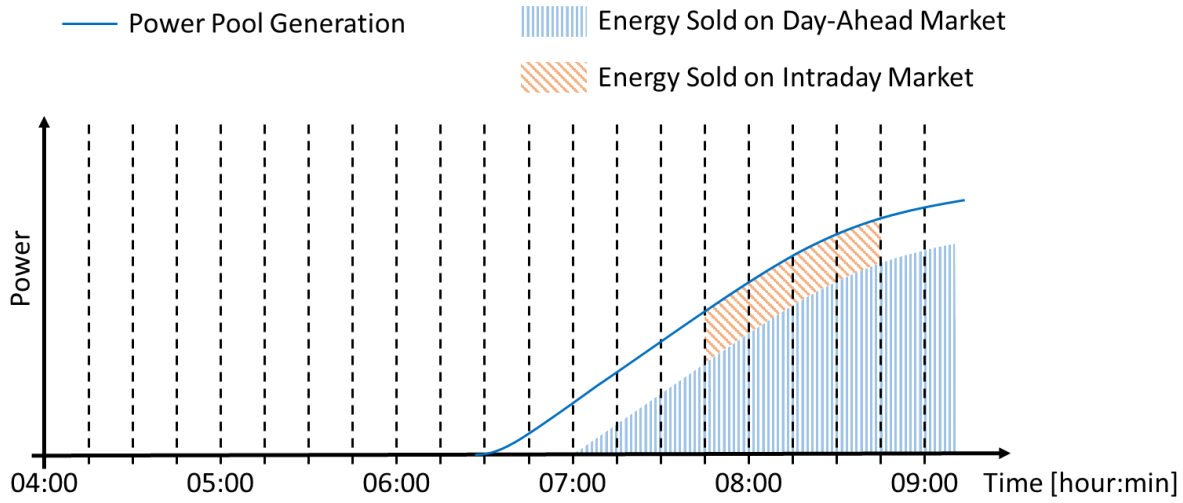

Figure 4-4: Non-Continuous Pool Generation Profile

The BESS must provide enough energy to answer a continuous full power aFRR request over that period. Due to energetic capacity limits of the BESS, the amount of aFRR capacity (MW) to offer on the market must be reduced. This work implements an algorithm to determine the maximum possible aFRR power as a function of the pool's generation profile, the power capabilities of the BESS and the energetic capacity of the BESS.

4.5.3 Active aFRR Period

For periods in which aFRR must be provided (auction success), this section describes how energy is dispatched within the pool and traded on the electricity market.

Each aFRR request triggered by the TSOs is instantaneously fulfilled by the BESS. Based on the merit-order position of the individual energy price bid, the set point power and request duration is derived. Since only positive aFRR is offered, the BESS only discharges.

As explained in section 4.5.2, a power band from the pool's generation profile is reserved to handle recharging the BESS. For each 15-minute block within the reserve band, a corresponding decision point marks the instance in time at which the decision to trade the

block on the intraday market or not (Figure 4-3) must be made. All energy discharged due to aFRR requests between two decision points will be recharged in the next possible 15-minute block.

As illustrated by the hatched blue area in Figure 4-3, generation capabilities beyond the reserve band are traded on the day-ahead market. Other trading options on the power exchange or Over-the-Counter (OTC) are possible as well (chapter 2) but due to simplicity are neglected in this work. The day-ahead market serves as a reference trade scenario.

Some generation types, such as thermal power plants, are often operated below their nominal capacity. The leftover generation capabilities can be used to recharge the BESS. Arising marginal costs due to for example lignite consumption are considered in this work.

If recharging from the pool generation is not possible, energy is recharged from the intraday market. Intraday recharge is only triggered as a last resort to bring the SoC back to 100% at the end of an aFRR product period. The latter applies for instance in BESS standalone operation or if the pool does not provide the generation capabilities. In each scenario of this work, the considered BESS (with an optional pool of generation units) fulfils the requirement of continuously providing aFRR for 4 h without relying on recharging from the intraday market.

Depending on the location of the BESS, additional expenses, as explained in subsection 4.5.1, might apply for recharging energy. This applies for example in scenarios in which the BESS is not located on-site of a coupled unit such as a wind farm. Recharging involves using the public electrical grid, which in turn causes aforementioned expenses. This work considers both scenarios, on-site and off-site coupling.

4.5.4 Inactive aFRR Period

This section describes the dispatch and trading of resources in time periods in which there is no obligation to provide aFRR (e.g. lost auction).

All power capabilities of the generation units are traded on the day-ahead market. As before, other trading options would be possible but are not subject to investigation in this work. The decision to trade all energy on the day-ahead market can be taken after the results of the aFRR auction are published. Market closing for the day-ahead market is at 12 pm and results of the aFRR auction are published at 9 am the day before delivery. As illustrated in Figure 4-5, no power is reserved for recharging the BESS.

If an active aFRR period is followed by an inactive aFRR period, energy might be discharged from the BESS at the end of the aFRR period. In such a case, recharging from the pool is not

possible since all energy is already sold on the day-ahead market. To bring the SoC of the BESS back to 100 %, energy is bought from the intraday market.

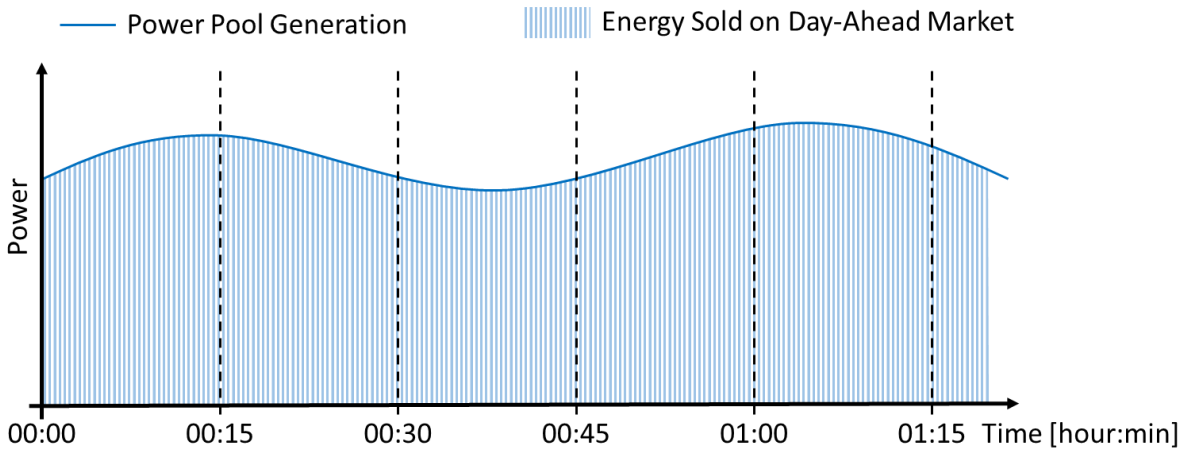

Figure 4-5: Trading of Pool Capabilities during Inactive aFRR Period

To utilize the otherwise unused capacity of the BESS, the operating strategy considers arbitrage trading on the intraday market. The arbitrage algorithm implemented in this work is based on [241,242] and has been extended to handle the properties of BESS. It was shown, that the algorithm reaches the global optimum for profit [233,241]. Within a predefined time period, the algorithm identifies pairs of charging/ discharging periods. The first pair consist of the quarter-hour block with the lowest and the quarter-hour block with the highest intraday price. To be considered a potential pair, the arbitrage algorithm forces a price spread above a predefined threshold. More on how the threshold can be quantified is given at the end of this subsection. The second pair covers the second highest price spread of all remaining quarter-hour blocks, and so on. According to the identified pairs, a schedule is created which maximizes the revenues. In the second step of the algorithm, the schedule is adapted in order to not violate the SoC boundaries of the battery. Only SoC values between 0 % and 100 % are possible. The least economic beneficial charging/discharging blocks are reduced accordingly. At the end of each inactive aFRR period, a target SoC of 100 % must be reached. The target SoC assures that the requirements for providing e.g. aFRR in the next block are satisfied. In the third step of the arbitrage algorithm, the schedule is again adapted to meet the target SoC requirement.

The predefined price spread threshold depends on the calendric battery ageing, cyclic battery ageing (section 4.6), energetic BESS efficiency and applying recharge taxes (subsection 4.5.1). From a battery ageing perspective, the end-of-life criterion can be reached first by either cyclic activity or calendric ageing. If the calendric lifetime exceeds the cyclic lifetime, the threshold in the arbitrage algorithm should be higher than the sum of the cyclic ageing costs, energetic losses and applying recharge taxes. Price spreads below latter

threshold would not be economically beneficial. If, however, the estimated calendric lifetime is lower than the estimated cyclic lifetime, the cyclic ageing costs can be neglected in the price spread threshold. In this scenario, the cyclic activity does not change the lifetime of the BESS. The price spread threshold is based only on the sum of energetic losses and applying recharge taxes. In general, latter considerations hold true if only little cyclic activity is targeted or the battery technology allows a long cycle life (e.g. lithium-titanate). So far, the calendric ageing costs were neglected in the derivation of the price spread threshold. If, however, two arbitrage blocks occur far apart in time from each other, the average SoC of the battery changes. The change of the average SoC has a direct impact on the calendric ageing (see section 4.6). Since in this work, most arbitrage activity is within a few hours, this effect is considered minor.

4.6 Battery Model

To estimate the costs associated with battery aging, this work implements a battery model based on [243]. The model was chosen since reasonably accurate results for arbitrary operating profiles can be achieved. In addition, the proposed model was fitted to a lithium ion manganese oxide (LMO) cell chemistry, which matches the largest battery technology used in the BESS located at the RWTH Aachen University. By combining theoretical battery degradation analysis with experimental observations, the model is described as semi-empirical. Battery deterioration is divided into a calendar component given by equation (46) and a cyclic component given by equation (47).

$$f_{\mathrm{cal}} = S_t(t) \cdot S_\sigma(\sigma) \cdot S_T(T) \tag{46}$$

$$f_{\mathrm{cyc}} = S_\delta(\delta) \cdot S_\sigma(\sigma) \cdot S_T(T) \tag{47}$$

Each factor represents a specific stress model, where $S_T(T)$ denotes a stress model for temperature based on Arrhenius' equation [244], $S_t(t)$ denotes a (linear) time stress model, $S_\sigma(\sigma)$ denotes a SoC stress model originating from [245] and $S_\delta(\delta)$ denotes a DoD stress model. For a more detailed description, reference is made to [243]. Battery degradation further depends on the current state of life, with a significantly higher rate during the early cycles than during the later cycles. A major cause of the early degradation is rooted in the formation of the Solid Electrolyte Interphase (SEI) film [246,247]. To correctly model the aging behavior, the proposed model implements a linear and non-linear component. The high accuracy of the proposed model was demonstrated on mixed-cycle operations (Dynamic Stress Test Cycling) data provided by the manufacturer of the LMO cell.

The model is adaptable to different types of lithium-ion batteries by fitting the coefficients to specifications provided either by the manufacturer or to conducted cell measurements.

Depending on the cell-chemistry, each stress model can be replaced with a suitable alternative.

To cope with the irregular charging/ discharging pattern resulting from the operating strategy (section 4.4), the frequently used Rainflow algorithm has been implemented. Originating from materials science, the algorithm has been used to analyze the aging of materials in stress-strain tests [248]. It is also widely used in battery ageing estimation since the problem structure is quite similar [243,249]. In its basic idea the charging and discharging can be considered separately and each process is counted as a half-cycle. Half cycles are counted by their depths of discharge and combined to full cycles.

Figure 4-6 illustrates the capacity degradation over the equivalent number of cycles performed by the LMO battery. In this work, the fast decay in capacity within the first around 500 cycles is not considered. The latter is justified by this work's simulation time range of less than one year, which corresponds to a few hundred cycles. Considering the non-linearity would overestimate the battery ageing.

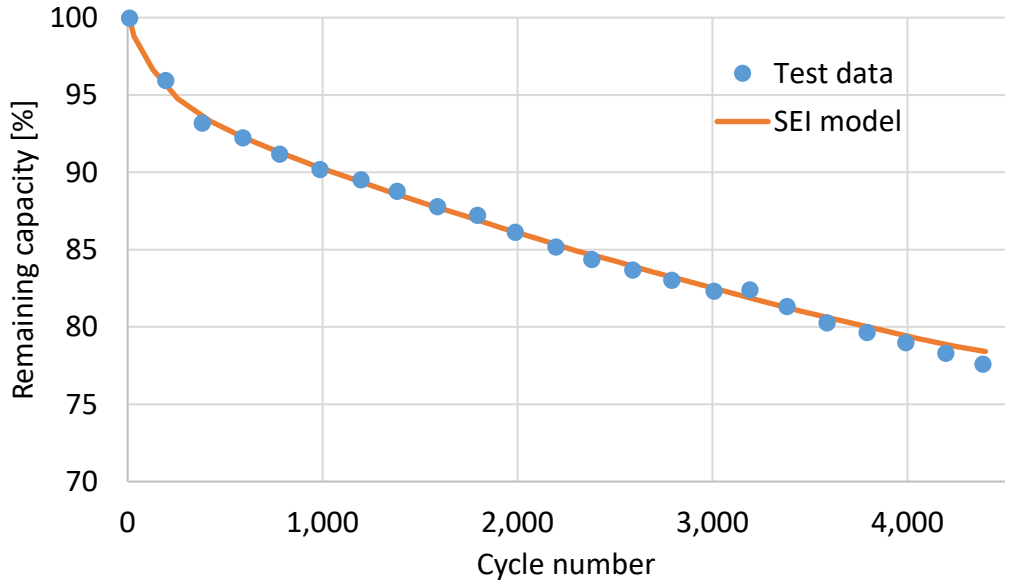

Figure 4-6: Degradation curve of lithium-ion LMO cell. Test data and fit of the non-linear SEI model. Figure based on [243].

Based on the charge/ discharge time series resulting from the operating strategy, this work derives the differential loss in capacity. The implemented battery-ageing model considers cyclic operations as well as standby periods to estimate the differential capacity loss. As described in section 4.4, a battery system price of 189 €/kWh is assumed. Together with the differential capacity loss, the monetary loss can be estimated.

4.7 Optimization

The economic viability of the proposed pool configurations (section 4.2) strongly depends on the submitted capacity bid and energy bid prices. This section presents the optimization approach of finding the most economic bid tuple for an individual pool configuration. Subsection 4.7.1 calculates the boundaries passed to the optimizer, subsection 4.7.2 derives an aFRR request time series based on a prediction of the total request duration (section 3.2), subsection 4.7.3 describes the objective function and subsection 4.7.4 briefly presents the algorithm of the solver.

4.7.1 Boundaries

For each aFRR product type under consideration, the search space of the optimization problem consists of a capacity price and an energy price. Both optimization variables are subject to certain boundaries applied in this work.

Currently, the aFRR regulations do not limit the capacity price, which in theory allows price offers between $\pm\infty$. In practice, however, capacity prices have not been negative and a capacity price of 0 €/MW corresponds to a very high acceptance probability in the auction process. This work sets the lower boundary to 0 €/MW and the upper boundary to 100 €/MW.

Due to energy price gambling in the past, the energy price has been regulated to be within ± 9999 €/MWh. This work further restricts the energy price to be not lower than the minimum intraday price payed during the aFRR period under consideration. If more revenues can be generated on the intraday market, there is no incentive to participate in the aFRR market. In addition, the energy price is forced to be higher than the cyclic ageing costs of the battery. Based on a full cycle analysis, the differential costs for charging and discharging 1 MWh of energy are derived from the battery model presented in section 4.6. Calendric ageing costs are excluded in the lower boundary since economic benefits can be achieved even if not the full calendric ageing costs are compensated. The upper boundary of the energy price is set to the highest energy bid of the past month.

4.7.2 Estimation of the aFRR Request Time Series

Since the accurate aFRR request time series is unknown at the time an aFRR bid tuple must be submitted, this section derives a strategy to predict an exemplary time series that can be used by the optimizer to estimate the revenues. The first step in deriving a time series is to obtain a prediction for the total expected aFRR request duration.

A prediction methodology for deriving key quantities of the aFRR market was presented in section 3.2. To obtain a prediction of the total aFRR request duration, the list of successful bids is first sorted ascending by energy price (merit order) and then grouped into 10 blocks

of equal capacity (MW). If the total tendered capacity is e.g. 1880 MW, each block covers 188 MW. For each of the 10 blocks, two prediction models are trained with data of the past. The first model is used to predict the mean energy price and the second model is used to predict the mean total aFRR request duration. Both models return a prediction for the next day. Figure 4-7 illustrates the prediction methodology for an exemplary day and aFRR product type. Each value marked with a cross represents the mean energy price prediction and each encircled value represents the prediction of the mean request duration. For an arbitrary choice of energy price, the corresponding request duration is graphically obtained as follows:

1. All energy price predictions are linearly interconnected (dashed line in Figure 4-7). Every possible energy price chosen by the optimizer is located somewhere on the dashed interconnection line. Possible positions are between two predicted energy prices, left from the first block mean value or right from the last block value.

2. All request duration predictions are linearly interconnected (continuous line in Figure 4-7). Starting from the position of the energy price, a vertical line is drawn until the continuous request duration line is crossed. The intersection point marks the desired request duration corresponding to the energy price.

In summary, the predicted request duration is obtained by linearly interpolating between the energy price predictions and the request duration predictions.

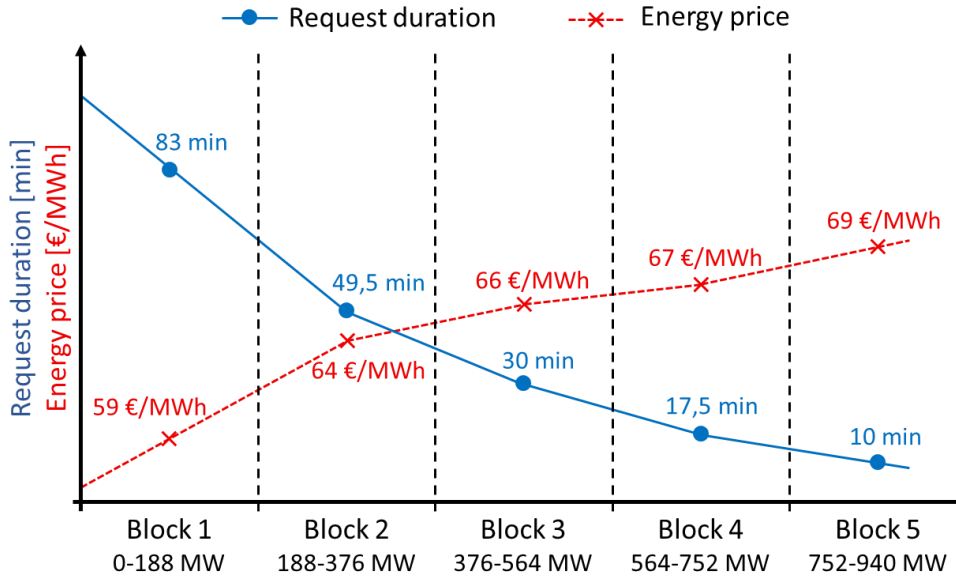

Figure 4-7: aFRR prediction methodology: Total request duration and energy price.

After having obtained a prediction for the total request duration, a high resolution time series must be generated which can be fed into the operating strategy. The process of

mapping one value to a high resolution time series involves many degrees of freedom. It is impossible to accurately predict the future request time series. However, the pattern of the time series influences the battery ageing. Long lasting continuous requests correspond to deep cycles and an increased capacity loss whereas many short requests correspond to less stress on the battery. In this work the following approach was conducted: The first hour of the total request duration is assumed to be continuously requested. All remaining time is assumed to be requested in multiple small cycles for the battery. This request distribution represents one an arbitrary realization which aims at not beeing extreme in any direction regarding battery ageing.

4.7.3 Objective Function

For each possible combination of capacity and energy price, the objective function is able to calculate the expected revenues by applying the operating strategy as described in section 4.5. As opposed to the approach presented in [15], a separate optimization process is conducted for each aFRR product type. This reduces the number of optimization variables to two (capacity and energy price). Aside from the significantly reduced computation time, a minor drawback is that arbitrage trading can only be considered within one aFRR product type range. However, when evaluating the overall profit based on the true auction outcome (section 4.9), arbitrage trading spanning multiple aFRR product types is considered.

In search of the maximum revenues, the optimizer samples various combinations of capacity and energy prices. As described in section 3.7, the acceptance probability $G(B_{\mathrm{C}}, B_{\mathrm{E}})$ depends on the choice of capacity price B_{C} and energy price B_{E}. For each choice, two outcomes are possible. Either the aFRR bid tuple is accepted or not. Equation (48) states the objective function which calculates the total expected revenues B_{Total} as a function of P_{C} (offered aFRR capacity), B_{C} and B_{E}. Table 4-3 describes each component of the objective function.

$$\begin{aligned} B_{\mathrm{Total}}(P_{\mathrm{C}}, B_{\mathrm{C}}, B_{\mathrm{E}}) &= G(B_{\mathrm{C}}, B_{\mathrm{E}}) \cdot \\ \big(B_{\mathrm{CaFRR}}(P_{\mathrm{C}}, B_{\mathrm{C}}) &+ B_{\mathrm{EaFRR}}(P_{\mathrm{C}}, B_{\mathrm{E}}) + B_{\mathrm{DA}} + B_{\mathrm{ID}} - C_{\mathrm{IdleGen}} - C_{\mathrm{BESSAge}}\big) \\ &+ \big(1 - G(B_{\mathrm{C}}, B_{\mathrm{E}})\big) \cdot (B_{\mathrm{DANoaFRR}} + B_{\mathrm{Arbitrage}} - C_{\mathrm{BESSAgeNoaFRR}}) \end{aligned} \tag{48}$$

The first summand of the objective function describes the case in which a successful bid tuple was submitted. All revenues generated from the operating strategy in section 4.5.3 are multiplied by the expected acceptance probability. The second summand covers the opposite case by multiplying the inverse probability with the revenue potential if no aFRR obligation exists. By using the optimization algorithm described in subsection 4.7.4, a bid tuple is searched which maximizes the total expected revenues B_{Total}.

Table 4-3: Components of the objective function

Variable	Meaning
$G(B_{\mathrm{C}}, B_{\mathrm{E}})$	Acceptance probability for a specific bid tuple in the aFRR auction. Depending on the auction design, this is a function of B_{C} only or of B_{C} and B_{E} (mixed price).
P_{C}	Offered aFRR capacity in MW
$B_{\mathrm{CaFRR}}(P_{\mathrm{C}}, B_{\mathrm{C}})$	Capacity based aFRR revenue based on P_{C} and B_{C}.
$B_{\mathrm{EaFRR}}(P_{\mathrm{C}}, B_{\mathrm{C}})$	Energy based aFRR revenue based on P_{C} and B_{E}.
B_{DA}	Revenues raised on the day-ahead market for trading some of the generation capabilities of the pool (section 4.5.3).
B_{ID}	Revenues raised on the intraday market resulting from trading the reserve band as explained in subsection 4.5.3.
C_{IdleGen}	Sum of marginal costs for activating the idle capacities of generation units (section 4.5.3).
C_{BESSAge}, $C_{\mathrm{BESSAgeNoaFRR}}$	Differential ageing costs for the BESS. This includes ageing of the battery cells due to calendar and cyclic ageing (section 4.6) as well as ageing of all other components in the system (section 4.4).
B_{DANoaFRR}	Revenues raised on the day-ahead market for periods without aFRR obligations (section 4.5.4).
$B_{\mathrm{Arbitrage}}$	Arbitrage revenues yielded on the intraday market for periods without aFRR obligations.

4.7.4 CMA-ES Optimization Algorithm

The calculations involved in evaluating the objective function are rather complex. For each evaluation, the operating strategy is executed which in turn includes the battery model and depends on the wholesale market prices, the relatively random aFRR call pattern and the generation capabilities of the pool. Because of this complexity, a direct formula to determine the perfect bid tuple does not exist. The optimization problem can be described as non-linear, derivative-free, not necessarily convex and potentially ill-conditioned.

In this work, the Covariance Matrix Adaption Evolutionary Strategy (CMA-ES) Optimizer is used [250]. CMA-ES is a flexible yet robust algorithm to solve black box problems. The algorithm belongs to the class of evolutionary strategies. These optimizers create a population of candidate solutions (individuals) which are spread out according to a multivariate normal distribution and the value of the objective function. In each iteration (generation) new individuals are generated which are closer to the optimum. CMA-ES has been successfully applied in numerous applications [251]. It has the convenient property of only having very few parameters to be set. This includes an initial solution guess, an initial

step size, boundaries for the search space and a population size (candidate solutions per iteration). The main challenge is to define a population size as such that a good trade-off between accuracy and calculation time is found. A too small population size potentially misses maxima while a too large population requires unnecessarily long calculations. In this work, a population size stated by equation (49) and recommended by [252] was followed. The number of optimization variables is represented by n_s.

$$n_{\mathrm{PopulationSize}} = 4 + 3 \cdot \ln(n_s) \tag{49}$$

4.8 Multi Agent Software Framework

Multi-agent environments are frequently used in the analysis of market structures in which participants can interact with one another. In this work, the JADE multi-agent environment developed by Telecom Italia Lab is used [253]. It allows the creation of so-called agents, which are individual software components able to interexchange messages with one another. Agents are executed simultaneously, each in an individual thread.

Figure 4-8 illustrates a flowchart of how agents interact when simulating an aFRR auction. The steps are as follows:

1. The Management Agent triggers an auction for a specific date and provides global parameters for the simulation.

2. The Auction Agents mimics the behavior of the TSOs by conducting the procurement process. Agents capable of providing aFRR are requested to submit a bid tuple.

3. Bidding Agents wishing to participate in the auction request data from the Data Agents. This data includes for example aFRR related data or prices on the wholesale market. Concurrently, data is requested from the Prediction Agents, which provide aFRR market prediction quantities for the corresponding date.

4. Data is received from the Data Agents and the Prediction Agents. The internal optimization process of the Bidding Agent is triggered to obtain the individual best bid tuple.

5. All bid tuples from participating Bidding Agents are send to the Auction Agent to evaluate which bids won the auction. A detailed revenue analysis as of section 4.9 is conducted.

The following subsections provide a more detailed description of each agent.

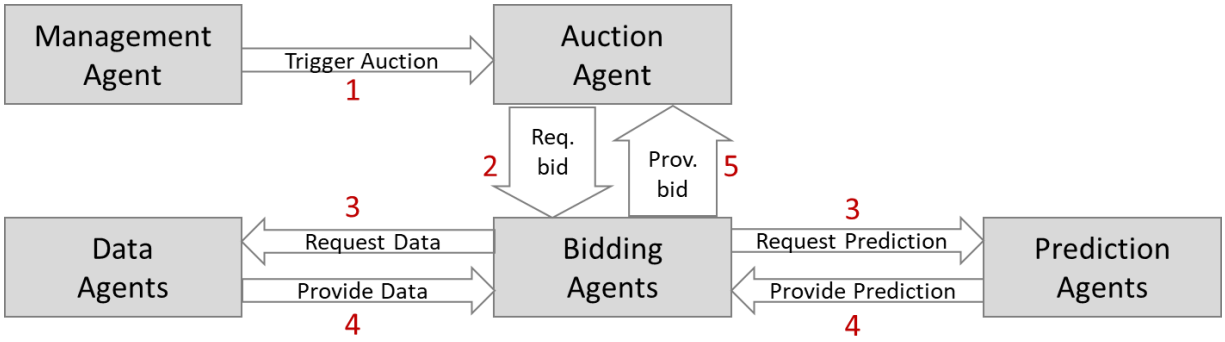

Figure 4-8: Schematic of the multi-agent framework for the aFRR market simulation

4.8.1 Management Agent

The Management Agent is the first instance that is executed within the developed software framework. Aside from the simulation period, the pool configuration (section 4.2) and market parameters (subsection 4.5.1) are defined. All subsequent agents are instantiated as well.

4.8.2 Auction Agent

The Auction Agent conducts the procurement and auction process for the aFRR market. It mimics the functionality of the web platform regelleistung.net operated by European TSOs. Auctions are instantiated, bids are received from all participants and successful bids are published.

4.8.3 Data Agents

Three different Data Agents provide access of historic data to the other agents in the framework. The first Data Agent parses relevant historic aFRR market data, which includes request time series, anonymous bids and mixed price factors. Pricing information of the intraday and day-ahead market is provided by the second agent. The third Data Agent covers generation profiles of various technical facilities such as thermal power plants or renewable generation.

4.8.4 Prediction Agents

The Prediction Agents used in this work implement the prediction methodology of the aFRR market as described in section 3.2. Each Bidding Agent can benefit from the predictions of the next day. The quantities being predicted include the aFRR capacity price, the aFRR mixed price, the aFRR energy prices and the aFRR request durations.

4.8.5 Bidding Agents

Bidding Agents participate in the auction process by submitting a bid tuple to the Auction Agent. This work considers two different types of Bidding Agents.

The first type mirrors the behavior of submitted bids in the real market. Each agent represents one historical bid tuple. This approach was followed because too little information is available about each market participant to derive the respective bidding strategy. Because of the anonymous bid result publishing, it is not even possible to track a participant across multiple consecutive auctions. Deriving bidding strategies based on incomplete information would thus decrease the reliability of the simulation results.

The second type of Bidding Agents implements the strategy as explained in this chapter. This includes amongst others the operating strategy (section 4.5), the battery model (section 4.6) and the optimization process for obtaining a bid tuple (section 4.7).

4.9 Simulation Output

This section describes the result output data, which is generated by running the aFRR simulation. For each submitted bid (including historical bids), the revenues generated on the aFRR market are derived. The total revenue stream is divided into capacity price based revenues and energy price based revenues for each aFRR product type.

For the bidding and operating strategy presented in this chapter, a detailed revenue and cost analysis is generated. The first part of the analysis provides a summary for a full day. This includes traded energy on each market (intraday and day-ahead), money exchanged on each market (intraday and day-ahead), marginal costs due to recharging from idle generation capabilities, differential battery ageing costs, battery capacity loss, differential system ageing costs, revenues for each aFRR product type (both capacity and energy price based), taxes and overhead due to annuity payments.

Further, a time series data file is written which at a 15-minute resolution includes the requested aFRR energy, SoC of the BESS, profile of the generation pool, traded energy on both intraday and day-ahead market and recharges from idle capabilities.

5 Results

This chapter is based largely on two previous publications of the author and is divided into two parts [5,224]. Section 5.1 presents the aFRR market prediction results, which serve as an input for the proposed bidding strategy. Building on these results, section 5.2 presents the simulation results of a battery storage system participating on the aFRR market by using the proposed bidding strategy of chapter 4.

5.1 Electricity Market Prediction

Following the market prediction methodology described in section 3.2, three different prediction quantities are considered. Subsection 5.1.1 presents prediction results of various models for the marginal mixed price. Results for predicting the average energy price for a group of participants can be found in subsection 5.1.2. Predictions on the deployment duration are presented in subsection 5.1.3. All predictions and simulations are conducted for the time period between October 20th, 2018 and June 20th, 2019.

5.1.1 Mixed Price Prediction

Since a separate aFRR auction is held for each of the six negative and positive time slices, twelve marginal mixed prices are subject to prediction. The following four subsections analyze the prediction results for each of the four models presented in section 3.13. A detailed result presentation is provided for the NEG_00_04 and POS_08_12 aFRR product. These two products serve as examples for all aFRR product types and were chosen randomly. An overall result summary for each aFRR product and prediction model is provided in subsection 5.1.1.5.

5.1.1.1 Exponential Smoothing

This subsection is structured as follows: Starting with the NEG_00_04 product, results for the persistence and exponential smoothing model are presented. The same steps are repeated for the POS_08_12 product.

Table 5-1 lists the performance of various exponential smoothing models on the time series. The first nine columns represent parameters of the model as described in section 3.13.2. If a model parameter is set to “auto”, it is automatically optimized by the underlying framework with respect to the properties of the time series. Both, the trend and seasonal component can be either additive (“add”) or multiplicative (“mul”). The latter six columns state the error measures as described in section 3.8 for both training and test set. The best performance on a particular error measure in is printed in bold.

Table 5-1: Performance of five best exponential smoothing models and persistence model (last row) on the NEG_00_04 product.

α	β	γ	φ	trend	damped	seasonal	seasonal periods	boxcox	$RMSE_{train}$	$RMSE_{test}$	MAE_{train}	MAE_{test}	Dir_{train} [%]	Dir_{test} [%]
auto	auto	auto	auto	mul	no	mul	7	yes	**23.7**	27.6	**13.4**	13.4	56	57
auto	auto	auto	auto	add	no	mul	7	yes	23.8	**26.5**	13.7	12.4	54	**62**
auto	auto	auto	auto	none	no	mul	7	yes	23.8	**26.5**	13.7	12.4	54	**62**
auto	auto	auto	auto	add	yes	mul	7	yes	23.8	26.6	13.7	12.4	54	**62**
auto	auto	auto	auto	none	no	add	7	yes	24.0	26.6	13.8	**12.1**	**59**	**62**
1	0	0	0	none	no	none	0	no	30.0	28.4	15.4	14.0		

An 85 %/15 % training/test set division was applied. The persistence model (subsection 3.13.1) is a special case of the exponential smoothing model with a parameter set as given by the last row of Table 5-1. Due to the simplicity of the model, all corresponding error measures serve as a reference for more sophisticated models.

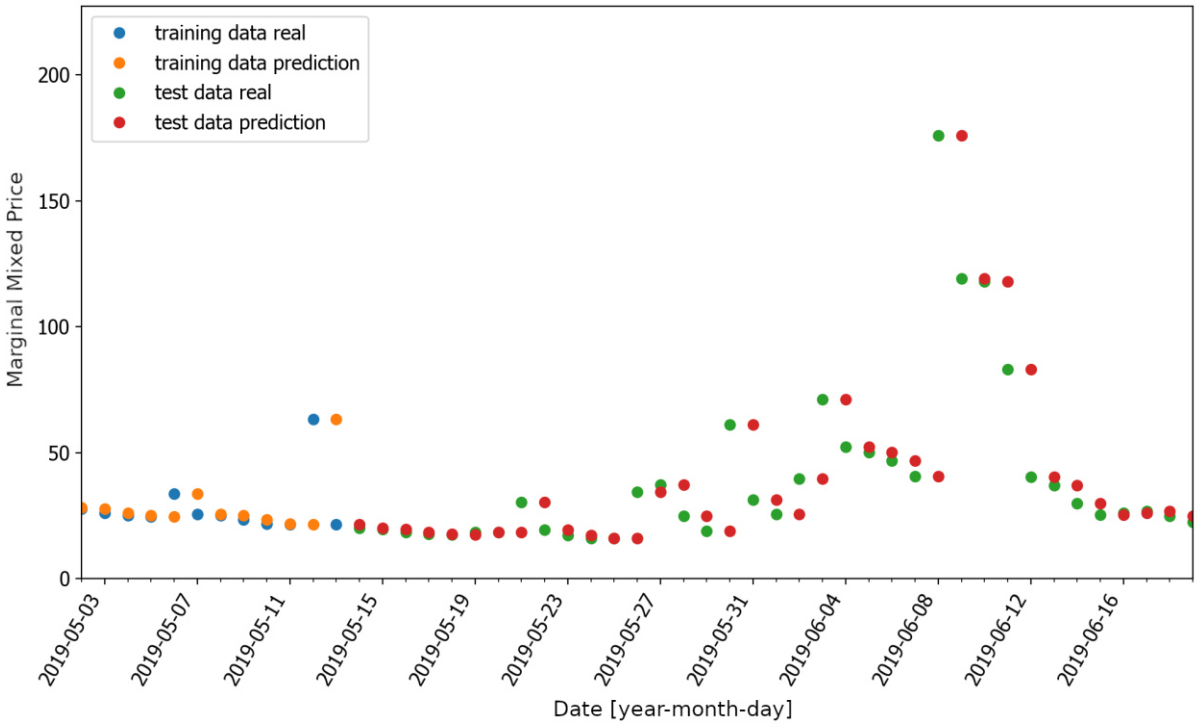

Figure 5-1: One-step ahead forecasts of the persistence model. The figure shows an extract of the full time series for the NEG_00_04 product. For both training and test data, real values and forecasts are illustrated.

Figure 5-1 illustrates the last 50 days of the time series with corresponding one-step ahead predictions of the persistence model. Each predicted value is equal to the corresponding real time series value one time step (day) backwards.

A detailed residual analysis of the persistence model on the test set is illustrated by the four plots in Figure 5-2. Reference is made to section 3.12, which states four properties indicating a good model fit. None of the spikes in the bottom right correlogram is above the significance level illustrated by the blue shaded area, thus indicating uncorrelated residuals. With a value of 0.03, the mean of the residuals is close to zero. As illustrated by the histogram and the Q-Q plot, residuals are not normally distributed. In particular, the mid-June 2019 spike was not captured well by the model. Overall, the persistence model performs remarkably well on the time series. The strong correlation with the previous time step indicates that bidders make strong use of previous auction outcomes rather than relying on external factors or variable costs. However, the results encourage applying more sophisticated models, which could reveal even better results.

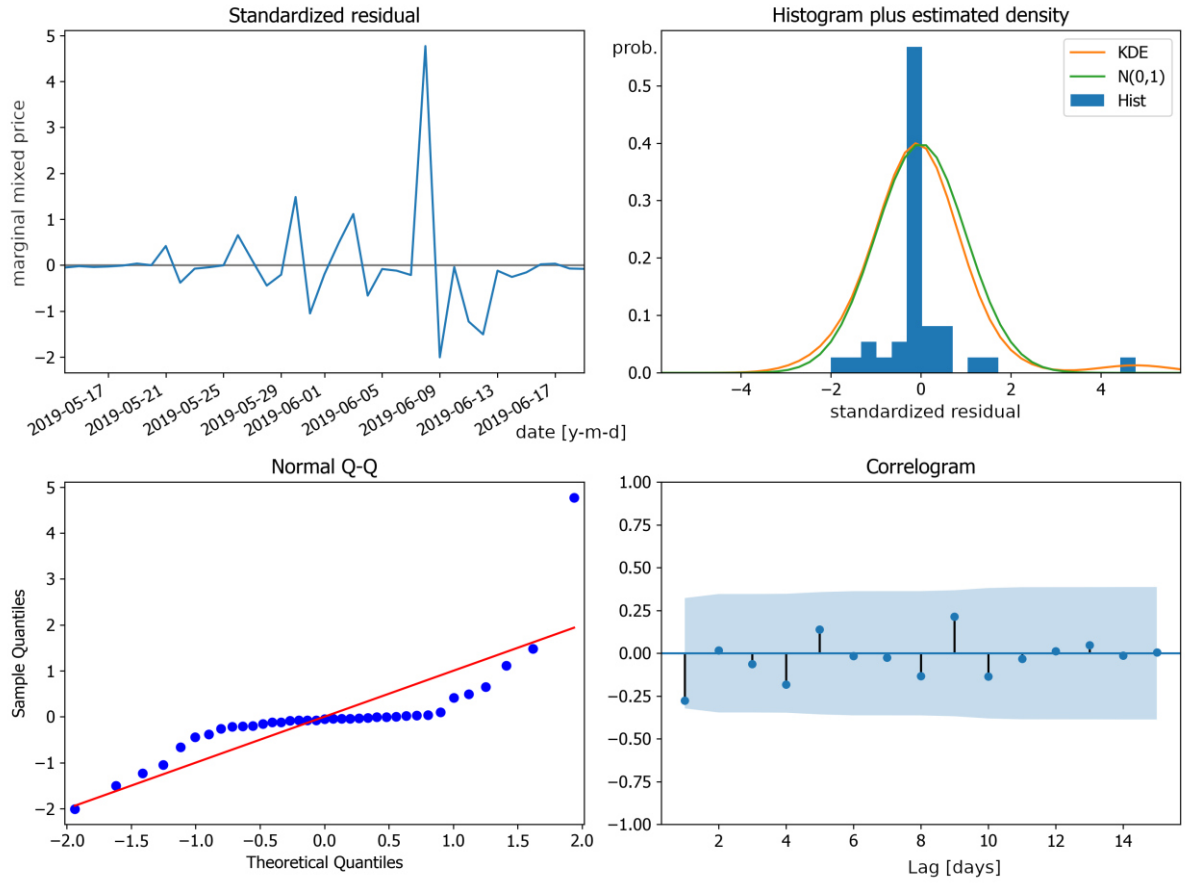

Figure 5-2: Residuals of the persistence model on the NEG_00_04 product.

As for the exponential smoothing model, all possible parameter combinations were evaluated (grid-search). Subsection 3.13.2 describes the parameters in more detail. The first

five rows of Table 5-1 show the best performing parameter sets according to the MAE of the training set. The model with the lowest MAE_{train} value is shown in the first row. Best model selection is based on the MAE to prevent overweighting the effects of outliers present in the time series. Outliers have a stronger influence on the RMSE than on the MAE. This thesis favors predictions that over a wide range of data samples are close to the true values as opposed to lucky guesses of outliers. Since the exponential smoothing model only has very few internal parameters, overfitting is less a problem than for more complex models such as neural networks. A separate validation set is therefore not required and model selection can be done by considering the performance on the training set. The performance of the test set must not be used for model selection since this corresponds to fitting to the test data, which subsequently falsifies conclusions on unseen data. All five best models have very similar performance values across the various measures. Notably, the best model in terms of performance on the training set is does not yield the best performance on the training set data. Common to the five best models is the weekly seasonality and the applied Box-Cox transformation. Whether the trend or seasonal component is additive or multiplicative does not significantly influence the performance.

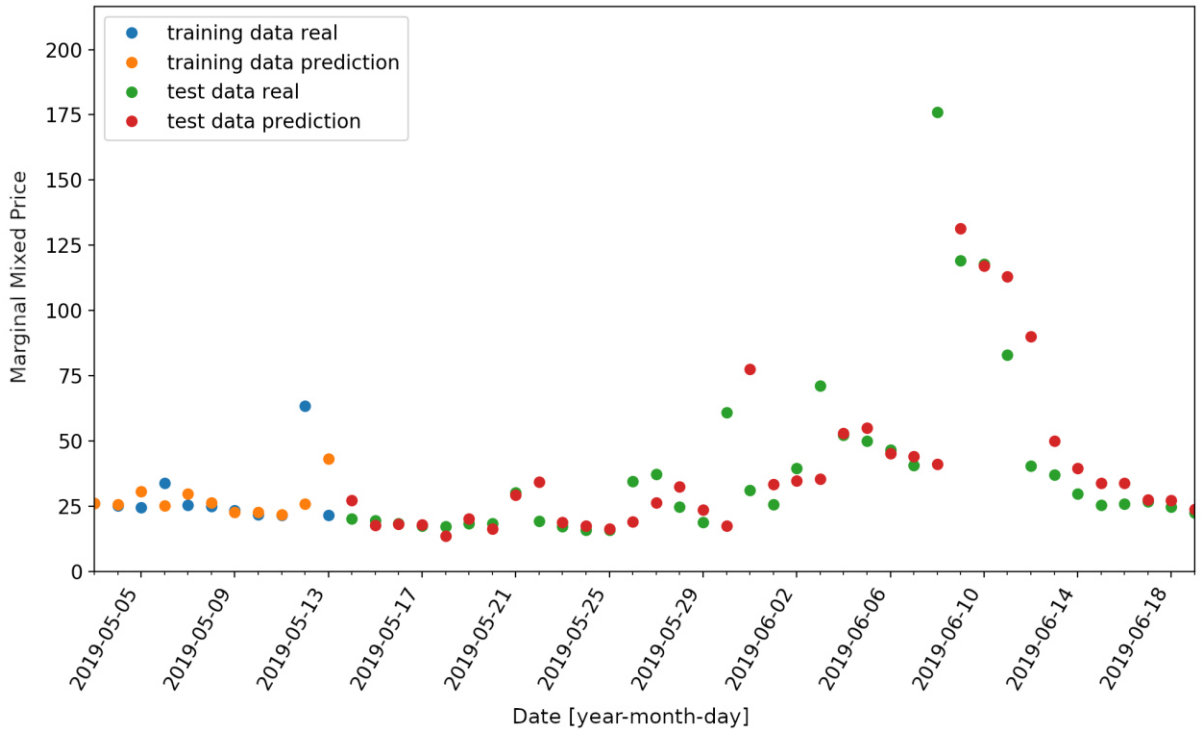

Figure 5-3: One-step ahead forecasts of the exponential smoothing model that yields the best performance on the training set. The figure shows an extract of the full time series for the NEG_00_04 product. For both training and test data, real values and forecasts are illustrated.

As expected, though, the performance of the best exponential smoothing model is better than the performance of the persistence model. However, as illustrated by Figure 5-3, not all trends are predicted accurately with the highest deviation at the outlier in mid-June 2019. Residuals, as illustrated by the four plots in Figure 5-4, are similar to the residuals of the persistence model. However, both the histogram and the Q-Q plot reveal a slightly more Gaussian-like distribution.

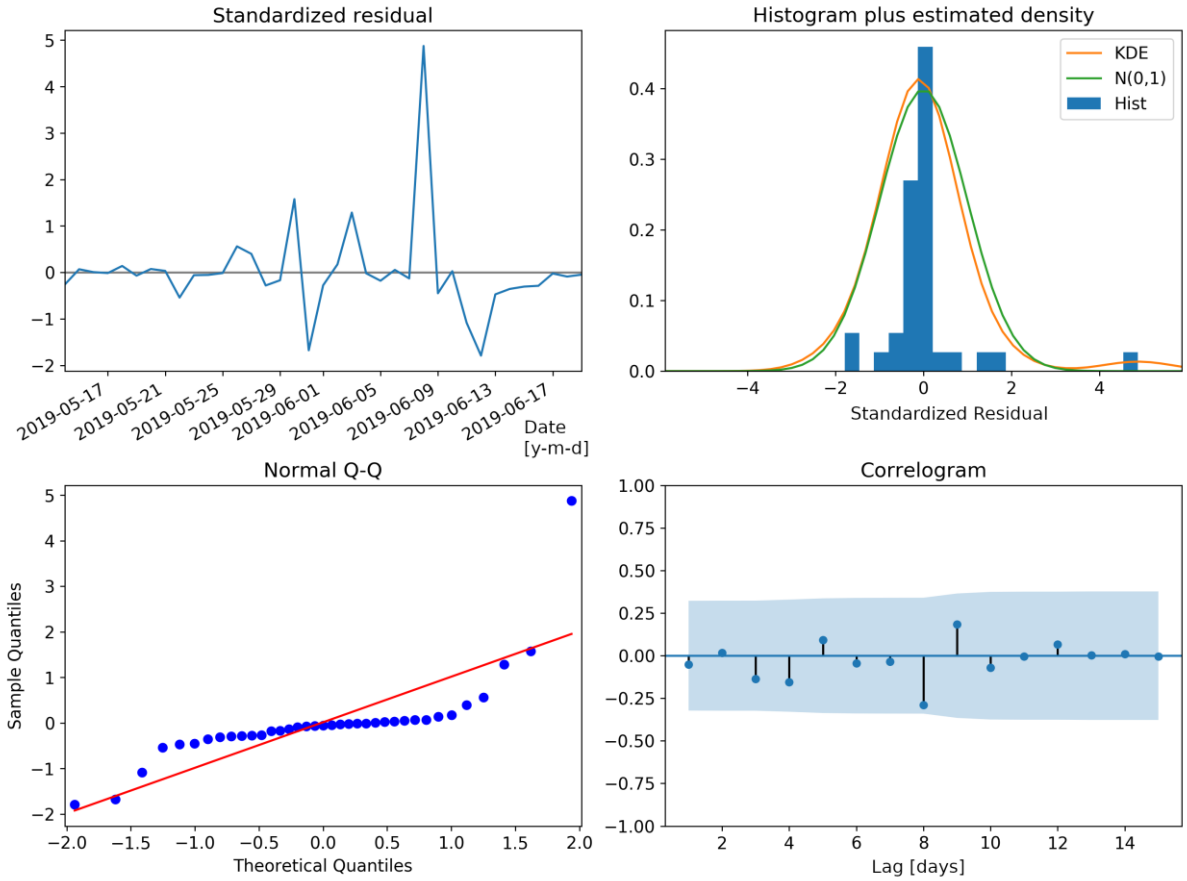

Figure 5-4: Residuals of the exponential smoothing model that yields the best performance on the training set for the NEG_00_04 product.

Table 5-2 summarizes the results of the three best performing exponential smoothing models and the persistence model on the POS_08_12 marginal mixed price time series. In terms of the training set errors, the exponential smoothing models perform better than the persistence model. Surprisingly, the two models with the lowest errors ($RMSE_{train}$ and MAE_{train}) on the training data perform worse on the test set data than the persistence model.

Table 5-2: Performance of three best exponential smoothing models and persistence model (last row) on the POS_08_12 product.

α	β	γ	φ	trend	damped	seasonal	seasonal periods	boxcox	$RMSE_{train}$	$RMSE_{test}$	MAE_{train}	MAE_{test}	Dir_{train} [%]	Dir_{test} [%]
auto	auto	auto	auto	add	no	mul	7	yes	**17.5**	7.0	**7.7**	4.8	**67**	62
auto	auto	auto	auto	none	no	mul	7	yes	**17.5**	7.0	**7.7**	4.8	**67**	62
auto	auto	auto	auto	mul	no	none	0	yes	18.6	**6.0**	8.4	**4.1**	52	**68**
1	0	0	0	none	no	none	0	no	22.6	6.2	9.5	4.3		

5.1.1.2 Seasonal Autoregressive Integrating Moving Average

Together with the parameters as explained in subsection 3.13.3, Table 5-3 lists the five best performing SARIMA models. The best models were obtained by conducting a grid-search over a wide parameter range. In comparison with one another, the models achieve very similar performance. All models have in common that autoregressive predictors up until order 9 (parameter p) are used and differencing is not applied (parameters d and D). The order of the moving average component (parameter q) does not significantly influence the outcome. In addition, seasonal components do not increase the performance.

Table 5-3: Performance of five best SARIMA models on NEG_00_04 product

p	d	q	P	D	Q	m	$RMSE_{train}$	$RMSE_{test}$	MAE_{train}	MAE_{test}	Dir_{train} [%]	Dir_{test} [%]
9	0	3	0	0	0	0	**24.5**	27.9	**14.0**	15.4	**49**	51
9	0	2	0	0	0	0	**24.5**	27.8	**14.0**	15.4	**49**	51
9	0	1	0	0	0	0	24.6	**27.7**	14.1	15.3	**49**	52
9	0	0	0	0	0	0	24.6	**27.7**	14.1	15.3	**49**	52
9	0	4	0	0	0	0	24.6	28.3	14.1	**15.0**	**49**	**57**

Comparing the performance of the SARIMA models with the persistence model reveals a better performance on the training data but worse performance on the test data. This is confirmed by *Figure 5-5* which illustrates high deviations between predictions and real values of the test set. The latter is surprising but might be due to overfitting the internal model parameters to the training data.

Residuals of the best performing SARIMA model are analyzed in Figure 5-6. The histogram and the KDE plot show a Gaussian-like distribution with certain deviations from an ideal

Gaussian distribution. Due to these deviations, native prediction intervals (see section 3.13.3) might not be accurate (see also Q-Q plot). The mean of the residuals is 1.79 for the training set and 1.59 for the test set. Latter non-zero means are due to price spikes not predictable by the SARIMA model and only occurring in positive direction. Downward spikes with very low mixed marginal prices are not present in the time series (see Figure 2-10). None of the spikes in the correlogram is above the significance level, thus changing model parameters is unlikely to improve the performance. The latter is verified by the grid-search parameter evaluation.

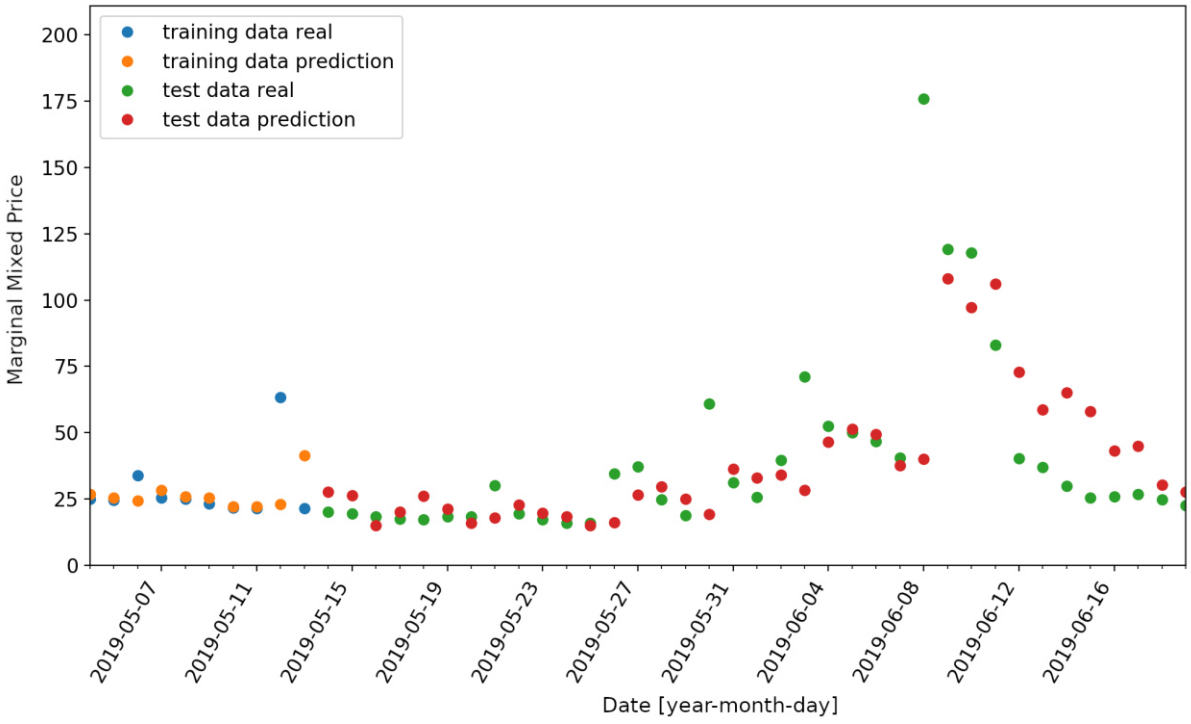

Figure 5-5: One-step ahead forecasts of the SARIMA model that yields the best performance on the training set. The figure shows an extract of the full time series for the NEG_00_04 product. For both training and test data, real values and forecasts are illustrated.

Applying various SARIMA models on the POS_08_12 time series reveals different results. The best-performing models as regards the MAE_{train} use autoregressive predictors of order 5 or 6 and no other SARIMA components. Other models with a higher or lower order of the p-parameter achieve slightly worse results. As with the NEG_00_04 time series, differencing is not applied and seasonal components are not used for best results. In terms of the MAE_{train}, all top five models perform better than the persistence model. On the test set however, only two models achieve similar or better results.

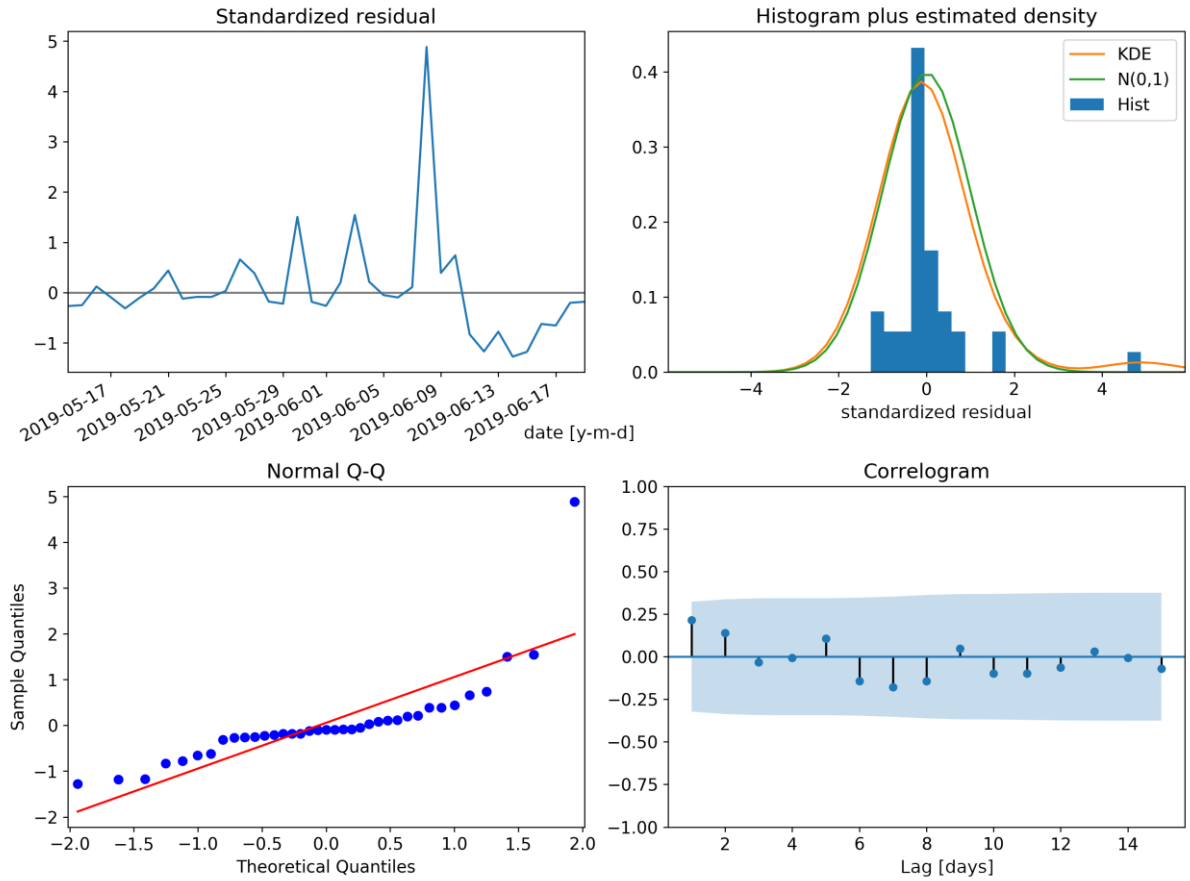

Figure 5-6: Residuals of the SARIMA model that yields the best performance on the training set of the NEG_00_04 product.

Table 5-4: Performance of the five best SARIMA models on the POS_08_12 product

p	d	q	P	D	Q	m	$RMSE_{train}$	$RMSE_{test}$	MAE_{train}	MAE_{test}	Dir_{train} [%]	Dir_{test} [%]
5	0	0	0	0	0	0	18.1	6.3	**8.2**	4.7	58	65
6	0	0	0	0	0	0	18.0	6.3	**8.2**	4.4	59	68
7	0	0	0	0	0	0	17.9	**6.1**	8.3	**4.2**	58	**70**
4	0	0	0	0	0	0	18.1	6.4	8.3	4.7	**60**	65
9	0	2	0	0	0	0	**17.7**	**6.1**	8.4	4.3	**60**	68

5.1.1.3 Neural Network

Due to the complexity of neural networks and the large hyperparameter space, a Bayesian hyperparameter optimization approach as described in section 3.10 was chosen. Table 5-5 gives an overview of the hyperparameter space available to the optimizer. In total, 800 models were evaluated for each aFRR product type to find well performing hyperparameter sets.

Table 5-5: Hyperparameter space used for Bayesian optimization of neural network models

Hyperparameter	**Parameter Range**
Feature vector	1,2,3,4,5
Normalization method	minmax, z-score
Hidden layers	1 – 70
Neurons	5 – 150
Activation function	ReLU, tanh
Learning rate	0.0 – 0.2
Batch size	1 – 40 (data samples)
Lasso regression (L1)	0.0 – 0.5
Ridge regression (L2)	0.0 – 0.5
Dropout	0.0 – 0.4
Loss function	MAE, MSE

The computational effort to train and evaluate a model depends on the model complexity (hyperparameter selection). On a 32-core Intel Xeon E5-4620 v2 CPU based system, the average processing time for a single model is 2 min, 20 s. Because of the high computational effort for each model, time series cross validation (see section 3.11) or ensemble learning with differently initialized weights were not applied during the hyperparameter optimization process. As described in section 3.4, samples of the time series are divided into a training (70 %), validation (15 %) and test (15 %) set. The validation set is used to early-stop the learning process to prevent overfitting to training data. Models are compared with one another based on the MAE performance on the validation set. Table 5-6 and Table 5-7 list different model realizations with the first three models representing those with the best MAE_{valid} performance (NEG_00_04 aFRR product type). The best performing models have some properties in common. They either use feature vector 1 or 4, which indicates that exogenous data sources (see section 3.3) support the prediction. Both aforementioned feature vectors include all data sources (see section 3.3). A detailed analysis as to which data sources contribute the most to the performance was not conducted. For most model evaluations, min-max normalization in combination with ReLU activation functions performed best. However, model 5 of *Table 5-6* yields a remarkably high performance with z-score normalization and tanh activation functions. Superior results are achieved on the RMSE of the validation and test set as well as on direction of change forecasting for the validation set (Dir_{valid}).

Model 4 has the same hyperparameter set than model 1 but for demonstration purposes uses time series cross validation to predict the test set samples. If cross validation is applied, the MAE on the test set decreases from 25.6 to 18.1. The latter is according to expectations, since more data samples are used during the learning process. However, the performance on the training and validation set unexpectedly decreases. In theory though, the

performance on the training and validation set should not change by cross validation since the process for obtaining predictions is the same.

Table 5-6: Hyperparameter configuration for six neural network models applied on the NEG_00_04 product.

Model	Feature vector	Normalization	Hidden layer	Neurons	Learning rate	Batch size	L1	L2	Dropout	Activation	Loss function	Cross validation
1	4	minmax	1	70	0.1	23	0.37	0.25	0.02	ReLU	MSE	no
2	4	minmax	5	38	0.01	23	0.07	0.03	0.03	ReLU	MSE	no
3	4	minmax	1	38	0.1	23	0.37	0.25	0.02	ReLU	MSE	no
4	4	minmax	1	70	0.1	23	0.37	0.25	0.02	ReLU	MSE	yes
5	1	z-score	1	51	0.1	32	0.37	0.26	0.01	tanh	MSE	yes
6	4	z-score	2	30	0.01	24	0.02	0.02	0.02	ReLU	MSE	no

Table 5-7: Performance of neural network models as defined in Table 5-6. Of all 800 model evaluations, the first three models perform best as regards the MAE_{valid}.

Model	$RMSE_{train}$	$RMSE_{valid}$	$RMSE_{test}$	MAE_{train}	MAE_{valid}	MAE_{test}	Dir_{train} [%]	Dir_{valid} [%]	Dir_{test} [%]
1	20.1	16.1	37.8	13.1	**7.7**	25.6	73	50	62
2	20.0	16.7	29.6	13.1	8.0	**16.2**	73	53	**70**
3	20.1	16.4	40.4	13.3	8.1	26.8	73	50	**70**
4	22.1	15.7	32.6	17.0	9.2	18.1	59	44	59
5	7.2	**14.0**	**29.0**	4.7	8.2	16.5	86	**61**	65
6	**1.4**	20.5	57.2	**1.1**	12.6	28.4	**93**	42	62

Most likely, the difference arises from the fact that weights in the neural network are initialized with different random values at each execution. As explained in the following, this thesis does not use a constant seed for the pseudorandom number generator. If the model is repeatedly evaluated with the same set of hyperparameters, each time a different result is obtained. In contrast, a constant seed would generate the same results in each run. However, using a constant seed does not capture the stochastic behavior of neural networks. In consequence, a preselected constant seed could just be lucky or unlucky outlier for a particular choice of hyperparameters and therefore give a very biased view on that particular choice of hyperparameters. The Bayesian hyperparameter optimization technique used in this work is capable of working with stochastic functions. It not just holds an

estimate of the true underlying function (outcome of neural network) but also captures information on how uncertain that estimate is. For variance estimation, a model can be evaluated multiple times. To present an insight into the variance associated with the random weight initialization, Table 5-8 gives an overview of 100 model evaluations (with differently initialized weights) for a hyperparameter set according to model 1.

Table 5-8: Statistical properties of 100 evaluations of the first NN model on the NEG_00_04 product type. Weights are randomly initialized for each training process.

	$RMSE_{train}$	$RMSE_{valid}$	$RMSE_{test}$	MAE_{train}	MAE_{valid}	MAE_{test}
Mean	20.3	16.1	38.9	14.3	8.6	24.5
Standard deviation	1.4	0.4	2.2	1.8	0.5	1.9

Most of the mean error measures are close to the error measures of the one specific model realization in *Table 5-7*. However, the mean MAE on the validation set with a value of 8.6 is much higher than the best performing models as of Table 5-7. Together with the standard deviation of 0.5, the one specific model appears to be a lucky outlier. The standard deviations in Table 5-8 quantify to which extend the performance varies with respect to the weight initialization.

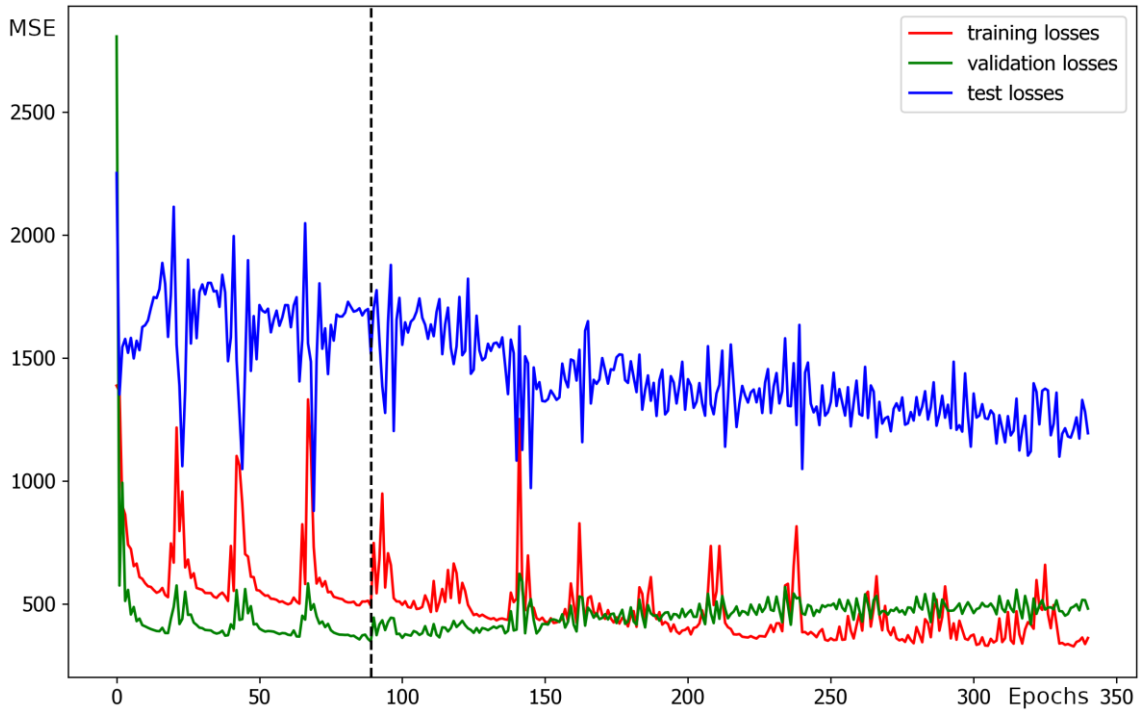

Figure 5-7: Epochs plot of the best performing neural network model.

All best performing models use MSE as a loss function during the training process. If instead MAE is used as the loss function, the model does not properly learn the dynamics of the time series and often returns the average time series value for all samples.

Further, the best performing neural networks are not deep and do not exhibit many neurons. All models in Table 5-6 have less than 5 hidden layers and less than 70 neurons per hidden layer.

No clear tendency as regards L1 and L2 regularization was observed since within the top 10 best performing models almost the whole hyperparameter range as of Table 5-5 is present. Dropout probability though is less than 0.15 for the top 10 best performing models.

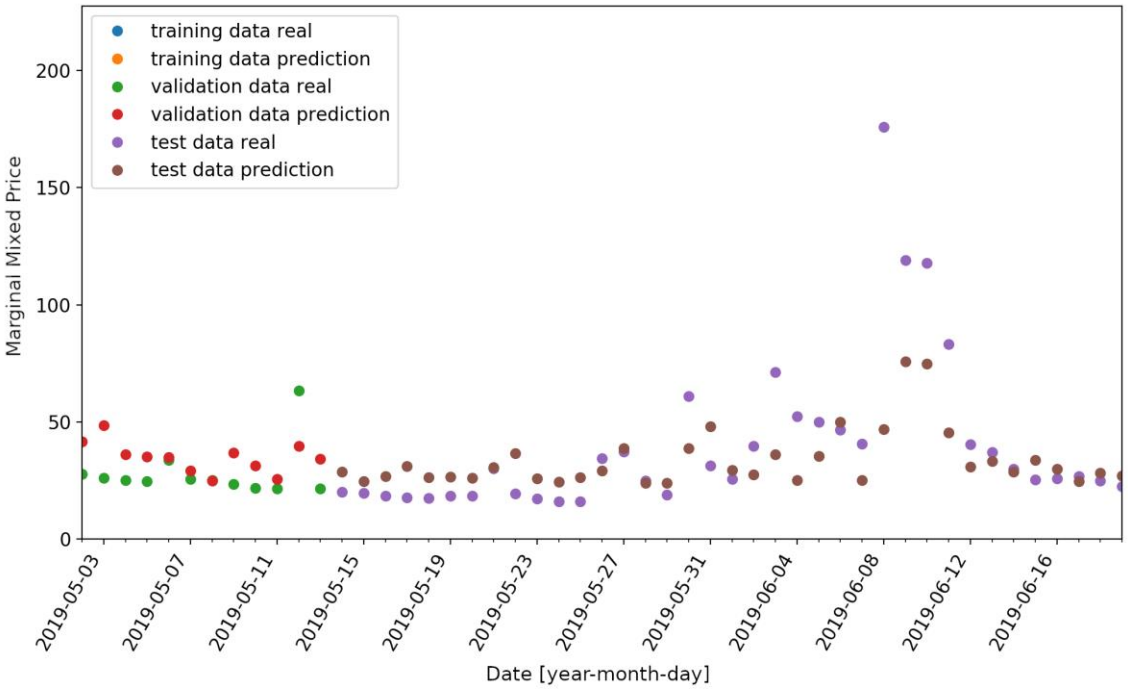

Figure 5-8: One-step ahead forecasts of the best performing neural network model. The figure shows an extract of the full time series for the NEG_00_04 product. Real values and forecasts are illustrated for both validation and test data.

Figure 5-7 illustrates the MSE performance on the three data sets over the training epochs of model one. Within each epoch, the full training set data is used once to adapt the weights of the neural network. After each epoch, the current weights are evaluated by calculating predictions (and error measures) for the training, validation and test data. Overfitting occurs if the training losses decrease and the validation losses increase. As indicated by the black dashed line (*Figure 5-7*), early stopping captures the neural network weights when performance on the validation set is best. Usually latter model weights perform best on unseen data such as the test set. However, Figure 5-7 reveals a continuous decrease in the test set error while the validation error is increasing. In addition, the test losses are by a

factor of 3-4 higher than the training and validation losses. This deviation is most likely due to the mid-June 2019 outlier and changes in the cause-and-effect relationship of the time series with exogenous data.

Figure 5-8 illustrates the real and predicted values of the best performing model. In around 62% of the predictions on the test set, the direction of change was correctly predicted. However, as with the exponential smoothing and SARIMA model, the mid-June outlier could not be predicted.

Model 6 (see Table 5-6) consists of 2 hidden layers, each with 30 neurons. The model was trained with early stopping deactivated and 12,000 epochs. A MAE of 1.1 on the training set suggests that the model complexity is sufficient to capture the behavior of the training samples. Of course, in this case the model overfits to training data and produces a large generalization error. Predictions and real values of model 6 on the training data are illustrated in Figure 5-9. The model is overfitted to the training data and reveals almost perfect predictions. However, performance on the test set is much worse (not visible in Figure 5-9).

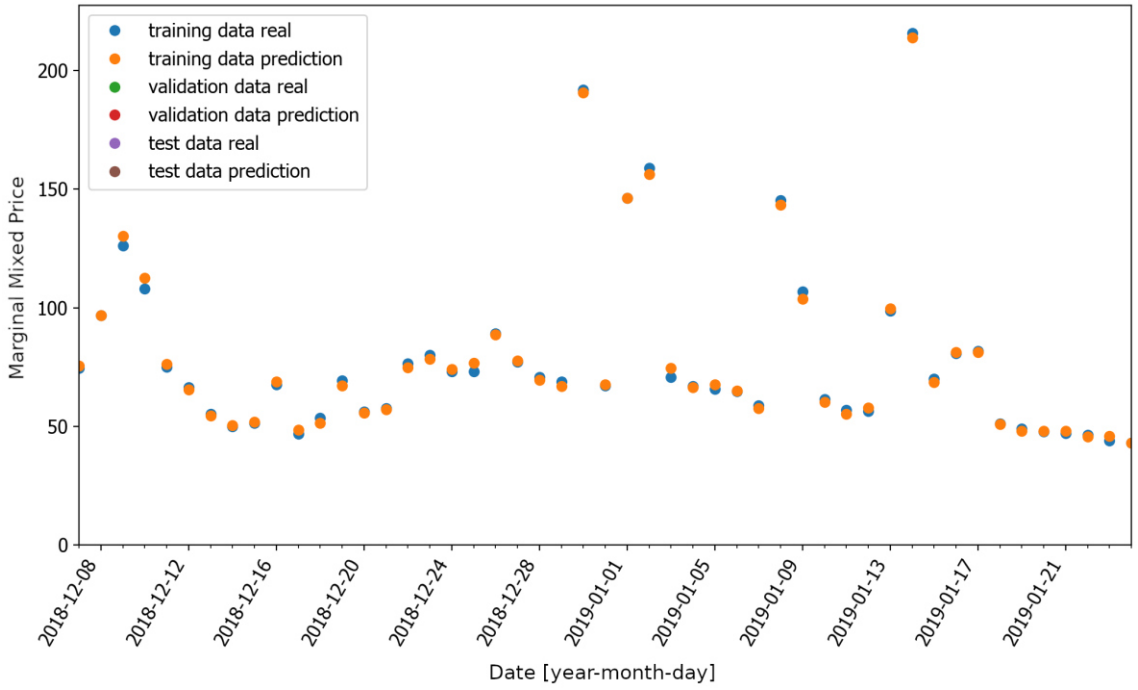

Figure 5-9: One-step ahead predictions of a neural network on the training data. The figure shows an extract of the full time series for the NEG_00_04 product. A model with 2 hidden layers and 30 neurons per layer was trained without early stopping and 12,000 epochs.

Results for the POS_08_12 product are illustrated in Table 5-9 and Table 5-10. Similar to the NEG_00_04 product, the best performing model has a small number of hidden layers and neurons. In addition, all data sources (feature vector 4) are used as predictors, MSE is used

as the loss function, ReLU activation functions are used and min-max normalization is applied. However, the 2nd to 4th best models have a significantly different set of hyperparameters. These models exhibit up to 63 hidden layers, have up to 116 neurons per layer, use MAE as the loss function and use different predictors. In particular, feature vectors 2 and 3 are used which do not contain any exogenous data sources except for date/ time related data (see section 3.3). The latter is surprising, since these models perform only slightly worse than the best performing model with all exogenous data sources. Latter finding also indicates that market participants are much more influenced by previous auction outcomes than by any other exogenous factors (weather, stock exchange, etc.).

Table 5-9: Hyperparameter configuration for the four best performing neural network models applied on the POS_08_12 product.

Model	Feature vector	Normalization	Hidden layer	Neurons	Learning rate	Batch size	L1	L2	Dropout	Activation	Loss function	Cross validation
1	4	minmax	5	38	0.01	23	0.25	0.19	0.27	ReLU	MSE	no
2	3	z-score	55	33	0.20	14	0.48	0.13	0.34	ReLU	MAE	no
3	3	zscore	63	116	0.08	29	0.35	0.35	0.11	tanh	MAE	no
4	2	minmax	34	77	0.14	24	0.31	0.31	0.31	tanh	MAE	no

Table 5-10: Performance measures of the four models described by Table 5-9.

Model	$RMSE_{train}$	$RMSE_{valid}$	$RMSE_{test}$	MAE_{train}	MAE_{valid}	MAE_{test}	Dir_{train} [%]	Dir_{valid} [%]	Dir_{test} [%]
1	**22.4**	**6.7**	**7.2**	**11.9**	**5.0**	**5.5**	63	61	**57**
2	23.0	6.9	7.4	12.3	5.1	5.6	63	58	**57**
3	23.0	6.9	7.4	12.3	5.1	5.6	63	61	**57**
4	23.0	6.9	7.4	12.3	5.1	5.6	**64**	**64**	**57**

5.1.1.4 Recurrent Neural Network

Due to the high computational effort to train recurrent neural networks and the large hyperparameter space, a Bayesian hyperparameter optimization approach as described in section 3.10 was applied. Table 5-11 gives an overview of the hyperparameter space available to the optimizer. Reference is made to subsection 3.13.5. The sequence length describes the number of previous time steps (lagged predictors) fed into each model for making one prediction. During the learning process, RNNs are unfolded sequence length times. The resolution of the predictors is introduced as a hyperparameter and can be

selected to be either daily or hourly. If the raw data is not in the target resolution, the data is either up- or down-sampled (see section 3.4). In total, 800 models were evaluated for each aFRR product type.

Table 5-11: Hyperparameter space used for Bayesian optimization of recurrent neural network models

Hyperparameter	**Parameter Range**
Feature vector	1,2,3,4,5
Normalization method	minmax, z-score
Sequence length	2 – 35
Resolution	daily, hourly
Cell type	Simple, LSTM, GRU
Hidden layers	1 – 70
Neurons	5 – 150
Activation function	ReLU, tanh
Learning rate	0.0 – 0.2
Batch size	1 – 40 (data samples)
Lasso regression (L1)	0.0 – 0.5
Ridge regression (L2)	0.0 – 0.5
Dropout	0.0 – 0.4
Loss function	MAE, MSE

The computational effort to train and evaluate a model depends on the selection of hyperparameters. On a 32-core Intel Xeon E5-4620 v2 CPU based system, the average processing time for a single model evaluation is 6 min, 41 s. Time series cross validation (see section 3.11) or ensemble learning with differently initialized weights were not applied during the hyperparameter optimization process. Samples of the time series are divided into a training (70 %), validation (15 %) and test (15 %) set (section 3.4). Table 5-12 and Table 5-13 list the five best model realizations with respect to the MAE_{valid} performance. The best performing models have some properties in common. All use feature vector 4 indicating that exogenous data sources (see section 3.3) support the prediction.

All best performing models use MSE as a loss function during the training process. If instead MAE is used as the loss function, the model does not properly learn the dynamics of the time series and often returns the average time series value for all samples. Table 5-12 suggests that the best performing RNNs are not deep and do not exhibit many neurons. All listed models have less than 5 hidden layers and less than 25 neurons per hidden layer. Denoted as “Simple” in Table 5-12, the Elman model (section 3.13.5, Figure 3-14) is dominantly present. However, among the top ten best performing RNNs, LSTM and GRU type models also reveal high performances. As of Table 5-12, the sequence length is in the order of a week. Best results are achieved with a daily data resolution for the predictors.

Table 5-12: Hyperparameter configuration for six recurrent neural network models applied on the NEG_00_04 product.

Model	Feature vector	Normalization	Cell type	Hidden layers	Neurons	Sequence length	resolution	Learning rate	Batch size	L1	L2	Dropout	Activation	Loss function
1	4	z-score	Simple	1	8	7	day	0.047	32	0.14	0.05	0.06	tanh	MSE
2	4	z-score	Simple	5	19	13	day	0.042	31	0.20	0.26	0.37	ReLU	MSE
3	4	minmax	Simple	2	24	8	day	0.009	6	0.11	0.02	0.05	ReLU	MSE
4	4	minmax	GRU	1	21	6	day	0.055	33	0.23	0.16	0.06	ReLU	MSE
5	4	minmax	Simple	1	24	6	day	0.041	17	0.19	0.01	0.13	ReLU	MSE

Table 5-13: Performance of recurrent neural network models as defined by Table 5-12. Of all 800 model evaluations, these models perform best as regards MAE_{valid}.

Model	$RMSE_{train}$	$RMSE_{valid}$	$RMSE_{test}$	MAE_{train}	MAE_{valid}	MAE_{test}	Dir_{train} [%]	Dir_{valid} [%]	Dir_{test} [%]
1	17.7	14.0	29.3	10.9	**6.6**	17.2	69	58	64
2	23.9	17.3	38.3	15.1	7.8	21.0	61	54	66
3	16.5	**12.4**	30.7	12.4	8.0	17.2	68	49	67
4	17.2	14.8	35.1	**10.8**	8.3	20.0	72	**61**	**78**
5	**15.5**	14.3	**26.8**	11.4	8.3	**14.1**	**70**	50	64

No clear tendency as regards L2 and dropout regularization was observed since within the top 10 best performing models, almost the whole hyperparameter range as of Table 5-11 was present. However, L1 regularization greater than 0.1 is present in all best performing models.

The characteristics of each trained model depends on the random initialization of weights within the RNN. Since this thesis does not make use of a constant random seed (pseudorandom number generator, see subsection 5.1.1.3 for explanation), 100 models with the same hyperparameter set but with differently initialized weights were evaluated. Table 5-14 shows the statistical properties for the best performing model as of Table 5-13.

Substantial deviations between the mean values of Table 5-14 and the model performance as of Table 5-13 can be observed. In addition, the standard deviations on the error measure are rather high, indicating a strong influence of the weight initialization. Model one of Table

5-13 appears to be a lucky outlier within the 100 model evaluations of the same hyperparameter set.

Table 5-14: Statistical properties of 100 evaluations of first RNN model on NEG_00_04. Weights are randomly initialized for each training process.

	$RMSE_{train}$	$RMSE_{valid}$	$RMSE_{test}$	MAE_{train}	MAE_{valid}	MAE_{test}
Mean	34.2	19.4	32.8	24.3	10.6	19.8
Standard deviation	14.2	3.4	3.5	12.5	2.0	2.3

Figure 5-10 illustrates the real and predicted values of the best performing RNN model. In around 64% of the predictions on the test set, the direction of change was correctly predicted. However, as with the other models, the mid-June outlier could not be accurately predicted.

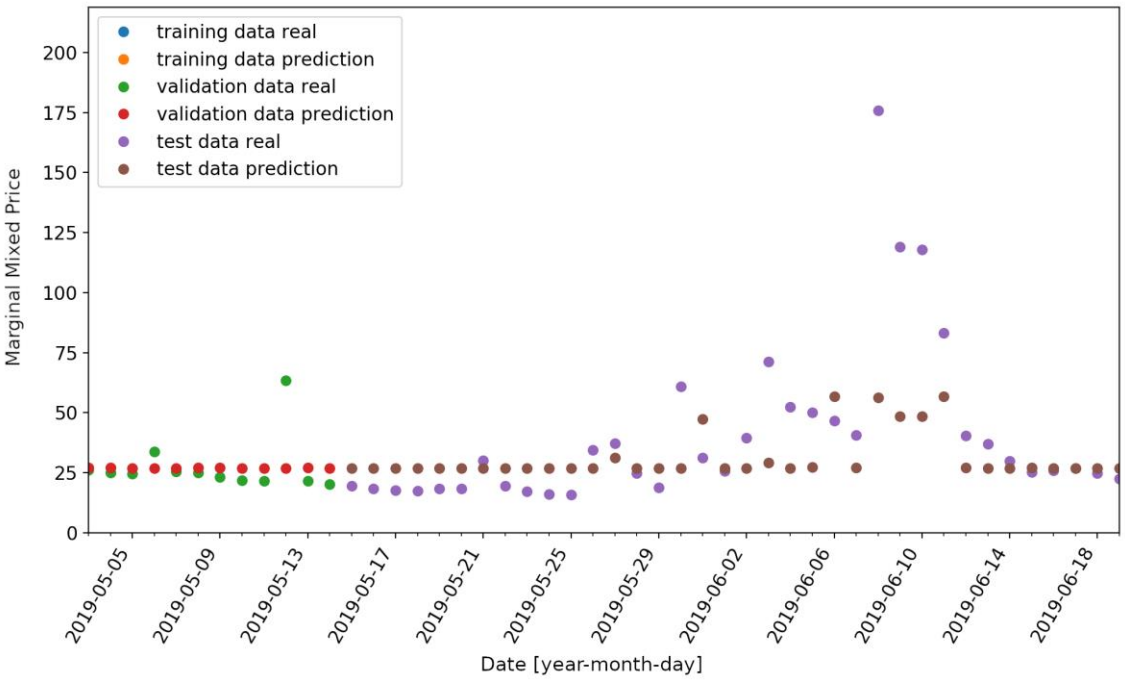

Figure 5-10: One-step ahead forecasts of the best performing recurrent neural network model. The figure shows an extract of the full time series for the NEG_00_04 product. Real values and forecasts are illustrated for both validation and test data.

The five best performing models on the POS_08_12 product are illustrated in Table 5-15 and Table 5-16. Similar to the NEG_00_04 product, the best performing model has a small number of hidden layers and neurons. Best performance is achieved with the Elman cell type but LSTM and GRU cells are also present in the top five. All have in common to use the

MSE loss function, ReLU activation functions and min-max normalization. As opposed to the NEG_00_04 case, the best performing model works on predictors with an hourly resolution and makes use of feature vector 5 which uses a reduced set of exogenous predictors. In addition, feature vector 3, which only includes the time series itself and time related data, is part of the top five list. In most best performing models, the sequence length covers data of at least 6 days. The sequence length for models operating on an hourly resolution must be 4 times as large (4 h per day and product) as corresponding models with a daily resolution.

Table 5-15: Hyperparameter configuration for five recurrent neural network models applied on the POS_08_12 product.

Model	Feature vector	Normalization	Cell type	Hidden layers	Neurons	Sequence length	resolution	Learning rate	Batch size	L1	L2	Dropout	Activation	Loss function
1	5	minmax	Simple	2	99	28	hour	0.011	34	0.15	0.39	0.31	ReLU	MSE
2	3	minmax	Simple	1	25	6	day	0.110	30	0.48	0.03	0.06	ReLU	MSE
3	4	minmax	LSTM	2	12	7	day	0.171	26	0.16	0.20	0.11	ReLU	MSE
4	4	minmax	LSTM	2	33	11	day	0.093	20	0.37	0.26	0.09	ReLU	MSE
5	3	minmax	GRU	2	97	16	hour	0.110	33	0.39	0.26	0.11	ReLU	MSE

Table 5-16: Performance of recurrent neural network models as defined by Table 5-15. Of all 800 model evaluations, these models perform best as regards MAE_{valid}.

Model	$RMSE_{train}$	$RMSE_{valid}$	$RMSE_{test}$	MAE_{train}	MAE_{valid}	MAE_{test}	Dir_{train} [%]	Dir_{valid} [%]	Dir_{test} [%]
1	**16.9**	**5.0**	10.3	11.8	**3.8**	7.2	58	67	61
2	20.7	5.8	**6.9**	**9.7**	3.9	**4.8**	**72**	67	**72**
3	18.3	5.4	10.9	10.7	3.9	8.8	59	**75**	58
4	23.0	5.3	9.5	16.8	4.2	7.3	49	57	69
5	18.2	5.8	7.3	9.9	4.2	5.5	60	58	61

5.1.1.5 Comparison and Summary

After each model type has been considered independently in the last subsections, this subsection compares the performances with one another and draws a conclusion. Table 5-17 offers a side-by-side comparison of all negative product types and all applied prediction

models. For each time series corresponding to a product type, one-step ahead predictions were conducted. Table 5-17 lists the best performance of each model type based on the error measures defined in section 3.8. The best performing model was obtained by evaluating the hyperparameter space as described in the corresponding model subsections. For instance, the neural networks were evaluated 800 times for each time series (see subsection 5.1.1.3).

Except for two cases, all models perform better than the persistence model in terms of the RMSE and MAE measure on the training set. Throughout, the best performance of all models on the training set is achieved by the neural network models. Apparently, the weights of the neural networks were successfully adapted to cover the properties of the training data. However, a good performance on the training set does not necessarily result in a good performance on the test set since in many cases the performance of more elaborate models is worse than the performance of the persistence model. On the NEG_08_12 product for instance, the persistence model performs best regarding the test set (MAE measure). Only for the NEG_12_16 product, the two neural network models outperform their contestants. For the remaining product types, either the exponential smoothing or the SARIMA model yield the best performance. In terms of predicting the direction of change, the two neural network models usually perform best. In summary, no clear winning model can be determined. Often the performances are rather close to one another. In a few instances, particular models perform significantly worse than others as it is the case for e.g. the exponential smoothing model on the test set of the NEG_08_12 product. The SARIMA model yields a decent performance over all products without any outliers.

Table 5-18 offers a side-by-side comparison of all positive product types and the performances of all applied prediction models. In contrast to the negative aFRR products, the neural network models perform worse on the training data than the competing models. As explained in subsection 5.1.1.3, the learning process stops early if the performance on the validation set does not further improve. This prevents a large generalization error and is the reason for the bad performance on the training set. However, for most products, the performance of the two neural networks on the test set is also worse than for the other models. In most disciplines, the exponential smoothing and SARIMA model outperform their alternatives. For the POS_08_12 product, the persistence model is ahead of the others. The high error measure magnitudes on the test set of the POS_12_16 product are due to an outlier in the marginal mixed price time series. On May 16th, 2019, the marginal mixed price reached a value of 107,710 (see subsection 2.1.2.4.1). In summary, none of the models shows superior performance regarding all disciplines. However, the exponential smoothing and SARIMA model provide more constant and usually better performance than their contestants.

Table 5-17: Result summary for all negative aFRR products and models on the marginal mixed price. The best performance is indicated in bold.

Product type	Model type	$RMSE_{train}$	$RMSE_{valid}$	$RMSE_{test}$	MAE_{train}	MAE_{valid}	MAE_{test}	Dir_{train} [%]	Dir_{valid} [%]	Dir_{test} [%]
NEG_00_04	Persistence	30.0		28.4	15.4		14.0			
	Exp. Smoothing	23.7		**27.6**	13.4		**13.4**	56		57
	SARIMA	24.5		27.9	14.0		15.4	49		51
	Neural Network	20.1	16.1	37.8	13.1	7.7	25.6	**73**	50	62
	Recurrent NN	**17.7**	**14.0**	29.3	**10.9**	**6.6**	17.2	69	**58**	**64**
NEG_04_08	Persistence	23.1		36.8	12.9		16.1			
	Exp. Smoothing	19.1		**33.7**	**11.5**		**14.0**	**67**		54
	SARIMA	20.3		34.6	11.8		15.3	59		57
	Neural Network	**18.1**	16.7	36.1	12.6	10.4	18.4	**67**	53	**73**
	Recurrent NN	22.5	**14.4**	43.5	14.7	**9.2**	20.5	62	**54**	67
NEG_08_12	Persistence	23.4		39.0	12.4		**17.0**			
	Exp. Smoothing	18.9		80.6	10.0		25.3	67		62
	SARIMA	20.0		**29.7**	10.7		17.8	64		59
	Neural Network	**11.9**	**11.4**	45.2	**8.8**	**8.6**	21.7	65	**58**	65
	Recurrent NN	16.1	15.5	38.9	9.6	9.2	17.7	**69**	53	**72**
NEG_12_16	Persistence	28.3		63.1	15.7		37.5			
	Exp. Smoothing	22.6		54.9	13.6		36.1	**71**		65
	SARIMA	24.4		58.3	13.9		36.3	69		59
	Neural Network	**14.9**	**27.7**	56.1	11.7	**13.7**	31.2	63	**78**	**81**
	Recurrent NN	15.8	39.3	**53.3**	**10.0**	21.0	**28.6**	70	69	**81**
NEG_16_20	Persistence	15.3		38.2	7.7		17.2			
	Exp. Smoothing	14.9		47.0	7.3		17.6	**68**		73
	SARIMA	14.4		**34.7**	7.4		**14.3**	57		59
	Neural Network	**6.6**	**20.5**	41.3	**4.8**	**11.8**	19.9	61	64	70
	Recurrent NN	10.3	24.8	39.4	6.6	13.9	19.5	63	**67**	**72**
NEG_20_24	Persistence	14.2		36.8	7.9		13.6			
	Exp. Smoothing	12.6		**33.5**	7.3		**11.6**	**75**		76
	SARIMA	12.3		34.4	7.5		12.4	60		68
	Neural Network	**8.1**	**8.8**	38.7	**6.3**	**5.7**	14.8	62	**69**	**92**
	Recurrent NN	14.2	14.9	41.3	8.5	**5.7**	14.9	70	50	69

Table 5-18: Result summary for all positive aFRR products and models on the marginal mixed price. The best performance is indicated in bold.

Product type	Model type	$RMSE_{train}$	$RMSE_{valid}$	$RMSE_{test}$	MAE_{train}	MAE_{valid}	MAE_{test}	Dir_{train} [%]	Dir_{valid} [%]	Dir_{test} [%]
POS_00_04	Persistence	5.4		7.2	2.5		3.7			
	Exp. Smoothing	5.3		7.1	**2.4**		3.6	56		43
	SARIMA	**5.1**		**6.9**	**2.4**		**3.5**	61		51
	Neural Network	12.0	3.5	10.6	9.8	2.3	6.9	60	69	**78**
	Recurrent NN	11.9	**3.3**	11.9	9.6	**1.8**	8.1	**68**	**73**	76
POS_04_08	Persistence	11.3		6.4	4.2		3.4			
	Exp. Smoothing	4.8		6.8	**2.9**		3.9	64		43
	SARIMA	**4.7**		**6.1**	**2.9**		**3.0**	63		54
	Neural Network	11.4	4.2	8.1	5.4	3.1	5.3	61	47	**65**
	Recurrent NN	7.8	**3.8**	8.7	5.9	**2.6**	5.7	**66**	**55**	55
POS_08_12	Persistence	22.6		**6.2**	9.5		**4.3**			
	Exp. Smoothing	17.5		7.0	**7.7**		4.8	**67**		62
	SARIMA	18.1		6.3	8.2		4.7	58		**65**
	Neural Network	22.4	6.7	7.2	11.9	5.0	5.5	63	61	57
	Recurrent NN	**16.9**	**5.0**	10.3	11.8	**3.8**	7.2	58	**67**	61
POS_12_16	Persistence	12.5		25,028.9	5.1		5,825.5			
	Exp. Smoothing	**10.6**		17,705.3	**4.8**		**2,917.6**	59		57
	SARIMA	**10.6**		44,467.3	**4.8**		9,841.2	**65**		59
	Neural Network	19.7	2.8	**17,705.1**	14.1	1.9	2,921.3	62	**75**	62
	Recurrent NN	11.7	**1.9**	18,317.1	6.6	**1.3**	4,116.1	63	74	**69**
POS_16_20	Persistence	27.0		5.8	10.7		3.0			
	Exp. Smoothing	**13.3**		5.8	**7.7**		3.2	64		54
	SARIMA	13.5		**5.5**	**7.7**		**2.7**	62		**65**
	Neural Network	34.5	5.0	7.2	24.1	3.6	4.9	61	61	51
	Recurrent NN	20.0	**3.9**	8.1	12.7	**3.0**	6.7	**75**	**63**	50
POS_20_24	Persistence	5.4		28.5	2.9		12.7			
	Exp. Smoothing	5.0		**21.8**	2.6		**9.3**	57		**62**
	SARIMA	4.7		25.7	**2.5**		13.1	**61**		54
	Neural Network	**3.6**	**8.8**	23.2	2.9	5.6	11.8	51	53	**62**
	Recurrent NN	4.1	10.0	22.5	3.4	**5.4**	10.3	52	**56**	58

5.1.2 Energy Price Prediction

This subsection presents results for the prediction of energy prices in the aFRR market. Each model type was applied on all aFRR product types. The error measures shown in Table 5-19 represent the best performing set of hyperparameters for each model type. All bids are sorted in ascending order by the energy price. The time series under consideration refers to the daily average energy prices for the lowest 10% of the capacity (bids).

Table 5-19: Result summary of energy price predictions on negative aFRR products. The energy price refers to the average within the 10 % quantile of all bids (1st group).

Product type	Model type	$RMSE_{train}$	$RMSE_{valid}$	$RMSE_{test}$	MAE_{train}	MAE_{valid}	MAE_{test}	Dir_{train} [%]	Dir_{valid} [%]	Dir_{test} [%]
NEG_00_04	Persistence	7.8		3.1	5.3		2.1			
	Exp. Smoothing	7.2		5.2	5.2		2.1	62		**70**
	SARIMA	**6.8**		**2.6**	**4.6**		**1.8**	**63**		**70**
	Neural Network	8.6	2.7	2.9	7.0	2.2	**1.8**	62	67	78
	Recurrent NN	11.9	**2.4**	4.4	10.0	**1.8**	3.2	60	**71**	66
NEG_04_08	Persistence	8.1		3.8	5.5		2.7			
	Exp. Smoothing	6.9		3.9	5.1		3.0	66		62
	SARIMA	**6.8**		**3.2**	**4.7**		2.3	63		68
	Neural Network	7.1	**2.4**	3.6	5.8	**1.8**	**2.1**	**73**	**72**	**76**
	Recurrent NN	9.4	3.0	5.6	7.7	2.3	4.3	65	61	62
NEG_08_12	Persistence	7.1		6.2	5.0		4.6			
	Exp. Smoothing	5.8		5.1	4.2		3.4	73		62
	SARIMA	5.5		**4.5**	4.0		**3.0**	69		**73**
	Neural Network	5.2	3.3	6.3	**3.7**	**2.5**	4.4	**80**	**89**	60
	Recurrent NN	**5.1**	**3.1**	5.9	3.9	**2.5**	4.4	75	78	62
NEG_12_16	Persistence	7.1		6.4	5.2		4.1			
	Exp. Smoothing	5.9		**4.0**	4.3		3.0	71		65
	SARIMA	5.8		4.3	4.2		**2.8**	73		**78**
	Neural Network	**3.5**	**4.0**	5.5	**2.8**	**2.9**	4.3	79	**83**	73
	Recurrent NN	4.0	5.1	5.7	3.0	4.2	4.4	**82**	72	62
NEG_16_20	Persistence	7.2		6.8	4.8		4.5			
	Exp. Smoothing	6.2		5.8	4.3		**4.0**	69		**59**
	SARIMA	6.1		**5.6**	4.2		**4.0**	64		**59**
	Neural Network	**2.9**	**6.2**	6.9	**2.2**	**3.5**	5.5	**82**	78	41
	Recurrent NN	3.7	6.9	6.7	2.9	4.2	5.0	81	**86**	**59**
NEG_20_24	Persistence	6.2		3.4	4.3		2.3			
	Exp. Smoothing	5.6		3.5	**4.0**		2.5	62		65
	SARIMA	5.5		**3.2**	**4.0**		**2.2**	62		57
	Neural Network	**5.1**	**2.4**	3.5	**4.0**	**1.9**	2.5	**69**	67	62
	Recurrent NN	5.4	**2.4**	3.8	4.1	**1.9**	2.6	68	**75**	**70**

Across all product types and error measures, the persistence model never achieves the best performance. For all but one product type, the SARIMA model outperforms all other models with regard the MAE of the test set. Overall, the SARIMA model followed by the exp. smoothing model perform the steadiest and best. The neural network model performs slightly better than other models on the NEG_04_08 product but performs worse on the

test set of the NEG_16_20 product than the persistence model. High fluctuations in the performance also apply for the recurrent neural network.

The best performing SARIMA model on the NEG_00_04 product type is illustrated in Figure 5-11. Overall the time series is rather constant at energy prices around -20€/MWh and -10€/MWh.

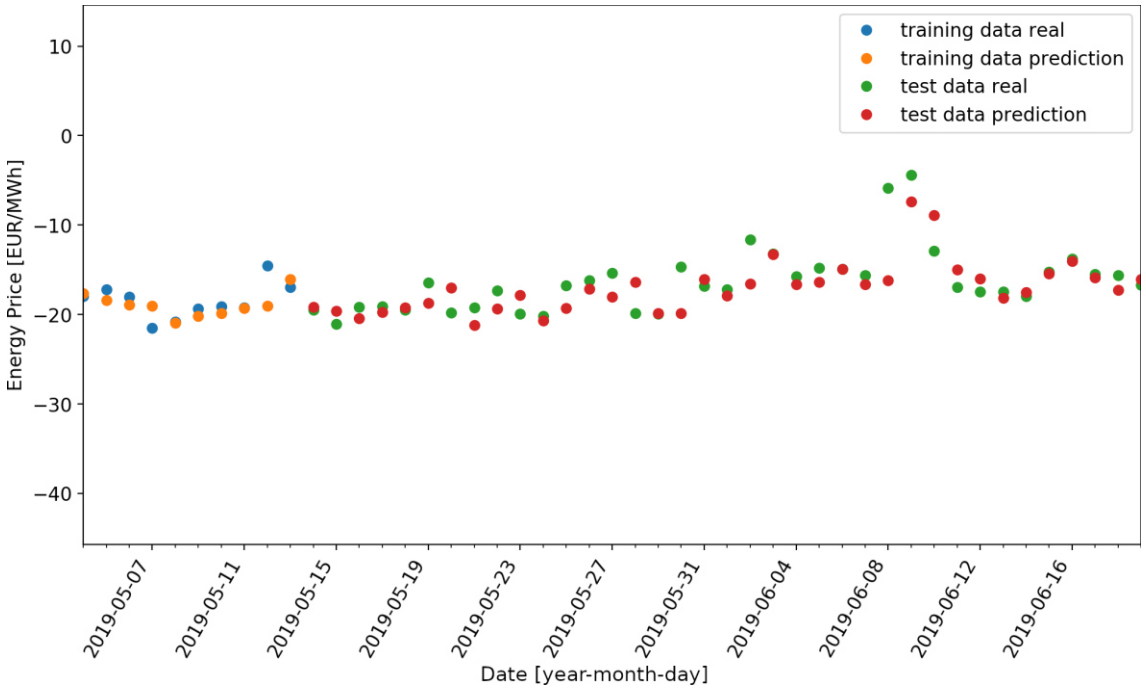

Figure 5-11: Energy price prediction of SARIMA(0,1,8) $(1,0,0)_7$ model on NEG_00_04 product type and 10% bid quantile.

Results for all positive aFRR product types are presented in Table 5-20. The energy prices refer to an average over the 10% quantile of all bids. On the POS_04_08 product type, the persistence model yields the best performance on the MAE measure of the test set. As with the negative aFRR products, the SARIMA and exp. smoothing model outperform both neural network model types. In almost all disciplines, both neural network model types perform worse than the persistence model.

Results for all negative product types on the 50% to 60% capacity range are illustrated in Table 5-21. For the NEG_00_04 product type, the persistence model reveals the best performance on the test set (MAE). The machine learning based models outperform their contestants in 4 out of 6 product types. In 3 out of 6 cases, the neural network model yields a significantly better performance.

Table 5-20: Result summary of energy price predictions on positive aFRR products. The energy price refers to the average within the 10 % quantile.

Product type	Model type	$RMSE_{train}$	$RMSE_{valid}$	$RMSE_{test}$	MAE_{train}	MAE_{valid}	MAE_{test}	Dir_{train} [%]	Dir_{valid} [%]	Dir_{test} [%]
POS_00_04	Persistence	6.6		1.8	3.5		1.4			
	Exp. Smoothing	5.4		1.8	**3.1**		1.3	51		**68**
	SARIMA	**5.2**		**1.7**	3.2		**1.2**	53		**68**
	Neural Network	8.5	1.9	2.1	7.1	1.4	1.8	54	**58**	54
	Recurrent NN	8.3	**1.0**	1.9	6.5	**0.8**	1.5	**57**	**58**	49
POS_04_08	Persistence	5.7		2.1	3.3		**1.4**			
	Exp. Smoothing	**4.4**		2.1	**2.8**		1.6	**71**		**73**
	SARIMA	4.7		**2.0**	2.9		1.6	59		62
	Neural Network	15.6	2.2	2.8	13.9	1.7	2.4	49	**67**	62
	Recurrent NN	14.3	**1.9**	2.6	12.3	**1.4**	2.1	51	66	64
POS_08_12	Persistence	5.7		2.5	3.8		2.0			
	Exp. Smoothing	4.8		2.5	**3.2**		1.9	72		57
	SARIMA	4.8		**2.1**	**3.2**		**1.8**	66		**65**
	Neural Network	**4.1**	**1.8**	3.1	**3.2**	**1.4**	2.6	**69**	**75**	46
	Recurrent NN	7.9	2.2	4.1	6.5	1.7	3.4	58	67	56
POS_12_16	Persistence	5.5		2.6	3.5		1.9			
	Exp. Smoothing	5.3		**2.3**	3.5		**1.8**	55		**76**
	SARIMA	**4.8**		2.4	**3.2**		2.0	58		68
	Neural Network	6.0	**2.1**	4.7	4.2	**1.7**	3.5	**65**	**64**	62
	Recurrent NN	5.2	2.4	4.6	4.1	2.0	3.6	63	58	64
POS_16_20	Persistence	6.1		2.3	3.8		1.8			
	Exp. Smoothing	5.3		**2.1**	3.5		**1.6**	**68**		**68**
	SARIMA	**5.2**		2.2	**3.4**		1.8	63		**68**
	Neural Network	6.5	2.7	4.4	4.5	2.2	4.1	66	58	49
	Recurrent NN	8.3	**1.8**	2.6	6.1	**1.4**	2.1	58	**69**	54
POS_20_24	Persistence	4.4		2.4	2.8		1.7			
	Exp. Smoothing	3.8		**2.1**	2.5		**1.5**	65		**73**
	SARIMA	**3.7**		2.2	**2.4**		1.6	**66**		62
	Neural Network	6.6	2.2	2.8	9.6	1.7	2.3	51	**67**	59
	Recurrent NN	5.7	**2.0**	2.3	4.1	**1.5**	1.8	57	52	59

Results for all positive product types on the 50% to 60% capacity range are illustrated in Table 5-22. For two product types, the persistence model yields the best performance on the test set (MAE). Compared to the statistical models, the machine learning based models perform significantly worse (on the test set) across the product types.

Table 5-21: Result summary of energy price predictions on negative aFRR products. The energy price refers to the average within the 50% to 60% range.

Product type	**Model type**	**$RMSE_{train}$**	**$RMSE_{valid}$**	**$RMSE_{test}$**	**MAE_{train}**	**MAE_{valid}**	**MAE_{test}**	**Dir_{train} [%]**	**Dir_{valid} [%]**	**Dir_{test} [%]**
NEG_00_04	Persistence	22.5		13.1	11.3		**6.9**			
	Exp. Smoothing	21.1		15.0	12.0		7.8	55		51
	SARIMA	19.3		**12.5**	11.7		7.8	56		54
	Neural Network	17.0	**8.7**	14.6	9.1	**4.7**	8.1	68	69	73
	Recurrent NN	**13.1**	10.3	13.3	**7.7**	6.4	8.5	**70**	**72**	**76**
NEG_04_08	Persistence	20.9		15.0	11.1		6.6			
	Exp. Smoothing	20.0		17.2	11.8		8.2	54		49
	SARIMA	17.5		13.8	10.7		6.9	58		59
	Neural Network	**5.7**	**4.3**	18.7	**4.2**	**3.6**	8.0	**73**	**72**	**68**
	Recurrent NN	18.7	6.9	**12.3**	12.7	4.6	**6.3**	58	69	**68**
NEG_08_12	Persistence	18.0		31.3	9.3		14.9			
	Exp. Smoothing	16.0		26.6	9.6		16.7	68		**73**
	SARIMA	15.3		26.9	8.4		15.5	71		68
	Neural Network	**6.0**	**8.2**	**20.1**	**5.0**	**5.3**	**10.4**	**72**	**72**	59
	Recurrent NN	15.7	9.2	26.2	10.2	6.0	15.0	57	69	65
NEG_12_16	Persistence	21.9		40.1	11.2		21.2			
	Exp. Smoothing	18.5		30.8	11.9		18.7	64		65
	SARIMA	18.2		30.8	10.4		17.4	67		73
	Neural Network	**7.0**	15.2	**26.8**	**4.9**	**10.0**	**13.7**	**70**	72	**68**
	Recurrent NN	12.5	**14.6**	28.0	8.3	10.4	16.0	63	**75**	**68**
NEG_16_20	Persistence	15.9		30.8	7.8		16.4			
	Exp. Smoothing	14.9		25.4	8.3		16.3	56		68
	SARIMA	13.2		24.6	7.9		14.7	66		70
	Neural Network	**8.8**	**9.3**	**18.9**	**6.7**	**5.9**	**10.9**	**67**	**72**	76
	Recurrent NN	12.6	12.3	21.3	8.7	6.5	10.5	62	**72**	**78**
NEG_20_24	Persistence	19.1		16.2	9.5		6.3			
	Exp. Smoothing	17.3		14.4	9.7		**6.2**	60		48
	SARIMA	16.5		13.9	9.5		6.9	55		51
	Neural Network	**10.1**	**4.3**	**12.2**	**6.3**	3.2	7.2	**72**	**78**	**62**
	Recurrent NN	19.1	4.5	14.5	11.2	**3.1**	6.1	53	69	43

Table 5-22: Result summary of energy price predictions on positive aFRR products. The energy price refers to the average within the 50 % to 60 % range.

Product type	Model type	$RMSE_{train}$	$RMSE_{valid}$	$RMSE_{test}$	MAE_{train}	MAE_{valid}	MAE_{test}	Dir_{train} [%]	Dir_{valid} [%]	Dir_{test} [%]
POS_00_04	Persistence	7.0		2.2	3.9		**1.4**			
	Exp. Smoothing	4.4		3.0	**3.1**		2.2	59		56
	SARIMA	**4.7**		**2.1**	**3.1**		**1.4**	**63**		51
	Neural Network	7.6	3.1	3.2	6.0	2.7	2.7	62	56	54
	Recurrent NN	7.3	**2.2**	2.3	5.0	**1.8**	1.5	62	**78**	**68**
POS_04_08	Persistence	6.4		2.5	3.9		**1.5**			
	Exp. Smoothing	**5.2**		2.3	**3.5**		1.8	**66**		62
	SARIMA	5.3		2.0	**3.5**		**1.5**	59		**73**
	Neural Network	18.2	3.1	2.8	15.9	2.5	2.5	52	**64**	57
	Recurrent NN	9.2	**2.6**	**1.9**	6.9	**2.0**	1.6	51	52	71
POS_08_12	Persistence	8.9		2.6	5.3		2.0			
	Exp. Smoothing	**7.1**		**2.3**	**4.3**		1.9	**70**		70
	SARIMA	**7.1**		2.4	4.4		**1.8**	68		73
	Neural Network	9.1	**2.1**	3.6	7.1	**1.5**	3.1	65	**83**	**68**
	Recurrent NN	7.9	2.3	3.7	5.9	1.8	3.0	64	78	65
POS_12_16	Persistence	7.8		2.7	4.2		1.9			
	Exp. Smoothing	**6.6**		**2.3**	**3.9**		**1.7**	**67**		65
	SARIMA	7.1		**2.3**	4.1		**1.7**	60		**68**
	Neural Network	7.7	3.3	3.8	5.6	2.8	3.0	53	58	59
	Recurrent NN	8.9	**2.6**	2.6	5.4	**2.1**	2.1	59	**61**	62
POS_16_20	Persistence	10.5		2.9	6.5		2.0			
	Exp. Smoothing	**8.1**		**2.2**	**5.2**		**1.7**	**69**		**78**
	SARIMA	8.5		2.9	5.4		2.4	67		65
	Neural Network	11.5	3.8	5.8	8.1	3.1	5.2	57	58	59
	Recurrent NN	10.8	**2.8**	2.8	7.2	**2.1**	2.2	63	**64**	61
POS_20_24	Persistence	5.6		3.1	3.7		2.3			
	Exp. Smoothing	**4.6**		2.9	**3.2**		2.4	**65**		**67**
	SARIMA	4.7		**2.7**	3.4		**2.1**	62		65
	Neural Network	4.9	3.3	6.6	3.7	2.6	5.8	69	**75**	59
	Recurrent NN	6.9	**3.0**	5.9	5.5	**2.3**	4.4	59	**75**	50

5.1.3 Deployment Duration Prediction

This subsection presents results for the prediction of the aFRR deployment duration. The error measures shown in Table 5-23 represent the best performing set of hyperparameters for each model type on the 10 % quantile (lowest energy price bids) of the tendered capacity.

Table 5-23: Result summary of deployment duration predictions on negative aFRR products. The deployment duration refers to the average within the 10 % quantile of all bids.

Product type	**Model type**	**$RMSE_{train}$**	**$RMSE_{valid}$**	**$RMSE_{test}$**	**MAE_{train}**	**MAE_{valid}**	**MAE_{test}**	**Dir_{train} [%]**	**Dir_{valid} [%]**	**Dir_{test} [%]**
NEG_00_04	Persistence	82.1		69.4	66.3		54.4			
	Exp. Smoothing	61.8		52.6	50.1		41.2	78		75
	SARIMA	62.8		56.1	51.8		45.6	78		68
	Neural Network	**59.3**	64.0	**51.2**	**48.5**	51.5	**40.9**	78	69	**84**
	Recurrent NN	59.8	**59.6**	69.0	49.1	**50.7**	61.2	**79**	**78**	62
NEG_04_08	Persistence	76.4		75.2	58.5		59.7			
	Exp. Smoothing	57.4		53.6	44.7		**41.8**	73		81
	SARIMA	56.2		54.1	44.7		45.1	73		76
	Neural Network	46.2	50.3	**45.6**	37.5	37.8	35.6	83	**72**	**86**
	Recurrent NN	**38.4**	**49.4**	68.1	**30.2**	**37.1**	57.1	**86**	67	70
NEG_08_12	Persistence	87.8		80.5	66.7		63.3			
	Exp. Smoothing	66.8		70.9	**51.2**		57.5	73		**65**
	SARIMA	**66.2**		67.0	54.1		59.1	**76**		**65**
	Neural Network	69.1	**40.7**	**60.4**	58.1	**32.8**	**51.9**	73	**78**	**65**
	Recurrent NN	68.4	43.8	63.7	55.8	34.0	54.5	74	75	**65**
NEG_12_16	Persistence	79.4		88.5	63.8		65.1			
	Exp. Smoothing	57.4		80.7	46.3		62.8	75		68
	SARIMA	59.2		**64.8**	48.5		**52.3**	**76**		**78**
	Neural Network	64.2	**52.4**	70.7	50.8	**43.4**	58.7	72	**67**	73
	Recurrent NN	**57.0**	53.7	93.4	**44.4**	45.8	74.0	**76**	69	70
NEG_16_20	Persistence	68.5		54.3	53.5		43.8			
	Exp. Smoothing	52.1		46.9	42.6		38.1	70		68
	SARIMA	50.7		43.5	42.1		34.4	75		62
	Neural Network	46.6	**38.6**	**42.6**	37.0	**31.5**	**33.3**	82	**67**	**73**
	Recurrent NN	**31.0**	45.0	75.0	**23.9**	36.5	42.6	**85**	**67**	**73**
NEG_20_24	Persistence	80.2		58.4	63.1		44.9			
	Exp. Smoothing	57.3		49.0	47.3		40.5	73		70
	SARIMA	64.6		47.9	50.3		**37.4**	72		62
	Neural Network	**46.6**	**58.8**	**43.1**	**37.2**	**49.1**	**37.4**	**82**	**78**	70
	Recurrent NN	67.9	60.0	45.9	56.1	49.9	40.6	73	67	**74**

Across all product types and error measures, the persistence model never achieves the best performance. Regarding the performance on the test set, the neural network model outperforms the other models on most negative aFRR product types. However, on the NEG_12_16 and NEG_20_24 product types, the SARIMA model reveals an equal or better performance on the test set. Overall, the MAE measure is in the order of 30 to 60 min. Considering the deployment duration time series as illustrated in Figure 2-11, the prediction

error is very high. A high prediction error was expected since aFRR requests depend on unpredictable events such as a power plant outage.

Table 5-24: Result summary of deployment duration predictions on positive aFRR products. The deployment duration refers to the average within the 10 % quantile.

Product type	**Model type**	**$RMSE_{train}$**	**$RMSE_{valid}$**	**$RMSE_{test}$**	**MAE_{train}**	**MAE_{valid}**	**MAE_{test}**	**Dir_{train} [%]**	**Dir_{valid} [%]**	**Dir_{test} [%]**
POS_00_04	Persistence	63.5		90.6	48.7		72.9			
	Exp. Smoothing	50.2		67.6	37.8		55.6	78		73
	SARIMA	49.0		68.0	38.9		55.3	74		76
	Neural Network	41.5	**57.4**	**67.2**	33.6	47.5	**51.6**	**81**	75	**78**
	Recurrent NN	**41.1**	54.8	71.3	**33.5**	**45.5**	58.1	80	**78**	**78**
POS_04_08	Persistence	68.5		75.1	55.1		62.9			
	Exp. Smoothing	52.1		62.9	42.6		48.8	79		68
	SARIMA	51.7		59.4	41.9		47.5	80		65
	Neural Network	**47.3**	**47.5**	71.1	**38.5**	**36.9**	59.1	**82**	**81**	62
	Recurrent NN	53.5	49.9	**58.4**	44.2	39.3	**45.4**	79	58	**78**
POS_08_12	Persistence	85.2		87.6	66.2		69.6			
	Exp. Smoothing	63.5		72.9	**51.4**		54.7	**75**		**76**
	SARIMA	64.4		76.8	53.0		61.8	72		59
	Neural Network	**60.6**	**51.7**	68.6	52.9	39.9	52.7	71	64	73
	Recurrent NN	68.0	53.5	**67.4**	55.5	**37.1**	**51.4**	72	**81**	**76**
POS_12_16	Persistence	80.7		91.7	65.5		73.9	49		51
	Exp. Smoothing	58.6		87.8	46.2		73.6	**75**		76
	SARIMA	58.9		**75.2**	48.5		**62.1**	74		76
	Neural Network	**55.5**	**50.4**	98.7	**43.6**	**40.2**	75.2	75	**81**	76
	Recurrent NN	68.2	53.6	82.7	54.5	47.3	67.4	70	76	**77**
POS_16_20	Persistence	72.9		74.1	59.0		58.9			
	Exp. Smoothing	53.3		**60.4**	44.1		**50.2**	78		62
	SARIMA	52.5		61.0	42.8		52.7	77		65
	Neural Network	**44.7**	**49.8**	70.8	**35.9**	**40.1**	55.7	**82**	**89**	64
	Recurrent NN	57.2	60.6	65.3	48.1	51.7	52.4	73	73	**67**
POS_20_24	Persistence	63.0		66.6	49.0		46.6			
	Exp. Smoothing	45.9		74.6	36.4		65.3	78		65
	SARIMA	47.9		**52.0**	39.6		**41.6**	75		70
	Neural Network	46.9	60.1	73.0	40.5	49.4	48.6	72	75	**78**
	Recurrent NN	**41.0**	**59.0**	66.0	**32.3**	**46.8**	53.8	**79**	**81**	64

For all positive aFRR product types, Table 5-24 summarizes the best performing model realizations. As opposed to the negative aFRR product types, the neural network does not reveal superior performance as regards the test set performance. In two out of six product

types, the recurrent neural network performs best. However, no clear winning candidate can be observed.

Results for all negative product types and the 50% to 60% capacity range are illustrated in *Table 5-25*. On five product types, the machine learning based models yield the best performance on the test set (MAE). However, the performance gain compared to the SARIMA model is minor.

Table 5-25: Result summary of deployment duration predictions on negative aFRR products. The energy price refers to the average within the 50% to 60% range.

Product type	**Model type**	**$RMSE_{train}$**	**$RMSE_{valid}$**	**$RMSE_{test}$**	**MAE_{train}**	**MAE_{valid}**	**MAE_{test}**	**Dir_{train} [%]**	**Dir_{valid} [%]**	**Dir_{test} [%]**
NEG_00_04	Persistence	20.4		3.3	9.0		1.1			
	Exp. Smoothing	**12.4**		2.4	6.9		1.3	**96**		**100**
	SARIMA	14.1		**2.3**	5.5		0.7	94		**100**
	Neural Network	18.2	**10.1**	**2.3**	6.3	**2.9**	**0.6**	94	**100**	**100**
	Recurrent NN	15.5	10.4	2.4	**5.1**	3.0	**0.6**	19	8	5
NEG_04_08	Persistence	20.2		18.8	8.8		6.2			
	Exp. Smoothing	**12.3**		13.6	7.0		4.5	91		62
	SARIMA	13.6		13.6	**5.3**		3.5	**94**		89
	Neural Network	16.6	**5.4**	**13.5**	6.3	**1.2**	**3.2**	**94**	**100**	**97**
	Recurrent NN	14.5	5.6	13.9	5.4	1.3	3.5	23	6	9
NEG_08_12	Persistence	18.9		21.4	9.4		10.2			
	Exp. Smoothing	**12.8**		16.4	8.5		10.3	**95**		95
	SARIMA	15.0		16.1	6.0		5.5	**95**		**100**
	Neural Network	14.9	17.6	16.1	5.9	7.6	5.6	**95**	92	**100**
	Recurrent NN	13.9	**17.3**	**15.3**	**5.8**	**7.4**	**5.2**	**95**	**97**	**100**
NEG_12_16	Persistence	20.4		13.6	9.9		5.8			
	Exp. Smoothing	14.4		11.6	8.3		8.3	82		**100**
	SARIMA	15.8		**9.6**	5.7		**2.9**	**97**		**100**
	Neural Network	14.4	**21.4**	9.7	5.5	**8.5**	3.1	20	**22**	11
	Recurrent NN	**14.3**	**21.4**	9.9	**5.3**	8.6	3.2	20	19	11
NEG_16_20	Persistence	20.1		9.4	9.2		2.2			
	Exp. Smoothing	**13.3**		8.8	8.1		5.3	83		65
	SARIMA	15.6		**6.6**	**5.5**		**1.1**	**97**		**100**
	Neural Network	16.5	**9.8**	**6.6**	6.2	**3.2**	**1.1**	96	**97**	**100**
	Recurrent NN	15.7	**9.8**	**6.6**	6.5	3.4	1.6	77	58	35
NEG_20_24	Persistence	22.5		9.2	9.9		3.6			
	Exp. Smoothing	**14.0**		**6.5**	7.8		2.9	**93**		**100**
	SARIMA	18.2		**6.5**	**6.8**		1.9	62		51
	Neural Network	21.9	10.2	**6.5**	8.3	**3.8**	**1.8**	**93**	**94**	**100**
	Recurrent NN	22.0	**10.1**	**6.5**	8.5	3.9	2.1	**93**	**94**	**100**

Results for all positive product types and the 50% to 60% capacity range are presented in *Table 5-26*. The SARIMA model yields the best performance on the test set (MAE) across all product types. In four cases, the neural network model performs equally well.

Table 5-26: Result summary of deployment duration predictions on positive aFRR products. The energy price refers to the average within the 50 % to 60 % range.

Product type	**Model type**	**$RMSE_{train}$**	**$RMSE_{valid}$**	**$RMSE_{test}$**	**MAE_{train}**	**MAE_{valid}**	**MAE_{test}**	**Dir_{train} [%]**	**Dir_{valid} [%]**	**Dir_{test} [%]**
POS_00_04	Persistence	5.7		5.0	1.3		2.1			
	Exp. Smoothing	**3.1**		4.2	1.0		1.9	98		87
	SARIMA	4.1		**4.0**	0.7		**1.3**	**99**		**95**
	Neural Network	3.8	**5.3**	**4.0**	**0.5**	**1.4**	**1.3**	98	**100**	**95**
	Recurrent NN	3.8	**5.3**	**4.0**	**0.5**	**1.4**	1.4	6	8	8
POS_04_08	Persistence	11.4		23.1	5.7		10.7			
	Exp. Smoothing	7.8		**15.5**	4.9		7.4	**97**		95
	SARIMA	8.7		16.3	3.2		**5.4**	96		**97**
	Neural Network	8.1	10.5	16.1	3.7	4.6	5.8	96	**100**	**97**
	Recurrent NN	**3.0**	**6.5**	17.5	**1.4**	**2.9**	8.5	**97**	**100**	**97**
POS_08_12	Persistence	22.5		39.9	9.9		12.2			
	Exp. Smoothing	**17.1**		**28.0**	9.2		10.3	94		**100**
	SARIMA	19.6		28.3	6.6		**6.7**	94		**100**
	Neural Network	20.9	11.9	28.3	7.2	5.3	**6.7**	91	97	**100**
	Recurrent NN	18.6	**9.5**	30.3	**5.8**	**4.6**	7.6	**95**	**100**	**100**
POS_12_16	Persistence	15.2		13.9	5.5		6.5			
	Exp. Smoothing	**9.5**		**10.5**	4.3		5.1	76		**100**
	SARIMA	12.1		10.9	**3.3**		**3.8**	**95**		**100**
	Neural Network	13.1	**5.7**	10.9	3.8	**1.3**	**3.8**	14	8	11
	Recurrent NN	13.2	**5.7**	11.1	3.9	**1.3**	3.9	94	**100**	**100**
POS_16_20	Persistence	17.8		**12.8**	8.8		6.9			
	Exp. Smoothing	10.9		13.8	6.5		9.2	**95**		89
	SARIMA	11.4		15.1	4.3		**6.6**	**95**		**95**
	Neural Network	13.0	15.7	15.2	4.9	**6.1**	6.7	23	22	24
	Recurrent NN	**10.1**	**15.6**	15.3	**4.0**	6.2	6.8	59	**47**	53
POS_20_24	Persistence	7.4		14.5	2.5		8.9			
	Exp. Smoothing	5.7		**10.5**	2.1		7.1	95		**95**
	SARIMA	6.0		11.8	1.5		**5.6**	97		92
	Neural Network	**2.4**	13.2	11.8	**0.6**	5.8	**5.6**	**99**	89	92
	Recurrent NN	3.9	**11.4**	11.9	1.6	**5.0**	6.2	98	**94**	91

5.2 Bidding Strategy

This section presents the results of applying the bidding strategy presented in chapter 4 on real market data. All simulations are conducted for the time period between October, 30th 2018 and July 31st, 2019. In the latter time period the aFRR mixed price auction scheme was in effect (subsection 2.1.2.1). A separate simulation is conducted for each day within the time range. To simulate under realistic conditions, only data until the aFRR auction closure one day before the day of simulation is used. All forecasts required for running the bidding strategy are obtained from applying the prediction framework of chapter 3.

Subsections 5.2.1 to 5.2.3 compare the earning potentials of operating virtual power plants (VPPs) with and without the contribution of a BESS. In subsection 5.2.1 a wind park of 100 MW nominal capacity is considered. In addition, the BESS standalone operation on the aFRR market is analyzed. Subsection 5.2.2 investigates a virtual power plant comprising both wind and PV generation. In subsection 5.2.3, a configuration comprising wind, PV and a thermal power plant is considered. A sensitivity analysis in which mainly cost related parameters are varied is conducted in subsection 5.2.4. Revenue potentials yielded on the aFRR market are compared to revenue potentials on the FCR market in subsection 5.2.5.

5.2.1 BESS in Standalone Operation and with Wind-Generation

This subsection considers three different scenarios. In the first scenario, a BESS with a nominal power output of 20 MW and an energetic capacity of 20 MWh (configuration 1, section 4.2) is operated in standalone mode without a supporting VPP. A wind park with a nominal capacity of 100 MW is operated in standalone mode in the second scenario. In the third scenario, a BESS with 30 MW nominal power output and an energetic capacity of 20 MWh is operated in conjunction with aforementioned wind park (configuration 2, section 4.2).

Table 5-27 summarizes the simulation results for above three scenarios. Each value in the table represents the daily average over the simulation period. Aside from the average capacity and energy price revenues on the aFRR market (row 1-2), for each aFRR product type, the average offered capacity (MW) and acceptance rate of the submitted bid is listed (row 4-9). The sold energy and yielded revenues on the intraday market correspond to the reserve band described in subsection 4.5.3 (row 10-11). If no energy is needed for recharging the BESS, the energy can be traded on the intraday market. All table entries denoted by “Arbitrage” correspond to intraday market activity triggered by the BESS (row 12-15). The latter can have two causes. Firstly, the BESS is increasing its revenues by buying energy at times of low prices and selling the energy at times of high prices (subsection 4.5.4). Secondly, the BESS must recharge energy to reach the target SoC at the end of an aFRR period. This is necessary if the BESS has no opportunity to recharge energy from the generation pool, e.g. in standalone mode. For this reason, the arbitrage buying costs can

exceed the arbitrage selling costs, as it is the case with the BESS in standalone mode (Table 5-27). As described in subsection 4.5.1, various fees and apportionments apply if the BESS recharges energy from the generation pool via the electrical grid. The row “Recharge Taxes” covers all costs associated with the energy exchange between the generation units and the BESS. It is assumed, that the BESS is not located on the same premises as the generation units. If that was the case, a private grid could be used for energy exchange to circumvent the recharge fees. Both calendric and cyclic ageing effects are included in the battery deterioration (section 4.6). The percentage value states the average decrease in capacity per day (row 19). If the total accumulated capacity decrease is above 20 %, the battery cells are considered to have reached their end-of-life. All other BESS components are expected to have a lifetime of 15 years (section 4.4). Their daily differential cost impact is stated in row 21 - 25.

This work does not incorporate any fixed or variable costs related to the generation units (wind, PV and thermal units) of the considered VPPs. Any investment costs, maintenance costs etc. of the generation units are not considered in this work. The total cash flow of the generation units only accounts for the revenues of having traded (sold) the generated energy (row 26). This work only answers the questions, whether a BESS is economically beneficial for an existing VPP. For this reason, only the full cost breakdown of the BESS is included in the total cash flow. For a BESS to be economically beneficial, the total cash flow of the VPP with BESS should be higher than without BESS.

As shown in Table 5-27, the average daily total cash flow of the BESS in standalone mode is negative (row 26). This indicates an uneconomical operation. Neither on the aFRR market, nor on the intraday market is the price spread between charging and discharging sufficient to cover all costs. Due to the 4 h criterion on the aFRR market, the BESS is only capable of offering 5MW of capacity to the aFRR market.

Across the aFRR product types, the acceptance rate of the submitted bids varies between 30 % (POS_16_20) and 73 % (POS_20_24). The low aFRR acceptance rates can have multiple causes. First, the prediction model predicts a mixed price that deviates from the real auction outcome. If the mixed price is overestimated, the optimizer of the bidding strategy overestimates the acceptance probability as well. Second, the cyclic ageing costs of the battery set a lower threshold to the offered aFRR energy price. Bids below the threshold would generate higher costs on the battery side than the yielded revenues. Consequently, the bidding strategy must choose an energy price that covers the arising costs but does not necessarily have a high acceptance probability. Third, a too high energy price does not only reduce the acceptance probability but also decreases the aFRR provision duration (merit order effect). With a decreased aFRR provision duration, the energy revenues might decrease as well.

Table 5-27: Result summary of three scenarios: BESS standalone, Wind and BESS + Wind. Each value represents the daily average over the simulation period.

Row		BESS Standalone	Wind	BESS + Wind
1	aFRR Capacity Price Revenue [€/day]	303	0	560
2	aFRR Energy Price Revenue [€/day]	353	0	778
3	aFRR Total Revenue [€/day]	657	0	1,339
4	POS_00_04: Accept Cap. [MW/day] / Accept. rate [%/day]	5 / 66	0 / 0	20 / 24
5	POS_04_08: Accept Cap. [MW/day] / Accept. rate [%/day]	5 / 55	0 / 0	19 / 24
6	POS_08_12: Accept Cap. [MW/day] / Accept. rate [%/day]	5 / 47	0 / 0	17 / 19
7	POS_12_16: Accept Cap. [MW/day] / Accept. rate [%/day]	5 / 38	0 / 0	19 / 19
8	POS_16_20: Accept Cap. [MW/day] / Accept. rate [%/day]	5 / 30	0 / 0	18 / 19
9	POS_20_24: Accept Cap. [MW/day] / Accept. rate [%/day]	5 / 73	0 / 0	18 / 17
10	Intraday Market: Sold Energy [MWh/day]	0	0	60
11	Intraday Market Revenue [€/day]	0	0	2,070
12	Arbitrage: Bought Energy [MWh/day]	6.6	0	3.5
13	Arbitrage: Costs [€/day]	367	0	127
14	Arbitrage: Sold Energy [MWh/day]	1.4	0	1.8
15	Arbitrage: Revenue [€/day]	140	0	163
16	Day-ahead Market: Sold Energy [MWh/day]	0	521	447
17	Day-ahead Market: Revenue [€/day]	0	20410	17,996
18	Recharge Taxes [€/day]	0	0	125
19	Battery Deterioration [%/day]	0.0049	0	0.0053
20	Battery Deterioration [€/day]	1,111	0	1,189
21	Differential Inverter Costs [€/day]	304	0	456
22	Differential BOS Costs [€/day]	352	0	352
23	Differential EPC and Soft Costs [€/day]	500	0	500
24	Differential Maintenance and Operation Costs [€/day]	222	0	245
25	Differential Contingency Costs [€/day]	59	0	64
26	Total Cash Flow incl. Degradation BESS Costs [€/day]	-2118	20,410	18,511

Fourth, the expected arbitrage earnings due to high price spreads on the intraday market might exceed the expected revenues on the aFRR market. In this case the bidding strategy submits a very high capacity price (€/MW) which is unlikely to be accepted. Consequently, the acceptance rate as of Table 5-27 decreases and this is desired behavior.

On average, the standalone BESS recharges 5.2 MWh per day from the intraday market and trades 1.4 MWh in arbitrage (row 12, 14). The intraday recharge costs therefore exceed the revenue from sold energy (row 13). Under consideration of the 80 % end-of-life criterion, the battery model estimates the battery life to 11.1 years. If the prediction framework is replaced by perfect knowledge of the simulation day (prices and request duration), the total cash flow incl. BESS degradation costs amounts to -1,959 €/day on average.

In case the BESS is operated in conjunction with the wind park, the total revenue on the aFRR market is more than doubled (row 3). Depending on the aFRR product type, the average offered capacity is between 17 to 20 MW. Compared to the BESS standalone operation this aFRR capacity offer increase arises from the possibility to recharge from the pool. The BESS does not need to provide 4 h of full offered capacity by itself. However, the average offered capacity is lower than the theoretical maximum of 24 MW because the wind generation profile does not always provide sufficient reserve power to recharge the BESS (see subsection 4.5.2 for explanation). Arbitrage trading plays minor role as regards exchanged energy and profits. Depending on the day, either the price spread is lower than the cyclic ageing costs of the BESS or the revenue potential on the aFRR market is higher. The battery model reveals an estimated lifetime of 10.4 years and therefore a slightly higher ageing than for the BESS standalone operation.

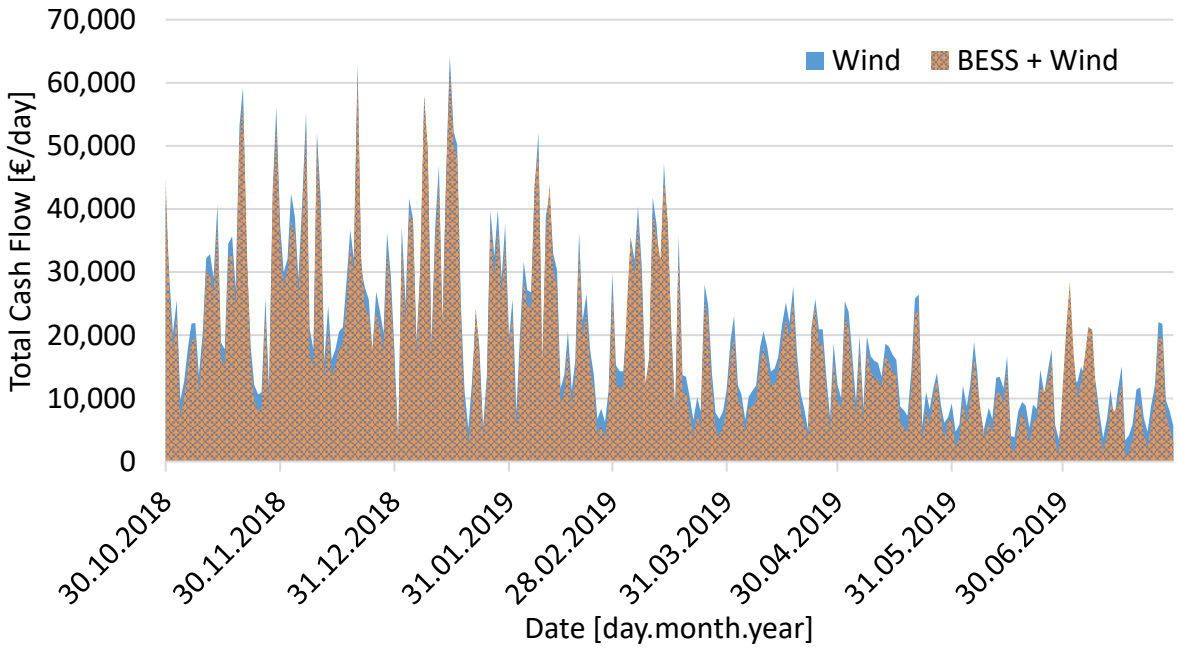

Figure 5-12: Total cash flow per day for 2 scenarios: Wind and BESS + Wind.

As explained in subsection 4.5.4, the revenue potential of generation units without a coupled BESS are estimated by trading all generation capabilities on the day-ahead market. The wind park by itself yields an average revenue of 20,410 €/day whereas the wind park in combination with the BESS yields 21,441 €/day. However, the total cash flow of the pooled

operation (18,511 €/day) is lower than in the wind only scenario (row 26). The additional revenues do not compensate for the costs of the BESS. Adding a BESS to an existing wind park is not economical beneficial. Figure 5-12 illustrates the daily total cash flow for both the wind and BESS + Wind configuration over the simulation period. Because of varying wind generation and day-ahead prices, the total cash flow fluctuates significantly. In only 9.9 % (27/274 days) of the days, the total cash flow of the BESS + Wind configuration is higher than for the wind only configuration. If the prediction framework is replaced by perfect knowledge of the simulation day (prices and request duration), the total cash flow amounts to 18,872 €/day on average.

For an exemplary day, Figure 5-13 provides detailed time series of the BESS + Wind operating strategy and prices on the various markets. The operating strategy strictly follows the methodology presented in section 4.5 and is the unaltered output of the simulation framework. As illustrated in the uppermost chart (SoC), the BESS undergoes two full cycles and one-quarter cycle at that specific day. The VPP participates in the aFRR market between 12 am and 8 pm with offered energy prices as indicated in the bottom chart. All offered aFRR energy prices are at any time above the day-ahead and intraday prices. During the aFRR delivery period, a part of the pool generation capabilities is traded on the day-ahead market and another part is reserved for recharging the BESS. In time periods of no aFRR requests, e.g. between 9 am and 8 pm, the reserve band is traded on the intraday market. All intraday market activity conducted by the wind park is denoted by “Intraday Market Power Pool” whereas all intraday market activity triggered by the BESS is denoted by “Intraday Market Power BESS”. The BESS intraday market activity includes all arbitrage trading and necessary recharge operations. If an aFRR request is triggered by the TSOs, the BESS provides the required power by discharging its battery cells. The discharged energy is later recharged from the reserve band of the pool (“Reserved Recharge Power”). At times of recharge, the pool cannot sell the reserve band to the intraday market. Between 8 pm and 12 am, the BESS does not provide aFRR but instead conducts arbitrage. At 8 pm, energy is sold for 53 €/MWh and at 11:45 pm, energy is bought for -4.6 €/MWh (negative energy price on intraday market). The target SoC of 100 % is reached at the end of the day.

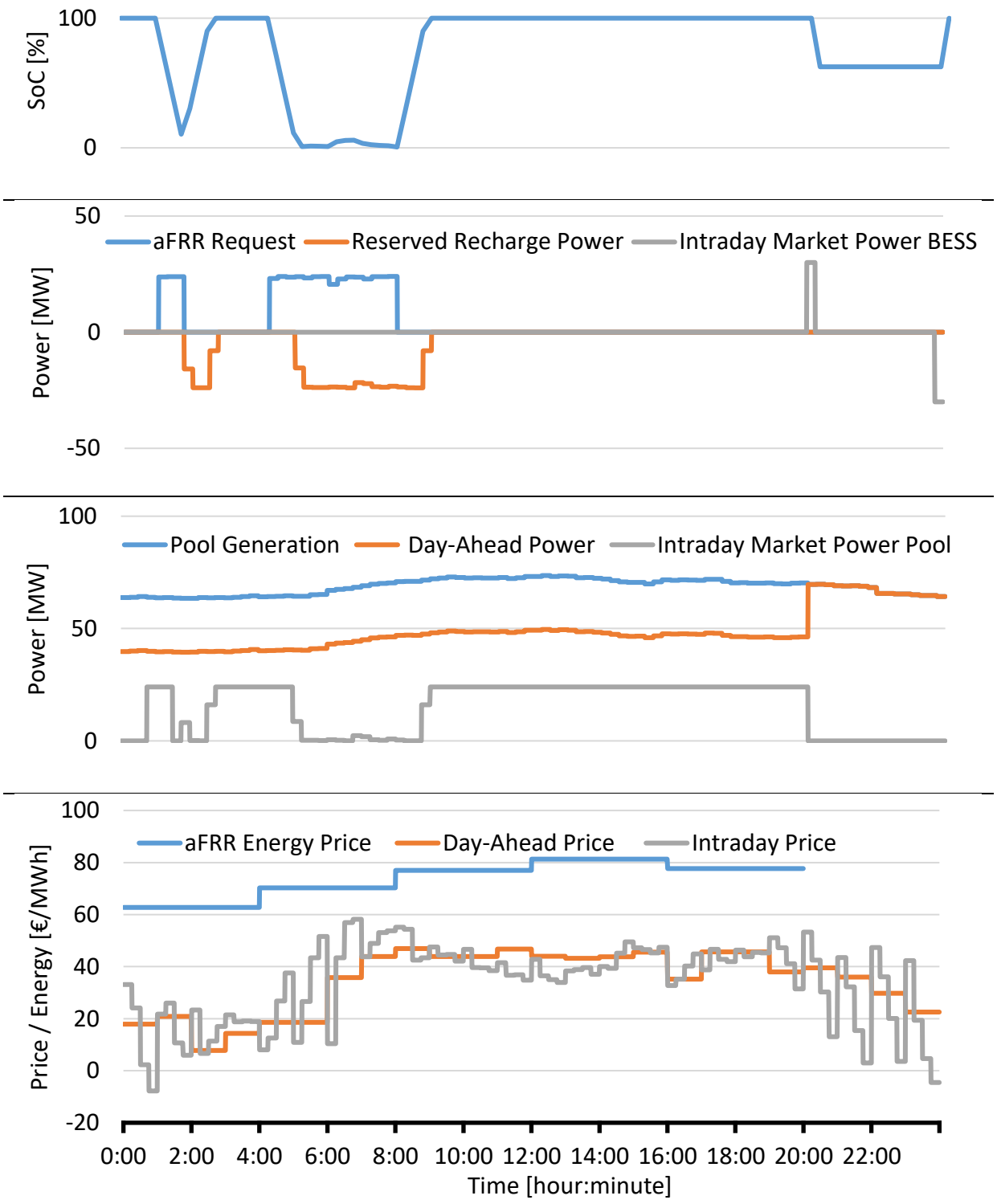

Figure 5-13: Operation and trading of the BESS + Wind pool on January 8th, 2019.

5.2.2 BESS with Wind- and PV-Generation

This subsection reveals if a BESS can positively contribute to the operation of a pooled wind park and a PV system with each having a nominal capacity of 100 MW (configuration 3,

section 4.2). The considered BESS has a nominal power output of 30 MW and an energetic capacity of 20 MWh.

Table 5-28: Result summary of 2 scenarios: Wind + PV and BESS + Wind + PV. Each value represents the daily average over the simulation period.

Row		**Wind + PV**	**BESS + Wind + PV**
1	aFRR Capacity Price Revenue [€/day]	0	638
2	aFRR Energy Price Revenue [€/day]	0	917
3	aFRR Total Revenue [€/day]	0	1,556
4	POS_00_04: Accept Cap. [MW/day] / Accept. rate [%/day]	0 / 0	20 / 24
5	POS_04_08: Accept Cap. [MW/day] / Accept. rate [%/day]	0 / 0	19 / 26
6	POS_08_12: Accept Cap. [MW/day] / Accept. rate [%/day]	0 / 0	21 / 22
7	POS_12_16: Accept Cap. [MW/day] / Accept. rate [%/day]	0 / 0	22 / 18
8	POS_16_20: Accept Cap. [MW/day] / Accept. rate [%/day]	0 / 0	19 / 18
9	POS_20_24: Accept Cap. [MW/day] / Accept. rate [%/day]	0 / 0	18 / 16
10	Intraday Market: Sold Energy [MWh/day]	0	67
11	Intraday Market Revenue [€/day]	0	2,420
12	Arbitrage: Bought Energy [MWh/day]	0	3.4
13	Arbitrage: Costs [€/day]	0	100
14	Arbitrage: Sold Energy [MWh/day]	0	3.4
15	Arbitrage: Revenue [€/day]	0	108
16	Day-ahead Market: Sold Energy [MWh/day]	756	672
17	Day-ahead Market: Revenue [€/day]	29,420	26,588
18	Recharge Taxes [€/day]	0	148
19	Battery Deterioration [%/day]	0	0.0054
20	Battery Deterioration [€/day]	0	1,215
21	Differential Inverter Costs [€/day]	0	456
22	Differential BOS Costs [€/day]	0	352
23	Differential EPC and Soft Costs [€/day]	0	500
24	Differential Maintenance and Operation Costs [€/day]	0	245
25	Differential Contingency Costs [€/day]	0	64
26	Total Cash Flow incl. Degradation BESS Costs [€/day]	29,420	27,592

Table 5-28 summarizes the simulation results for the operation with and without the BESS. On average, between 18 MW and 22 MW of capacity were offered to the aFRR market (row 4 - 9). Due to the availability of PV generation during the day, more recharge opportunities arise for the BESS than for e.g. a pool of only wind generation (subsection 5.2.1).

Consequently, more aFRR capacity can be traded and more revenues can be generated. With the same reasoning as explained in subsection 5.2.1, the aFRR acceptance rate is rather low, ranging between 16 % and 26 %. Revenues arising from arbitrage trading are minor. The battery model reveals an expected lifetime of 10.2 years. Due to the high costs of the BESS and the relatively low revenue margin on the aFRR market, the total cash flow with BESS is lower than without BESS. Economically, it is not beneficial to operate the BESS with this strategy.

Figure 5-14 illustrates the daily total cash flow for both configuration over the simulation period. Because of varying renewable generation and day-ahead prices, the total cash flow fluctuates significantly. In only 9.9 % (27/274 days) of the days, the total cash flow with BESS is higher than without BESS. For an exemplary day, *Figure A-1* provides detailed time series of the operating strategy and prices on the various markets for an exemplary day.

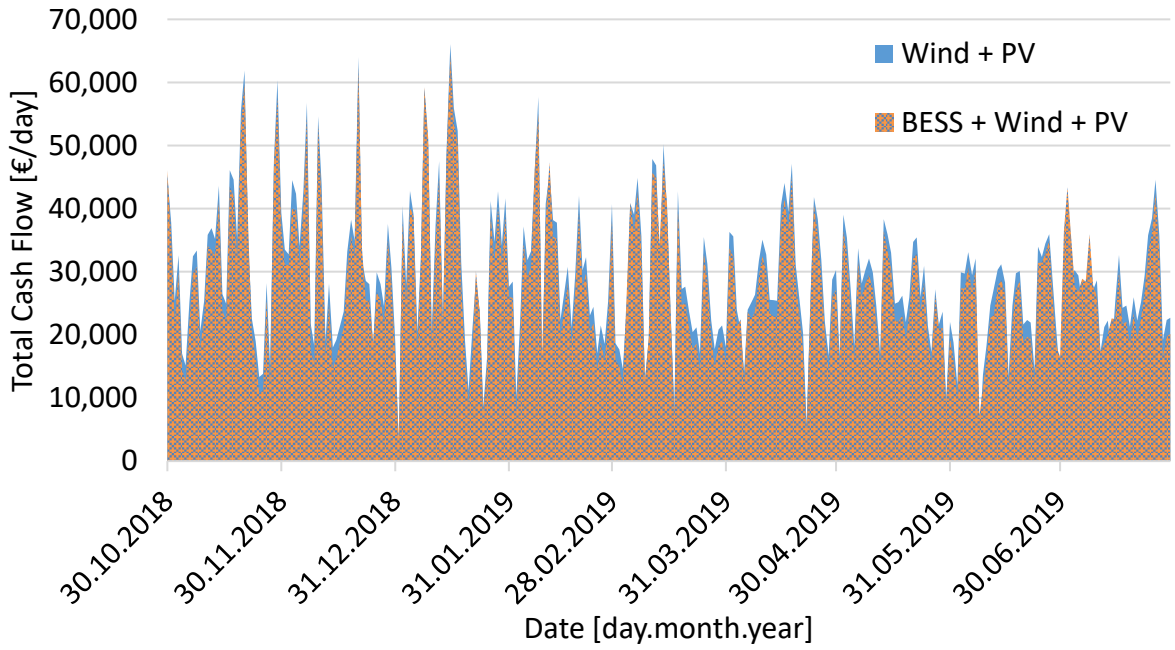

Figure 5-14: Total cash flow per day for 2 scenarios: Wind + PV and BESS + Wind + PV

5.2.3 BESS with Wind-, PV- and Thermal-Generation

This subsection reveals if a BESS can positively contribute to the operation of a pool comprising a 100 MW wind park, a 100 MW PV system and a lignite power plant with a nominal capacity of 400 MW (configuration 4, section 4.2). As in the previous subsection, the BESS has a nominal power output of 30 MW and an energetic capacity of 20 MWh. Table 5-29 summarizes the simulation results for the operation with and without the BESS. By using the standby capacity of the lignite power plant, the BESS is able to recharge at any given instance in time. For this reason, the maximum possible aFRR capacity (24 MW) can be offered to the market (row 4 – 9). Compared to subsections 5.2.1 and 5.2.2, the highest

total aFRR revenues are therefore yielded (row 3). The aFRR acceptance rate is similarly low and the arbitrage revenues are negligibly.

Table 5-29: Result summary of 2 scenarios: Wind+PV+Thermal and BESS+Wind+PV+Thermal. Each value represents the daily average over the simulation period.

Row		**Wind + PV + Thermal**	**BESS + Wind + PV + Thermal**
1	aFRR Capacity Price Revenue [€/day]	0	692
2	aFRR Energy Price Revenue [€/day]	0	934
3	aFRR Total Revenue [€/day]	0	1,627
4	POS_00_04: Accept Cap. [MW/day] / Accept. rate [%/day]	0 / 0	23 / 22
5	POS_04_08: Accept Cap. [MW/day] / Accept. rate [%/day]	0 / 0	23 / 22
6	POS_08_12: Accept Cap. [MW/day] / Accept. rate [%/day]	0 / 0	23 / 19
7	POS_12_16: Accept Cap. [MW/day] / Accept. rate [%/day]	0 / 0	24 / 17
8	POS_16_20: Accept Cap. [MW/day] / Accept. rate [%/day]	0 / 0	24 / 16
9	POS_20_24: Accept Cap. [MW/day] / Accept. rate [%/day]	0 / 0	23 / 15
10	Intraday Market: Sold Energy [MWh/day]	0	73
11	Intraday Market Revenue [€/day]	0	2,782
12	Arbitrage: Bought Energy [MWh/day]	0	3.4
13	Arbitrage: Costs [€/day]	0	103
14	Arbitrage: Sold Energy [MWh/day]	0	1.5
15	Arbitrage: Revenue [€/day]	0	104
16	Day-ahead Market: Sold Energy [MWh/day]	6,278	6,187
17	Day-ahead Market: Revenue [€/day]	282,330	279,128
18	Recharge Taxes [€/day]	0	148
19	Battery Deterioration [%/day]	0	0.0054
20	Battery Deterioration [€/day]	0	1,224
21	Differential Inverter Costs [€/day]	0	456
22	Differential BOS Costs [€/day]	0	352
23	Differential EPC and Soft Costs [€/day]	0	500
24	Differential Maintenance and Operation Costs [€/day]	0	245
25	Differential Contingency Costs [€/day]	0	64
26	Total Cash Flow incl. Degradation BESS Costs [€/day]	282,330	280,549

As explained in subsection 5.2.1, the total cash flow (row 26) only includes the revenues for selling energy on the intraday and day-ahead market. Variable costs such as for raw material (e.g. lignite) or CO_2 emissions are not considered for sold energy. Latter variable costs are

only included if the BESS recharges from the lignite power plant. For this reason, the results of Table 5-29 should only be used to evaluate if it is beneficial to add a BESS to an existing VPP.

The battery model reveals an expected lifetime of 10.1 years. Due to the high costs of the BESS and the relatively low revenue margin on the aFRR market, the total cash flow with BESS is lower than without BESS. Economically, it is not beneficial to operate the BESS with this strategy.

Figure 5-15 illustrates the daily total cash flow for both configuration over the simulation period. In only 10.2 % (28/274 days) of the days, the total cash flow with BESS is higher than without BESS. For an exemplary day, Appendix B *Figure B-1* provides detailed time series of the operating strategy and prices on the various markets for an exemplary day.

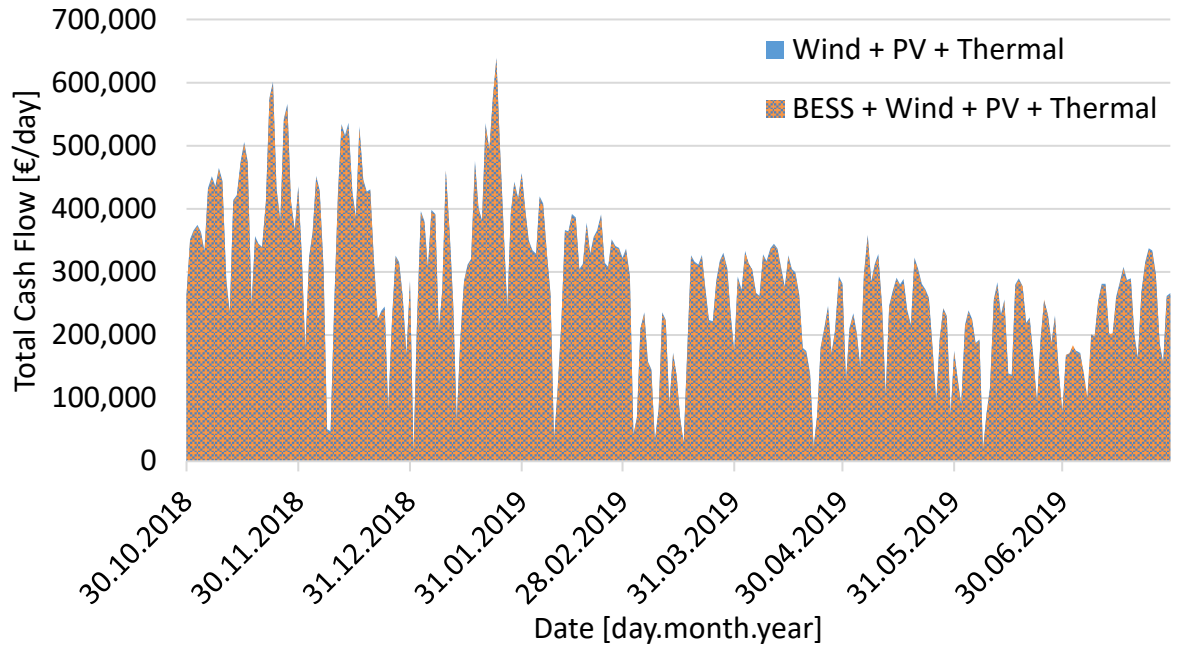

Figure 5-15: Total cash flow per day for 2 scenarios: Wind + PV + Thermal and BESS + Wind + PV + Thermal

5.2.4 Parameter Variation

Adding a BESS to the pool configurations as described in the previous subsections caused a decrease of the total cash flows. However, all simulations were based on BESS cost parameters of the year 2019 (section 4.4). This subsection presents an outlook into the year 2025 by running the same simulations with an altered set of system parameters. Since future market design changes (see subsection 2.1.2.1), control reserve demands and prices are impossible to accurately predict, this subsection uses the same underlying market model for the year 2025 as for the year 2019.

To grant the market an opportunity to react on bids placed on the intraday market, a sale opportunity time of t_{Sale} = 30mins was considered so far. As trading processes are increasing in speed, this subsection considers a sale opportunity time of t_{Sale} = 15mins. With this measure, BESS can offer more aFRR capacity (MW) to the market, since less energy must be reserved for aFRR request fulfilments.

The previous subsections derived differential battery ageing costs by considering an end-of-life (EoL) criterion of 80 % of the nominal capacity. However, various battery ageing measurements and research articles suggest that batteries can be used beyond the predefined end-of-life criterion [254–256]. In particular, multiple investigations recommend a stationary usage after the battery cells have been aged to the EoL criterion in a primary use case (e.g. electric vehicle). Results show that 2nd life battery lifespan can be multiple years [254]. The decrease in capacity beyond the end-of-life can be non-linear and the speed depends on the cell chemistry. For the simulation in this subsection, an EoL criterion of 75 % was chosen and the capacity decline is assumed linear. Investigations beyond this point would require a more sophisticated and specialized battery model.

The highest cost influence on the total cash flow arises from the containerized BESS solution. Table 5-30 summarizes the predicted costs of the various components for the year 2025. The source of the prediction is stated behind each cost value. Due to economies of scale, all hardware component costs are expected to decline by more than 50 percent until 2025 (see Table 5-30). Due to gained experience within construction companies and more standardized processes, the EPC and soft costs decline as well. Aside from the battery system (section 4.6), all components are simulated with a lifetime of 20 years.

Table 5-30: Predicted utility-scale cost parameters of containerized BESS for the year 2025.

Component	**Costs**
Battery system	99 €/kWh [238,257]
Bi-directional Inverter	50 €/kW [258]
BOS	53 €/kWh [238]
EPC	40 €/kWh [238]
Soft Costs	35 €/kWh [238]
Maintenance and Operation	1 % of hardware invest per year
Contingency	3 % of invest [236]

Simulation results for the parameter set as described above are provided in Table 5-31. Four columns state the results for the BESS standalone scenario, the BESS + Wind scenario, the BESS + Wind + PV scenario and the BESS + Wind + PV + Thermal scenario. For comparison, the last row in Table 5-31 states the total cash flow of the pool without incorporating the BESS. Despite the cost reductions, a BESS cannot be operated economically beneficial in

standalone mode. As in subsection 5.2.1, the respective total cash flow is negative (-673 €/day).

Table 5-31: Result summary with an altered parameter set. Each value represents the daily average over the simulation period.

Row		BESS Stand-alone	BESS + Wind	BESS + Wind + PV	BESS + Wind + PV + Thermal
1	aFRR Capacity Price Revenue [€/day]	309	823	944	1,126
2	aFRR Energy Price Revenue [€/day]	569	2,083	2,301	2,841
3	aFRR Total Revenue [€/day]	878	2,905	3,245	3,967
4	POS_00_04: Cap. [MW/day] / Acc. rate [%/day]	5 / 69	23 / 36	23 / 37	30 / 35
5	POS_04_08: Cap. [MW/day] / Acc. rate [%/day]	5 / 64	21 / 46	22 / 47	28 / 42
6	POS_08_12: Cap. [MW/day] / Acc. rate [%/day]	5 / 50	20 / 25	25 / 29	29 / 26
7	POS_12_16: Cap. [MW/day] / Acc. rate [%/day]	5 / 47	21 / 29	27 / 26	29 / 26
8	POS_16_20: Cap. [MW/day] / Acc. rate [%/day]	5 / 39	21 / 30	22 / 30	29 / 27
9	POS_20_24: Cap. [MW/day] / Acc. rate [%/day]	5 / 65	21 / 24	21 / 23	29 / 23
10	Intraday Market: Sold Energy [MWh/day]	0	102	118	143
11	Intraday Market Revenue [€/day]	0	3,756	4,503	5,844
12	Arbitrage: Bought Energy [MWh/day]	11.7	12.2	11.5	10.9
13	Arbitrage: Costs [€/day]	626	495	433	371
14	Arbitrage: Sold Energy [MWh/day]	3.1	8.6	8.1	8.0
15	Arbitrage: Revenue [€/day]	226	574	498	477
16	Day-ahead Market: Sold Energy [MWh/day]	0	385	599	6,085
17	Day-ahead Market: Revenue [€/day]	0	15,554	23,700	274,900
18	Recharge Taxes [€/day]	0	355	400	511
19	Battery Deterioration [%/day]	0.0054	0.0070	0.0072	0.0076
20	Battery Deterioration [€/day]	513	664	675	716
21	Battery Lifetime [years/day]	12.6	9.7	9.6	9.0
22	Differential Inverter Costs [€/day]	82	245	245	245
23	Differential BOS Costs [€/day]	173	173	173	173
24	Differential EPC and Soft Costs [€/day]	245	245	245	245
25	Differential Maint. and Operation Costs [€/day]	115	148	148	148
26	Differential Contingency Costs [€/day]	25	30	30	30
27	Total Cash Flow incl. Degrad. BESS Costs [€/day]	-673	20,421	29,599	282,751
28	Total Cash Flow without BESS [€/day]	0	20,410	29,420	282,330

However, in all other scenarios, adding a BESS to the pool configuration increases the total cash flow. It is a key finding of this work, that a BESS in conjunction with an existing generation pool can in the near future be operated economically beneficial. This in particular applies to generation pools comprising only renewables. Compared to the parameter set of the previous subsections, the total revenues on the aFRR market have more than doubled (row 3). Due to the reduced battery system costs (in particular cyclic ageing costs), the bidding strategy can offer lower energy prices (€/MWh). Consequently, a lower position in the merit order list is obtained which then leads to an increased energetic throughput. The higher energetic throughput is reflected in an increased average daily battery deterioration. Despite the lower EoL threshold, the estimated battery lifetime is around 1 year lower than with the parameter set of the previous subsection. The arbitrage revenues are increased but as before do not substantially contribute to the revenue.

5.2.5 Comparison with FCR

The vast majority of stationary BESS located in Europe/Germany operate on the FCR market (section 2.1.1). As of November 2019, 380 MW of BESS capacity were prequalified for FCR provision [259]. This amounts to 5.5 % of the total prequalified capacity. However, decreasing capacity prices lead to uncertainties in the business model for BESS [260]. This subsection provides a rough assessment of the revenue potentials for BESS and compares with the revenue potentials on the aFRR market. Reference is made to literature which more thoroughly analyses FCR provision with BESS [249,260–262].

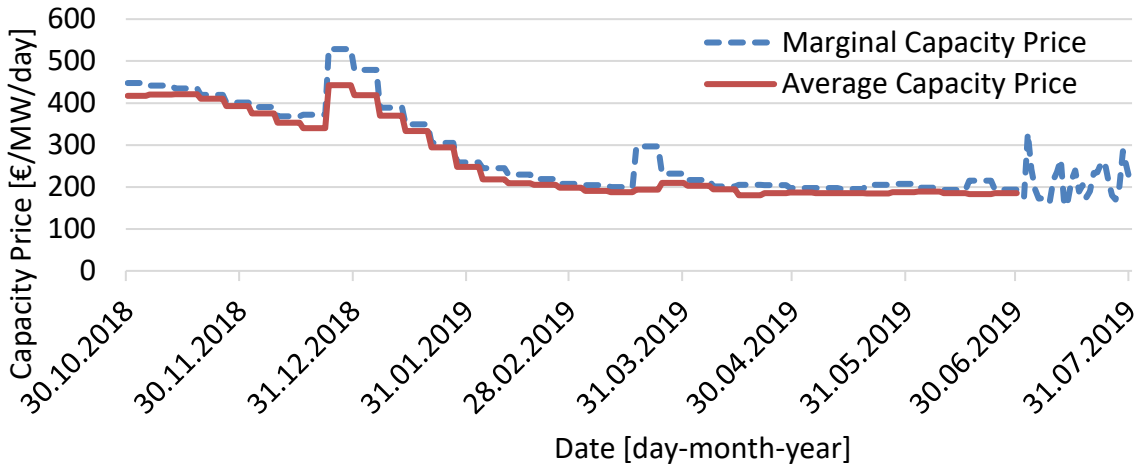

Figure 5-16: Daily capacity prices of FCR in the German control zone [14].

Figure 5-16 illustrates both the marginal capacity price and the average paid capacity price on the German FCR market for the simulation period as specified in section 5.1. Before July 2019, FCR was auctioned in weekly blocks with a service compensation based on the individually submitted capacity price (pay-as-bid). Starting with July 1st, 2019, each day is auctioned independently (section 2.1.1) and a uniform capacity price is paid to all successful

participants. The daily average paid capacity price during the aforementioned time period is 258.55 €/MW.

Before May 2019, each FCR prequalified unit was required to provide the auctioned power for 30 min in both fulfilment directions. Following new regulations coming into place at start of May 2019, the minimum delivery duration was reduced to 15 min. To get prequalified, each BESS must be able to provide the minimum delivery duration and present a functioning recharge strategy to compensate for FCR calls as well as losses within the system. An in-depth analysis regarding the minimum required energy buffer per MW FCR offered was conducted by [263]. The analysis includes the application of a recharge strategy, which is also implemented on a stationary, grid-connected BESS located in Aachen, Germany (M5BAT). Equation (50) states the minimum required energetic capacity (E_{buffer}) a BESS should have for providing a FCR power of P_{FCR} [263].

$$\begin{gathered} E_{\mathrm{buffer}}(P_{\mathrm{FCR}}, t_{\mathrm{lead}}, t_{\mathrm{idle}}) = \\ 2 \cdot (E_{\mathrm{worstCase}}(P_{\mathrm{FCR}}, t_{\mathrm{lead}}, t_{\mathrm{idle}}) + E_{\mathrm{15MinCriterion}}(P_{\mathrm{FCR}})) = \\ 2 \cdot \left(5\,\mathrm{min} \cdot P_{\mathrm{FCR}} + 10\,\mathrm{min} \cdot \frac{1}{2} \cdot P_{FCR} + 5\,\mathrm{min} \cdot \frac{1}{4} \cdot P_{\mathrm{FCR}} + 15\,\mathrm{min} \cdot P_{\mathrm{FCR}}\right) = \\ = 0.875h \cdot P_{\mathrm{FCR}} \end{gathered} \tag{50}$$

The formula includes the lead-time $t_{\mathrm{lead}}(= 5\,min)$, which accounts for the delay between triggering a recharge (set point adjustment) and the actual delivery. Further, an idle time $t_{\mathrm{idle}}(= 15\,min)$, which arises from the block size on the intraday market, is considered. The capacity reserved for providing the 15-minute minimum delivery duration ($E_{\mathrm{15MinCriterion}}$) may only be used in a so-called alert state. Three different conditions define when the alert state is active. A worst-case estimate of how much additional energy is required before the reserve capacity can be used, is provided by $E_{\mathrm{worstCase}}$ [263]. Applying equation (50) on the 30 MW, 20 MWh BESS considered in the previous subsections reveals a maximum FCR power (P_{FCR}) of 22 MW. The remaining 8 MW can be used for recharging during FCR operation (recharge strategy).

In total, the average daily revenue on the FCR market amounts to $22\,MW \cdot 258.55\,€/MW = 5688.1\,€$. The estimated FCR revenue is higher than the revenue potential on the aFRR market. The latter holds true for all considered aFRR scenarios including the reduced cost scenario of the year 2025 (subsection 5.2.4). Since large frequency deviations are very rare in the European integrated grid, the BESS has long idle times (~43 % of the time) and mostly performs small cycles [263]. Battery ageing is dominated by calendar ageing [260]. For this reason, the battery deterioration costs are lower when providing FCR than aFRR.

6 Summary and Conclusion

This work introduced with an overview of the European electricity market design and a special focus on the automatic Frequency Restoration Reserve (aFRR) market for which historical bids of successful auction participants were evaluated. Different bidding strategies were revealed by analyzing submitted capacity prices, energy prices and deployment durations. The analysis revealed a dominant impact of the individually submitted energy prices (€/MWh) on the revenues. Across all positive aFRR products in the considered period, the 25 % of participants which submitted the lowest energy price bids (€/MWh) revealed a daily average revenue of 384.95 €/MW (Table 2-1). Of these revenues, the capacity price only makes up a share of 14.49 €/MW. The remaining share is attributed to the energy price based revenues. Further, revenues significantly drop with increasing energy price bids. The next higher 25 % block of participants, in terms of the submitted energy prices, only reveals a daily average revenue of 123.18 €/MW. The latter is due to a highly reduced average deployment duration with increasing energy price bids (merit order effect). Market participants with bidding strategies that submit high energy prices are likely to either have no alternative business case for that period or follow a high-risk strategy which waits for a very rare aFRR energy request at extremely high energy prices. On the negative aFRR market, energy price bids are usually negative, corresponding to participants paying for the energy consumption or generation decrease. Revenues can only indirectly be generated by obtaining energy at prices lower than on other electricity markets.

Revenues on the aFRR market are subject to bids submitted by other market participants and to the future request pattern. Since latter components are unknown at the time of bid submission, a market prediction methodology was presented. Key market quantities were derived which assist a bidding strategy in deriving an optimal bid. These quantities include the marginal mixed price, energy prices and the deployment durations. Multiple statistical and artificial intelligence based models were used for prediction. The models are supported by various data sources, which amongst other include weather, stock exchange, bank holiday and load forecast data. Based on the predictions, the acceptance probability associated to any choice of bid was derived. In a large hyperparameter space, each model was evaluated numerous times until the best parameter set was found (hyperparameter optimization).

Comparing the performances of each model with one another did not reveal a superior model, which outperforms its contestants in all disciplines. Because of the use of exogenous data sources and the ability to generate nonlinear output, (recurrent) neural networks were expected to perform best. However, this turned out not to be true since across every time series predicted in this work, either the exponential smoothing or SARIMA model provided

the best performance on the test set in 67 % of all cases. Most neural network hyperparameter optimizations revealed slightly better performance for models using feature vectors with exogenous data sources. However, the performance benefits against not using exogenous data sources were minor and could not withstand a statistical significance test. In general, models with a small number of layers (< 5) and few neurons per layer (< 50) performed better than deep neural networks. Recurrent neural networks did not reveal performance benefits, even though, RNNs should in theory better capture events from previous time steps. The statistical variance of the RNN performance was highest among all models. Across all 60 time series, the SARIMA and exponential smoothing model provided the steadiest performance.

In the next part of this work, the earning potentials of BESS participating on the aFRR market were investigated. Both the standalone operation as well as the joint operation with three different VPPs was considered. A detailed operating strategy was presented, which maximizes the sale of generation capabilities, instantly provides aFRR power when requested and recharges the BESS from the VPP. During hours of no aFRR obligation, the BESS conducts arbitrage on the intraday market. The maximum possible aFRR capacity (MW) to offer was derived as a function of the VPP's generation profile and the energetic storage capacity (MWh) of the BESS. Based on the aFRR market predictions and the derivation of the acceptance probability, a bidding strategy was presented which finds the optimal bid to submit in the auction process. The bidding strategy solves an optimization problem which considers a cost breakdown of the BESS and involves a battery model to estimate the cell ageing.

Results indicate that an economically feasible operation in the year 2019 was not possible. This applies to all VPP configurations considered in this work. The price spread between the optimized aFRR energy price and the intraday market price does not suffice to compensate the differential BESS costs. However, for a predicted cost parameter set of the year 2025, an economically feasible operation is possible. This applies to a BESS operated in conjunction with a VPP but does not hold true for a BESS in standalone mode. One important finding of this work is that the economic feasibility strongly depends on the diversity of the VPP composition. VPPs comprising e.g. wind, PV and thermal generation show a more continuous generation profile over time than e.g. a VPP only comprising PV without any night-time generation. A continuous generation profile gives the aFRR participating BESS more recharge opportunities which consequently allows for less required energetic battery capacity (MWh) and therefore a better business case.

The economic feasibility is very sensitive as regards prices on the aFRR market and costs of the BESS. Small changes in either direction make a substantial difference. Intraday market

lead times further impact the economic feasibility. Smaller market lead times lead to less required energetic capacity of the BESS and a higher maximum aFRR capacity (MW) to offer.

One option in the optimization process conducted in this work is to provide intraday market based arbitrage in hours of no aFRR obligations. The optimizer can choose between aFRR provision and arbitrage trading. As a side effect, this work revealed that arbitrage is no economic feasible option for a BESS. In only very few instances, the optimizer decided in favor of arbitrage. Usually, the price spread on the intraday market does not compensate for the differential BESS aging costs in addition to the country-specific expenses (transmission fees, taxes, etc.).

A cost breakdown for a containerized stationary BESS revealed a battery system related contribution to the total costs of only 28 %. Aside from the cells, the battery system includes modules, cell state monitoring devices, racks, DC circuit breaker, DC bus bar, DC connection point and the battery management system. Therefore, the cost contribution of the pure battery cells is even lower.

Compared to the FCR market, profits on the aFRR market were found to be lower throughout the scenarios of this work.

6.1 Relevance of Results

Due to a university operated stationary BESS, all results generated for this thesis refer to the German/Austrian aFRR market design conditions applying between October 30th, 2018 and July 31st, 2019. Due to frequent design changes in the control reserve markets, the statements of this work are relatively short-lived and results should continuously be re-evaluated in the future. However, this section investigates why the presented results have a more wide-spread indication.

Efforts are made to consolidate and merge the various market designs across Europe based on the German/Austrian model. A European-wide auction and energy request collaboration is expected to bring synergy effects. Due to the auction similarity, the methodology and results presented in this work have a more widespread statement. Further, the methodology presented in this work can easily be adapted to predict similar quantities corresponding to different market rules. The underlying results, such as the dependency on exogenous data sources, provide an indication for other international auction-based control reserve markets.

The revenues generated by the proposed bidding strategy are based on the aFRR mixed price awarding scheme. However, they also serve as an indication for auctions based on a capacity price awarding scheme. In the past, both awarding schemes were in place in the

German/Austrian consolidation area. Revenues in either scheme are largely based on the individually submitted energy price (€/MWh) rather than on the capacity price (€/MW) or the derived mixed price. The capacity prices are close to zero in both auction schemes. A notable difference between the two auction schemes is that capacity price based awarding auctions reveal more aggressive bidding behavior. For both positive and negative fulfilment directions, a few very high (~10,000 €/MWh) energy price bids can be observed. Latter bidding strategies are targeted at making high profits at very rare and extreme conditions of the electrical grid. In an expected future auction scheme amendment, aggressive bidding behavior shall be prevented by allowing energy price bids after auction closing. For this reason, the author believes that the revenues derived by the bidding strategy in this work do not substantially deviate from the future auction scheme revenues.

6.2 Suggestions for Future Work

The prediction methodology as well as the bidding strategy can in the future be extended and improved.

Since the exogenous data sources did not generate a significant performance gain on the predictions, other data sources such as the availability of thermal power plants could be implemented. Current literature further suggests the use of qualitative sources such as news feeds or social media posts [50]. Techniques such as text mining and sentiment analysis allow the integration into the learning process. Also, the neural network models might benefit from adding autoregressive components with multiple lags to the feature vector. Due to the frequent market design changes, this work is based on a data range of less than one year. Annual seasonal effects could for instance not be considered in this work. Longer market periods can in the future be used for training the various models. In general, machine learning based models perform better, the more data is available. Various alternative time-series prediction models have been proposed in literature and could be added to the prediction framework developed for this work (e.g. support vector regression) [159,264]. Ensemble learning techniques have generated promising results in other fields and could be applied as well [265].

The bidding strategy could be extended to a holistic approach which covers the participation in multiple markets. If for instance a bid on the aFRR auction was not awarded, a subsequent bid could be submitted to the mFRR auction. Market participation on the FCR market could also be implemented. The arbitrage algorithm could be extended to simultaneously trade on both the day-ahead and intraday market to find higher price spreads. For all simulations conducted in this work, the minimum end-of-life (EoL) criterion of the battery cells was set to either 80 % or 75 %. However, various measurements and research show that battery cells can be used beyond this point. Since deep ageing effects

are not covered by the implemented battery model, a more sophisticated and specialized battery model could be used instead. A better usage of the battery lifetime would decrease the differential ageing costs and increase the earning potential.

Appendix A BESS with Wind- and PV-Generation

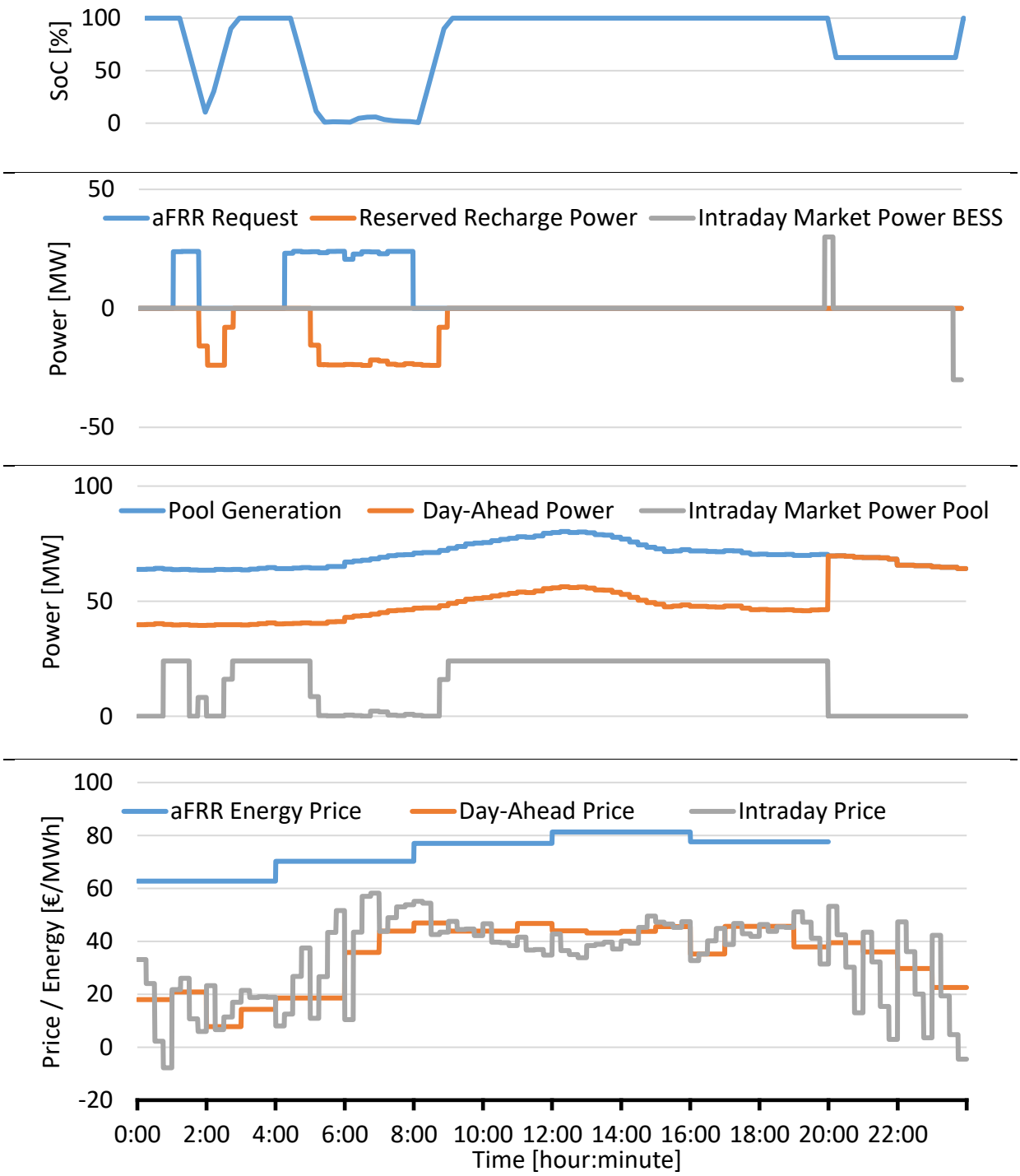

Figure A-1: Operation and trading of the BESS + Wind + PV pool on January 8th, 2019.

Appendix B BESS with Wind-, PV- and Thermal-Generation

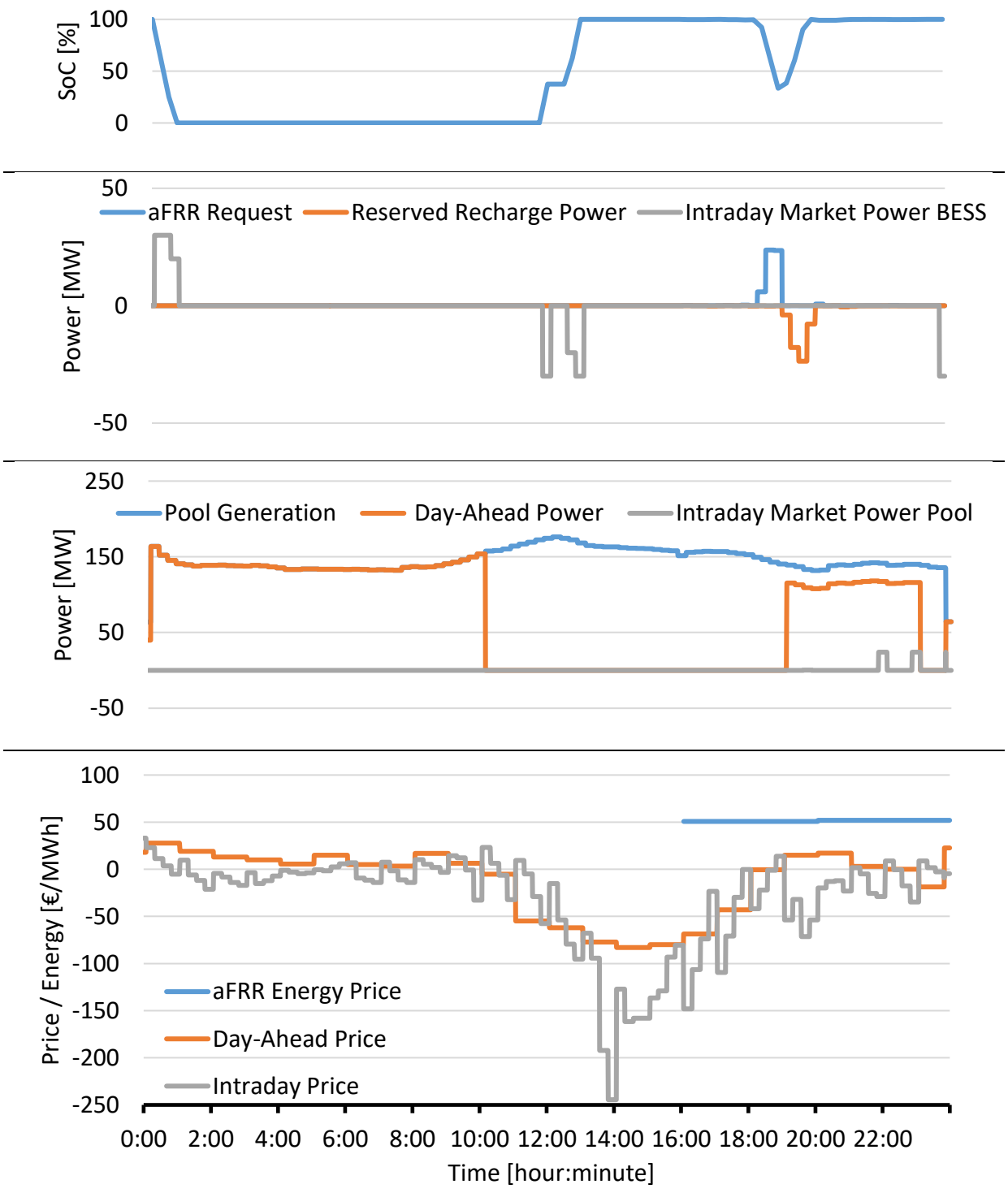

Figure B-1: Operation and trading of the BESS + Wind + PV + Thermal pool on April 22nd, 2019

List of Acronyms

ADF	Augmented Dickey Fuller
aFRR	automatic Frequency Restoration Reserve
BESS	Battery Energy Storage System
BPTT	Backpropagation Through Time
EPF	Electricity Price Forecasting
EPF	Electricity Price Forecasting
FCR	Frequency Control Reserve
GRU	Gated Recurrent Unit
KPSS	Kwiatkowski–Phillips–Schmidt–Shin
LSTM	Long Short-Term Memory
MAE	Mean Average Error
mFRR	manual Frequency Restoration Reserve
NN	Neural Network
PHS	Pumped Hydro Storages
PV	Photo Voltaic
ReLU	Rectified Linear Unit
RMSE	Root Mean Squared Error
RNN	Recurrent Neural Network
SARIMA	Seasonal Autoregressive Integrated Moving Average
SBP	Secondary Balancing Power
SCR	Secondary Control Reserve
SEATS	Seasonal Extraction in ARIMA Time Series
SoC	State of Charge
STL	Seasonal And Trend Decomposition Using Loess
TSO	Transmission System Operator
VPP	Virtual Power Plant

List of Symbols

Symbol	Unit	Meaning
$\overrightarrow{x_t}$	-	Feature vector at time step t
$\mathrm{b_t}$	-	ETS model: Smoothing component for the trend
$\mathrm{e_{t\_std}}$	-	Standardized residuals
$\mathrm{KDE_t}$	-	Estimated density function at time step t
$\mathrm{l_t}$	-	ETS model: Smoothing component for the level
$\mathrm{o_{k,j}}$	-	Output of a neural network
$\mathrm{s_t}$	-	ETS model: Smoothing component for the seasonality
$\hat{\mathrm{y}}_{\mathrm{t+1}}$	-	One-step ahead point forecast of a time series
σ_{re}	-	Standard deviation of the residuals
$B_{\mathrm{Arbitrage}}$	€	Arbitrage revenues yielded on the intraday market for periods without aFRR obligations.
B_{C}	€/MW	aFRR capacity price
$B_{\mathrm{CaFRR}}(P_{\mathrm{C}}, B_{\mathrm{C}})$	€	Capacity based aFRR revenue based on P_{C} and B_{C}
B_{Cmin}	€/MW	Lowest reasonable aFRR capacity price for an inframarginal power plant
B_{DA}	€	Revenues raised on the day-ahead market for trading some of the generation capabilities of the pool (section 4.5.3)
B_{DANoaFRR}	€	Revenues raised on the day-ahead market for periods without aFRR obligations (section 4.5.4)
B_{E}	€/MWh	aFRR energy price
$B_{\mathrm{EaFRR}}(P_{\mathrm{C}}, B_{\mathrm{C}})$	€	Energy based aFRR revenue based on P_{C} and B_{E}
B_{EE}	€/MW	Expected revenues based on the energy price
B_{ID}	€	Revenues raised on the intraday market resulting from trading the reserve band as explained in subsection 4.5.3
B_{M}	€/MW	Potential market revenues
B_{MP}	-	The mixed price for one aFRR product

C_{BESSAge}, $C_{\mathrm{BESSAgeNoaFRR}}$	€	Differential ageing costs for the BESS
C_{IdleGen}	€	Sum of marginal costs for activating the idle capacities of generation units (section 4.5.3)
C_{R}	€/MW	Power plant ramp-up costs
C_{U}	€/MW	Power plant usage costs
C_V	€/MW	Variable costs of the power plant
$E_{\mathrm{15MinCriterion}}$	MWh	Capacity reserved for providing the 15-minute minimum delivery duration for FCR provision
E_{buffer}	MWh	Energetic buffer capacity a BESS should have for providing FCR
E_{Nom}	MWh	Energetic capacity
I_{C}	-	Confidence interval
I_{P}	-	Prediction interval
$P_{\mathrm{aFRR\_Pool\_max}}$	MW	Maximum capacity a BESS in conjunction with a pool can offer on the aFRR market
$P_{\mathrm{aFRR\_Standalone}}$	MW	Maximum capacity a standalone BESS can offer on the aFRR market
P_{C}	MW	Offered aFRR capacity
P_{FCR}	MW	FCR capacity to offer on the market
P_{Nom}	MW	Nominal capacity
$S_T(T)$	-	Temperature stress component of the battery model
$S_t(t)$	-	Linear time stress component of the battery model
$S_\delta(\delta)$	-	DoD stress component of the battery model
$S_\sigma(\sigma)$	-	SoC stress component of the battery model
a_{M}	-	aFRR factor quarterly published by TSOs
$b_{k,j}$	-	Bias for a neuron within a neural network
e_t	-	Residual at time step t
f_{cal}	-	Calendric battery deterioration
f_{cyc}	-	Cyclic battery deterioration
$m_{\mathrm{valid}}(\overrightarrow{x_t})$	-	Mean model estimate of validation set data (bootstrap technique)

$n_{\mathrm{PopulationSize}}$	-	Population size of the CMA-ES optimization
n_{run}	-	Number of bootstrap evaluations
t_{Block}	min	Block size on the intraday market
t_{Delivery}	min	Minimum aFRR delivery time of a BESS
t_{Lead}	min	Lead time on the intraday market
t_{Sale}	min	Sale opportunity time on the intraday market
y_t	-	Actual values of a time series
y_t'	-	Differenced time series at time step t
z^*	-	The realization of hyperparameters resulting in the lowest value of $k(z)$
σ_{fe}	-	Standard deviation of the forecast error
σ_c	-	Standard deviation of the confidence interval
c	-	Coverage probability (critical value from the Gaussian distribution)
d	-	SARIMA model: Order of the differencing component
D	-	SARIMA model: Order of the seasonal differencing component
$\mathrm{erf}(x)$	-	Gaussian error function
h	-	Bandwidth of the kernel function $\mathrm{KDE_t}$
$\mathrm{m}(\overrightarrow{x_t})$	-	Mean model estimate (bootstrap or ensemble learning)
n	-	Number of data pairs $\{\overrightarrow{x_t}, y_t\}$
p	-	SARIMA model: Order of the autoregression component
P	-	SARIMA model: Order of the seasonal autoregression component
$\mathrm{P}(B_{\mathrm{MP}})$	-	Acceptance probability $\mathrm{P}(B_{\mathrm{MP}})$ of a mixed price B_{MP}
q	-	SARIMA model: Order of the moving-average component
Q	-	SARIMA model: Order of the seasonal moving-average component
$\mathrm{Q(x)}$	-	Q-function
T	K	Temperature
t	s	time

$\mathrm{y}(\overrightarrow{x_t})$	-	Target function
β	-	ETS model: Smoothing parameter for the trend
γ	-	ETS model: Smoothing parameter for the seasonality
$G(B_{\mathrm{C}}, B_{\mathrm{E}})$	%	Acceptance probability for a specific bid tuple in the aFRR auction.
Z	-	All possible hyperparameter realizations
$f(\overrightarrow{x_t})$	-	True regression function as a function of $\overrightarrow{x_t}$
$g(\overrightarrow{x_t})$	-	output of a trained prediction model as a function of $\overrightarrow{x_t}$
$k(z)$	-	Objective function
m	-	Frequency of the seasonality
z	-	One realization of hyperparameters
α	-	ETS model: Smoothing parameter for the level
δ	%	Depth of discharge
$\xi(\overrightarrow{x_t})$	-	Noise component of feature vector of $\overrightarrow{x_t}$
$\varphi(x)$	-	Activation function within a neural network
$\chi^2(\overrightarrow{x_t})$	-	A model fit to the remaining residuals

List of Figures

List of Tables

Bibliography

[1] Powering Past Coal Alliance (PPCA) (ed.). Third Generation Environmentalism Ltd, Members List, 2019 https://poweringpastcoal.org/about/Powering_Past_Coal_Alliance_Members (accessed 13 December 2019).

[2] Deutscher Bundestag, Dreizehntes Gesetz zur Änderung des Atomgesetzes. Bundesgesetzblatt Jahrgang 2011 Teil I Nr. 43. 31.07.2011 http://fzu.rewi.hu-berlin.de/doc/rechtsentwicklung/bgbl111s1704.pdf (accessed 18 April 2020).

[3] V. Kaminski, Energy markets, Risk Books, London, 2012. ISBN:9781906348793 http://search.ebscohost.com/login.aspx?direct=true&scope=site&db=nlebk&db=nlabk&AN=668322.

[4] 50Hertz Transmission GmbH, Amprion GmbH, TenneT TSO GmbH, TransnetBW GmbH (eds.), Präqualifizierte Anbieter je Regelenergieart. Regelleistung.net, 2019 (last update: 2 March 2020) https://www.regelleistung.net/ext/download/anbieterliste (accessed 18 April 2020).

[5] M. Merten, F. Rücker, I. Schoeneberger, D.U. Sauer, Automatic Frequency Restoration Reserve Market Prediction: Methodology and Comparison of Various Approaches, Applied Energy 268 (2020) 114978. https://doi.org/10.1016/j.apenergy.2020.114978. APEN-D-19-12341.

[6] European Parliament, Council of the European Union, Directive 96/92/EC of the European Parliament and of the Council of 19 December 1996 concerning common rules for the internal market in electricity. 19.12.1996 COM/91/0548-01 COM/93/0643-01 https://eur-lex.europa.eu/legal-content/EN/TXT/HTML/?uri=CELEX:31996L0092&from=EN (accessed 18 April 2020).

[7] European Parliament, Council of the European Union, Directive 2003/54/EC of the European Parliament and of the Council of 26 June 2003 concerning common rules for the internal market in electricity and repealing Directive 96/92/EC - Statements made with regard to decommissioning and waste management activities. 26.06.2003 2001/0077/COD https://eur-lex.europa.eu/legal-content/EN/TXT/HTML/?uri=CELEX:32003L0054&from=en (accessed 18 April 2020).

[8] European Parliament, Council of the European Union, Directive 2009/72/EC of the European Parliament and of the Council of 13 July 2009 concerning common rules for the internal market in electricity and repealing Directive 2003/54/EC (Text with EEA relevance). 13.07.2009 2007/0195/COD https://eur-lex.europa.eu/legal-content/EN/TXT/HTML/?uri=CELEX:32009L0072&from=en (accessed 18 April 2020).

[9] B. Burgholzer, Evaluation of different balancing market designs with the EDisOn+Balancing model, in: 2016 13th International Conference on the European Energy Market (EEM): 6-9 June 2016, Porto, Portugal, Porto, Portugal, IEEE, Piscataway, NJ, 2016, pp. 1–6. https://doi.org/10.1109/EEM.2016.7521271.

[10] Institute of Power Systems an Economics and E-Bridge Consulting GmbH. 50Hertz Transmission GmbH, Amprion GmbH, Elia System Operator NV, TenneT TSO B.V., TenneT TSO GmbH, TransnetBW GmbH, Potential cross-border balancing cooperation between the Belgian, Dutch and German electricity Transmission System Operators, 2014 https://www.regelleistung.net/ext/download/studie20081014 (accessed 18 April 2020).

[11] T. Thien, H. Axelsen, M. Merten, S. Zurmühlen, J. Münderlein, M. Leuthold, D.U. Sauer, Planning of Grid-Scale Battery Energy Storage Systems Lessons Learned from a 5 MW Hybrid Battery Storage Project in Germany. 19. Battcon International Stationary Battery Conference. Orlando, Florida, USA. 12.05.2015-14.04.2015, 2015 https://core.ac.uk/download/pdf/36657235.pdf (accessed 18 April 2020).

[12] E. Kraft, D. Keles, W. Fichtner, Analysis of Bidding Strategies in the German Control Reserve Market, in: 2018 15th International Conference on the European Energy Market (EEM): 27-29 June 2018, Lodz, IEEE, Piscataway, NJ, 2017, pp. 1–6. https://doi.org/10.1109/EEM.2018.8469903.

[13] Deutscher Bundestag, Gesetz zur Weiterentwicklung des Strommarktes (Strommarktgesetz), in: Bundesanzeiger Verlag, 29 July 2016, pp. 1786–1817 http://www.bgbl.de/xaver/bgbl/start.xav?startbk=Bundesanzeiger_BGBl&jumpTo=bgbl116s1786.pdf (accessed 18 April 2020).

[14] 50Hertz Transmission GmbH, Amprion GmbH, TenneT TSO GmbH, TransnetBW GmbH (eds.), General information on control reserve - technical aspects: Regelleistung.net - Internetplattform zur Vergabe von Regelleistung, 2020 https://www.regelleistung.net/ext/static/technical (accessed 18 April 2020).

[15] C. Olk, D.U. Sauer, M. Merten, Bidding strategy for a battery storage in the German secondary balancing power market, Journal of Energy Storage 21 (2019) 787–800. https://doi.org/10.1016/j.est.2019.01.019.

[16] Consentec GmbH, Description of load-frequency control concept and market for control reserves: Study commissioned by the German TSOs, 2014 https://www.consentec.de/wp-content/uploads/2014/08/Consentec_50Hertz_Regelleistungsmarkt_en__20140227.pdf (accessed 22 July 2019).

[17] F. Ocker, K.-M. Ehrhart, M. Ott, Bidding strategies in Austrian and German balancing power auctions, WIREs Energy Environ 7 (2018) e303. https://doi.org/10.1002/wene.303.

[18] B. Burgholzer, Interdependencies of harmonised procurement of manually and automatically activated FRR in selected Central European balancing markets, in: 2017 14th International Conference on the European Energy Market (EEM): 6-9 June 2017, Dresden, Germany, Dresden, Germany, IEEE, Piscataway, NJ, 2017, pp. 1–6. https://doi.org/10.1109/EEM.2017.7981919.

[19] H. Berndt, M. Hermann, H.D. Kreye, R. Reinisch, S. Ulrich, J. Vanzetta, TransmissionCode 2007: Netz- und Systemregeln der deutschen Übertragungsnetzbetreiber. Verband der Netzbetreiber - VDN – e.V. beim VDEW (ed.), 2007 https://www.vde.com/resource/blob/937758/14f1b92ea821e9e19ee13fc798c1ee0e/transmissioncode-2007--netz--und-systemregeln-der-deutschen-uebertragungsnetzbetreiber-data.pdf (accessed 18 April 2020).

[20] Bundesnetzagentur -Beschlusskammer 6, BK6-18-006. 25.01.2019 https://www.bundesnetzagentur.de/DE/Service-Funktionen/Beschlusskammern/1_GZ/BK6-GZ/2018/BK6-18-006/BK6-18-006_beschluss_vom_13_12_2018.html (accessed 18 April 2020).

[21] S. Camal, A. Michiorri, G. Kariniotakis, A. Liebelt, Short-term forecast of automatic frequency restoration reserve from a renewable energy based virtual power plant, in: 2017 IEEE PES Innovative Smart Grid Technologies Conference Europe (ISGT-Europe): Torino, Italy, 26-29 September 2017 conference proceedings, Torino, Italy, IEEE, Piscataway, NJ, 2017, pp. 1–6. https://doi.org/10.1109/ISGTEurope.2017.8260311.

[22] 50Hertz Transmission GmbH, Amprion GmbH, TenneT TSO GmbH, TransnetBW GmbH (eds.), Information on grid control cooperation and international development: Further TSOs joins IGCC (International Grid Control Cooperation). IGCC price model - transmission system operator market information, 2020 (last update: 1 April 2020) https://www.regelleistung.net/ext/download/marktinformationenApg (accessed 18 April 2020).

[23] F. Ocker, K.-M. Ehrhart, M. Belica, Harmonization of the European balancing power auction: A game-theoretical and empirical investigation, Energy Economics 73 (2018) 194–211. https://doi.org/10.1016/j.eneco.2018.05.003.

[24] TenneT TSO GmbH, PICASSO Project: Further development in integration of European balancing market, 2017 https://www.tennet.eu/news/detail/picasso-project-further-development-in-integration-of-european-balancing-market/ (accessed 22 July 2019).

[25] A. Knaut, F. Obermüller, F. Weiser. Köln: Institute of Energy Economics at the University of Cologne (EWI), Tender frequency and market concentration in balancing power markets. EWI Working Paper 17/04, 2017 https://www.econstor.eu/bitstream/10419/162229/1/879456817.pdf (accessed 18 April 2020).

[26] A. Kauffmann, M. Schlossarczyk, Einführung des Mischpreisverfahrens im Regelenergiemarkt mischt die Karten neu - enervis, 2018 https://enervis.de/einfuehrung_mischpreisverfahren_regelenergiemarkt/ (accessed 24 July 2019).

[27] J. Asker, E. Cantillon, Properties of scoring auctions, The RAND Journal of Economics 39 (2008) 69–85. https://doi.org/10.1111/j.1756-2171.2008.00004.x.

[28] S. Enkhardt. https://www.facebook.com/pvmagazine/, Erfolg für Next Kraftwerke – OLG Düsseldorf kippt Mischpreisverfahren für Regelenergie, 2019 https://www.pv-magazine.de/2019/07/22/erfolg-fuer-next-kraftwerke-olg-duesseldorf-kippt-mischpreisverfahren-fuer-regelenergie/ (accessed 24 July 2019).

[29] Bundesnetzagentur - Federal Network Agency, Einführung eines Regelarbeitsmarktes: Neue Konditionen für Anbieter von Sekundärregelung und Minutenreserve, 2019 (last update: 8 October 2019) https://www.bundesnetzagentur.de/SharedDocs/Pressemitteilungen/DE/2019/20191008_Regelenergiemarkt.html (accessed 20 April 2020).

[30] F. Müsgens, A. Ockenfels, M. Peek, Economics and design of balancing power markets in Germany, International Journal of Electrical Power & Energy Systems 55 (2014) 392–401. https://doi.org/10.1016/j.ijepes.2013.09.020.

[31] S. Just, C. Weber, Pricing of reserves: Valuing system reserve capacity against spot prices in electricity markets, Energy Economics 30 (2008) 3198–3221. https://doi.org/10.1016/j.eneco.2008.05.004 http://www.sciencedirect.com/science/article/pii/S0140988308000789.

[32] M. Aoyagi, Efficient collusion in repeated auctions with communication, Journal of Economic Theory 134 (2007) 61–92. https://doi.org/10.1016/j.jet.2005.07.016 http://www.sciencedirect.com/science/article/pii/S0022053106000755.

[33] R.C. Marshall, L.M. Marx, Bidder collusion, Journal of Economic Theory 133 (2007) 374–402. https://doi.org/10.1016/j.jet.2005.12.004 http://www.sciencedirect.com/science/article/pii/S0022053105002784.

[34] A. Hortaçsu, S.L. Puller, Understanding strategic bidding in multi-unit auctions: a case study of the Texas electricity spot market, John Wiley & Sons, Ltd (10.1111), The RAND Journal of Economics 39 (2008) 86–114. https://doi.org/10.1111/j.0741-

6261.2008.00005.x https://onlinelibrary.wiley.com/doi/full/10.1111/j.0741-6261.2008.00005.x.

[35] S. Heim, G. Götz, Do Pay-as-bid Auctions Favor Collusion? Evidence from Germany's Market for Reserve Power. Zentrum für Europäische Wirtschaftsforschung GmbH (ed.) 13-035, 2013 http://ftp.zew.de/pub/zew-docs/dp/dp13035.pdf (accessed 18 April 2020).

[36] F. Ocker, K.-M. Ehrhart, The "German Paradox" in the balancing power markets, Renewable and Sustainable Energy Reviews 67 (2017) 892–898. https://doi.org/10.1016/j.rser.2016.09.040 http://www.sciencedirect.com/science/article/pii/S1364032116305330.

[37] Next Kraftwerke GmbH (ed.), Minutenreserve: Was ist Minutenreserveleistung (MRL)?, 2011 https://www.next-kraftwerke.de/wissen/minutenreserve-tertiaerregelung (accessed 3 August 2019).

[38] EPEX SPOT SE (ed.), Marktdaten: Day-Ahead-Auktion https://www.epexspot.com/de/marktdaten/dayaheadauktion (accessed 16 May 2019).

[39] N.J. Cutler, N.D. Boerema, I.F. MacGill, H.R. Outhred, High penetration wind generation impacts on spot prices in the Australian national electricity market, Energy Policy 39 (2011) 5939–5949. https://doi.org/10.1016/j.enpol.2011.06.053 http://www.sciencedirect.com/science/article/pii/S030142151100509X.

[40] E. Fanone, A. Gamba, M. Prokopczuk, The case of negative day-ahead electricity prices, Energy Economics 35 (2013) 22–34. https://doi.org/10.1016/j.eneco.2011.12.006 http://www.sciencedirect.com/science/article/pii/S014098831100301X.

[41] T. Weibbach, S. Remppis, H. Lens, Impact of Current Market Developments in Europe on Deterministic Grid Frequency Deviations and Frequency Restauration Reserve Demand, in: 2018 15th International Conference on the European Energy Market (EEM): 27-29 June 2018, Lodz, IEEE, Piscataway, NJ, 2017, pp. 1–6. https://doi.org/10.1109/EEM.2018.8469210.

[42] S. Camal, A. Michiorri, G. Kariniotakis, Probabilistic forecasting and bidding strategy of ancillary services for aggregated renewable power plants. 6th International Conference Energy & Meteorology. Copenhagen, Denmark. 24.06.2019 - 27.06.2019, 2019 https://hal.archives-ouvertes.fr/hal-02177537 (accessed 18 April 2020).

[43] Y. Ma, P.B. Luh, K. Kasiviswanathan, E. Ni, A neural network-based method for forecasting zonal locational marginal prices, in: IEEE Power Engineering Society

General Meeting, 2004, Denver, CO, USA, IEEE, 6-10 June 2004, pp. 296–302. https://doi.org/10.1109/PES.2004.1372802.

[44] M. Olsson, L. Soder, Modeling Real-Time Balancing Power Market Prices Using Combined SARIMA and Markov Processes, IEEE Trans. Power Syst. 23 (2008) 443–450. https://doi.org/10.1109/TPWRS.2008.920046.

[45] R. Weron, Electricity price forecasting: A review of the state-of-the-art with a look into the future, International Journal of Forecasting 30 (2014) 1030–1081. https://doi.org/10.1016/j.ijforecast.2014.08.008.

[46] V. Gonzalez, J. Contreras, D.W. Bunn, Forecasting Power Prices Using a Hybrid Fundamental-Econometric Model, IEEE Trans. Power Syst. 27 (2012) 363–372. https://doi.org/10.1109/TPWRS.2011.2167689.

[47] C. Wan, Z. Xu, Y. Wang, Z.Y. Dong, K.P. Wong, A Hybrid Approach for Probabilistic Forecasting of Electricity Price, IEEE Trans. Smart Grid 5 (2014) 463–470. https://doi.org/10.1109/TSG.2013.2274465.

[48] R. Weron, A. Misiorek, Forecasting spot electricity prices: A comparison of parametric and semiparametric time series models, International Journal of Forecasting 24 (2008) 744–763. https://doi.org/10.1016/j.ijforecast.2008.08.004 http://www.sciencedirect.com/science/article/pii/S0169207008000952.

[49] A. Andalib, F. Atry, Multi-step ahead forecasts for electricity prices using NARX: A new approach, a critical analysis of one-step ahead forecasts, Energy Conversion and Management 50 (2009) 739–747. https://doi.org/10.1016/j.enconman.2008.09.040 http://www.sciencedirect.com/science/article/pii/S0196890408003889.

[50] A. Pathak, N.P. Shetty, Indian Stock Market Prediction Using Machine Learning and Sentiment Analysis, in: H.S. Behera, J. Nayak, B. Naik, A. Abraham (Eds.), Computational Intelligence in Data Mining, Springer Singapore, Singapore, 2019, pp. 595–603. https://doi.org/10.1007/978-981-10-8055-5_53.

[51] Y. Zhai, A. Hsu, S.K. Halgamuge, Combining News and Technical Indicators in Daily Stock Price Trends Prediction, in: D. Liu, S. Fei, Z. Hou, H. Zhang, C. Sun (Eds.), Advances in Neural Networks – ISNN 2007, Springer Berlin Heidelberg, Berlin, Heidelberg, 2007, pp. 1087–1096. https://doi.org/10.1007/978-3-540-72395-0_132.

[52] V.S. Pagolu, K.N. Reddy, G. Panda, B. Majhi, Sentiment analysis of Twitter data for predicting stock market movements, in: International Conference on Signal Processing, Communication, Power and Embedded System (SCOPES)-2016: 3rd-5th October 2016 IEEE conference proceedings, Paralakhemundi, Odisha, India, IEEE, Piscataway, NJ, 2016, pp. 1345–1350. https://doi.org/10.1109/SCOPES.2016.7955659.

[53] T. Jonsson, P. Pinson, H.A. Nielsen, H. Madsen, T.S. Nielsen, Forecasting Electricity Spot Prices Accounting for Wind Power Predictions, IEEE Trans. Sustain. Energy 4 (2013) 210–218. https://doi.org/10.1109/TSTE.2012.2212731.

[54] T. Kristiansen, Forecasting Nord Pool day-ahead prices with an autoregressive model, Energy Policy 49 (2012) 328–332. https://doi.org/10.1016/j.enpol.2012.06.028 http://www.sciencedirect.com/science/article/pii/S0301421512005381.

[55] J. Janczura, S. Trück, R. Weron, R.C. Wolff, Identifying spikes and seasonal components in electricity spot price data: A guide to robust modeling, Energy Economics 38 (2013) 96–110. https://doi.org/10.1016/j.eneco.2013.03.013 http://www.sciencedirect.com/science/article/pii/S0140988313000625.

[56] A.J. Conejo, M.A. Plazas, R. Espinola, A.B. Molina, Day-Ahead Electricity Price Forecasting Using the Wavelet Transform and ARIMA Models, IEEE Trans. Power Syst. 20 (2005) 1035–1042. https://doi.org/10.1109/TPWRS.2005.846054.

[57] M. Bubak, G.D. van Albada, P.M.A. Sloot, J. Dongarra, M. Bierbrauer, S. Trück, R. Weron, Modeling Electricity Prices with Regime Switching Models: Computational Science - ICCS 2004, Springer Berlin Heidelberg. Berlin, Heidelberg, 2004. ISBN:978-3-540-25944-2.

[58] Deutscher Wetterdienst - DWD Climate Data Center. CDC - Vertrieb Klima und Umwelt (ed.), Most recent 10-minute station observations of mean wind speed and wind direction for Germany. version recent, 2019 ftp://ftp-cdc.dwd.de/climate_environment/CDC/observations_germany/climate/10_minutes/wind/now/DESCRIPTION_obsgermany_climate_10min_wind_now_en.pdf (accessed 18 April 2020).

[59] R.B. Alley, K.A. Emanuel, F. Zhang, Advances in weather prediction, Science 363 (2019) 342–344. https://doi.org/10.1126/science.aav7274.

[60] Marlene Weiß. Süddeutsche.de GmbH (ed.), Die geheime Wetter-Revolution, Munich, Germany, 2019 (last update: 30 January 2019) https://www.sueddeutsche.de/wissen/wettervorhersage-genauer-meteorologie-prognose-wettersatellit-1.4306028 (accessed 18 April 2020).

[61] ENTSO-E (ed.), ENTSO-E Transparency Platform: Central collection and publication of electricity generation, transportation and consumption data and information for the pan-European market., 2019 (last update: 14 May 2019) https://m-transparency.entsoe.eu/dashboard/show (accessed 18 April 2020).

[62] I. Guyon, A. Elisseeff, An introduction to variable and feature selection, The Journal of Machine Learning Research (2003) https://dl.acm.org/doi/10.5555/944919.944968 (accessed 18 April 2020).

[63] Davis Kirkendall. Github (ed.), German Bank Holidays, 2019 https://github.com/daviskirk/german-holidays (accessed 18 April 2020).

[64] Deutscher Wetterdienst - DWD Climate Data Center. CDC - Vertrieb Klima und Umwelt (ed.), Most recent 10-minute station observations of solar incoming radiation,longwave downward radiation and sunshine duration for Germany,. version recent, 2019 ftp://ftp-cdc.dwd.de/climate_environment/CDC/observations_germany/climate/10_minutes/solar/now/DESCRIPTION_obsgermany_climate_10min_solar_now_en.pdf (accessed 18 April 2020).

[65] Deutscher Wetterdienst - DWD Climate Data Center. CDC - Vertrieb Klima und Umwelt (ed.), Most recent 10-minute station observations of pressure, air temperature (at 5cm and 2m height), humidity and dew point for Germany. version recent, 2019 ftp://ftp-cdc.dwd.de/climate_environment/CDC/observations_germany/climate/10_minutes/air_temperature/now/DESCRIPTION_obsgermany_climate_10min_tu_now_en.pdf (accessed 18 April 2020).

[66] Verizon Media (ed.). Yahoo Finance, Global X DAX Germany ETF (DAX) https://finance.yahoo.com/quote/DAX/history (accessed 18 April 2020).

[67] U.S. Energy Information Administration (ed.), Crude Oil Prices: Brent - Europe, 2019 https://fred.stlouisfed.org/series/DCOILBRENTEU (accessed 14 May 2019).

[68] finanzen.net GmbH, Kohlepreis in EUR - Historische Kurse https://www.boerse-online.de/rohstoffe/historisch/kohlepreis/euro (accessed 14 May 2019).

[69] wallstreet:online AG (ed.), Index Zertifikat auf ECX EUA [CO2-Emission] Future 12/2019 (ICE-Europe) Open-End (COBA) https://www.wallstreet-online.de/zertifikat/dr1wbm-ecx-eua-co2-emission-future-12-2019-ice-europe-index-zertifikat-open-end-coba (accessed 14 May 2019).

[70] wallstreet:online AG (ed.), Erdgaspreis: ISIN: XD0002745517 | Symbol: NG https://www.wallstreet-online.de/rohstoffe/erdgaspreis/historische-kurse (accessed 14 May 2019).

[71] S.I. Vagropoulos, G.I. Chouliaras, E.G. Kardakos, C.K. Simoglou, A.G. Bakirtzis, Comparison of SARIMAX, SARIMA, modified SARIMA and ANN-based models for short-term PV generation forecasting, in: 2016 IEEE International Energy Conference (ENERGYCON): The 2016 IEEE International Energy Conference (ENERGYCON) took place in Leuven from 4 to 8 April 2016, Leuven, Belgium, IEEE, Piscataway, NJ, 2016, pp. 1–6. https://doi.org/10.1109/ENERGYCON.2016.7514029.

[72] S. Raschka, V. Mirjalili, Python machine learning: Machine learning and deep learning with Python, scikit-learn, and TensorFlow, Packt Publishing, Birmingham, Mumbai, 2018. ISBN:9781787125933.

[73] P.P. Angelov, X. Gu. Springer International Publishing AG, Empirical approach to machine learning, Springer, Cham, 2019. ISBN:9783030023843 http://www.springer.com/.

[74] H. Saleh, Machine learning fundamentals: Use Python and scikit-learn to get up and running with the hottest developments in machine learning, Packt Publishing, Birmingham, 2018. ISBN:9781789801767.

[75] M. Kuhn, K. Johnson, Applied predictive modeling, 5th ed., Springer, New York, 2016. ISBN:9781461468493.

[76] B. d. Ripley, Pattern recognition and neural networks, 1st ed., Cambridge Univ. Press, Cambridge, 2009. ISBN:9780521717700.

[77] S.J. Russell, P. Norvig, Artificial intelligence: A modern approach, Pearson, Boston, Columbus, Indianapolis, 2016. ISBN:9780132071482.

[78] M. Gori, Machine learning: A constraint-based approach, Morgan Kaufmann, Amsterdam, 2017. ISBN:9780081006702 http://www.sciencedirect.com/science/book/9780081006597.

[79] R.J. Hyndman, G. Athanasopoulos, Forecasting: Principles and practice, 2nd ed., 2018. ISBN:9780987507112.

[80] E.B. Dagum, S. Bianconcini, Seasonal adjustment methods and real time trend-cycle estimation, Springer, Cham, 2016. ISBN:9783319318202 http://dx.doi.org/10.1007/978-3-319-31822-6.

[81] D. Ladiray, B. Quenneville, Seasonal Adjustment with the X-11 Method, Springer, New York, NY, 2001. ISBN:9780387951713 http://dx.doi.org/10.1007/978-1-4613-0175-2.

[82] R.B. Cleveland, W.S. Cleveland, J.E. McRae, I. Terpenning, STL: A seasonal-trend decomposition procedure based on loess, Journal of official statistics 6 (1990) 3–33 https://www.scb.se/contentassets/ca21efb41fee47d293bbee5bf7be7fb3/stl-a-seasonal-trend-decomposition-procedure-based-on-loess.pdf (accessed 18 April 2020).

[83] R.A. Yaffee, M. McGee, An Introduction to Time Series Analysis and Forecasting: With Applications of SAS® and SPSS®, 1st ed., Elsevier textbooks, s.l., 2000. ISBN:0127678700 http://site.ebrary.com/lib/alltitles/docDetail.action?docID=10185912.

[84] P.S.P. Cowpertwait, A. v. Metcalfe, Introductory time series with R, Springer, Dordrecht, 2009. ISBN:9780387886978 http://dx.doi.org/10.1007/978-0-387-88698-5.

[85] G.E.P. Box, D.R. Cox, An Analysis of Transformations, [Royal Statistical Society, Wiley], Journal of the Royal Statistical Society. Series B (Methodological) 26 (1964) 211–252 https://www.ime.usp.br/~abe/lista/pdfQWaCMboK68.pdf (accessed 18 April 2020).

[86] T. Bollerslev, Generalized autoregressive conditional heteroskedasticity, Journal of Econometrics 31 (1986) 307–327. https://doi.org/10.1016/0304-4076(86)90063-1 http://www.sciencedirect.com/science/article/pii/0304407686900631.

[87] A. Röthig, Microeconomic Risk Management and Macroeconomic Stability, Springer-Verlag Berlin Heidelberg, Berlin, Heidelberg, 2009. ISBN:9783642015649 http://www.springerlink.com.library.myebs.de/content/u27266/.

[88] H. Lütkepohl, M. Krätzig (Eds.), Applied time series econometrics, Cambridge Univ. Press, Cambridge, 2009. ISBN:9780521547871.

[89] W.Q. Meeker, G.J. Hahn, L.A. Escobar, Statistical intervals: A guide for practitioners and researchers, John Wiley & Sons Inc, Hoboken, New Jersey, 2017. ISBN:9781118595169 http://onlinelibrary.wiley.com/book/10.1002/9781118594841.

[90] J. Landon, N.D. Singpurwalla, Choosing a Coverage Probability for Prediction Intervals, The American Statistician 62 (2008) 120–124. https://doi.org/10.1198/000313008X304062.

[91] C.W.J. Granger, P. Newbold, K. Shell, Forecasting Economic Time Series, 2nd ed., Elsevier Reference Monographs, s.l., 2014. ISBN:0122951832 http://gbv.eblib.com/patron/FullRecord.aspx?p=1876880.

[92] H.M. Wadsworth, Handbook of statistical methods for engineers and scientists, 2nd ed., McGraw-Hill, New York, NY, 1998. ISBN:007067678X.

[93] T. Heskes, Practical Confidence and Prediction Intervals, in: Advances in Neural Information Processing Systems 9, MIT press, 1997, pp. 176–182 https://papers.nips.cc/paper/1306-practical-confidence-and-prediction-intervals.pdf (accessed 18 April 2020).

[94] G. Petneházi, Recurrent Neural Networks for Time Series Forecasting, 2019 http://arxiv.org/pdf/1901.00069v1 (accessed 18 April 2020).

[95] G. James, D. Witten, T. Hastie, R. Tibshirani, An introduction to statistical learning: With applications in R, 8th ed., Springer, New York, Heidelberg, Dordrecht, London, 2017. ISBN:9781461471387.

[96] R.J. Hyndman, A. Koehler, K. Ord, R. Snyder, Forecasting with Exponential Smoothing: The State Space Approach, Springer, Berlin, Heidelberg, 2008. ISBN:9783540719168 http://d-nb.info/989924998/34.

[97] P.J. Brockwell, R.A. Davis, Introduction to Time Series and Forecasting, Springer, Cham, 2016. ISBN:9783319298528 http://dx.doi.org/10.1007/978-3-319-29854-2.

[98] R.D. Snyder, J.K. Ord, A.B. Koehler, Prediction Intervals for ARIMA Models, [American Statistical Association, Taylor & Francis, Ltd.], Journal of Business & Economic Statistics 19 (2001) 217–225 http://www.jstor.org/stable/1392165 (accessed 18 April 2020).

[99] R.J. Hyndman, Y. Khandakar, Automatic Time Series Forecasting: the forecast Package for R, Monash University, Department of Econometrics and Business Statistics …, Journal of Statistical Software (2008). https://doi.org/10.18637/jss.v027.i03 (accessed 18 April 2020).

[100] E. Dhamo, L. Puka. University of Tirana, Faculty of Natural Science, Department of Mathematics, Using the R-package to forecast time series: ARIMA models and Application https://www.researchgate.net/publication/274249061_Using_the_R-package_to_forecast_time_series_ARIMA_models_and_Application (accessed 18 April 2020).

[101] S. Seabold, J. Perktold, Statsmodels: Econometric and Statistical Modeling with Python, Proceedings of the 9th Python in Science Conference 2010 (2010) https://www.researchgate.net/publication/264891066_Statsmodels_Econometric_and_Statistical_Modeling_with_Python (accessed 18 April 2020).

[102] D.J.C. MacKay, The Evidence Framework Applied to Classification Networks, Neural Computation 4 (1992) 720–736. https://doi.org/10.1162/neco.1992.4.5.720.

[103] C.M. Bishop, Neural networks for pattern recognition, Oxford Univ. Press, Oxford, 2010. ISBN:9780198538646.

[104] J.T.G. Hwang, A.A. Ding, Prediction Intervals for Artificial Neural Networks, Journal of the American Statistical Association 92 (1997) 748–757. https://doi.org/10.1080/01621459.1997.10474027.

[105] R. d. de Veaux, J. Schumi, J. Schweinsberg, L.H. Ungar, Prediction Intervals for Neural Networks via Nonlinear Regression, Technometrics 40 (1998) 273. https://doi.org/10.2307/1270528.

[106] B. Efron, Bootstrap Methods: Another Look at the Jackknife, Ann. Statist. 7 (1979) 1–26. https://doi.org/10.1214/aos/1176344552.

[107] L.A. Thombs, W.R. Schucany, Bootstrap Prediction Intervals for Autoregression, Taylor & Francis, Journal of the American Statistical Association 85 (1990) 486–492. https://doi.org/10.1080/01621459.1990.10476225.

[108] B. Efron, R. Tibshirani, An introduction to the bootstrap, Chapman & Hall, Boca Raton, Fla., 1998. ISBN:9780412042317.

[109] D.A. Nix, A.S. Weigend, Estimating the mean and variance of the target probability distribution, in: Proceedings of 1994 IEEE International Conference on Neural Networks (ICNN'94), Orlando, FL, USA, IEEE, 28.06.1994 - 02.07.1994, 55-60 vol.1. https://doi.org/10.1109/ICNN.1994.374138.

[110] N.A. Shrivastava, A. Khosravi, B.K. Panigrahi, Prediction Interval Estimation of Electricity Prices Using PSO-Tuned Support Vector Machines, IEEE Trans. Ind. Inf. 11 (2015) 322–331. https://doi.org/10.1109/TII.2015.2389625.

[111] R. Errouissi, J. Cardenas-Barrera, J. Meng, E. Castillo-Guerra, X. Gong, L. Chang, Bootstrap prediction interval estimation for wind speed forecasting, in: 2015 IEEE Energy Conversion Congress and Exposition (ECCE): 20 - 24 Sept. 2015, Montreal, Quebec, Canada, Montreal, QC, Canada, IEEE, Piscataway, NJ, 2015, pp. 1919–1924. https://doi.org/10.1109/ECCE.2015.7309931.

[112] A. Khosravi, S. Nahavandi, D. Creighton, A.F. Atiya, Comprehensive review of neural network-based prediction intervals and new advances, IEEE Trans. Neural Netw. 22 (2011) 1341–1356. https://doi.org/10.1109/TNN.2011.2162110.

[113] D.K. Agrafiotis, W. Cedeño, V.S. Lobanov, On the Use of Neural Network Ensembles in QSAR and QSPR, J. Chem. Inf. Comput. Sci. 42 (2002) 903–911. https://doi.org/10.1021/ci0203702.

[114] J.G. Carney, P. Cunningham, U. Bhagwan, Confidence and prediction intervals for neural network ensembles, in: IJCNN'99: Proceedings, International Joint Conference on Neural Networks, Washington, DC, July 10-16, 1999, Washington, DC, USA, Institute of Electrical and Electronics Engineers, New York, 1999, pp. 1215–1218. https://doi.org/10.1109/IJCNN.1999.831133.

[115] C. Sheng, J. Zhao, W. Wang, H. Leung, Prediction intervals for a noisy nonlinear time series based on a bootstrapping reservoir computing network ensemble, IEEE Trans. Neural Netw. Learn. Syst. 24 (2013) 1036–1048. https://doi.org/10.1109/TNNLS.2013.2250299.

[116] R. Davidson, J.G. MacKinnon, Bootstrap tests: how many bootstraps?, Econometric Reviews 19 (2000) 55–68. https://doi.org/10.1080/07474930008800459.

[117] R.R. Wilcox, Fundamentals of Modern Statistical Methods: Substantially Improving Power and Accuracy, 2nd ed., Springer Science+Business Media LLC, New York, NY, 2010. ISBN:978-1-4419-5525-8 http://dx.doi.org/10.1007/978-1-4419-5525-8.

[118] H.J. Adèr, G.J. Mellenbergh, D.J. Hand, Advising on Research Methods: A consultant's companion, 1st ed., 2011. ISBN:9789079418091.

[119] M.P. Clements, N. Taylor, Bootstrapping prediction intervals for autoregressive models, International Journal of Forecasting 17 (2001) 247–267. https://doi.org/10.1016/S0169-2070(00)00079-0 http://www.sciencedirect.com/science/article/pii/S0169207000000790.

[120] J.A. Miguel, P. Olave, Bootstrapping forecast intervals in ARCH models, Test 8 (1999) 345–364. https://doi.org/10.1007/BF02595875 https://doi.org/10.1007/BF02595875.

[121] C. Wan, Y. Song, Z. Xu, G. Yang, A.H. Nielsen, Probabilistic Wind Power Forecasting with Hybrid Artificial Neural Networks, Electric Power Components and Systems 44 (2016) 1656–1668. https://doi.org/10.1080/15325008.2016.1198437.

[122] X. Chen, Z.Y. Dong, K. Meng, Y. Xu, K.P. Wong, H.W. Ngan, Electricity Price Forecasting With Extreme Learning Machine and Bootstrapping, IEEE Trans. Power Syst. 27 (2012) 2055–2062. https://doi.org/10.1109/TPWRS.2012.2190627.

[123] E.M. Oliveira, F.L.C. Oliveiraa, Forecasting mid-long term electric energy consumption through bagging ARIMA and exponential smoothing methods, Pergamon, Energy 144 (2018) 776–788. https://doi.org/10.1016/j.energy.2017.12.049.

[124] P.F. Dunn, Measurement and Data Analysis for Engineering and Science, Third Edition, Taylor & Francis, 2014. ISBN:9781466594968 https://books.google.de/books?id=LsySAwAAQBAJ.

[125] M.K. Simon, Probability distributions involving gaussian random variables: A handbook for engineers and scientists, Springer Science + Business Media LLC, Boston, MA, 2006. ISBN:9781402070587 http://dx.doi.org/10.1007/978-0-387-47694-0.

[126] R.J. Hyndman, A.B. Koehler, Another look at measures of forecast accuracy, International Journal of Forecasting 22 (2006) 679–688. https://doi.org/10.1016/j.ijforecast.2006.03.001 http://www.sciencedirect.com/science/article/pii/S0169207006000239.

[127] S. Raschka, Model Evaluation, Model Selection, and Algorithm Selection in Machine Learning, 2018 http://arxiv.org/pdf/1811.12808v2.

[128] A. Pal, P.K.S. Prakash, Practical time series analysis: Master time series data processing, visualization, and modeling using python, 2017. ISBN:9781788290227.

[129] A.C. Müller, S. Guido, Introduction to machine learning with Python: A guide for data scientists, O'Reilly Media, Sebastopol, CA, 2017. ISBN:9781449369415 http://proquest.tech.safaribooksonline.de/9781449369880.

[130] G. Zaccone, M.R. Karim, Deep Learning with TensorFlow - Second Edition, Packt Publishing, Birmingham, England, 2018. ISBN:1788831101.

[131] J. Bergstra, Y. Bengio, Random Search for Hyper-Parameter Optimization, Journal of Machine Learning Research 13 (2012) https://pdfs.semanticscholar.org/8e28/30fb6ba9ea201d4ec5d2d800ab9a9bf9677c.pdf (accessed 18 April 2020).

[132] M. Bernico, Deep learning quick reference: Useful hacks for training and optimizing deep neural networks with TensorFlow and Keras, 2018. ISBN:9781788838917.

[133] J. Bergstra, R. Bardenet, Y. Bengio, B. Kégl, Algorithms for hyper-parameter optimization, Curran Associates Inc (2011) https://papers.nips.cc/paper/4443-algorithms-for-hyper-parameter-optimization.pdf (accessed 18 April 2020).

[134] P. Jiang, C.A. Shoemaker, X. Liu, Time-varying hyperparameter strategies for radial basis function surrogate-based global optimization algorithm, in: 2017 IEEE International Conference on Industrial Engineering & Engineering Management: IEEE IEEM2017 10-13 Dec, Singapore, Singapore, IEEE, Piscataway, NJ, 2017, pp. 984–988. https://doi.org/10.1109/IEEM.2017.8290039.

[135] E. Real, S. Moore, A. Selle, S. Saxena, Y.L. Suematsu, J. Tan, Le Quoc, A. Kurakin, Large-Scale Evolution of Image Classifiers, 2017 http://arxiv.org/pdf/1703.01041v2.

[136] M. Feurer, F. Hutter, Hyperparameter Optimization, in: F. Hutter, L. Kotthoff, J. Vanschoren (Eds.), Automated Machine Learning: Methods, Systems, Challenges, Springer International Publishing, Cham, 2019, pp. 3–33. https://doi.org/10.1007/978-3-030-05318-5_1.

[137] J. Snoek, H. Larochelle, R.P. Adams, Practical Bayesian Optimization of Machine Learning Algorithms, 2012 http://arxiv.org/pdf/1206.2944v2.

[138] J. Bergstra, D. Yamins, D.D. Cox, Making a Science of Model Search, 2012 http://arxiv.org/pdf/1209.5111v1.

[139] B. Shahriari, K. Swersky, Z. Wang, R.P. Adams, N. de Freitas, Taking the Human Out of the Loop: A Review of Bayesian Optimization, Proc. IEEE 104 (2016) 148–175. https://doi.org/10.1109/JPROC.2015.2494218.

[140] T. Hastie, R. Tibshirani, J.H. Friedman, The elements of statistical learning: Data mining, inference, and prediction, 12th ed., Springer, New York, NY, 2017. ISBN:9780387848587.

[141] M. Stone, Cross-Validatory Choice and Assessment of Statistical Predictions, [Royal Statistical Society, Wiley], Journal of the Royal Statistical Society. Series B (Methodological) 36 (1974) 111–147 http://www.jstor.org/stable/2984809.

[142] C. Bergmeir, R.J. Hyndman, B. Koo, A note on the validity of cross-validation for evaluating autoregressive time series prediction, Computational Statistics & Data Analysis 120 (2018) 70–83. https://doi.org/10.1016/j.csda.2017.11.003 http://www.sciencedirect.com/science/article/pii/S0167947317302384.

[143] C. Bergmeir, J.M. Benítez, On the use of cross-validation for time series predictor evaluation, Information Sciences 191 (2012) 192–213. https://doi.org/10.1016/j.ins.2011.12.028.

[144] C. Bergmeir, R.J. Hyndman, B. Koo, A Note on the Validity of Cross-Validation for Evaluating Time Series Prediction, Department of Econometrics and Business Statistics (2015) https://pdfs.semanticscholar.org/1dec/48d4f811350786312398299b7ae9621769ea.pdf (accessed 18 April 2020).

[145] G.M. LJUNG, G.E.P. Box, On a measure of lack of fit in time series models, Biometrika 65 (1978) 297–303. https://doi.org/10.1093/biomet/65.2.297.

[146] C.C. Aggarwal, Data mining: The textbook, Springer, Cham, 2015. ISBN:9783319141411.

[147] E. Parzen, On Estimation of a Probability Density Function and Mode, The Annals of Mathematical Statistics 33 (1962) 1065–1076. https://doi.org/10.1214/aoms/1177704472.

[148] M. Rosenblatt, Remarks on Some Nonparametric Estimates of a Density Function, The Annals of Mathematical Statistics 27 (1956) 832–837. https://doi.org/10.1214/aoms/1177728190.

[149] M.C. Jones, J.S. Marron, S.J. Sheather, A brief survey of bandwidth selection for density estimation, Journal of the American Statistical Association 91 (1996) 401–407. https://doi.org/10.2307/2291420.

[150] B.U. Park, J.S. Marron, Comparison of data-driven bandwidth selectors, Journal of the American Statistical Association 85 (1990) 66–72. https://doi.org/10.1080/01621459.1990.10475307.

[151] J. M. C. Jones, S. Marron, S. J. Sheather, The performance of six popular bandwidth selection methods on some real data sets (with discussion), Journal of the American Statistical Association 91 (1996) 401-407 http://www.jstor.org/stable/2291420?origin=JSTOR-pdf (accessed 18 April 2020).

[152] B.A. Turlach, Bandwidth Selection in Kernel Density Estimation: A Review Vol. 19 (1993) http://citeseerx.ist.psu.edu/viewdoc/download?doi=10.1.1.44.6770&rep=rep1&type=pdf (accessed 18 April 2020).

[153] D.W. Scott, Multivariate density estimation: Theory, practice, and visualization, Wiley, New York, NY, 1992. ISBN:9780471547709 http://site.ebrary.com/lib/alltitles/docDetail.action?docID=10344014.

[154] Z.I. Botev, J.F. Grotowski, D.P. Kroese, Kernel density estimation via diffusion, Institute of Mathematical Statistics, The Annals of Statistics 38 (2010) 2916–2957. https://doi.org/10.1214/10-AOS799 https://projecteuclid.org/download/pdfview_1/euclid.aos/1281964340.

[155] P. Hall, J.S. Marron, B.U. Park, Smoothed cross-validation, Probability Theory and Related Fields 92 (1992) 1–20. https://doi.org/10.1007/BF01205233 https://doi.org/10.1007/BF01205233.

[156] R.M. Heiberger, B. Holland, Statistical analysis and data display: An intermediate course with examples in S-Plus, R, and SAS, Springer, New York, NY, 2004. ISBN:9780387402703 http://www.loc.gov/catdir/enhancements/fy0817/2004048200-d.html.

[157] J.G. de Gooijer, R.J. Hyndman, 25 years of time series forecasting, International Journal of Forecasting 22 (2006) 443–473. https://doi.org/10.1016/j.ijforecast.2006.01.001.

[158] R. Adhikari, R.K. Agrawal, An Introductory Study on Time Series Modeling and Forecasting, LAP Lambert Academic Publishing http://arxiv.org/pdf/1302.6613v1.

[159] Mahmoud K. Okasha, Using Support Vector Machines in Financial Time Series Forecasting, Department of Applied Statistics International Journal of Statistics and Applications (2014). https://doi.org/10.5923/j.statistics.20140401.03.

[160] C.C. Holt, Forecasting seasonals and trends by exponentially weighted moving averages, International Journal of Forecasting (1957) 5–10. https://doi.org/10.1016/j.ijforecast.2003.09.015 http://www.sciencedirect.com/science/article/pii/S0169207003001134.

[161] R.G. Brown, Statistical forecasting for inventory control, McGraw-Hill, New York, 1959 https://openlibrary.org/books/OL21251092M/Statistical_forecasting_for_inventory_control (accessed 18 April 2020).

[162] P.R. Winters, Forecasting Sales by Exponentially Weighted Moving Averages, Management Science 6 (1960) 324–342. https://doi.org/10.1287/mnsc.6.3.324.

[163] G.P. McCormick, Communications to the Editor—Exponential Forecasting: Some New Variations, Management Science 15 (1969) 311–320. https://doi.org/10.1287/mnsc.15.5.311.

[164] E.S. Gardner, E. Mckenzie, Forecasting Trends in Time Series, Management Science 31 (1985) 1237–1246. https://doi.org/10.1287/mnsc.31.10.1237.

[165] M. Akpinar, N. Yumusak, Day-ahead natural gas forecasting using nonseasonal exponential smoothing methods, in: Conference proceedings 2017 IEEE International Conference on Environment and Electrical Engineering and 2017 IEEE Industrial and Commercial Power Systems Europe (EEEIC/I & CPS Europe): 6-9 June, 2017, Milan, Italy, Milan, Italy, IEEE, Piscataway, NJ, 2017, pp. 1–4. https://doi.org/10.1109/EEEIC.2017.7977756.

[166] J. Lian, L. Li, Predictive Analysis of E-Commerce Enterprises Soft Operating Costs Based on Exponential Smoothing Technique, in: Ninth International Conference on Information Technology in Medicine and Education: ITME 2018 proceedings 19-21 October 2018, Hangzhou, Zhejiang, China, Hangzhou, IEEE, Piscataway, NJ, 2018, pp. 911–915. https://doi.org/10.1109/ITME.2018.00203.

[167] J. Lian, L. He, Research on Production Prediction Based on Exponential Smoothing Method, in: Ninth International Conference on Information Technology in Medicine and Education: ITME 2018 proceedings 19-21 October 2018, Hangzhou, Zhejiang, China, Hangzhou, IEEE, Piscataway, NJ, 2018, pp. 961–963. https://doi.org/10.1109/ITME.2018.00214.

[168] H. Zhou, X. Wu, W. Wang, L. Chen, Forecast of next day clearing price in deregulated electricity market, in: IEEE International Conference on Systems, Man and Cybernetics, 2009: SMC 2009 ; 11 - 14 Oct. 2009, San Antonio, Texas, USA ; proceedings, San Antonio, TX, USA, IEEE, Piscataway, NJ, 2009, pp. 4397–4401. https://doi.org/10.1109/ICSMC.2009.5346934.

[169] J. Huang, D. Srinivasan, D. Zhang, Electricity Demand Forecasting Using HWT Model with Fourfold Seasonality, in: ICCAIRO 2017: 2017 International Conference on Control, Artificial Intelligence, Robotics & Optimization Prague, Czech Republic, 20-22 May 2017 proceedings, Prague, IEEE, Piscataway, NJ, 2017, pp. 254–258. https://doi.org/10.1109/ICCAIRO.2017.55.

[170] M.R. Milici, L.-D. Milici, P. Atanasoae, V. Stefanescu, Studies on Energy Consumption Using Methods of Exponential Smoothing, in: 2019 11th International Symposium on Advanced Topics in Electrical Engineering (ATEE), Bucharest, Romania, IEEE, 3/28/2019 - 3/30/2019, pp. 1–4. https://doi.org/10.1109/ATEE.2019.8724946.

[171] R. Beigaite, T. Krilavicius, K.L. Man, Electricity Price Forecasting for Nord Pool Data, in: 2018 International Conference on Platform Technology and Service (PlatCon): 29-31 Jan. 2018, Jeju, IEEE, Piscataway, NJ, 2018, pp. 1–6. https://doi.org/10.1109/PlatCon.2018.8472762.

[172] R.J. Hyndman, A.B. Koehler, R.D. Snyder, S. Grose, A state space framework for automatic forecasting using exponential smoothing methods, International Journal of Forecasting 18 (2002) 439–454. https://doi.org/10.1016/S0169-2070(01)00110-8.

[173] J.K. Ord, A.B. Koehler, R.D. Snyder, Estimation and Prediction for a Class of Dynamic Nonlinear Statistical Models, Journal of the American Statistical Association 92 (1997) 1621. https://doi.org/10.2307/2965433.

[174] J.H. Cochrane. Graduate School of Business, University of Chicago, Time Series for Macroeconomics and Finance, University of Chicago, 1997 http://econ.lse.ac.uk/staff/wdenhaan/teach/cochrane.pdf (accessed 18 April 2020).

[175] K.W. Hipel, A.I. McLeod. ScienceDirect (Online service), Time series modelling of water resources and environmental systems, Elsevier, Amsterdam, New York, 1994. ISBN:9781281778734 http://site.ebrary.com/lib/alltitles/docDetail.action?docID=10259230.

[176] J.C. Ramesh, T. Ganesh, Forecasting of Monthly Mean Rainfall in Rayalaseema, IJCRR (2017). https://doi.org/10.7324/IJCRR.2017.9244.

[177] H. Nguyen, C.K. Hansen, Short-term electricity load forecasting with Time Series Analysis, in: 2017 IEEE International Conference on Prognostics and Health Management (ICPHM): took place June 19-21, 2017 in Dallas, TX, USA, Dallas, TX, USA, IEEE, Piscataway, NJ, 2017, pp. 214–221. https://doi.org/10.1109/ICPHM.2017.7998331.

[178] F. Fahmi, H. Sofyan, Forecasting household electricity consumption in the province of Aceh using combination time series model, in: "Advancing Knowledge, Research, and Technology for Humanity": Proceedings 2017 International Conference on Electrical Engineering and Informatics Banda Aceh, Aceh, Indonesia, October 18-20, 2017, Banda Aceh, IEEE, Piscataway, NJ, 2017, pp. 97–102. https://doi.org/10.1109/ICELTICS.2017.8253239.

[179] G.E.P. Box, G.M. Jenkins, Time Series Analysis Forecasting and Control, Operational Research Quarterly (1970-1977) 22 (1971) 199. https://doi.org/10.2307/3008255.

[180] R.J. Hyndman, Y. Khandakar, Automatic Time Series Forecasting: The forecast Package for R, J. Stat. Soft. 27 (2008). https://doi.org/10.18637/jss.v027.i03.

[181] H. Akaike, This Week's Citation Classic: A new look at the statistical model identification, Current Contents Engineering, Technology, and Applied Sciences 12 (1981) 42 http://www.garfield.library.upenn.edu/classics1981/A1981MS54100001.pdf (accessed 18 April 2020).

[182] T.W. ARNOLD, Uninformative Parameters and Model Selection Using Akaike's Information Criterion, The Journal of Wildlife Management 74 (2010) 1175–1178. https://doi.org/10.1111/j.1937-2817.2010.tb01236.x.

[183] G. Ciaburro, P. Joshi, Python Machine Learning Cookbook - Second Edition, Packt Publishing, Birmingham, England, 2019. ISBN:1789808456.

[184] J.G. Taylor, The Promise of Neural Networks, Springer London, 2012. ISBN:9781447103950 https://books.google.de/books?id=GbnkBwAAQBAJ.

[185] W.S. McCulloch, W. Pitts, A logical calculus of the ideas immanent in nervous activity, The bulletin of mathematical biophysics 5 (1943) 115–133. https://doi.org/10.1007/BF02478259 https://doi.org/10.1007/BF02478259.

[186] K. Hornik, M. Stinchcombe, H. White, Multilayer feedforward networks are universal approximators, Neural Networks 2 (1989) 359–366. https://doi.org/10.1016/0893-6080(89)90020-8 http://www.sciencedirect.com/science/article/pii/0893608089900208.

[187] A. Navlani. DataCamp, Neural Network Models in R https://www.datacamp.com/community/tutorials/neural-network-models-r (accessed 9 July 2019).

[188] A. Hajian, P. Styles, Application of Soft Computing and Intelligent Methods in Geophysics, Springer International Publishing, 2018. ISBN:9783319665320 https://books.google.de/books?id=93hhDwAAQBAJ.

[189] J. Heaton, Introduction to neural networks with Java, 2nd ed., Heaton Research, St. Louis, Mo., 2008. ISBN:9781604390087.

[190] I. Goodfellow, Y. Bengio, A. Courville, Deep learning, MIT press, Cambridge, Massachusetts, London, England, 2016. ISBN:9780262035613 http://www.deeplearningbook.org/.

[191] X. Glorot, A. Bordes, Y. Bengio, Deep Sparse Rectifier Neural Networks 315–323 http://proceedings.mlr.press/v15/glorot11a/glorot11a.pdf (accessed 18 April 2020).

[192] A. Krizhevsky, I. Sutskever, G.E. Hinton, ImageNet Classification with Deep Convolutional Neural Networks, pp. 1097–1105 http://papers.nips.cc/paper/4824-imagenet-classification-with-deep-convolutional-neural-networks.pdf (accessed 18 April 2020).

[193] K. Jarrett, K. Kavukcuoglu, M.'A. Ranzato, Y. LeCun, What is the best multi-stage architecture for object recognition?, in: IEEE 12th International Conference on Computer Vision, 2009: Kyoto, Japan, 29 September - 2 October 2009, Kyoto, IEEE, Piscataway, NJ, 2009, pp. 2146–2153. https://doi.org/10.1109/ICCV.2009.5459469.

[194] K. He, X. Zhang, S. Ren, J. Sun, Delving Deep into Rectifiers: Surpassing Human-Level Performance on ImageNet Classification, 2015 http://arxiv.org/pdf/1502.01852v1.

[195] J. Brownlee, Clever algorithms: Nature-inspired programming recipes, 2nd ed., LuLu.com, s.l., 2012. ISBN:9781446785065.

[196] Y. Zhao, W. Lang, B. Li, Performence analysis of neural network with improved weight training process, in: 2019 IEEE 3rd Information Technology, Networking, Electronic and Automation Control Conference (ITNEC), Chengdu, China, IEEE, 3/15/2019 - 3/17/2019, pp. 1760–1764. https://doi.org/10.1109/ITNEC.2019.8729535.

[197] L.M. Waghmare, N.N. Bidwai, P.P. Bhogle, Neural Network Weight Initialization, in: International Conference on Mechatronics and Automation, 2007: ICMA 2007 ; 5 - 8 Aug. 2007, Harbin, China, Harbin, China, IEEE Service Center, Piscataway, NJ, 2007, pp. 679–681. https://doi.org/10.1109/ICMA.2007.4303625.

[198] X. Glorot, Y. Bengio, Understanding the difficulty of training deep feedforward neural networks, Journal of Machine Learning Research - Proceedings Track 9 (2010) 249–256 http://proceedings.mlr.press/v9/glorot10a/glorot10a.pdf (accessed 18 April 2020).

[199] C.C. Aggarwal, Neural Networks and Deep Learning: A Textbook, Springer International Publishing, Cham, 2018. ISBN:9783319944647.

[200] S. Ruder, An overview of gradient descent optimization algorithms, 2017 https://arxiv.org/pdf/1609.04747.

[201] A.C. Wilson, R. Roelofs, M. Stern, N. Srebro, B. Recht, The Marginal Value of Adaptive Gradient Methods in Machine Learning, 2017 http://arxiv.org/pdf/1705.08292v2.

[202] J. Duchi, E. Hazan, Y. Singer, Adaptive Subgradient Methods for Online Learning and Stochastic Optimization, JMLR.org, Journal of Machine Learning Research 12 (2011) 2121–2159 http://dl.acm.org/ft_gateway.cfm?id=2021068&type=pdf (accessed 18 April 2020).

[203] M.D. Zeiler, ADADELTA: An Adaptive Learning Rate Method, 2012 https://arxiv.org/pdf/1212.5701.

[204] D.P. Kingma, J. Ba, Adam: A Method for Stochastic Optimization, 2014 http://arxiv.org/pdf/1412.6980v9.

[205] N.S. Keskar, R. Socher, Improving Generalization Performance by Switching from Adam to SGD, 2017 https://arxiv.org/pdf/1712.07628.

[206] S.J. Reddi, S. Kale, S. Kumar, On the Convergence of Adam and Beyond (2018) https://arxiv.org/abs/1904.09237 (accessed 18 April 2020).

[207] H. Zou, T. Hastie, Regularization and variable selection via the elastic net, J Royal Statistical Soc B 67 (2005) 301–320. https://doi.org/10.1111/j.1467-9868.2005.00503.x.

[208] F. Chollet, Deep learning with Python, Manning, Shelter Island, NY, 2018. ISBN:9781617294433 http://proquest.safaribooksonline.com/9781617294433.

[209] N. Srivastava, G. Hinton, A. Krizhevsky, I. Sutskever, R. Salakhutdinov, Dropout: A Simple Way to Prevent Neural Networks from Overfitting, Journal of Machine Learning Research 15 (2014) 1929–1958 http://jmlr.org/papers/volume15/srivastava14a/srivastava14a.pdf (accessed 18 April 2020).

[210] M.C. Mozer, A Focused Backpropagation Algorithm for Temporal Pattern Recognition, Department of Computer Science and Institute of Cognitive Science, University of Colorado, Boulder, CO 80309, USA, Complex Systems 3 137–169 https://wpmedia.wolfram.com/uploads/sites/13/2018/02/03-4-4.pdf (accessed 18 April 2020).

[211] A.J. Robinson, F. Fallside, The utility driven dynamic error propagation network, Cambridge University, Engineering Department (1987) https://www.bibsonomy.org/bibtex/269a88ecbac9a51cbf0b4be189c412820/idsia (accessed 18 April 2020).

[212] P.J. Werbos, Generalization of backpropagation with application to a recurrent gas market model, Neural Networks 1 (1988) 339–356. https://doi.org/10.1016/0893-6080(88)90007-x.

[213] C. Olah, Understanding LSTM Networks -- colah's blog, 2019 (last update: 25 June 2019) https://colah.github.io/posts/2015-08-Understanding-LSTMs/ (accessed 12 July 2019).

[214] L. Peng, S. Liu, R. Liu, L. Wang, Effective long short-term memory with differential evolution algorithm for electricity price prediction, Energy 162 (2018) 1301–1314. https://doi.org/10.1016/j.energy.2018.05.052.

[215] Z. Chang, Y. Zhang, W. Chen, Effective Adam-Optimized LSTM Neural Network for Electricity Price Forecasting, in: 2018 IEEE 9th International Conference on Software

Engineering and Service Science (ICSESS), Beijing, China, IEEE, 11/23/2018 - 11/25/2018, pp. 245–248. https://doi.org/10.1109/ICSESS.2018.8663710.

[216] R. Pascanu, T. Mikolov, Y. Bengio, On the difficulty of training Recurrent Neural Networks, 30th International Conference on Machine Learning, ICML 2013 (2012) https://arxiv.org/pdf/1211.5063.pdf (accessed 18 April 2020).

[217] J. Hochreiter, Untersuchungen zu dynamischen neuronalen Netzen. Institut für Informatik - Technische Universität München (ed.), 1991 http://people.idsia.ch/~juergen/SeppHochreiter1991ThesisAdvisorSchmidhuber.pdf (accessed 18 April 2020).

[218] S. Hochreiter, J. Schmidhuber, Long Short-Term Memory, Neural Computation 9 (1997) 1735–1780. https://doi.org/10.1162/neco.1997.9.8.1735.

[219] Z.C. Lipton, J. Berkowitz, C. Elkan, A Critical Review of Recurrent Neural Networks for Sequence Learning, 2015 http://arxiv.org/pdf/1506.00019v4.

[220] K. Cho, B. van Merrienboer, C. Gulcehre, D. Bahdanau, F. Bougares, H. Schwenk, Y. Bengio, Learning Phrase Representations using RNN Encoder-Decoder for Statistical Machine Translation, 2014 https://arxiv.org/pdf/1406.1078.

[221] J. Chung, C. Gulcehre, K. Cho, Y. Bengio, Empirical Evaluation of Gated Recurrent Neural Networks on Sequence Modeling, 2014 https://arxiv.org/pdf/1412.3555.

[222] K. Yao, T. Cohn, K. Vylomova, K. Duh, C. Dyer, Depth-Gated LSTM, 2015 https://arxiv.org/pdf/1508.03790.

[223] J. Koutník, K. Greff, F. Gomez, J. Schmidhuber, A Clockwork RNN, 2014 https://arxiv.org/pdf/1402.3511.

[224] M. Merten, C. Olk, I. Schoeneberger, D.U. Sauer, Bidding Strategy for Battery Storage Systems in the Secondary Control Reserve Market, Applied Energy 268 (2020) 114951. https://doi.org/10.1016/j.apenergy.2020.114951. APEN-D-20-00475.

[225] T. Drees, N.V. Bracht, A. Moser, Reserve providing in future generation systems considering renewable energy sources, in: 2014 11th International Conference on the European Energy Market (EEM): 28-30 May 2014, Kraków, Poland, Krakow, Poland, IEEE, Piscataway, NJ, 2014, pp. 1–6. https://doi.org/10.1109/EEM.2014.6861301.

[226] A. Maaz. RWTH Aachen; Print Production M. Wolff GmbH, Auswirkungen von strategischem Bietverhalten auf die Marktpreise am deutschen Day-Ahead-Spotmarkt und an den Regelleistungsauktionen. Dissertation, 1st ed. ISBN:9783941704671.

[227] A. Bublitz, P. Ringler, M. Genoese, D. Keles, W. Fichtner, Agent-Based Simulation of Interrelated Wholesale Electricity Markets, in: Twenty-Fifth International Workshop

on Database and Expert Systems Applications: Proceedings DEXA 2014 1-4 September 2014, Munich, Germany, Munich, Germany, IEEE Computer Society, Los Alamitos, CA, 2014, pp. 103–108. https://doi.org/10.1109/DEXA.2014.35.

[228] M. Genoese, Energiewirtschaftliche Analysen des deutschen Strommarkts mit agentenbasierter Simulation, 1st ed., Nomos, Baden-Baden, 2010. ISBN:9783845227443.

[229] European Commission, Directorate-General for Energy, Commission Regulation (EU) 2017/2195 - Establishing a Guideline on Electricity Balancing. 2017 http://data.europa.eu/eli/reg/2017/2195/oj (accessed 18 April 2020).

[230] A.G. Morinec, F.E. Villaseca, Optimal generator bidding strategies for power and ancillary services using game theory, in: 40th North American Power Symposium: September 28-September 30 2008, University of Calgary, Calgary, Alberta, Canada, Calgary, AB, Canada, IEEE, [Piscataway, N.J.], 2008, pp. 1–8. https://doi.org/10.1109/NAPS.2008.5307329.

[231] T. Soares, P. Pinson, T.V. Jensen, H. Morais, Optimal Offering Strategies for Wind Power in Energy and Primary Reserve Markets, IEEE Trans. Sustain. Energy 7 (2016) 1036–1045. https://doi.org/10.1109/TSTE.2016.2516767.

[232] S. Camal, A. Michiorri, G. Kariniotakis, Optimal Offer of Automatic Frequency Restoration Reserve From a Combined PV/Wind Virtual Power Plant, IEEE Trans. Power Syst. 33 (2018) 6155–6170. https://doi.org/10.1109/TPWRS.2018.2847239.

[233] I. Staffell, M. Rustomji, Maximising the value of electricity storage, Journal of Energy Storage 8 (2016) 212–225. https://doi.org/10.1016/j.est.2016.08.010 http://www.sciencedirect.com/science/article/pii/S2352152X1630113X.

[234] H. Khani, Optimal Scheduling of Energy Storage for Energy Shifting and Ancillary Services to the Grid, Electronic Thesis and Dissertation Repository (2016) https://ir.lib.uwo.ca/etd/3933 (accessed 18 April 2020).

[235] A. Gitis, M. Leuthold, D.U. Sauer, Applications and Markets for Grid-Connected Storage Systems, in: P.T. Moseley (Ed.), Electrochemical energy storage for renewable sources and grid balancing, Elsevier, Amsterdam u.a., 2015, pp. 33–52. https://doi.org/10.1016/B978-0-444-62616-5.00004-8.

[236] R. Fu, T. Remo, R. Margolis, Evaluating the Cost Benefits of U.S. Utility-Scale Photovoltaics Plus Energy Storage Systems, in: 2018 IEEE 7th World Conference on Photovoltaic Energy Conversion (WCPEC): (a joint conference of 45th IEEE PVSC, 28th PVSEC & 34th EU PVSEC) 10-15 June 2018, Waikoloa Village, HI, IEEE, Piscataway, NJ, 2018, pp. 1–4. https://doi.org/10.1109/PVSC.2018.8547852.

[237] R. Fu, T. Remo, R. Margolis, 2018 U.S. Utility-Scale Photovoltaics-Plus-Energy Storage System Costs Benchmark. National Laboratory of the U.S. Department of Energy (NREL) https://www.nrel.gov/docs/fy19osti/71714.pdf (accessed 18 April 2020).

[238] D. Frankel, S. Kane, C. Tryggestad, The new rules of competition in energy storage, 2018 (last update: June 2018) https://www.mckinsey.com/industries/electric-power-and-natural-gas/our-insights/the-new-rules-of-competition-in-energy-storage# (accessed 21 November 2019).

[239] M. Sieg. PV Magazine, Marktübersicht große Batteriespeicher, 2019 https://www.pv-magazine.de/marktuebersichten/grosse-batteriespeicher/ (accessed 21 November 2019).

[240] Bundesministerium der Justiz und für Verbraucherschutz, Verordnung über die Entgelte für den Zugang zu Elektrizitätsversorgungsnetzen (Stromnetzentgeltverordnung - StromNEV). § 19 Sonderformen der Netznutzung. 25.07.2005 https://www.gesetze-im-internet.de/stromnev/StromNEV.pdf (accessed 18 April 2020).

[241] H. Lund, G. Salgi, B. Elmegaard, A.N. Andersen, Optimal operation strategies of compressed air energy storage (CAES) on electricity spot markets with fluctuating prices, Applied Thermal Engineering 29 (2009) 799–806. https://doi.org/10.1016/j.applthermaleng.2008.05.020 http://www.sciencedirect.com/science/article/pii/S1359431108002469.

[242] D. Connolly, H. Lund, P. Finn, B.V. Mathiesen, M. Leahy, Practical operation strategies for pumped hydroelectric energy storage (PHES) utilising electricity price arbitrage, Energy Policy 39 (2011) 4189–4196. https://doi.org/10.1016/j.enpol.2011.04.032 http://www.sciencedirect.com/science/article/pii/S0301421511003156.

[243] B. Xu, A. Oudalov, A. Ulbig, G. Andersson, D. Kirschen, Modeling of lithium-ion battery degradation for cell life assessment, in: 2017 IEEE Power & Energy Society General Meeting: 16-20 July 2017, Chicago, IL, IEEE, Piscataway, NJ, 2017, p. 1. https://doi.org/10.1109/PESGM.2017.8274005.

[244] G. Ning, B. Popov, Cycle Life Modeling of Lithium-Ion Batteries, Journal of The Electrochemical Society - J ELECTROCHEM SOC 151 (2004). https://doi.org/10.1149/1.1787631.

[245] A. Millner, Modeling Lithium Ion battery degradation in electric vehicles, in: IEEE Conference on Innovative Technologies for an Efficient and Reliable Electricity Supply (CITRES), 2010: Waltham, Massachusetts, USA, 27 - 29 Sept. 2010, Waltham, MA, USA, IEEE, Piscataway, NJ, 2010, pp. 349–356. https://doi.org/10.1109/CITRES.2010.5619782.

[246] J. Vetter, P. Novák, M.R. Wagner, C. Veit, K.-C. Möller, J.O. Besenhard, M. Winter, M. Wohlfahrt-Mehrens, C. Vogler, A. Hammouche, Ageing mechanisms in lithium-ion batteries, Journal of Power Sources 147 (2005) 269–281. https://doi.org/10.1016/j.jpowsour.2005.01.006 http://www.sciencedirect.com/science/article/pii/S0378775305000832.

[247] I. Laresgoiti, S. Käbitz, M. Ecker, D.U. Sauer, Modeling mechanical degradation in lithium ion batteries during cycling: Solid electrolyte interphase fracture, Journal of Power Sources 300 (2015) 112–122. https://doi.org/10.1016/j.jpowsour.2015.09.033 http://www.sciencedirect.com/science/article/pii/S0378775315302949.

[248] G. Marsh, C. Wignall, P.R. Thies, N. Barltrop, A. Incecik, V. Venugopal, L. Johanning, Review and application of Rainflow residue processing techniques for accurate fatigue damage estimation, International Journal of Fatigue 82 (2016) 757–765. https://doi.org/10.1016/j.ijfatigue.2015.10.007 http://www.sciencedirect.com/science/article/pii/S0142112315003333.

[249] J. Münderlein, M. Steinhoff, S. Zurmühlen, D.U. Sauer, Analysis and evaluation of operations strategies based on a large scale 5 MW and 5 MWh battery storage system, Elsevier, Journal of Energy Storage 24 (2019) 100778. https://doi.org/10.1016/j.est.2019.100778.

[250] N. Hansen, The CMA Evolution Strategy: A Comparing Review, in: J.A. Lozano, E. Bengoetxea, I. Inza, P. Larrañaga (Eds.), Towards a New Evolutionary Computation: Advances in the Estimation of Distribution Algorithms, Springer-Verlag Berlin Heidelberg, Berlin, Heidelberg, 2006, pp. 75–102. https://doi.org/10.1007/3-540-32494-1_4 https://doi.org/10.1007/3-540-32494-1_4.

[251] N. Hansen. Ecole Polytechnique (ed.), References to CMA-ES Applications, Paris http://www.cmap.polytechnique.fr/~nikolaus.hansen/cmaapplications.pdf (accessed 24 November 2019).

[252] N. Hansen. Github (ed.), CMA-ES written in ANSI C https://github.com/cma-es/c-cmaes (accessed 24 November 2019).

[253] F. Bellifermine, G. Caire, A. Poggi, G. Rimassa, JADE: A software framework for developing multi-agent applications. Lessons learned, Elsevier, Information and Software Technology 50 (2008) 10–21. https://doi.org/10.1016/j.infsof.2007.10.008.

[254] L.C. Casals, B. Amante García, C. Canal, Second life batteries lifespan: Rest of useful life and environmental analysis, Journal of Environmental Management 232 (2019) 354–363. https://doi.org/10.1016/j.jenvman.2018.11.046 http://www.sciencedirect.com/science/article/pii/S0301479718313124.

[255] A. Podias, A. Pfrang, F. Di Persio, A. Kriston, S. Bobba, F. Mathieux, M. Messagie, L. Boon-Brett, Sustainability Assessment of Second Use Applications of Automotive Batteries: Ageing of Li-Ion Battery Cells in Automotive and Grid-Scale Applications, Multidisciplinary Digital Publishing Institute, World Electric Vehicle Journal 9 (2018) 24. https://doi.org/10.3390/wevj9020024 https://www.mdpi.com/2032-6653/9/2/24/pdf.

[256] S. Bobba, F. Mathieux, F. Ardente, G.A. Blengini, M.A. Cusenza, A. Podias, A. Pfrang, Life Cycle Assessment of repurposed electric vehicle batteries: an adapted method based on modelling energy flows, Journal of Energy Storage 19 (2018) 213–225. https://doi.org/10.1016/j.est.2018.07.008 http://www.sciencedirect.com/science/article/pii/S2352152X18300677.

[257] W.J. Cole, A. Frazier, Cost Projections for Utility-Scale Battery Storage. National Renewable Energy Lab. (NREL), Golden, CO (United States) NREL/TP-6A20-73222. https://doi.org/10.2172/1529218 https://www.osti.gov/servlets/purl/1529218 (accessed 18 April 2020).

[258] D. Fürstenwerth, M.M. Kleiner, Current and Future Cost of Photovoltaics. Long-term Scenarios for Market Development, System Prices and LCOE of Utility-Scale PV Systems.: Study on behalf of Agora Energiewende. Fraunhofer ISE (ed.), 2015 https://www.ise.fraunhofer.de/content/dam/ise/de/documents/publications/studies/AgoraEnergiewende_Current_and_Future_Cost_of_PV_Feb2015_web.pdf (accessed 18 April 2020).

[259] 50Hertz Transmission GmbH, Amprion GmbH, TenneT TSO GmbH, TransnetBW GmbH (eds.), Prequalified Capacity in Germany. Regelleistung.net, 2019 (last update: November 2019) https://www.regelleistung.net/ext/download/pq_capacity (accessed 18 April 2020).

[260] J. Fleer, S. Zurmühlen, J. Meyer, J. Badeda, P. Stenzel, J.-F. Hake, D. Uwe Sauer, Price development and bidding strategies for battery energy storage systems on the primary control reserve market, Energy Procedia 135 (2017) 143–157. https://doi.org/10.1016/j.egypro.2017.09.497 http://www.sciencedirect.com/science/article/pii/S1876610217346003.

[261] A. Zeh, M. Müller, M. Naumann, H.C. Hesse, A. Jossen, R. Witzmann, Fundamentals of Using Battery Energy Storage Systems to Provide Primary Control Reserves in Germany, Multidisciplinary Digital Publishing Institute, Batteries 2 (2016) 29. https://doi.org/10.3390/batteries2030029 https://www.mdpi.com/2313-0105/2/3/29/pdf.

[262] P. Iurillia, C. Briviob, M. Merloa, SoC management strategies in Battery Energy Storage System providing Primary Control Reserve, Elsevier, Sustainable Energy, Grids and Networks 19 (2019) 100230. https://doi.org/10.1016/j.segan.2019.100230.

[263] T. Thien, D. Schweer, D. Vom Stein, A. Moser, D.U. Sauer, Real-world operating strategy and sensitivity analysis of frequency containment reserve provision with battery energy storage systems in the german market, Elsevier, Journal of Energy Storage 13 (2017) 143–163. https://doi.org/10.1016/j.est.2017.06.012.

[264] K.-j. Kim, Financial time series forecasting using support vector machines, Neurocomputing 55 (2003) 307–319. https://doi.org/10.1016/S0925-2312(03)00372-2.

[265] Z.-H. Zhou, Ensemble Learning, Springer, Boston, MA, Encyclopedia of Biometrics (2015). https://doi.org/10.1007/978-1-4899-7488-4_293.

Own Publications

During my time as a research associate at the institute, multiple publications as listed below were created. The contents of these publications are in accordance with the doctoral degree regulations of the Faculty of Electrical Engineering and Information Technology at RWTH Aachen University and in agreement with the supervising professor Dirk Uwe Sauer.

Scientific Journals

- Michael Merten, Christopher Olk, Ilka Schoeneberger, Dirk Uwe Sauer, “Bidding Strategy for Battery Storage Systems in the Secondary Control Reserve Market”, Elsevier, *Journal of Applied Energy*, 2020, DOI: 10.1016/j.apenergy.2020.114951
- Michael Merten, Fabian Rücker, Ilka Schoeneberger, Dirk Uwe Sauer, “Automatic Frequency Restoration Reserve Market Prediction: Methodology and Comparison of Various Approaches”, Elsevier, *Journal of Applied Energy*, 2020, DOI: 10.1016/j.apenergy.2020.114978
- Georg Angenendt, Michael Merten, Sebastian Zurmühlen, Dirk Uwe Sauer, “Evaluation of the effects of frequency restoration reserves market participation with photovoltaic battery energy storage systems and power-to-heat coupling”, Elsevier, *Journal of Applied Energy, Volume 260*, DOI: 10.1016/j.apenergy.2019.114186
- Christopher Olk, Michael Merten, Dirk Uwe Sauer, “Bidding strategy for a battery storage in the German secondary balancing power market”, Elsevier, *Journal of Energy Storage, 2019, Volume 21 p. 787-800,* DOI: 10.1016/j.est.2019.01.019
- Fabian Rücker, Michael Merten, Jingyu Gong, Roberto Villafáfila-Robles, Ilka Schoeneberger, Dirk Uwe Sauer, “Evaluation of the Effects of Smart Charging Strategies and Frequency Restoration Reserves Market Participation of an Electric Vehicle”, MDPI, Energies, Open Access Journal, DOI: 10.3390/en13123112

Conference Proceedings

- Tjark Thien, Michael Merten, Hendrik Axelsen, Sebastian Zurmühlen, Jeanette Münderlein et al., “Planning of Grid-Scale Battery Energy Storage Systems: Lessons Learned from a 5 MW Hybrid Battery Storage Project in Germany”, Battcon International Stationary Battery Conference, 2015, Orlando, Florida, USA

Supervised Theses

During my time as a research associate at the institute, I supervised the following graduate theses:

2018	Data Repository at a 5 MW Battery Storage System (bachelor's thesis)
2018	Pooling of Battery Storages for the Provision of Secondary Control Reserve (master's thesis)
2018	Development of a Self-Learning System for Predicting the Secondary Control Reserve Market (master's thesis)
2017	Development of a Self-Learning System for Predicting the Secondary Control Reserve Market - Entwicklung eines selbstlernenden Systems zur Prädiktion des Sekundärregelleistungsmarktes (master's thesis)
2017	Development of a Bidding Strategy for a Battery Storage to Participate in the German Secondary Balancing Power Market (master's thesis)
2017	Implementation and Sizing of a Controller for Active and Reactive Power Flow Optimization for a Stationary Battery Storage System - Auslegung eines Reglers zur Optimierung von Wirk- und Blindleistung für das M5BAT System (bachelor's thesis)
2016	Development of a Web-based Visualization System for a Grid-connected 5 MW Stationary Battery Storage System - Entwurf einer Webvisualisierung für einen Netzgekoppelten 5 MW Batteriespeicher (bachelor's thesis)
2015	Development of an Operator Control and Monitoring System for the SCADA (Supervisory Control and Data Acquisition) System of a 5 MW Grid-Integrated Battery Storage - Entwurf eines Bedien- und Beobachtungssystems mit zugehöriger Datenhaltung für die Leittechnik eines Netzgekoppelten 5 MW Batteriespeichers (master's thesis)
2014	Design and Implementation of an Operation, Diagnostic and Database System for Extending the SCADA (Supervisory Control and Data Acquisition) System of a 5 MW Grid-Integrated Battery Storage - Systementwurf und Realisierung eines Datenbankbasierten Kontroll- und Diagnosesystems zur Optimierung der Leittechnik eines Netzgekoppelten 5 MW Batteriespeichers (master's thesis)

ABISEA Band 1
Eßer, Albert
Berührungslose, kombinierte Energie- und Informations-übertragung für bewegliche Systeme
1. Aufl. 1992, 129 S.
ISBN 3-86073-046-0

ABISEA Band 2
Vogel, Ulrich
Entwurf und Beurteilung von Verfahren zur Hochausnutzung des Rad-Schiene-Kraftschlusses durch Triebfahrzeuge
1. Aufl. 1992, 131 S.
ISBN 3-86073-060-6

ABISEA Band 3
Reckhorn, Thomas
Stromeinprägendes Antriebssystem mit fremderregter Synchron-maschine
1. Aufl. 1992, 128 S.
ISBN 3-86073-061-4

ABISEA Band 4
Ackva, Ansgar
Spannungseinprägendes Antriebssystem mit Synchronmaschine und direkter Stromregelung
1. Aufl. 1992, 137 S.
ISBN 3-86073-062-2

ABISEA Band 5
Mertens, Axel
Analyse des Oberschwingungsverhaltens von taktsynchronen Delta - Modulationsverfahren zur Steuerung von Pulsstrom-richtern bei hoher Taktzahl
1. Aufl. 1992, 178 S.
ISBN 3-86073-069-X

ABISEA Band 6
Geuer, Wolfgang
Untersuchungen über das Alterungsverhalten von Blei-Akkumulatoren
1. Aufl. 1993, 97 S.
ISBN 3-86073-097-5

ABISEA Band 7
Langheim, Jochen
Einzelradantrieb für Elektrostraßenfahrzeuge
1. Aufl. 1993, 213 S.
ISBN 3-86073-123-8
(vergriffen)

ABISEA Band 8
Fetz, Joachim
Fehlertolerante Regelung eines Asynchron-Doppelantriebes für ein Elektrospeicherfahrzeug
1. Aufl. 1993, 136 S.
ISBN 3-86073-124-6
(vergriffen)

ABISEA Band 9
Schülting, Ludger
Optimierte Auslegung induktiver Bauelemente für den Mittelfrequenzbereich
1. Aufl. 1993, 126 S.
ISBN 3-86073-174-2
(vergriffen)

ABISEA Band 10
Skudelny, H.-Ch.
Stromrichtertechnik
4. Aufl. 1997, 259 S.
ISBN 3-86073-189-0

ABISEA Band 11
Skudelny, H.-Ch.
Elektrische Antriebe
3. Aufl. 1997, 124 S.
ISBN 3-86073-231-5

ABISEA Band 12
Schöpe, Friedhelm
Batterie-Management für Nickel-Cadmium Akkumulatoren
1. Aufl. 1994, 148 S.
ISBN 3-86073-232-3
(vergriffen)

ABISEA Band 13
v. d. Weem, Jürgen
Schmalbandige aktive Filter für Schienentriebfahrzeuge am Gleichspannungs-fahrdraht
1. Aufl. 1995, 126 S.
ISBN 3-86073-233-1

ABISEA Band 14
Backhaus, Klaus
Spannungseinprägendes Direktantriebssystem mit schnelllaufender geschalteter Reluktanzmaschine
1. Aufl. 1995, 146 S.
ISBN 3-86073-234-X
(vergriffen)

ABISEA Band 15
Reinold, Harry
Optimierung dreiphasiger Pulsdauermodulations-verfahren
1. Aufl. 1996, 107 S.
ISBN 3-86073-235-8

ABISEA Band 16
Köpken, Hans-Georg
Regelverfahren für Parallelschwingkreis-umrichter
1. Aufl. 1996, 125 S.
ISBN 3-86073-236-6

ABISEA Band 17
Mauracher, Peter
Modellbildung und Verbundoptimierung bei Elektrostraßenfahrzeugen
1. Aufl. 1996, 192 S.
ISBN 3-86073-237-4

ABISEA Band 18
Protiwa, Franz-Ferdinand
Vergleich dreiphasiger Resonanz-Wechselrichter in Simulation und Messung
1. Aufl. 1997, 178 S.
ISBN 3-86073-238-2

ABISEA Band 19
Brockmeyer, Ansgar
Dimensionierungswerkzeug für magnetische Bau-elemente in Stromrichter-anwendungen
1. Aufl. 1997, 175 S.
ISBN 3-86073-239-0

ABISEA Band 20
Apeldoorn, Oscar
Simulationsgestützte Bewertung von Steuerverfahren für netzgeführte Stromrichter mit verringerter Netzrückwirkung
1. Aufl. 1997, 134 S.
ISBN 3-86073-680-9

ABISEA Band 21
Lohner, Andreas
Batteriemanagement für verschlossene Blei-Batterien am Beispiel von Unterbrechungsfreien Stromversorgungen
1. Aufl. 1998, 126 S.
ISBN 3-86073-681-7

ABISEA Band 22
Reinert, Jürgen
Optimierung der Betriebseigenschaften von Antrieben mit geschalteter Reluktanzmaschine
1. Aufl. 1998, 153 S.
ISBN 3-86073-682-5

ABISEA Band 23
Nagel, Andreas
Leitungsgebundene Störungen in der Leistungselektronik: Entstehung, Ausbreitung und Filterung
1. Aufl. 1999, 140 S.
ISBN 3-86073-683-3

ABISEA Band 24
Menne, Marcus
Drehschwingungen im Antriebsstrang von Elektrostraßenfahrzeugen - Analyse und aktive Dämpfung
1. Aufl. 2001, 169 S.
ISBN 3-86073-684-1

ABISEA Band 25
von Bloh, Jürgen
Multilevel-Umrichter zum Einsatz in Mittelspannungs-Gleichspannungs-Übertragungen
1. Aufl. 2001, 137 S.
ISBN 3-86073-685-X

ABISEA Band 26
Karden, Eckhard
Using low-frequency impedance spectroscopy for characterization, monitoring, and modeling of industrial batteries
1. Aufl. 2002, 137 S.
ISBN 3-8265-9766-4

ABISEA Band 27
Karipidis, Claus-Ulrich
A Versatile DSP/ FPGA Structure optimized for Rapid Prototyping and Digital Real-Time Simulation of Power Electronic and Electrical Drive Systems
1. Aufl. 2001, 164 S.
ISBN 3-8265-9738-9

ABISEA Band 28
Kahlen, Klemens
Regelungsstrategien für permanentmagnetische Direktantriebe mit mehreren Freiheitsgraden
1. Aufl. 2002, 154 S.
ISBN 3-8322-1222-1

ABISEA Band 29
Inderka, Robert B.
Direkte Drehmomentregelung Geschalteter Reluktanzantriebe
1. Aufl. 2003, 182 S.
ISBN 3-8322-1175-6

ABISEA Band 30
Schröder, Stefan
Circuit-Simulation Models of High-Power Devices Based on Semiconductor Physics
1. Aufl. 2003, 123 S.
ISBN 3-8322-1250-7

ABISEA Band 31
Buller, Stephan
Impedance-Based Simulation Models for Energy Storage Devices in Advanced Automotive Power Systems
1. Aufl. 2003, 138 S.
ISBN 3-8322-1225-6

ABISEA Band 32
Schönknecht, Andreas
Topologien und Regelungsstrategien für das induktive Erwärmen mit hohen Frequenz-Leistungsprodukten
1. Aufl. 2004, 157 S.
ISBN 3-8322-2408-4

ABISEA Band 33
Tolle, Tobias
Konvertertopologien für ein aufwandsarmes, zweistufiges Schaltnetzteil zum Laden von Batterien aus dem Netz
1. Aufl. 2004, 148 S.
ISBN 3-8322-2676-1

ABISEA Band 34
Götting, Gunther
Dynamische Antriebsregelung von Elektrostraßenfahrzeugen unter Berücksichtigung eines schwingungsfähigen Antriebsstrangs
1. Aufl. 2004, 157 S.
ISBN 3-8322-2804-7

ABISEA Band 35
Dieckerhoff, Sibylle
Transformatorlose Stromrichterschaltungen für Bahnfahrzeuge am 16 2/3Hz Netz
1. Aufl. 2004, 147 S.
ISBN 3-8322-3094-7

ABISEA Band 36
Hu, Jing
Bewertung von DC-DC-Topologien und Optimierung eines DC-DC-Leistungsmoduls für das 42-V-Kfz-Bordnetz
1. Aufl. 2004, 148 S.
ISBN 3-8322-3201-X

ABISEA Band 37
Detjen, Dirk-Oliver
Characterization and Modeling of Si-Si Bonded Hydrophobie Interfaces for Novel High-Power BIMOS Devices
1. Aufl. 2004, 135 S.
ISBN 3-8322-2963-9

ABISEA Band 38
Walter, Jörg
Simulationsbasierte Zuverlässigkeitsanalyse in der modernen Leistungselektronik
1. Aufl. 2004, 121 S.
ISBN 3-8322-3481-0

ABISEA Band 39
Schwarzer, Ulrich
IGBT versus GCT in der Mittelspannungsanwendung - ein experimenteller und simulativer Vergleich
1. Aufl. 2005, 170 S.
ISBN 3-8322-4489-1

ABISEA Band 40
Bartram, Markus
IGBT-Umrichtersysteme für Windkraftanlagen: Analyse der Zyklenbelastung, Modellbildung, Optimierung und Lebensdauervorhersage
1. Aufl. 2006, 185 S.
ISBN 3-8322-5039-5

ABISEA Band 41
Ponnaluri, Srinivas
Generalized Design, Analysis and Control of Grid side converters with integrated UPS or Islanding functionality
1. Aufl. 2006, 163 S.
ISBN 3-8322-5281-9

ABISEA Band 42
Jacobs, Joseph
Multi-Phase Series Resonant DC-to-DC Converters
1. Aufl. 2006, 185 S.
ISBN 3-8322-5532-X

ABISEA Band 43
Linzen, Dirk
Impedance-Based Loss Calculation and Thermal Modeling of Electrochemical Energy Storage Devices for Design Considerations of Automotive Power Systems
1. Aufl. 2006, 185 S.
ISBN 3-8322-5706-3

ABISEA Band 44
Fiedler, Jens
Design of Low-Noise Switched Reluctance Drives
1. Aufl. 2007, 176 S.
ISBN 978-3-8322-5864-1

ABISEA Band 45
Fuengwarodsakul, Nisai
Predictive PWM-based Direct Instantaneous Torque Control for Switched Reluctance Machines
1. Aufl. 2007, 141 S.
ISBN 978-3-8322-6210-5

ABISEA Band 46
Meyer, Christoph
Key Components for Future Offshore DC Grids
1. Aufl. 2007, 187 S.
ISBN 978-3-8322-6571-7

ABISEA Band 47
Fujii, Kansuke
Characterization and Optimization of Soft-Switched Multi-Level Converters for STATCOMs
1. Aufl. 2008, 199 S.
ISBN 978-3-8322-6981-4

ABISEA Band 48
Carstensen, Christian
Eddy Currents in Windings of Switched Reluctance Machines
1. Aufl. 2008, 179 S.
ISBN 978-3-8322-7118-3

ABISEA Band 49
Bohlen, Oliver
Impedance-based battery monitoring
1. Aufl. 2008, 190 S.
ISBN 978-3-8322-7606-5

ABISEA Band 50
Thele, Marc
A contribution to the modelling of the charge acceptance of lead-acid batteries - using frequency and time domain based concepts
1. Aufl. 2008, 165 S.
ISBN 978-3-8322-7659-1

ABISEA Band 51
König, Andreas
High Temperature DC-to-DC Converters for Downhole Applications
1. Aufl. 2009, 154 S.
ISBN 978-3-8322-8489-3

ABISEA Band 52
Dick, Christian Peter
Multi-Resonant Converters as Photovoltaic Module-Integrated Maximum Power Point Tracker
1. Aufl. 2010, 182 S.
ISBN 978-3-8322-9199-0

ABISEA Band 53
Kowal, Julia
Spatially resolved impedance of nonlinear inhomogeneous devices: using the example of lead-acid batteries
1. Aufl. 2010, 203 S.
ISBN 978-3-8322-9483-0

ABISEA Band 54
Roscher, Michael Andreas
Zustandserkennung von LiFeP04-Batterien für Hybrid- und Elektrofahrzeuge
1. Aufl. 2011, 186 S.
ISBN 978-3-8322-9738-1

ABISEA Band 55
Hirschmann, Dirk
Highly Dynamic Piezoelectric Positioning
1. Aufl. 2011, 146 S.
ISBN 978-3-8322-9746-6

ABISEA Band 56
Rigbers, Klaus
Highly Efficient Inverter Architectures for Three-Phase Grid Connection of Photovoltaic Generators
1. Aufl. 2011, 244 S.
ISBN 978-3-8322-9816-9

ABISEA Band 57
Kasper, Knut
Analysis and Control of the Acoustic Behavior of Switched Reluctance Drives
1. Aufl. 2011, 205 S.
ISBN 978-3-8322-9869-2

ABISEA Band 58
Köllensperger, Peter
The Internally Commutated Thyristor - Concept, Design and Application
1. Aufl. 2011, 214 S.
ISBN 978-3-8322-9909-5

ABISEA Band 59
Schoenen, Timo
Einsatz eines DC/DC-Wandlers zur Spannungsanpassung zwischen Antrieb und Energiespeicher in Elektro-und Hybridfahrzeugen
1. Aufl. 2011, 128 S.
ISBN 978-3-8440-0622-3

ABISEA Band 60
Hennen, Martin
Switched Reluctance Direct Drive with Integrated Distributed Inverter
1. Aufl. 2012, 141 S.
ISBN 978-3-8440-0731-2

ABISEA Band 61
van Treek, Daniel
Position Sensorless Torque Control of Switched Reluctance Machines
1. Aufl. 2012, 144 S.
ISBN 978-3-8440-1014-5

ABISEA Band 62
Bragard, Michael
The Integrated Emitter Turn-Off Thyristor. An Innovative MOS-Gated High-Power Device
1. Aufl. 2012, 164 S.
ISBN 978-3-8440-1152-4

ABISEA Band 63
Gerschler, Jochen B.
Ortsaufgelöste Modellbildung von Lithium-Ionen-Systemen unter spezieller Berücksichtigung der Batteriealterung
1. Aufl. 2012, 334 S.
ISBN 978-3-8440-1307-8

ABISEA Band 64
Neuhaus, Christoph R.
Schaltstrategien für Geschaltete Reluktanzantriebe mit kleinem Zwischenkreis
1. Aufl. 2012, 133 S.
ISBN 978-3-8440-1487-7

ABISEA Band 65
Butschen, Thomas
Dual-ICT- A Clever Way to Unite Conduction and Switching Optimized Properties in a Single Wafer
1. Aufl. 2012, 168 S.
ISBN 978-3-8440-1771-7

ABISEA Band 66
Plum, Thomas
Design and Realization of High-Power MOS Turn-Off Thyristors
1. Aufl. 2013, 113 S.
ISBN 978-3-8440-1884-4

ABISEA Band 67
Kiel, Martin
Impedanzspektroskopie an Batterien unter besonderer Berücksichtigung von Batteriesensoren für den Feldeinsatz
1. Aufl. 2013, 226 S.
ISBN 978-3-8440-1973-5

ABISEA Band 68
Brauer, Helge
Schnelldrehender Geschalteter Reluktanzantrieb mit extremem Längendurchmesserverhältnis
1. Aufl. 2013, 192 S.
ISBN 978-3-8440-2345-9

ABISEA Band 69
Thomas, Stephan
A Medium-Voltage Multi-Level DC/DC Converter with High Voltage Transformation Ratio
1. Aufl. 2014, 226 S.
ISBN 978-3-8440-2605-4

ABISEA Band 70
Richter, Sebastian
Digitale Regelung von PWM Wechselrichtern mit niedrigen Trägerfrequenzen
1. Aufl. 2014, 126 S.
ISBN 978-3-8440-2641-2

ABISEA Band 71
Bösing, Matthias
Acoustic Modeling of Electrical Drives - Noise and Vibration Synthesis based on Force Response Superposition
1. Aufl. 2014, 188 S.
ISBN 978-3-8440-2752-5

ABISEA Band 72
Waag, Wladislaw
Adaptive algorithms for monitoring of lithium-ion batteries in electric vehicles
1. Aufl. 2014, 232 S.
ISBN 978-3-8440-2976-5

ABISEA Band 73
Sanders, Tilman
Spatially Resolved Electrical In-Situ Measurement Techniques for Fuel Cells
1. Aufl. 2014, 126 S.
ISBN 978-3-8440-3121-8

ABISEA Band 74
Baumhöfer, Thorsten
Statistische Betrachtung experimenteller Alterungsuntersuchungen an Lithium-Ionen Batterien
1. Aufl. 2015, 157 S.
ISBN 978-3-8440-3423-3

ABISEA Band 75
Andre, Dave
Systematic Characterization of Ageing Factors for High-Energy Lithium-Ion Cells and Approaches for Lifetime Modelling Regarding an Optimized Operating Strategy in Automotive Applications
1. Aufl. 2015, 196 S.
ISBN 978-3-8440-3587-2

ABISEA Band 76
Merei, Ghada
Optimization of off-grid hybrid PV-wind-diesel power supplies with multi-technology battery systems taking into account battery aging
1. Aufl. 2015, 184 S.
ISBN 978-3-8440-4148-4

ABISEA Band 77
Schulte, Dominik
Modellierung und experimentelle Validierung der Alterung von Blei-Säure Batterien durch inhomogene Stromverteilung und Säureschichtung
1. Aufl. 2016, 165 S.
ISBN 978-3-8440-4216-0

ABISEA Band 78
Schenk, Mareike
Simulative Untersuchung der Wicklungsverluste in Geschalteten Reluktanzmaschinen
1. Aufl. 2016, 126 S.
ISBN 978-3-8440-4282-5

ABISEA Band 79
Wang, Yu
Development of Dynamic Models with Spatial Resolution for Electrochemical Energy Converters as Basis for Control and Management Strategies
1. Aufl. 2016, 188 S.
ISBN 978-3-8440-4303-7

ABISEA Band 80
Ecker, Madeleine
Lithium Plating in Lithium-Ion Batteries:
An Experimental and Simulation Approach
1. Aufl. 2016, 154 S.
ISBN 978-3-8440-4525-3

ABISEA Band 81
Zhou, Wei
Modellbasierte Auslegungsmethode von Temperierungssystemen für Hochvolt-Batterien in Personenkraftfahrzeugen
1. Aufl. 2016, 175 S.
ISBN 978-3-8440-4589-5

ABISEA Band 82
Lunz, Benedikt
Deutschlands Stromversorgung im Jahr 2050
Ein szenariobasiertes Verfahren zur vergleichenden Bewertung von Systemvarianten und Flexibilitätsoptionen
1. Aufl. 2016, 187 S.
ISBN 978-3-8440-4627-4

ABISEA Band 83
Hofmann, Andreas G.
Direct Instantaneous Force Control: Key to Low-Noise Switched Reluctance Traction Drives
1. Aufl. 2016, 228 S.
ISBN 978-3-8440-4715-8

ABISEA Band 84
Budde-Meiwes, Heide
Dynamic Charge Acceptance of Lead-Acid Batteries for Micro-Hybrid Automotive Applications
1. Aufl. 2016, 157 S.
ISBN 978-3-8440-4733-2

ABISEA Band 85
Engel, Stefan P.
Thyristor-Based High-Power On-Load Tap Changers Control under Harsh Load Conditions
1. Aufl. 2016, 156 S.
ISBN 978-3-8440-4986-2

ABISEA Band 86
Van Hoek, Hauke
Design and Operation Considerations of Three-Phase Dual Active Bridge Converters for Low-Power Applications with Wide Voltage Ranges
1. Aufl. 2017, 231 S.
ISBN 978-3-8440-5011-0

ABISEA Band 87
Diekhans, Tobias
Wireless Charging of Electric Vehicles - a Pareto-Based Comparison of Power Electronic Topologies
1. Aufl. 2017, 151 S.
ISBN 978-3-8440-5048-6

ABISEA Band 88
Lehner, Susanne
Reliability Assessment of Lithium-Ion Battery Systems with Special Emphasis on Cell Performance Distribution
1. Aufl. 2017, 184 S.
ISBN 978-3-8440-5090-5

ABISEA Band 89
Käbitz, Stefan
Untersuchung der Alterung von Lithium-Ionen-Batterien mittels Elektroanalytik und elektrochemischer Impedanzspektroskopie
1. Aufl. 2016, 258 S.
DOI: 10.18154/RWTH-2016-12094

ABISEA Band 90
Witzenhausen, Heiko
Elektrische Batteriespeichermodelle: Modellbildung, Parameteridentifikation und Modellreduktion
1. Aufl. 2017, 266 S.
DOI: 10.18154/RWTH-2017-03437

ABISEA Band 91
Münnix, Jens
Einfluss von Stromstärke und Zyklentiefe auf graphitische Anoden
1. Aufl. 2017, 171 S.
DOI: 10.18154/RWTH-2017-01915

ABISEA Band 92
Pilatowicz, Grzegorz
Failure Detection and Battery Management Systems of Lead-Acid Batteries for Micro-Hybrid Vehicles
1. Aufl. 2017, 212 S.
DOI: 10.18154/RWTH-2017-09156

ABISEA Band 93
Drillkens, Julia
Aging in Electrochemical Double Layer Capacitors: An Experimental and Modeling Approach
1. Aufl. 2017, 179 S.
DOI: 10.18154/RWTH-2018-223434

ABISEA Band 94
Magnor, Dirk
Globale Optimierung netzgekoppelter PV-Batteriesysteme unter besonderer Berücksichtigung der Batteriealterung
1. Aufl. 2017, 210 S.
DOI: 10.18154/RWTH-2017-06592

ABISEA Band 95
Iliksu, Merve
Elucidation and Comparison of the Effects of Lithium Salts on Discharge Chemistry of Nonaqueous Li-O_2 Batteries
1. Aufl. 2018, 160 S.
DOI: 10.18154/RWTH-2018-223782

ABISEA Band 96
Schmalstieg, Johannes
Physikalisch-elektrochemische Simulation von Lithium-Ionen-Batterien: Implementierung, Parametrierung und Anwendung
1. Aufl. 2017, 168 S.
DOI: 10.18154/RWTH-2017-04693

ABISEA Band 97
Soltau, Nils
High-Power Medium-Voltage DC-DC Converters: Design, Control and Demonstration
1. Aufl. 2017, 176 S.
DOI: 10.18154/RWTH-2017-04084

ABISEA Band 98
Stieneker, Marco
Analysis of Medium-Voltage Direct-Current Collector Grids in Offshore Wind Parks
1. Aufl. 2017, 144 S.
DOI: 10.18154/RWTH-2017-04667

ABISEA Band 99
Masomtob, Manop
A New Conceptual Design of Battery Cell with an Internal Cooling Channel
1. Aufl. 2017, 167 S.
DOI: 10.18154/RWTH-2018-223281

ABISEA Band 100
Marongiu, Andrea
Performance and Aging Diagnostic on Lithium Iron Phosphate Batteries for Electric Vehicles and Vehicle-to-Grid Strategies
1. Aufl. 2017, 222 S.
DOI: 10.18154/RWTH-2017-09944

ABISEA Band 101
Gitis, Alexander
Flaw detection in the coating process of lithium-ion battery electrodes with acoustic guided waves
1. Aufl. 2017, 109 S.
DOI: 10.18154/RWTH-2017-099519

ABISEA Band 102
Neeb, Christoph
Packaging Technologies for Power Electronics in Automotive Applications
1. Aufl. 2017, 132 S.
DOI: 10.18154/RWTH-2018-224569

ABISEA Band 103
Adler, Felix
A Digital Hardware Platform for Distributed Real-Time Simulation of Power Electronic Systems
1. Aufl. 2017, 156 S.
DOI: 10.18154/RWTH-2017-10761

ABISEA Band 104
Becker, Jan
Flexible Dimensionierung und Optimierung hybrider Lithium-Ionenbatterie-speichersysteme mit verschiedenen Auslegungs-zielen
1. Aufl., 2017, 157 S.
DOI: 10.18154/RWTH-2017-09278

ABISEA Band 105
Warnecke, Alexander J.
Degradation Mechanisms in NMC Based Lithium-Ion Batteries
1. Aufl. 2017, 158 S.
DOI: 10.18154/RWTH-2017-09646

ABISEA Band 106
Taraborrelli, Silvano
Bidirectional Dual Active Bridge Converter using a Tap Changer for Extended Voltage Ranges
1. Aufl. 2017, 94 S.
DOI: 10.18154/RWTH-2018-228242

ABISEA Band 107
Sarriegi, Garikoitz
SiC and GaN Semiconductors: The Future Enablers of Compact and Efficient Converters for Electromobility
1. Aufl. 2017, 106 S.
DOI: 10.18154/RWTH-2018-227548

ABISEA Band 108
Senol, Murat
Drivetrain Integrated Dc-Dc Converters utilizing Zero Sequence Currents
1. Aufl. 2017, 134 S.
DOI: 10.18154/RWTH-2018-226170

ABISEA Band 109
Kojima, Tetsuya
Efficiency Optimized Control of Switched Reluctance Machines
1. Aufl. 2017, 142 S.
DOI: 10.18154/RWTH-2018-226697

ABISEA Band 110
Lewerenz, Meinert
Dissection and Quantitative Description of Aging of Lithium-Ion Batteries Using Non-Destructive Methods Validated by Post-Mortem-Analyses
1. Aufl. 2018, 139 S.
DOI: 10.18154/RWTH-2018-228663

ABISEA Band 111
Büngeler, Johannes
Optimierung der Verfügbarkeit und der Lebensdauer von Traktionsbatterien für den Einsatz in Flurförderfahrzeugen
1. Aufl. 2018, 171 S.
DOI: 10.18154/RWTH-2018-226569

ABISEA Band 112
Wegmann, Raphael
Betriebsstrategien und Potentialbewertung hybrider Batteriespeichersysteme in Elektrofahrzeugen
1. Auflage 2018, 184 S.
DOI: 10.18154/RWTH-2018-228833

ABISEA Band 113
Nordmann, Hannes
Batteriemanagementsysteme unter besonderer Berücksichtigung von Fehlererkennung und Peripherieanalyse
1. Aufl. 2018, 222 S.
DOI: 10.18154/RWTH-2018-228763

ABISEA Band 114
Engelmann, Georges
Reducing Device Stress and Switching Losses Using Active Gate Drivers and Improved Switching Cell Design
1. Aufl. 2018, 195 S.
DOI: 10.18154/RWTH-2018-228973

ABISEA Band 115
Klein-Heßling, Annegret
Active DC-Power Filters for Switched Reluctance Drives during Single-Pulse Operation
1. Aufl. 2018, 166 S.
DOI: 10.18154/RWTH-2018-231030

ABISEA Band 116
Burkhart, Bernhard
Switched Reluctance Generator for Range Extender Applications - Design, Control and Evaluation
1. Aufl. 2018, 194 S.
DOI: 10.18154/RWTH-2019-00025

ABISEA Band 117
Biskoping, Matthias
Discrete Modeling and Control of a versatile Power Electronic Test Bench with Special Focus on Central Photovoltaic Inverter Testing
1. Aufl. 2018, 236 S.
DOI: 10.18154/RWTH-2019-03346

ABISEA Band 118
Schubert, Michael
High-Precision Torque Control of Inverter-Fed Induction Machines with Instantaneous Phase Voltage Sensing
1. Aufl. 2019, 221 S.
DOI: 10.18154/RWTH-2018-231364

ABISEA Band 119
Van der Broeck, Christoph
Methodology for Thermal Modeling, Monitoring and Control of Power Electronic Modules
1. Aufl. 2019, 290 S.
DOI: 10.18154/RWTH-2019-01370

ABISEA Band 120
Hust, Friedrich Emanuel
Physico-chemically motivated parameterization and modelling of real-time capable lithium-ion battery models – a case study on the Tesla Model S battery
1. Aufl. 2019, 203 S.
DOI: 10.18154/RWTH-2019-00249

ABISEA Band 121
Ralev, Iliya
Accurate Torque Control of Position Sensorless Switched Reluctance Drives
1. Aufl. 2019, 154 S.
DOI: 10.18154/RWTH-2019-03071

ABISEA Band 122
Ayeng'o, Sarah Paul
Optimization of number of PV cells connected in series for a direct-coupled PV system with lead-acid and lithium-ion batteries
1. Aufl. 2019, 114 S.
DOI: 10.18154/RWTH-2019-01843

ABISEA Band 123
Koschik, Stefan Andreas
Permanenterregte Synchronmaschinen mit verteilter Einzelzahnsteuerung - Regelkonzepte und Betriebsstrategien für hochintegrierte Antriebssysteme
1. Aufl. 2019, 158 S.
DOI: 10.18154/RWTH-2019-03446

ABISEA Band 124
Farmann, Alexander
A comparative study of reduced-order equivalent circuit models for state-of-available-power prediction of lithium-ion batteries in electric vehicles
1. Aufl. 2019, 214 S.
DOI: 10.18154/RWTH-2019-04700

ABISEA Band 125
Mareev, Ivan
Analyse und Bewertung von batteriegetriebenen, oberleitungsversorgten und brennstoffzellengetriebenen Lastkraftwagen für den Einsatz im Güterfernverkehr in Deutschland
1. Aufl. 2019, 158 S.
DOI: 10.18154/RWTH-2019-04698

ABISEA Band 126
Qi, Fang
Online Model-predictive Thermal Management of Inverter-fed Electrical Machines
1. Aufl. 2019, 154 S.
DOI: 10.18154/RWTH-2019-08304

ABISEA Band 127
Kairies, Kai-Philipp
Auswirkungen dezentraler Solarstromspeicher auf Netzbetreiber und Energieversorger
1. Aufl. 2019, 140 S.
DOI: 10.18154/RWTH-2019-06706

ABISEA Band 128
Fleischer, Michael
Traction control for Railway Vehicles
1. Aufl. 2019, 162 S.
DOI: 10.18154/RWTH-2019-10570

ABISEA Band 129
Teuber, Moritz
Lifetime Assessment and Degradation Mechanisms in Electric Double-Layer Capacitors
1. Aufl. 2019, 150 S.
DOI: 10.18154/RWTH-2019-10071

ABISEA Band 130
Bußar, Christian
Investigation of Optimal Transformation Pathways towards 2050 for the Successful Implementation of a Sustainable Reduction of Carbon Emissions from Power Generation
1. Aufl. 2019, 204 S.
DOI: 10.18154/RWTH-2019-09975

ABISEA Band 131
Wienhausen, Arne Hendrik
High Integration of Power Electronic Converters enabled by 3D Printing
1. Aufl. 2019, 146 S.
DOI: 10.18154/RWTH-2019-08746

ABISEA Band 132
Kwiecien, Monika
Electrochemical Impedance Spectroscopy on Lead-Acid Cells during Aging
1. Aufl. 2019, 138 S.
DOI: 10.18154/RWTH-2019-09480

ABISEA Band 133
Titiz, Furkan Kaan
A Three-phase Low-voltage Grid-connected Current Source Inverter
1. Aufl. 2019, 128 S.
DOI: 10.18154/RWTH-2020-00458

ABISEA Band 134
Wünsch, Martin
Separation der Kathoden-alterung in Lithium-Ionen-Batteriezellen mittels elektrochemischer Impedanzspektroskopie
1. Aufl. 2019, 177 S.
DOI: 10.18154/RWTH-2019-11017

ABISEA Band 135
Badeda, Julia
Modeling and Steering of Multi-Use Operation with Uninterruptible Power Supply Systems - utilizing the example of lead-acid batteries
1. Aufl. 2020, 282 S.
DOI: 10.18154/RWTH-2020-05456

ABISEA Band 136
Kleinsteinberg, Björn
Energy Efficiency Increase of a Vanadium Redox Flow Battery with a Power-Based Model
1. Aufl. 2020, 163 S.
DOI: 10.18154/RWTH-2020-06092

ABISEA Band 137
Cai, Zhuang
Optimization of dimension and operation strategy for a wind-battery energy system in German electricity market under consideration of battery ageing process
1. Aufl. 2020, 144 S.
DOI: 10.18154/RWTH-2020-06525

ABISEA Band 138
Sabet, Pouyan Shafiei
Analysis of Predominant Processes in Electrochemical Impedance Spectra and Investigation of Aging Processes of Lithium-Ion Batteries with Layered Oxide Cathodes and Graphitic Anodes
1. Aufl. 2020, 136 S.
DOI: 10.18154/RWTH-2020-07683

ABISEA Band 139
Angenendt, Georg
Operation, Optimization and Additional Market Participation of Households with PV Battery Storage System and Power-to-Heat Application
1. Aufl. 2020, 221 S.
DOI: 10.18154/RWTH-2020-05200

ABISEA Band 140
Oberdieck, Karl Friedrich
Measurement and Mitigation of Electromagnetic Emissions of Propulsion Inverters for Electric Vehicles
1. Aufl. 2020, S.
DOI: 10.18154/RWTH-2020-

ABISEA Band 141
Bubert, Andreas Martin
Optimierung des elektrischen Antriebsstrangs von Elektrofahrzeugen mit Betrachtung parasitärer Ströme innerhalb der elektrischen Maschine
1. Aufl. 2020, S.
DOI: 10.18154/RWTH-2020-

ABISEA Band 142
Fleischer, Christian Georg
Model-Driven Software Development and Verification Solutions for Safety Critical Battery Management Systems
1. Aufl. 2020, S.
DOI: 10.18154/RWTH-2020-

ABISEA Band 143
Arzberger, Arno
Thermografische Methoden zur zerstörungsfreien Messung der anisotropen Wärmeleitfähigkeit von Lithium-Ionen Zellen
1. Aufl. 2020, S.
DOI: 10.18154/RWTH-2020

ABISEA Band 144
Lange, Tobias
Oberwellenbasierte Modellierung, Regelung und Auslegung von Permanentmagnet- und Reluktanz-Synchronmaschinen
1. Aufl. 2020, S.
DOI: 10.18154/RWTH-2020-

ABISEA Band 145
Weiss, Claude
Fault Tolerant Switched Reluctance Machines with Distributed Inverters – Modeling and Control
1. Aufl. 2020, S.
DOI: 10.18154/RWTH-2020-

ABISEA Band 146
Huck, Moritz
Modelling the Transient Behaviour of Lead-Acid Batteries: Electrochemical Impedance of Adsorbed Species
1. Aufl. 2020, 151 S.
DOI: 10.18154/RWTH-2020-08362

ABISEA Band 147
Willenberg, Lisa
Volumenausdehnung und ihre Auswirkungen auf die Alterung einer zylindrischen Lithium-Ionen-Batterie
1. Aufl. 2020, S.
DOI: 10.18154/RWTH-2020-

ABISEA Band 148
Rogge, Matthias
Electrification of Public Transport Bus Fleets with Battery Electric Busses
1. Aufl. 2020, S.
DOI: 10.18154/RWTH-2020-

ABISEA Band 149
Münderlein, Jeanette
Numerische Methodik zur Auslegung eines Hybriden Speichersystems mit Multinutzen“
1. Aufl. 2020, S.
DOI: 10.18154/RWTH-2020-

Automatic Frequency Restoration Reserve (aFRR) is one of three control reserve services in continental Europe to compensate imbalances in the electrical grid. Due to the transition towards a high degree of renewable sources, fewer conventional power plants will be available in the future to stabilize the electrical grid. However, new technologies are facing various entrance barriers because of the complex market design. This work provides a detailed aFRR market analysis and derives earning potentials for different bidding strategies.

To assist the creation of bidding strategies, a market prediction methodology is presented. Both statistical and machine learning based models are used for predicting key market quantities. A model comparison reveals a usually better performance of statistical models. Exogenous data sources such as weather, electrical loads or market data did not significantly improve the prediction performance.

This work further developed an operating strategy for integrating Battery Energy Storage Systems (BESS) into existing Virtual Power Plants (VPP) to exploit the advantages of multiple technologies. Based on an optimization process, a bidding strategy is presented that optimizes the bids to submit to the aFRR auction. An in-depth cost breakdown and battery-ageing model support the derivation of optimal bids. With current costs of containerized BESS, an operation is not economically viable and earnings were found to be lower than on the Frequency Control Reserve (FCR) market. However, with a predicted cost breakdown for the year 2025, profits can be generated.

ISSN 1437-675X